ELECTROMAGNETIC PROPERTIES OF IRON DEFICIENT Ni-Cu-Zn FERRITES AND THE INFLUENCE OF ADDITIVES AS SINTERING AID

By

Md. Zakir Hossain Khan
Roll No: 0655751
Session: July-2006

A THESIS SUBMITED TO THE DEPARTMENT OF PHYSICS, KHULNA UNIVERSITY OF ENGINEERING & TECHNOLOGY, KHULNA- 9203 IN PARTIAL FULFILMENT OF THE REQUIRMENT FOR THE DEGREE OF DOCTOR OF PHILLOSOPHY

DEPARTMENT OF PHYSICS
KHULNA UNIVERSITY OF ENGINEERING AND TECHNOLOGY
KHULNA - 9203, BANGLADESH
January- 2013

DECLARATION

This is to certify that the thesis work entitled as **"Electromagnetic Properties of Iron deficient Ni-Cu-Zn Ferrites and the influence of additives as sintering AID"** has been carried out in partial fulfillment of the requirement for Ph. D. degree in the department of physics, Khulna University of Engineering & Technology, Khulna-9203, Bangladesh. The above research work or any part of this work has not been submitted to anywhere for the award of any degree or diploma. No other person's work has been used without due acknowledgement.

1. Supervisor

....
Prof. Dr. S. S. Sikder

Candidate

....
Md. Zakir Hossain Khan

2. Co-supervisor

....
Dr. A. K. M. Abdul Hakim

To
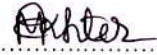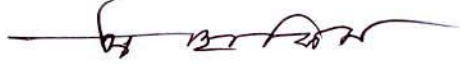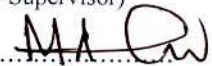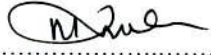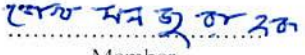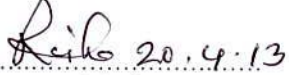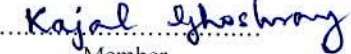
My Late Father and Mother

Approval

This is to certify that the thesis work submitted by *Md. Zakir Hossain Khan* entitled *"Electromagnetic Properties of Iron deficient Ni-Cu-Zn Ferrites and the influence of additives as sintering AID"* has been accepted by the board of examiners for the partial fulfillment of the requirements for the degree of *Doctor of Philosophy* in the Department of *Physics*, Khulna University of Engineering & Technology, Khulna, Bangladesh in April 2013.

Board of Examiners

Sl. No.	Name, Designation & Address	Signature
1.	Prof. Dr. Shibendra Shekher Sikder Department of Physics Khulna University of Engineering & Technology Khulna-9203	Chairman (Supervisor)
2.	Head Department of Physics Khulna University of Engineering & Technology Khulna-9203	Member
3.	Dr. A. K. M. Abdul Hakim Chief Engineer& Head (Ex) Materials Science Division Atomic Energy Center, Dhaka-1000	Member (Co- Supervisor)
4.	Prof. Dr. Md. Mahbub Alam Department of Physics Khulna University of Engineering & Technology Khulna-9203	Member
5.	Prof. Dr. Md. Rafiqul Islam Department of Electrical and Electronic Engineering Khulna University of Engineering & Technology Khulna-9203	Member
6.	Prof. Dr. Mohammad Abu Yousuf Department of Chemistry Khulna University of Engineering & Technology Khulna-9203	Member
7.	Dr. Sheikh Manjura Hoque Principal Scientific Officer Materials Science Division Atomic Energy Center, Dhaka-1000	Member
8.	Prof. Dr. Rabindra Chandra Sinha Chairman, Department of Physics Jahangirnagar University Saver, Dhaka-1342, Bangladesh	20.4.13 Member (External)
9.	Prof. Dr. Kajal Ghoshray Experimental Condensed Matter Physics Division Saha Institute of Nuclear Physics 1/AF, Bidhanagar, Kolkata 700064 West Bengal, India	Member (External)

March 14, 2013

Report on the thesis entitled "**Electromagnetic properties of iron deficient Ni-Cu-Zn Ferrites and the influence of additives as sintering aid**" submitted by Mr. Md. Zakir Hossain Khan (Roll No. 0655751), Ph. D student of the Dept. of Physics, Khulna University of Engineering and Technology, Khulna 9203, Bangladesh.

This thesis reports the detailed and systematic investigation on the effect of doping and sintering aids on the electromagnetic properties of Fe-deficient Ni-Cu-Zn ferrite. Three series of ferrite samples of the compositions $(Ni_{0.28}Cu_{0.10}Zn_{0.62}O)$ $(Fe_2O_3)_{1-x}$ (where x=0.0. 0.03, 0.06, 0.08), $Ni_{0.28}Cu_{0.10+x}Zn_{0.62-x}Fe_{1.98}O_4$ (where x=0.00. 0.03, 0.06, 0.09, 0.120 and $Ni_{0.28}Cu_{0.10}Zn_{0.62}Fe_{1.98}O_4$ doped with V_2O_5 and Li_2O were prepared by solid state reaction and characterized by X-Ray Diffraction (XRD) studies. All the samples were of single phase. Temperature and frequency dependence of the permeability, B-H loop at room temperature, and DC magnetization as a function of magnetic field and temperature were measured. The composition dependence of room temperature dc resistivity and the frequency dependence of ac resistivity and the dielectric constant were measured. The grain size of the samples was also determined using SEM micrograph. Effect of the grain size on the magnetic and dielectric properties along with the electrical resistivity were also investigated. Based on the different experimental results, the optimum composition resulting high initial permeability and minimum hysteresis loss was determined. Based on these results, the direction of the future research on soft ferrites for electronic device application is also highlighted.

Detail Report:

In chapter I, the candidate has elaborated the aims and objective of the present work. To compare the present results a review on the recent reports by other groups has also been made. The need for the further studies on the subject of ferrite in particular the effect of doping on the magnetic, electrical transport and micro-structural properties are discussed.

Chapter II deals with the theoretical aspects of magnetism and the magnetic materials with a special emphasis to ferrite. Starting from the description of the single crystal structure he described in detail the crystal structure of spinel with metal ions in different local structural environments, which affects the physical properties. Different types of magnetic exchange

साहा इंस्टिट्यूट ऑफ़ न्यूक्लियर फ़िज़िक्स

SAHA INSTITUTE OF NUCLEAR PHYSICS

सेक्टर-।, ब्लॉक 'ए.एफ़', विधाननगर / SECTOR-I, BLOCK-'AF', BIDHANNAGAR

कोलकाता-700 064, (भारत) / KOLKATA-700 064, INDIA

ग्रैम / GRAM : 'NUCLISTUTE' KOLKATA

दूरभाष / PHONE : 2337-5345-49 (5 LINES), फ़ैक्स / FAX : 091-33-2337-4637

Website : www.saha.ac.in

interactions present in spinel structure are described. Magnetic properties of ferrites are discussed using Molecular field theory and the expressions for sublattice magnetizations are derived. The nature of the magnetization curve as a function of the magnetic field and the hysteresis loop are discussed in detail. Effect of grain size and porosity on the hysteresis loop parameters has been discussed. Different types of domain wall motions and the interactions influencing such motions are discussed. Theory of magnetic permeability is discussed. Theoretical models used to explain the electronic transport property of ferrites are discussed.

In chapter III, experimental procedures adopted during the course of the work were explained. The details of the sample preparation were mentioned. Different techniques like XRD, measurement of porosity, magnetic permeability measurement including its frequency characteristics, low field hysteresis, AC and DC magnetization curve measurement and the details of DC and AC resistivity and Dielectric constant measurements were discussed in detail. Method of microstructure study using SEM was also discussed.

Chapter IV deals with the results and discussion on $(Ni_{0.28}Cu_{0.10}Zn_{0.62}O)$ $(Fe_2O_3)_{1-x}$, (where x = 0.0, 0.03, 0.06, 0.08). The motivation was to see the effects of small deficiency of iron on the structural, magnetic and transport properties.

The structural analysis was done on sintered samples from XRD studies. All the samples show well defined diffraction lines characteristic of single-phase cubic spinel structure. The lattice parameter, *decreases* linearly with decrease of iron concentration. The bulk density and the density determined from XRD data were studied as a function of x which is useful to explain the magnetic and the electrical properties of these samples. The magnetic property of the samples was determined by measuring the temperature and the frequency dependence of initial permeability for the toroid shaped samples. It was observed that permeability increases with the increase of Fe-deficiency and falls sharply at the Curie temperature, and this feature is independent of the annealing temperature. It was observed that the Curie temperature increases continuously with the increase of Fe-deficiency. This was explained as the introduction of Fe-deficiency might increase the exchange interaction between A and B site cations in this spinel structure. Frequency dependence of the permeability at room temperature was measured in samples with different x. It remains frequency (f) independent up to 5 MHz and then decrease sharply with further increase of f. These results were analyzed with respect to domain wall motion. Study of the frequency dependence of the quality factor (Q) shows a peak at a certain

साहा इंस्टिट्यूट ऑफ़ न्यूक्लियर फ़िज़िक्स
SAHA INSTITUTE OF NUCLEAR PHYSICS
सेक्टर-I, ब्लॉक 'ए.एफ़', बिधाननगर / SECTOR-I, BLOCK-'AF', BIDHANNAGAR
कोलकाता-700 064, (भारत) / KOLKATA-700 064, INDIA
ग्राम / GRAM : 'NUCLISTUTE' KOLKATA
दूरभाष / PHONE : 2337-5345-49 (5 LINES), फ़ैक्स / FAX : 091-33-2337-4637
Website : www.saha.ac.in

frequency. The fall in Q factor above a certain frequency is related to the phenomenon associated to the ferromagnetic resonance within the domains. At resonance, maximum energy is transferred from the applied ac magnetic field to the lattice resulting in a rapid decrease in the Q-factor. Low field B-H loop at room temperature reveals that coercivity decreases and permeability increases with the increase of Fe-deficiency. Therefore, increase of Fe-deficiency results more soft magnetic behavior of this ferrite. Magnetization versus magnetic field curve at 300 K did not show saturation up to a field of 16 kOe and was explained as due to magnetic anisotropy effect. The behavior of saturation magnetization as a function of temperature in a field of 5 kOe, reveal the presence of two magnetic sub-lattices unlike a ferromagnet. Determination of grain size using SEM micrograph clearly shows not appreciable change in grain size with increase of x. It increases with increase of sintering temperature, which is usual. The dc resistivity at 300 K increases continuously with x up to x=0.06 and then decreases sharply with further increase in x. This behavior was suggested as due to micro-structural modification taking place for reduction of Fe concentration. This should be clarified during viva. The ac resistivity decreases with the increase in frequency with in a small frequency range and above that it remains almost independent of frequency. The reason for this was not mentioned and should be explained during viva. The frequency dependence of the dielectric constant was explained due to contributions from well conducting large ferrite grains and low conducting grain boundaries.

In chapter V, results in $Ni_{0.28}Cu_{0.10+x}Zn_{0.62-x}Fe_{1.98}O_4$ (where x=0.00. 0.03, 0.06, 0.09, 0.120 have been presented. Single phase cubic spinel structure was confirmed from XRD studies. The decrease of lattice parameter and the increase of Curie temperature with increase of copper content were observed. The initial permeability increased with Cu content and sintering temperature but resonance frequency was shifted towards lower frequency obeying the Snoek's relation. Soft ferromagnetic nature was established from the low field B-H loop coercivity which decreased with the increase of Cu content. The saturation magnetization and dc resistivity increased with x. ac electrical resistivity and the dielectric constant decreased with frequency. All these features are more or less similar to that found in Fe deficient systems. Thus both these systems essentially show softer ferromagnetic properties with high resistivity.

In chapter VI, results in $Ni_{0.28}Cu_{0.10}Zn_{0.62}Fe_{1.98}O_4$ doped with V_2O_5 and Li_2O were presented. Effect of sintering additives on densification behavior and electromagnetic

properties were studied. A significant increase in initial permeability of the ferrite was found at small doping of 0.4 wt % of V_2O_5 and 0.4wt. % Li_2O substitution. The increased permeability was explained as due to better densification and increased grain size, on substitution. Better densification also resulted in improved electromagnetic properties of the V_2O_5 modified ferrites.

Chapter VII, presents the overall conclusion from the whole experimental investigations on three types of substitutions in Ni-Cu-Zn ferrites. The scope of future work in this area of research is also highlighted.

Details of the references have also been listed.

Recommendation:
Considering the overall presentation and the volume of work, results and analysis of the data, **I recommend that the candidate Md. Zakir Hossain Khan be awarded Ph. D. degree of the Khulna University of Engineering and Technology**.

Kajal Ghoshray

Kajal Ghoshray
Senior Professor
ECMP Division
Saha Institute of Nuclear Physics
1/AF, Bidhannagar, Kolkata 700064 India

K. GhoshRay
Professor
E.C.M P. Division
SAHA INSTITUTE OF NUCLEAR PHYSICS
I/AF, Bidhannagar, Kolkata-700 064

DR. RABINDRA CHANDRA SINHA

B.Sc.(Hons.), M. Sc. (DU), Ph.D (USSR)

Professor

Department of Physics

Department of Physics

Jahangirnagar University

Savar, Dhaka-1342

PABX- 7791045-51

Ext. 1426 (Office)

E-mail: rabindra.chandra.sinha@gmail.com

24 March, 2013.

Md. Toyebur Rahman

Controller of Examinations

Office of the Controller of Examination

Khulna University of Engineering and Technology (KUET)

Khulna-9203, Bangladesh.

Subject: Evaluation Report on the thesis entitled "Electromagnetic Properties of Iron Deficient Ni-Cu-Zn Ferrites and the Influence of Additives as Sintering Aid" submitted by Md. Zakir Hossain Khan in partial fulfillment of requirement of the degree of Doctor of Philosophy (Ph.D), Roll no. 0655751, Session: July 2006.

Ref. No. KUET/Exam/39 dated 12.02.2013

Dear Sir,

With reference to your letter dated 12.02.2013 I would like to inform you that I have gone through the thesis and please find a written evaluation report on the thesis as follows:

The thesis is a good piece of experimental research work with scientific thoughts and innovation. The research is focused on the influence of substitution and sintering aids on electromagnetic properties of Fe deficient Ni-Cu-Zn ferrites.

In the thesis attempts have been made to present a systematic review of different experimental research works related to this study.

This research work is important because there are a large number of applications of soft ferrites where high frequency electromagnetic energy use is involved.

In the present study an experimental research work regarding structural, magnetic and dielectric properties of several compositions of Ni-Cu-Zn soft ferrites with additives has been carried out and according to the results, a thorough scientific discussion has been made.

(Contd.)

JAHANGIRNAGAR UNIVERSITY
Savar, Dhaka-1342, Bangladesh

DR. RABINDRA CHANDRA SINHA
B.Sc.(Hons.), M. Sc. (DU), Ph.D (USSR)
Professor
Department of Physics

Department of Physics
Jahangirnagar University
Savar, Dhaka-1342
PABX- 7791045-51
Ext. 1426 (Office)
E-mail: rabindra.chandra.sinha@gmail.com

Throughout the experimental study of ferrite samples modern equipments have been employed such as X-ray diffractometer, Impedance Analyzer, B-H loop tracer, Vibrating Sample Magnetometer (VSM), SEM etc.

It is observed from the analyses of the experimental results that this study may play an important role to do more research for the development of efficient miniaturized devices for which soft magnetic materials are needed. With the advancement of nanotechnology a tremendous growth in research on miniaturization and high efficiency electronic devices is taking place.

Chapter wise evaluation as follows:

The thesis consists of seven chapters and an abstract.

Chapter-I contains a brief introduction of ferrites, aim and objectives of the research work, brief review works and an outline of the thesis. In this chapter an idea of the experimental methods have been given.

Chapter-II describes about theoretical aspects of the research work and has been written in a well manner.

Chapter-III contains the detailed description of the experimental works and has been written logically. It describes the methodology of ferrite sample preparation, composition of the studied ferrite system and gives description of the apparatus used for the characterization of the prepared ferrite samples.

Chapter- IV describes the results and discussion of $(Ni_{0.28}Cu_{0.10}Zn_{0.62}O)(Fe_2O_3)_{1-x}$ ferrites. This chapter gives an idea about the structure of the samples, bulk density, curie temperature, permeability, hysteresis behaviour and the dielectric properties of the samples. The results are explained scientifically and in a logical manner.

Chapter-V states the results and discussions of $Ni_{0.28}Cu_{0.10+x}Zw_{0.62-x}Fe_{1.98}O_4$ ferrites. This chapter describes the experimental results of the effect of Cu-substitution on the electrical and magnetic properties of Ni-Zn ferrites sintered at high temperature with various compositions.

(Contd.)

JAHANGIRNAGAR UNIVERSITY
Savar, Dhaka-1342, Bangladesh

DR. RABINDRA CHANDRA SINHA
B.Sc.(Hons.), M. Sc. (DU), Ph.D (USSR)
Professor
Department of Physics

Department of Physics
Jahangirnagar University
Savar, Dhaka-1342
PABX- 7791045-51
Ext. 1426 (Office)
E-mail: rabindra.chandra.sinha@gmail.com

In the chapter-VI, results and discussions of $Ni_{0.28}Cu_{0.10}Zn_{0.62}Fe_{1.98}O_4$ doped with V_2O_5 and Li_2O have been presented. Experimental results show that V_2O_5 doping evidently affect the magnetic properties. The mechanism involved has been discussed. The results also show that small amount of additives is able to enhance the densification. In this chapter it is reported that better densification results in improved electromagnetic properties of the V_2O_5 modified ferrites.

Chapter-VII states the conclusion and scope of future works of the present study.

Reference section contains the references for each chapter individually. It is written systematically.

Publication list is included in the thesis.

An extensive experimental research work has been carried out in this study. I think that the thesis is of Ph.D. standard and results obtained by the candidate may contribute to our knowledge in the field of science and technology. There are significant evidences of originality. Hence Mr. Md. Zakir Hossain Khan may be called for an oral examination to defend the thesis submitted by him for the degree of Doctor of Philosophy (Ph.D.) in Physics.

Prof. Dr. Rabindra Chandra Sinha
Department of Physics
Jahangirnagar University
Savar, Dhaka.

Acknowledgements

Abstract

The present work is focused on the influence of substitutions and sintering aids on electromagnetic properties of Fe-deficient Ni-Cu-Zn ferrite. Three series of ferrite samples of the compositions $(Ni_{0.28}Cu_{0.10}Zn_{0.62}O)$ $(Fe_2O_3)_{1-x}$ (where x=0.00, 0.02, 0.04, 0.06 & 0.08), $Ni_{0.28}Cu_{0.10+x}Zn_{0.62-x}Fe_{1.98}O_4$ (where x=0.00, 0.03, 0.06, 0.09 & 0.12) and $Ni_{0.28}Cu_{0.10}Zn_{0.62}Fe_{1.98}O_4$ doped with V_2O_5 and Li_2O were prepared by using the solid state reaction technique.

The phase identification was carried out by using the X-ray diffraction. The X-ray diffraction analysis revealed that all the samples of the studied three series were found to crystallize in single-phase cubic spinel structure. A slight increase of Curie temperature, T_c and saturation magnetization, M_s of $(Ni_{0.28}Cu_{0.10}Zn_{0.62}O)$ $(Fe_2O_3)_{1-x}$ series with increasing iron deficiency were observed. Lattice parameter of $(Ni_{0.28}Cu_{0.10}Zn_{0.62}O)(Fe_2O_3)_{1-x}$ series slightly decreases with x content. Initial permeability was found to increase with increasing iron deficiency and also with increasing sintering temperature which may be attributed to enhanced density and reduced anisotropy energy as well as increase in grain size of the studied samples. The permeability spectrum with frequency follows the Snoek's limit. From hysteresis parameters it was revealed that optimum soft magnetic properties corresponds to the composition with x=0.08 sintered at T_s=1150°C having highest permeability of 358, maximum induction, minimum coercivity and hysteresis losses.

From the detail study on the magnetic properties of $Ni_{0.28}Cu_{0.10+x}Zn_{0.62-x}Fe_{1.98}O_4$ series, it appeared that optimum soft magnetic properties were found in the composition with x=0.09 with the manifestation of highest permeability of 586 with low coercivity of 0.75 Oe and hysteresis loss of 15.5 W/kg. Saturation magnetization, M_s increases with x content with high value of 61.8 emu/g for x=0.09. Lattice parameter decreases linearly with increasing Cu content while Curie temperature increases linearly with Cu content. The decrease of Curie temperature may be attributed to the strengthening of A-B (J_{AB}) exchange interaction. Initial permeability increases gradually with increasing Cu content and sintering temperature, T_s attaining a maximum value for x=0.09 at T_s=1200°C. This enhancement of permeability may be correlated with improved microstructural features.

The effect of dopants such as V_2O_5 (0.4 wt %) and Li_2O (0.4 wt %) on the composition $Ni_{0.28}Cu_{0.10}Zn_{0.62}Fe_{1.98}O_4$ with $T_s=1150°C$ revealed that a substantial increase of initial permeability from 284 to 476 for V_2O_5 and 380 for Li_2O is observed. This may be accounted for due to increased density and grain size. A noticeable decrease of coercivity and increase of magnetization of the doped samples have been observed resulting in high permeability.

List of Symbols

Absolute value of admittance	$|Y|$
Absolute value of impedance	$|Z|$
AC current	I
Angular frequency	ω
Anisotropy field	H_k
Anisotropy constant	K_1
Average anisotropy	$<K>$
Bohr magneton	μB
Bragg's angle	θ
Bulk density	d_B
Charge of electron	e
Capacitance	C
Coercivity	H_c
Cross-sectional area of toroids	S
Curie temperature	T_c
DC resistivity	ρ_{dc}
Dielectric constant	ε'
Diffraction angle	θ
Energy per unit area of a 180° Bloch wall	γ
Exchange integral	J
Exchange coupling constant	J_{ij}
Exchange correlation length	L_o
Face centered cubic	fcc
Frequency	f
Full width at half maxima	FWHM
Ferromagnetism	FM
Grain size	D
Heating rate	β

Imaginary part of initial permeability	μ''
Impedance	Z
Inductance	L
Initial permeability	μ_i
Inter planner spacing	d
Loss factor	$\tan \delta$
Magnetization	M
Magnetic field	H
Magnetic induction	B
Magnetocrystalline anisotropy constant	K_1
Neel temperature	T_N
Nelson-Riley function	$F(\theta)$
Number of turns	N
Peak temperature	T_p
Permeability of in free space	μ_o
Quality factor	QF
Reactance	X
Real part of initial permeability	μ'
Retentivity	B_r
Remanent ratio	M_r
Resistance	R
Resistivity	ρ
Saturation magnetization	M_s
Saturation induction	B_s
Saturation polarizatin	J_s
Susceptance	B
Susceptibility	χ
X-density	d_x
X-ray diffraction	XRD
Yafet-Kittel	Y-K
Wavelength	λ

Contents

CHAPTER- I : Introduction

CHAPTER- II : Theoretical Aspects

CHAPTER- III : Experimental

CHAPTER- IV : Results and Discussion of $(Ni_{0.28}Cu_{0.10}Zn_{0.62}O)(Fe_2O_3)_{1-x}$ Ferrites

CHAPTER- V : Results and Discussion of $Ni_{0.28}Cu_{0.10+x}Zn_{0.62-x}Fe_{1.98}O_4$ Ferrites

CHAPTER- VI :   Results   and   Discussion   of $Ni_{0.28}Cu_{0.10}Zn_{0.62}Fe_{1.98}O_4$ doped with V_2O_5 and Li_2O

CHAPTER- VII : Conclusion

List of Tables

CHAPTER- III

CHAPTER- IV

CHAPTER- V

CHAPTER- VI

CHAPTER - I
Introduction

Introduction

1.1   Introduction

Ferrites pervade almost every sphere and modern technology. The present day technology owes a lot to the ferrite industry. Ranging from the very ordinary ratio sets to the complicated and exhaustive hardware involved in computers, ferrites have found their way to prove their importance. Ferrites constitute a special branch of ferrimagnatic. The term ferrite denotes a group of iron oxides, which have the general formula $MO.Fe_2O_3$, where M is a divalent metal ion such as Mn^{2+}, Fe^{2+}, Co^{2+}, Ni^{2+}, Cu^{2+}, Zn^{2+}, Mg^{2+} or Cd^{2+}. The typical Ferrite is magnetite, Fe_3O_4 ($FeO. Fe_2O_3$), which has been a well known magnetic oxide since ancient time. Ferrites are more useful because of their high resistivity. The resistivity of ferrites varies from 10^2 to 10^{10} ohm-cm, which is about 15 orders of magnitude higher than that of iron. Snoek had laid the foundation of the physics and technology of practical ferrites in 1945 and now embrace a very wide diversity of compositions, properties and applications [1.1]. Technological advances in a variety of areas have generated a growing demand for the soft magnetic materials in devices. Polycrystalline soft ferrites prepared from the metal oxides are magnetic semiconductors and have made important contributions, both technological and conceptual to the development and electronics. Soft ferrites still remain the best magnetic materials and can not be replaced by any other magnetic materials with respect to their very high frequency application because they are inexpensive, more stable, easily manufactured [1.2]. They have wide range of technological applications in transformer cores, inductors, high quality filters, radio frequency circuits, rod antennas, read/write heads for high-speed digital tape and operating devices [1.3-1.5].

Ferrites are ferrimagnetic cubic spinels that posses the combined properties of magnetic materials and insulators. They have been extensively investigated and become the subject of great interest because of their importance in many technological applications from both the fundamental and the applied research point of view. Spinel type ferrites are commonly used in many electronic and magnetic devices due to their high magnetic permeability and low magnetic losses [1.6-1.7] and also used in electrode materials for high temperature applications because of their

high thermodynamic stability, electrical resistivity, electrolytic activity and resistance to corrosion [1.8-1.9]. Moreover, these low cost materials are easy to synthesize and offer the advantages of greater shape formability than their metal and amorphous magnetic counterparts. Almost every item of electronic equipment produced today contains some ferrimagnetic spinel ferrite materials.

The magnetic ferrites mainly fall into two groups with different crystal structure.

i. **Cubic:** These have the general formula MO. Fe_2O_3, when M is a divalent metal ion like Mn, Ni, Fe, Co, Mg and Cu etc. Cobalt Ferrites is magnetically hard but all other cubic ferrite is magnetically soft.

ii. **Hexagonal:** The most important in this group is barium ferrite BaO. $6Fe_2O_3$ ($BaFe_{12}O_{19}$) which is magnetically hard.

High frequency ferrite application can be broadly divided into two categories: Microwave and Non microwaves applications. A Microwave ferrite can be defined as highly resistive magnetic materials used at frequencies between 100 MHz and 500 GHz, the highest microwave frequency now in use. Microwave ferrites are again of two types: Non- reciprocal and reciprocal devices. The Non-reciprocal devices for which ferrites are almost irreplaceable have greatest number of applications. These devices are essentially isolators or circulators which perform the following functions:

i. An isolator is merely a wave guide sections in which the incident electromagnetic wave (from input to output) can propagate without attenuation but an electromagnetic wave coming from reverse direction will be highly attenuated.

ii. An n-port circulator is a device having n ports or inputs and works in a rather complicated manner.

The device of this type provides easy isolation between different channels of a microwave circuit which is essential in present techniques for radar and radio links. The second category comprises of reciprocal devices, e.g. electrically controlled phase shifters.

2

On the other hand, the unique properties of non-microwave ferrites are magnetic permeability and high electrical resistivity. These are the ferrites used at frequencies from audio to about 500 MHz.

The computer technology got a new thrust when it was discovered that some polycrystalline spinel ferrite can have a rectangular hysteresis loop and therefore can be used as computer memory elements. Until 1970 nearly all main frame computer memories consisted of ferrite cores. Around 1968, according to Jacobs [1.10] the yearly world production of ferrite was about 2×10^{10} cores.

The main consumer products are TV sets and radio sets in which such parts as the line transformer, deflection coils, turners and rod antennas contain ferrite materials. About 0.7 kg of ferrite enters a black and white TV set and about 2 kg in a color set. On going ferrite research in unveiling may mysteries that concern the theoreticians and at the same time revealing many special properties having industrial importance.

Ferrites are posses the combined properties of magnetic materials and insulator. They from a complex system composed of grains, grain boundaries and pores. Ferrites exhibit a substantial spontaneous magnetization at room temperature, like the normal ferromagnetic. They have two unequal sub-lattice called tetrahedral (A-site) and Octahedral (B-site) and are ordered antiparallel to each other. In ferrites, the cations occupy the tetrahedral A-site and octahedral B-site of cubic spinel lattice and experience competing nearest neighbor (J_{AB}) and the next nearest neighbor (J_{AA} and J_{BB}) interactions with $|J_{AB}| \gg |J_{BB}| > |J_{AA}|$. The magnetic properties of ferrites are dependent on the type of magnetic ions residing on the A and B- sites and the relative strengths of the inter (J_{AB}) and intra sublattice (J_{BB}, J_{AA}) interactions. When the J_{AB} is much stronger than J_{BB} and J_{AA} interactions, the magnetic spins have a collinear structure in which the magnetic moments on the A sub lattice are antiparallel to the moments on the B sub lattice. But when J_{BB} or J_{AA} becomes comparable with J_{AB}, it may lead to non-collinear spin structure [1.11]. When magnetic dilution of the sub lattice is introduced by substituting non magnetic ions in the lattice, frustration and or disorder occurs leading to collapse of the collinearity of the ferromagnetic phase by local spin canting exhibiting a wide spectrum of magnetic ordering e.g.

antiferromagnetic, ferromagnetic, re-entrant spin-glass, spin- glass, cluster Spin-glass properties [1.12-1.13]. Small amount of site disorder i.e. cations redistribution between A and B site is sufficient to change the super-exchange interactions which are strongly dependent on thermal history i.e. on sintering temperature time and atmosphere as well as heating/cooling rates during materials preparation. Micro structure and magnetic properties of ferrites are highly sensitive to preparation method, sintering conditions, amount of constituent metal oxides, various additives including dopants and impurities [1.14-1.17].

Among the soft ferrites Nickel – Zinc (Ni-Zn), Magnesium - Zinc (Mg-Zn) and Manganese – Zinc (Mn-Zn) ferrites with various additives have enormous technological application and accordingly extensive research works have been carried out [1.18-1.22]. Magnetically soft ferities are ceramic materials having cubic (spinel) structure. The general composition of such ferrites is Me Fe_2O_4, where Me represent one or several of the divalent transition metals such as manganese (Mn), Zinc (Zn), Nickel (Ni), Cobalt (Co) , Copper (Cu), iron (Fe) or magnesium (Mg) etc. The most popular combination is Ni-Zn and Mn-Zn ferrite. Ferrite crystallizes with two magnetic sub-lattices, i.e. tetrahedral (A) site and octahedral (B) site based on Neel's model. Magnetic and electrical properties of ferrites are strongly dependent on distribution of cations in A and B sites and their valence state. The properties of Ni-Zn ferrites can be tailored by substituting them with different material ions such as Co^{2+}, Mg^{2+}, Mn^{2+}, Cu^{2+} etc.

The Ni-Zn ferrites are one of the most versatile, reasonable cost magnetic materials for general use in both low and high frequency devices because of their high resistivity, low dielectric losses, mechanical hardness, high Curie temperature and chemical stability. The typical Ni-Zn ferrites, are sintered satisfactory only above 1250°C, where their microstructure and properties being difficult to control because of the volatility of ZnO at such high temperature. High sintering temperature may cause anomalous densification, and high power consumption. So, from the view point of engineering, it is very interesting to prepare high permeability and low magnetic loss Ni-Zn ferrites at lower sintering temperature. Sintering temperature can be reduced by using CuO with Ni-Zn ferrites as well as with the addition of some oxides having low melting point. The addition of CuO in the Ni-Zn ferrite composition is

4

known to play a crucial role in increasing the sintering density and lowering the sintering temperature [1.19, 1.23]. The uses of nano particles in the starting materials for the synthesis of ferrites can also reduce sintering temperature and improve magnetic properties. Recently, there has been a growing interest in the low temperature sintering of Ni-Zn ferrite doped with CuO for attaining high density and high permeability than undoped Ni-Zn ferrite.

Ni-Cu- Zn ferrites have potential application in the fabrication of multilayer chip inductors (MLCI) and various electronic applications such as telecommunications because of their good electro-magnetic properties at high frequency and these oxides can be sintered at relatively low temperature with high density covering a wide range of compositions. Multilayer chip inductors are important components for the latest electronic products such as cellular phones, video cameras, note book computers, hard and floppy drives etc; which require small dimensions, light weight and better functions. Lowering of sintering temperature is important for co-firing the multilayer chips with silver (Ag) and also from energy saving point of view including the cost effective manufacture of ferrite components. Various additives such as V_2O_5, Bi_2O_3, PbO, MoO_3, WO_3, Eu_2O_3, P_2O_5, Li_2O, Na_2O etc, having low melting point facilitated to reduce the sintering temperature of these oxide materials due to liquid phase sintering. Although enormous research activities have been carried out on spinel soft ferrites in order to improve and optimize their electrical and magnetic properties, there does not exist an ideal ferrite sample that meets the requirements of high permeability and low eddy current loss at reasonably high frequency. Till now researchers have not yet been able to formulate at rigid set of rules for ferrites about a single property.

In the present research work efforts have been under taken to synthesize Ni-Cu-Zn ferrites and substituted Cu by using a solid state reaction technique and to study their structural, magnetic and electrical properties by varying sintering conditions. Study the effect of Fe deficiency on the composition $(Ni_{0.28}Cu_{0.10}Zn_{0.62}O)$ $(Fe_2O_3)_{1-x}$ and Zn substituting for Cu on the properties on $Ni_{0.28}Cu_{0.10+x}Zn_{0.62-x}Fe_{1.98}O_4$ ferrites. Further another work on additives such as V_2O_5 and Li_2O doped on Ni-Cu-Zn ferrites. However, attempts have been made to present a systematic review of various experimental and theoretical observed facts related to this study. The systematic

research is still necessary for a more comprehensive understanding and properties of such materials.

1.2   The Aim and Objectives of the Present Work

Soft ferrites are relatively cheap materials which are within our means and technical ability to develop. There are large numbers of applications of these soft magnetic materials where high frequency electromagnetic energy use is involved. At present, Bangladesh is totally dependent upon the imported ferrite cores and other soft magnetic materials. If we can develop a ferrite in our country, that may alleviate this problem. Research in this field will provide information in choosing appropriate materials for the above uses and ultimately high quality materials with desired characteristics and will open-up the possibility of indigenous development of ferrite technology.

The main objectives of the present work are made as bellows:
(i) $(Ni_{0.28}Cu_{0.10}Zn_{0.62}O)$ $(Fe_2O_3)_{1-x}$, where x= 0.00, 0.02, 0.04, 0.06 and 0.08
(ii) $Ni_{0.28}Cu_{0.10+x}Zn_{0.62-x}Fe_{1.98}O_4$, where x=0.03, 0.06. 0.09 and 0.12
(iii) Additives such as V_2O_5 and Li_2O.

The raw oxide materials that were used to synthesize Ni-Cu-Zn ferrites of composition $Ni_{1-x-y}Cu_yZn_xFe_{2-z}O_4$ samples were commercially available. The value of x, y and z have been maintained in such way so that high permeability, higher resonance frequency and low magnetic loss along with a low sintering temperature was ascertained. The Fe–deficiency in the chosen composition was proposed to have high resistivity and low sintering temperature. The amount of Fe deficiency have been maintained in such way so that prepared materials ensure high permeability as a prime requisite for a good inductor material.

The Cu- addition ensured good sinter ability. The low melting point additive as sintering aid was chosen to minimize the sintering temperature and to attain good soft magnetic properties. Finally the electromagnetic properties of all the prepared samples such as magnetization, Curie temperature, magnetic permeability, magnetic loss components, coercivity, resistivity, dielectric constant, dielectric loss tangents etc have been studied in detail to find out an optimum composition with appropriate

amount of sintering aid, Cu and Zn concentration for good soft magnetic properties required for an inductor. The various structural, electrical and magnetic properties of Ni-Cu-Zn ferrite doped with V_2O_5 and Li_2O. Ni-Cu-Zn ferrites are generally used as magnetic materials for their better properties at high frequencies than for Mn – Zn ferrites and their lower densification temperature than for Ni-Cu-Zn ferrites. Hence, if we carry on our research in soft magnetic materials and in ferrites, Bangladesh may develop a profitable ferrite industry and can thus strengthen its electronic industry.

1.3   Experimental Reason for this Research Work

Ferrites samples have been prepared by conventional double sintering ceramic technique using high purity oxide nanomaterials. The experimental methods that have been used in this work are as follows.

(i)   The prepared samples have been characterized in terms of their crystal structure, unit cell parameters and phases present in the prepared samples with the help of X-ray diffractometer (XRD). The porosity of the prepared samples has been calculated from the theoretical density (using XRD data) and the balk density.

(ii)   Sintering of the samples has been measured as a function of field and temperature furnace.

(iii)   Magnetization of the samples have been measured as a function of field and temperature using vibrating samples magnetometer (VSM)

(iv)   Permeability magnetic loss factor and relative quality factor as a function of frequency and temperature have been determined using an impedance analyzer.

(v)   Hysteresis parameters have been determined by B – H loop tracer.

(vi)   Curie temperature / magnetic phase transition temperature have been determined by permeability versus temperature measurement with the help of a oven using a LCR meter.

(vii)   DC/AC electrical resistively and dielectric properties as a function of frequency and temperature have been studied with the help of electrometer inductance meter.

1.4   Review Works

Ni-Cu-Zn ferrites with their case of preparation and versatility for use in wide ranging applications are very attractive materials from the commercial point of view. Microstructure and magnetic properties of these ferrites are highly sensitive to preparation method, sintering conditions and amount of constituent of metal oxides, including impurities or dopants. Many efforts are focused in obtaining low power loss material operating in the MHz region in accordance with the miniaturization of cores.

The polycrystalline ferrite has been used extensively in many electronic devices, because of its high permeability in the RF frequency region, high electrical resistivity, mechanical hardness and chemical stability. Nomura and Takaya [1-24] was engaged in the research work on the surface mounting devices that rapidly developed using multilayer chip inductors. These chip inductors are produced by coating ferrite and electrical phases alternately and the Co-firing. Since Ag is usually used as an electrode material, high temperature cofiring causes an unexpected lowering of the inductance due to the interfacial lowering of the inductance due to the interfacial reaction (diffusing) between the ferrite and the Ag electrode which have been studied by Nomura et. al. [1.25] and Nakano et. al. [1.26]. Nakamura [1.27] examined the low temperature sintering of Ni-Cu-Zn ferrite and clarified the relationship between the preparation conditions (calcinations temperature and particle size of starting materials) and some properties of the sintered ferrite (post – sintering density and complex permeability).

Hui Zhong et. al. [1.28] reported the effect of WO_3 addition on the electromagnetic properties of Ni-Cu-Zn ferrite prepared by usual ceramic technique. They observed that the substitution of W^{6+} ions in Ni-Cu-Zn ferrite improved not only electromagnetic properties but also microstructures of the sintered sample. The scanning electron microscope (SEM) microphotographs showed that the grain size of sintered ceramic decreases with the increasing WO_3 content. Number of pores entraps within the grains and the quantity of pores at grain boundaries is reduced with the

increase of W^{6+} ions concentration. The decrease of the grain size may be attributed to the presence of WO_3 as a secondary phase at the grain boundaries which hinders the grain growth in the microstructures of Ni-Cu-Zn ferrites. The bulk density and real permeability increases with increasing W^{6+} ions. The resonance frequency increases on account of the deterioration of the real part of complex permeability. Complex permeability spectra $\mu^* = \mu' - i\mu''$ for two types of spinel ferrites (Ni-Zn ferrites and Mn-Zn ferrites) and their composite materials have been investigated by Takanori Tsutoka [1.29].

Nakarmura et.al. [1.30] reported on frequency dispersion of permeability in ferrite composite materials. The permeability increases with increasing density of composite materials. As the ferrite content decreases, both the shoulder frequency of real part of permeability and the peak frequency of imaginary part of permeability shifts to higher frequency. Abdeen [1.31] studied electric conduction in Ni-Zn ferrite. The AC and DC electrical conductivities increase as the temperature increasing indicating the studied samples are semiconductors in nature. The AC electrical conductivity increases with increasing angular frequency below Curie point and above Curie point it is independent of nature. The values of Curie temperature decreases with increasing of Zn content and activation energy below and above T_c decreases with increasing Zn-content.

Ni-Cu-Zn ferrites are widely used in multilayer chip devices. These devices were studied by K. O. Low and Sale [1.32], such as multilayer chip inductors, are produced by co-firing ferrite layers with an internal silver conductor. Since silver has a melting point of 961°C, in order to suppress inter-diffusion between the ferrite core and silver, a lower temperature than 961°C is preferred. Ni-Cu-Zn ferrites are selected in these applications because these ferrites can be sintered lower than 950°C. The low sintering temperature is attributed to its Cu-content because the Cu-containing ferrites were claimed to suffer thermal dissociation at temperature around 900°C. Kin. O. Low et.al. [1.33] has design of Ni-Cu-Zn ferrites to suit a particular application where consideration was given on thermal dissociation temperature so that electromagnetic properties are not affected.

Manjura Hoque et.al [1.34] has studied the crystal structure density, compressive strength, microstructure magnetic and electrical properties of

$Ni_{1-x}Cu_xFe_2O_4$ ferrites. Tetragonal deformation was observed for the sample of composition x= 1.0, i.e. for pure $CuFe_2O_4$. SEM micrographs exhibit increase in grain size with the increase of copper content. Addition of copper behaves like a flux in $Ni_{1-x}Cu_xFe_2O_4$. SEM micrographs exhibit secondary recrystallization for x > 0.2, which leads to exaggerated grain growth and poor sintered product. The increase in the initial permeability between x = 0 and 0.5 is accompanied by a shift in the dispersion toward low frequencies. Saturation magnetization increases with the increase of Cu due to nonmagnetic content up to x = 0.2 and then decreases and also due to the intra granular porosity trapped within exaggerated grains due to secondary recrystallization. Rahman et. al. [1.35] studied on Ni-Cu-Zn based ferrite. Average crystallite size increase linearly with calcinations temperature. The lattice parameter and the ionic radius of octahedral sites increase with copper concentrations. The saturation magnetization decreases with increasing non-magnetic Cu-content.

To achieve a reliable performance of multilayer ferrites, it is necessary to co-fire the ferrite with Ag electrodes at low temperature and have been reported by Hirota et. al [1.36] and Aoyama et.al [1.37]. It can avoid increasing the resistivity of the thermal electrode resulting from the diffusion of electrode into ferrite and leading the deterioration of the magnetic properties due to the segregation of Cu from the ferrite. There has been a growing interest in Ni-Cu-Zn ferrites for the application in producing multi-layer-type chips mainly because these oxides can be sintered at relatively low temperatures with a wide range of compositions. In particular, the addition of Cu in the ferrite composition has been known to play a crucial role in dropping the firing temperature. In addition, Ni-Cu-Zn ferrite has better properties at high frequencies than Mn-Zn ferrite and lower densification temperature than Ni-Zn ferrites reported by Stoppels [1.38] and Sang et.al. [1.39].

Jingling Sun [1.40] measured the effects of La_2O_3 and Gd_2O_3 on some properties of Ni-Zn ferrites. The R_2O_3 [R= La or Gd] substitutions decrease samples density and increase lattice parameter of higher sintering temperature is necessary for densification with R_2O_3. R_2O_3 substitution tends to flatten dielectric constant versus frequency curves, increase the value of dielectric constant and lower the value of loss factor. Hu et. al. [1.41] has considered the ways of reducing sintering temperature of high permeability Ni-Zn ferrites. It was found that optimum additions of CuO and

V_2O_5 contributed to the grain growth and the densification of matrix in the sintering process leading to decrease in sintering temperatures of Ni-Zn ferrites. The post-sintering density and the initial permeability were also strongly affected by the average particle size of raw materials. The domain wall motion plays a predominant role in the magnetizing process and loss mechanism. The effect of Mn^{3+} doping on the high and low frequency electromagnetic properties of Ni-Cu-Zn ferrites has been investigated by Tsakloudi et.al. [1.42]. Mn additions influence the electromagnetic properties of Ni-Cu-Zn ferrites by influencing the microstructure. The optimum Mn^{3+} concentration depends on the Fe^{3+} content of the material and is subjected to the restriction that the concentration of both should be slightly below stoichiometry. When the addition of Mn is such that where the total trivalent cation amount of material remains slightly below stoichiometry (i.e. $Fe^{3+} + Mn^{3+} \leq 2$), Mn^{3+} ions act as grain growth promoters. This results in polycrystalline microstructures with large grain size and consequently high initial permeability and low coercivity. The low frequency losses decrease because of the positive influence on the hysteresis losses, while the high frequency losses increase because of the increased contribution of resonance losses. When Mn^{3+} is added to Ni-Cu-Zn ferrites under the condition that the total $Mn^{3+}+Fe^{3+}$ content exceeds stoichiometry grain growth is inhibited and the influence on the low or high frequency electromagnetic properties is reversed.

Ni-Cu-Zn ferrites are soft magnetic materials that are used for inductive multilayer devices because of their low sintering temperature and their good performance at intermediate at high frequencies, Ni-Cu-Zn ferrites are Co-fired with internal Ag conductor, because of the melting point of silver, the sintering temperature is limit $T \leq 950°C$. The first multilayer chip inductors were developed by Nomura et. al. [1.25] and Nakamura et al. [1.43]. Multilayer chip LC filters and hybrid circuit devices appeared as second generation of inductive multilayer. SMD components reported by Yasuda et. al. [1.44]. The required low sintering temperature it is crucial to use ferrite powders with high sintering activity at 900°C. This can be realized by two main routes: (i) Preparation of powders with small particles and high surface energy or (ii) addition of sintering additives. Several soft Chemistry routes have been explored in order to synthesize reactive powder, e.g. Sol-gel Synthesis [1.45] auto-combustion Synthesis studied [1.46] or Co-precipitation of Oxalates [1.47]. Different sintering additives have been proposed to enhance the densification

behavior of Ni-Cu-Zn ferrites, e.g. V_2O_5 [1.47], PbO [1.48] and glasses [1.49]. The preparation of highly reactive sub-micron Ni-Cu-Zn ferrite powders by milling of the calcined raw materials. The influence of powder particle size and bismuth oxide addition on the densification behavior ferrite microstructure and permeability are outlined, contrary to studied by Jeong et.al. [1.50] at intermediate concentration of Bi_2O_3 (0.3 – 0.5 wt %) an inhomogeneous microstructure with large grains is formed causing maximum permeability.

Hakim et.al. [1.51] have synthesized Mg-ferrite nanoparticles by using a chemical co precipitation method in three different methods. Metal nitrates were used for preparing $MgFe_2O_4$ nanoparticles. Akther Hossain et.al. [1.52] have studied $Ni_{1-x}Zn_xFe_2O_4$ (x= 0.2, 0.4) samples sintered at different temperatures. The DC electrical resistivity decreases as the temperature increases indicating that the samples have semiconductors like behavior. As the Zn content increases, the T_c, resistivity and activation energy decrease while the magnetization, initial permeability and the relative quality factor increases.

K. O. Low et.al. [1.45] and Hsiang et.al. [1.53] reported that Ni-Cu-Zn ferrites are well established soft magnetic material for MLCI applications because of their relatively low sintering temperature high permeability in the RF frequency region and high electrical resistivity. The magnetic properties of the ferrite are highly sensitive to the technology parameters, especially to the amount of constituent metal oxide or additives in their composition [1.54]. The magnetic properties can be changed by the substitution of various kinds of Mn^{2+} divalent cations (Co^{2+}, Mg^{2+}, Fe^{2+}, Mn^{2+}) or by introducing a relatively small amount of rare-earth ions [1.55]. Nowadays the rare earth oxides are becoming promising additives to improve the magnetic properties of ferrites [1.56]. Sun et.al. [1.57] reported that the permeability of Ni-Zn ferrite decreased with La substitution and that has been interpreted by a combination of low density, small grain size, secondary phase $LaFeO_3$ formation and creation of more lattice defects. However, Ahmed et.al. [1.58] reported an increase in susceptibility in Mn-Zn ferrite by the same substitution also an increase in permeability of Ni-Cu-Zn ferrite by the substitution has been reported by P. K. Roy [1.59]. Caltun et.al. [1.60] studied the microstructure and the permeability spectra of Ni-Cu-Zn ferrites. The particle size increases when the sintering temperature is raised. For the same chemical

composition and different sintering temperature it was found that the real permeability in the low frequency region decreases by addition of CuO. A sintering temperature increases, the natural resonance frequency, where the imaginary permeability had a maximum values, shifted towards low frequency from 3 to 0.5 MHz.

From the above mentioned review works it is observed that physical, magnetic, electrical transport and microstructural properties are strongly dependent on additives/ substitution in a very complicated way and there is no straight forward relationship between the nature and the quantity of doping on the magnetic characteristics to be understood by any simple theory. These are strongly dependent on several factors like sintering conditions preparation methods, compositions etc. In the present work it is aimed at determining experimentally microstructure exhibiting better magnetic and electrical properties as affected by sintering temperature / time, composition and the nature and amount of substitutions. The addition of additives as sintering aid will reduce the sintering temperature which may affect to obtain homogeneous microstructure and enhanced electromagnetic properties. Ni-Cu-Zn ferrites are generally used as magnetic materials for their better properties at high frequencies than for Mn-Zn ferrites and their lower densification temperature than for Ni-Cu-Zn ferrites. So that Ni-Zn ferrites with appropriate substitution can be obtained in respect of improving electromagnetic properties.

1.5   Outline of the Thesis

The thesis has been divided into seven Chapters: **Chapter-I** presents a brief introduction of Ni-Cu-Zn ferrite and organization of thesis. This chapter incorporates background information to assist in understanding the aims and objectives of this investigation, and also reviews recent reports by other investigator which these results can be compared. **Chapter-II** briefly describes the theories necessary to understand the present work. **Chapter-III** enunciates with the detail experimental process related to this research work. **Chapter-IV** describes the results and discussion about the structural, magnetic and electrical properties, of $(Ni_{0.28}Cu_{0.10}Zn_{0.62}O)(Fe_2O_3)_{1-x}$ ferrites. **Chapter-V** describes about the structural, magnetic and electrical properties of $Ni_{0.28}Cu_{0.10+x}Zn_{0.62-x}Fe_{1.98}O_4$ ferrites. **Chapter-VI** describes about the same measurements of $Ni_{0.28}Cu_{0.10}Zn_{0.62}Fe_{1.98}O_4$ doped with V_2O_5 and Li_2O. **Chapter VII** contains the concluding works.

Chapter - II

Theoretical Aspects

Theoretical Aspects

2.1　Introduction

A crystal is a solid in which the constituent atoms, molecules, or ions are packed in a regularly ordered, repeating pattern extending in all three spatial dimensions. All the atoms in the solid fit into the same crystal structure forms a single crystal structure. However, generally, many crystals form simultaneously during solidification, leading to a polycrystalline solid. Most of the metals encountered in everyday life are polycrystals. Crystals are often symmetrically intergrown to form crystal twins. In which, fluid forms a crystal structure, depends on the chemistry of the fluid, the conditions under which it is being solidified, and also on the ambient pressure. The process of forming a crystalline structure is often referred to as crystallization [2.1].

Almost all metal exists in a polycrystalline state; amorphous or single-crystal metals must be produced synthetically, often with great difficulty. Ionically bonded crystals can form upon solidification of salts, either from a molten fluid or when it condenses from a solution. Covalently bonded crystals are also very common, notable examples being diamond, silica and graphite. Weak Van der Waals forces can also play a role in a crystal structure; for example, this type of bonding loosely holds together the hexagonal-patterned sheets in graphite. Most crystalline materials have a variety of crystallographic defects. The types and structures of these defects can have a profound effect on the properties of the materials. While the term 'crystal' has a precise meaning within materials science and solid-state physics, colloquially "crystal" refers to solid objects that exhibit well-defined and often pleasing geometric shapes. The shape of these crystals is dependent on the types of molecular bonds between the atoms to determine the structure, as well as on the conditions under which they formed. Snowflakes, diamonds and common salt are common examples of crystals. Crystallography is the scientific study of crystals and crystal formation.

2.1.1　Single Crystal

A single crystal, also called monocrystal, is a crystalline solid in which the crystal lattice of the entire sample is continuous and unbroken to the edges of the sample, with no grain boundaries. The opposite of a single crystal sample is a polycrystalline sample,

which is made up of a number of smaller crystals known as crystallites. Because of a variety of entropic effects on the microstructure of solids, including the distorting effects of impurities and the mobility of crystallographic defects and dislocations, single crystals of meaningful size are exceedingly rare in nature, and can also be difficult to produce in the laboratory under controlled conditions. Because grain boundaries can have significant effects on the physical and electrical properties of a material, single crystals are of interest to industry, and have important industrial applications. The most notable of there is the use of single crystal silicon in the fabrication of semiconductors. On the quantum scale that microprocessors operate on, the presence of grain boundaries would have a significant impact on the functionality of field effect transistors by altering local electrical properties. Therefore, microprocessor fabricators have invested heavily in facilities to produce large single crystals of silicon. Fabrication of single crystals usually involves the building of a crystal layer by layer of atoms. Some thin film deposition techniques can be used for epitaxy, forming a new layer of material with the same structure on the surface of an existing single crystal.

2.1.2 Lattices

A crystal may be defined a s solid composed of atoms arranged in a pattern periodic in three dimensions. Not all solids are crystalline, however, some are amorphous, like glass and do not have any regular interior arrangement of atoms. In thinking about crystals, it is often convenient to ignore the actual atoms composing the crystals and their periodic arrangement in space, and to think instead of a set of imaginary points which has a fixed relation in space to the atoms of the crystals and which may be regarded as a sort of framework of skeleton on which the actual crystal is built [2.2]. The space dividing planes will intersect each other in a set of lines shown in Fig. 2.1, and these lines in turn in interest in the set of points so referred to above. A set of points so formed has an important property: it constitutes a point lattice, which is defined as an array of points in space so, arranged that each points has identical surrounding. By 'identical surrounding' mean that the lattice of points, when viewed in a particular direction from one lattice point would have exactly the same appearance when viewed in the same direction from any other lattice point.
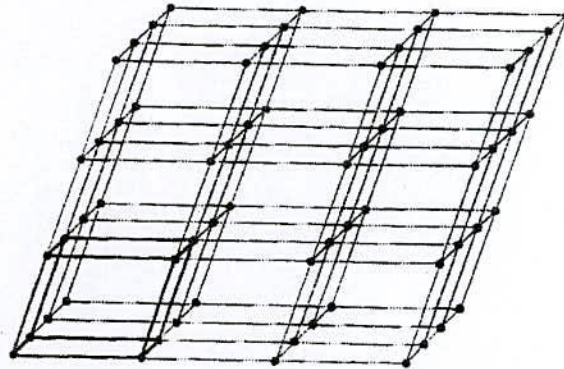
Fig. 2.1 A point lattice

According to the Fig. 2.1 all the cells of the lattices are identical, choose any one, for example the heaving out lined one, as a unit cell. The size and shape of the unit cell can in turn be described by the three vectors a, b and c drawn from one corner of the cell taken as origin as shown in Fig. 2.2. The cell is defined by these vectors called the crystallographic axes of the cell. They may also be described in terms of their lengths (a, b, c) and the angles between them (α, β, γ). These lengths and angles are the lattice constants or lattice parameters of the unit cell.
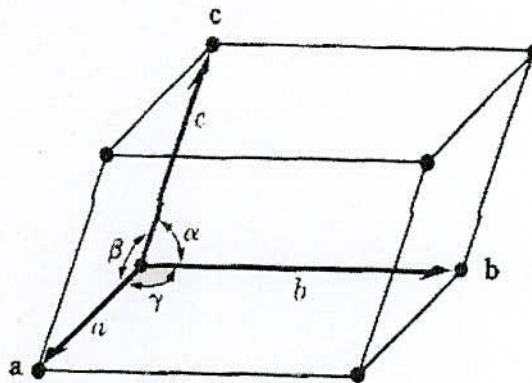
Fig. 2.2 A unit cell

2.2   Classification of Ferrites and its Relevance

Ferrites are essentially ceramic materials, compound of iron, boron, barium, strontium, lead, zinc, magnesium or manganese. The ingredients are mixed, preferred,

milled/crushed, dried, shaped and finally pressed and fired into their final hard and brittle state. Now a days newer family of ferrite materials have been discovered, which are rare-earth types. Additives of rare-earth metals like lanthanum oxide (La_2O_3) are used to study the effect of enhancing the magnetic properties. They are primarily used as permanent magnets. These ferrites are very stable with the excellent characteristic of high resistively.

Ferrites are classified two categories based on their coercive field strength. They are

   (i)   Soft ferrite with coercive field strength < 10 Oe

   (ii)   Hard ferrite with coercive field strength > 125 Oe

The unique feature of high coercivity and high-energy product of the hexagonal ferrites is their high uniaxial magnetocrystalline anisotropy about 100 times higher than the soft ferrite with cubic structured. Therefore, hard ferrites constitute the major fraction since they are used where energy per unit eight and cost are important considerations [2.3].

According to the crystallographic structures ferrites fall into three categories

   (i)   Cubic ferrites of spinel type

   (ii)   Cubic ferrites of the garnet type and

   (iii)   Hexagonal ferrites

Ferrites fallen into two groups with different crystal structures are shown in the following block diagram shown in Fig. 2.3
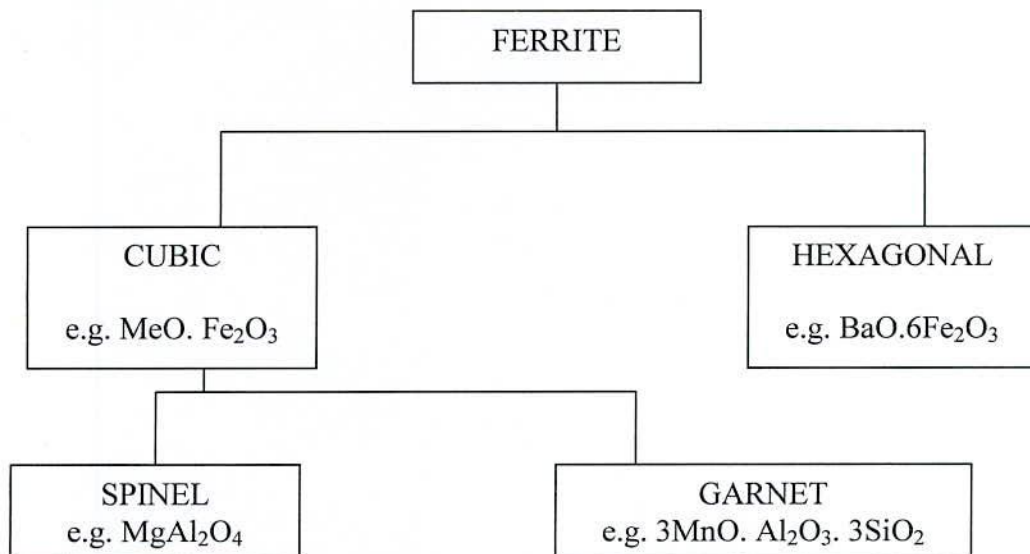
Fig. 2.3 Classification of Ferrites

2.2.1 Soft Magnetic Materials

The wide variety of magnetic materials can be divided into two groups, the magnetically soft and the magnetically hard. Soft magnetic materials are those materials that are easily magnetized and demagnetized. They have low magnetocrystalline anisotropy resulting in reduced coercivity and high permeability. They typically have intrinsic coercivity less than 1000 Am^{-1}. They are used primarily to enhance and/or channel the flux produced by an electric current. The important parameter, often used as a figure of merit for soft magnetic materials, is the high relative permeability (μ_r, where μ_r $= \dfrac{B}{\mu_o H}$), which is a measure of how readily the material responds to the applied magnetic field. The other main parameters of interest are the coercivity, the saturation magnetization and the electrical conductivity.

The types of applications for soft magnetic materials fall into two main categories: AC and DC. In DC applications the material is magnetized in order to perform an operation and then demagnetized at the conclusion of the operation, e.g. an electromagnet on a crane at a scrap yard will be switched on to attract the scrap steel and then switched off to drop the steel. In AC applications the material will be continuously cycled from being magnetized in one direction to the other, throughout the period of operation, e.g. a power supply transformer. A high permeability will be desirable for each type of application but the significance of the other properties varies.

For DC applications the main consideration for material selection is most likely to be the permeability. This would be the case, for example, in shielding applications where the flux must be channeled through the material. Where the material is used to generate a magnetic field or to create a force then the saturation magnetization may also be significant. For AC applications the important consideration is how much energy is lost in the system as the material is cycled around its hysteresis loop. The energy loss can originate from three different sources: (1) hysteresis loss, which is related to the area contained within the hysteresis loop; (2) eddy current loss, which is related to the generation of electric currents in the magnetic material and the associated resistive losses and (3) anomalous loss, which is related to the movement of domain walls within the material. Hysteresis losses can be reduced by the reduction of the intrinsic coercivity,

with a consequent reduction in the area contained within the hysteresis loop. Eddy current losses can be reduced by decreasing the electrical conductivity of the material and by laminating the material, which has an influence on overall conductivity and is important because of skin effects at higher frequency. Finally, the anomalous losses can be reduced by having a completely homogeneous material, within which there will be no hindrance to the motion of domain walls.

2.2.2 Soft Ferrites

At high frequency metallic soft magnetic materials simply cannot be used due to the eddy current losses. Therefore, soft ferrites, which are ceramic insulators, become the most desirable material. These materials are ferrimagnetic with a cubic crystal structure and the general composition $MO.Fe_2O_3$, where M is a transition metal such as nickel, manganese, magnesium or zinc. The magnetically soft ferrites first came into commercial production in 1948.

Mn Zn ferrite, sold commercially as ferroxcube, can be used at frequencies up to 10MHz, for example in telephone signal transmitters and receivers and in switch mode power supplies (also referred to as DC-DC converters). For these type of application the driving force to increase frequency is to allow miniaturization. Additionally, part of the family of soft ferrites, are the microwave ferrites, e.g. yttrium iron garnet. These ferrites are used in the frequency range from 100MHz to 500GHz, for waveguides for electromagnetic radiation and in microwave devices such as phase shifters.

2.2.3 Hard Ferrites

Hard magnets are characterized by high remanent inductions and high coercivities. They generally exhibit large hysteresis losses. Hard ferrite referred to as permanent magnets retain their magnetism after being magnetized. Hard ferrite likes Ba-ferrite, Sr-ferrite, Pb-ferrite are used in communication device operating with high frequency currents because of their high resistivity, negligible eddy currents and lower loss of energy due to Joule heating and hysteresis. These are found useful in many applications including fractional horse-power motors, automobiles, audio- and video-recorders, earphones, computer peripherals, and clocks.
According to the crystallographic structures ferrite fall into three categories.

(i) Cubic ferrites of spinel type
(ii) Cubic ferrites of garnet type and
(iii) Hexagonal Ferrites.

2.2.4 Cubic Ferrites with Spinel Structure

The cubic ferrite has the general formula $MO.Fe_2O_3$ where M is one of the divalent cations of the transition elements such as Mn, Ni, Mg, Zn, Cd, Cu, Co etc. A combination of these ions is also possible and it can be named as solid solution of two ferrites or mixed spinel ferrites. Generally, M represents a combination of ions which has an average valency of two. The trivalent iron ion in $MO.Fe_2O_3$ can partially be replaced by another trivalent ion such as Al^{3+} or Cr^{3+}, giving rise to mixed crystals. The structure of ferrite is derived from the mineral $MgAl_2O_4$ determined by Bragg [2.4]. These ferrites crystallize in the FCC spinel structure. The spinel lattice is composed of a close-packed oxygen arrangement in which 32 oxygen ions form the unit cell (the smallest repeating unit in the crystal network).

AB_2O_4

⊗ A   ⊙ B   ◯ o
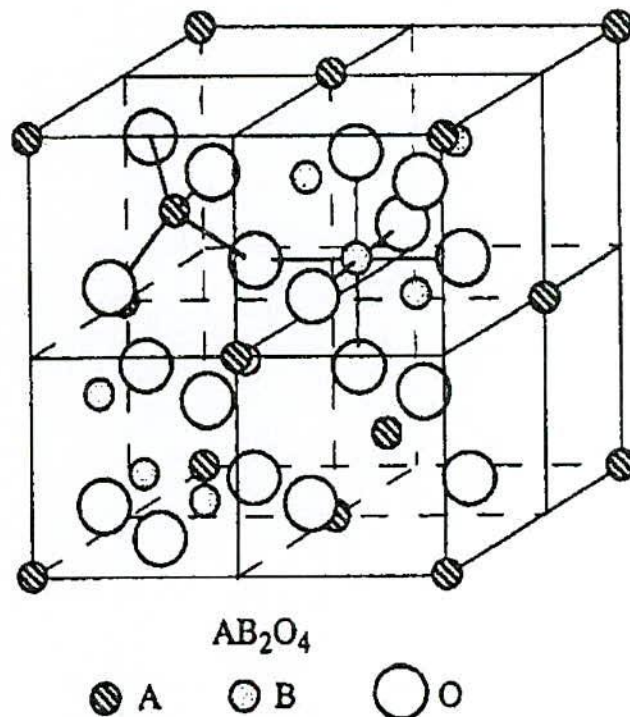
Fig. 2.4 Schematic of two subcells of a unit cell of the spinel structure, showing octahedral and tetrahedral sites

These anions are packed in a face centered cubic (FCC) arrangement leaving two kinds of spaces between anions: tetrahedral coordinated sites (A), surrounded by four

nearest oxygen atoms, and octahedral coordinated sites (B), surrounded by six nearest neighbor oxygen atoms. These are illustrated in Fig. 2.4. In total, there are 64 tetrahedral sites and 32 octahedral sites in the unit cell, of which only 8 tetrahedral sites and 16 octahedral sites are occupied, resulting in a structure that is electrically neutral [2.5, 2.6]. The localization of ions either in the A or B sites depends fundamentally on the ion and lattice sizes. Also it has been observed to depend on the temperature and the orbital preference for specific coordination. In general, divalent ions are larger than trivalent ions. This is because trivalent ion nuclei produce greater electrostatic attraction, hence their electron orbits contract. The octahedral sites are larger than the tetrahedral sites, thus, the divalent ions are localized in the octahedral sites whereas trivalent ions are in the tetrahedral sites [2.5].

According to the site occupancy of the metal ions, the spinel ferrites are classified as (a) normal spinel; where the tetrahedral (A-sites) are occupied by divalent metal ions and trivalent ions occupy B sites. A majority of these ferrites present paramagnetic behavior, (b) inverse spinel; where all the divalent ions are present in the octahedral site while trivalent ions are located on both A and B sites. The spin moments of the trivalent ions in an inverse spinel are canceled (direction of moment on A sites is opposed to B sites) whereas the spin moments of the divalent ions are aligned, resulting in a net magnetic moment [2.6] and (c) mixed spinel; where divalent ions are present both in tetrahedral and octahedral sites.

The cubic ferrite is easily magnetized and demagnetized; it has high permeability and saturation magnetization, low electrical conductivity, and the anisotropy energy is dominated by the anisotropy constant K_1. If K_1 is greater than zero, the easy direction is the cube edge direction (100) whereas if K_1 is less than zero, the body direction is preferred (111). For most ferrites the value of K_1 is negative, with the exception of cobalt ferrite [2.5].

2.2.5 The Spinel Structure

The ferrites have general formula $Me^{2+}Fe^{3+}O_4$ where Me^{2+} represents a divalent metal cation such as Mn, Fe, Co, Ni, Zn, Cd and Mg or combination of two divalent ions and Fe^{3+} is the trivalent iron cation. Ferrite's structure is derived from the mineral

21

$MgAl_2O_4$ determined by Bragg [2.4]. The unit cell consists of eight formula units ($8Me^{2+}Fe^{2+}O_4$) as shown in Fig. (2.5a). The 32 oxygen ions form an fcc lattice in which two types of interstitial sites are present namely (a) 64 tetrahedral sites surrounded by 4 oxygen (A-sites) and (b) 32 octahedral sites surrounded by 6 oxygen ions (B-sites). The space group is (O^7_h-F3dm), with following cationic position [2.7-2.8].

8-fold positions, 8 metal cations

$$000, \quad \frac{1}{4}\frac{1}{4}\frac{1}{4}$$

16-fold positions, 16 metal ions

$$\frac{5}{8}\frac{5}{8}\frac{5}{8}, \quad \frac{5}{8}\frac{7}{8}\frac{7}{8}, \quad \frac{7}{8}\frac{5}{8}\frac{7}{8}, \quad \frac{7}{8}\frac{7}{8}\frac{5}{8}$$

32- fold positions, 32 oxygen ions

$uuu, u\,\bar{u}\,\bar{u}$

$$\frac{1}{4}-u, \quad \frac{1}{4}-u, \quad \frac{1}{4}-u, \quad \frac{1}{4}-u, \quad \frac{1}{4}-u, \quad \frac{1}{4}-u,$$

$\bar{u}\,u\,\bar{u}, \bar{u}\,\bar{u}\,u$

$$\frac{1}{4}+u, \quad \frac{1}{4}+u, \quad \frac{1}{4}+u, \quad \frac{1}{4}+u, \quad \frac{1}{4}+u, \quad \frac{1}{4}+u,$$

with fcc translations $\left(0\ 0\ 0,\ 0\frac{1}{2}\frac{1}{2},\ \frac{1}{2}0\frac{1}{2},\ \frac{1}{2}\frac{1}{2}0 \right)$ and $u=\frac{3}{8}$

It is useful to divide the cubic lattice into two groups [2.9, 2.10];

(i) subshell consisting of four cubes with edge lengths, $\frac{a}{2}$, called octants. As shown in Fig. (2.5a), where two adjacent octants are illustrated, each of these small cubes contains four oxygen ions. In one of these octants, the oxygen ions lie along the main diagonal and are halfway from the divalent cations in the corner sites.

(ii) For the other type of octant the oxygen ions still lie along the main diagonal but lies half towards the divalent metal cations in the corners.

The left hand octant contains, in the center, a metal ion, in 8-fold position, which lies in the center of a tetrahedron of oxygen ions (A-sites). The right hand octant shows four metal cations in (16-fold) position, each surrounded by six oxygen ions (B-sites). Various features of the spinel structure are further illustrated in Fig. 2.5(b-e)
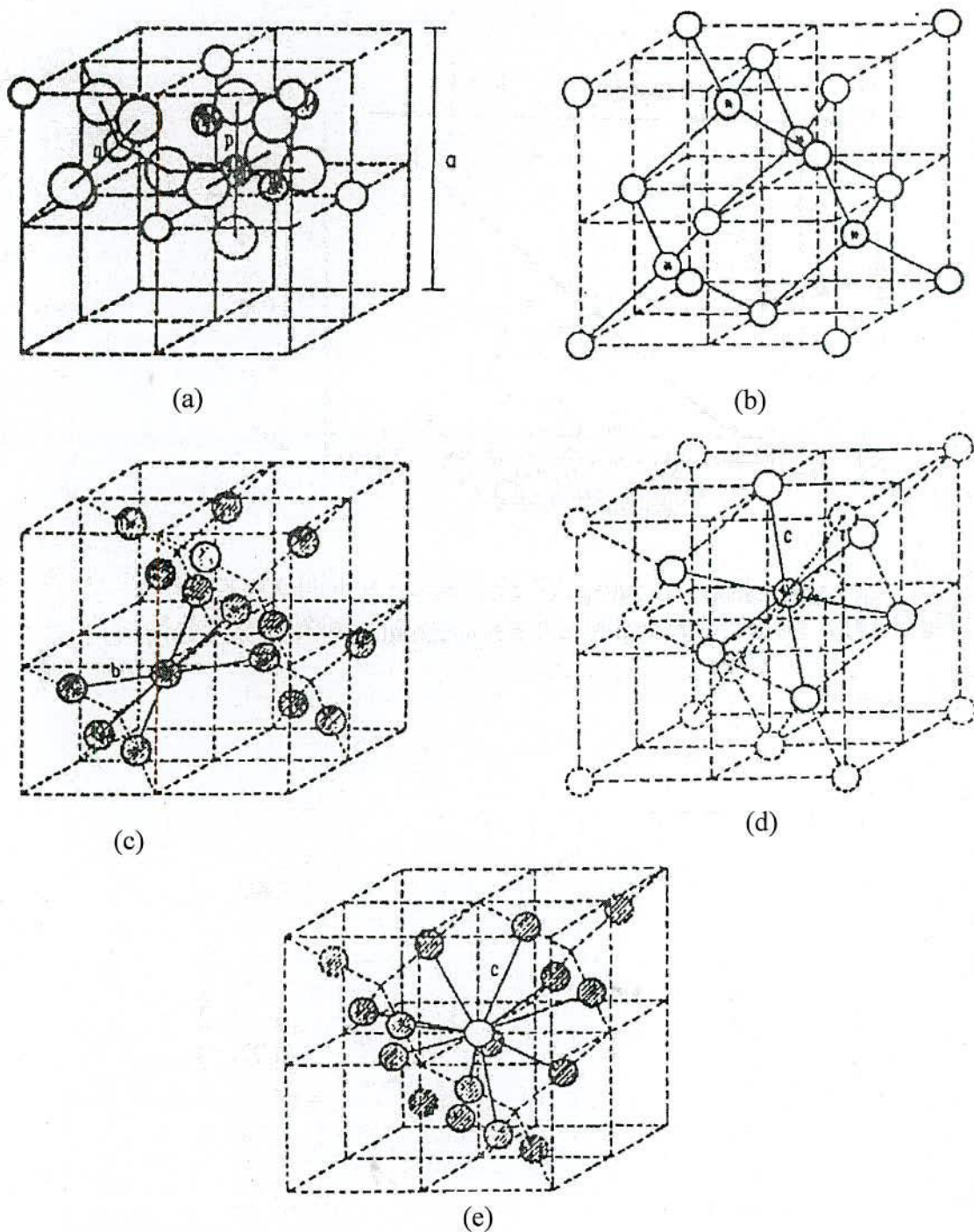
Fig. 2.5 Unit cells of the spinel structure (a) showing the tetrahedral and octahedral sites in two adjacent octants. Large circles: Oxygen ions; small hatched circles octahedral metal ions; small unhitched circles: tetrahedral metal ions, (b) positions of metal cations of tetrahedral sites only (c) positions of metal cations on octahedral sites only (d) position of one octahedral cation with its six nearest-neighbour tetrahedral cations (e) position of one tetrahedral cation with its six nearest-neighbour tetrahedral cations

It is further concluded that each A-ion has 12 nearest-neighbors of B-type, while each B 6 nearest-neighbors of A-type surround ion. The shortest distances are;

$$\Gamma_{AB} = \frac{a}{8}\sqrt{11}$$

$$\Gamma_{AB} = \frac{a}{4}\sqrt{3}$$

$$\Gamma_{AB} = \frac{a}{8}\sqrt{2}$$

The Me-O distances between nearest-neighbors are given by 0.216a and 0.25a, for tetrahedral and octahedral environments.

2.2.6 Cation Distribution in Spinels

The cation distribution in the spinel $Me^{2+}Me^{3+}O_4$ can be as follows [2.8, 2.9];

● **Normal**

The Me^{2+} cations are in tetrahedral positions, while the two Me^{3+} cations are in octahedral sites. The square brackets are generally used to represent the octahedral sites, i.e. $Me^{2+}[Me^{3+}]O_4$

● **Inverse**

In this case the Me^{2+} cation and one of the Me^{3+} cations are in octahedral positions while the second Me^{3+} cation occupies a tetrahedral site. The arrangement is as $Me^{3+}[Me^{2+}Me^{3+}]O_4$.

● **Intermediate**

The arrangement of the form like $Me_{1-\delta}^{3+}Me_{\delta}^{2+}\left[Me_{1-\delta}^{3+}Me_{1+\delta}^{2+}\right]O_4$ is often referred as intermediate, where δ is called the inversion parameter. $\delta = 0.0$ for completely normal and $\delta = 1.0$ for completely inverse spinels and $0 < \delta < 1$ for intermediate spinels.

The factors affecting the cation distribution over A and B-sites are as follows [2.10, 2.11];

● the size of the cations
● the electronic configurations of the cations
● the electronic energy
● the saturation magnetization of the lattice

Smaller cations (trivalent ions) prefer to occupy the A-sites. The cations have special preference for A and B-sites and the preference depends on the following factors.

- ionic radius
- size of interstices
- temperature
- Orbital preference for the specific coordination

The preference of cations is according to Verway-Heilman scheme [2.12, 2.13];

- ions with preference for A-sites Zn^{2+}, Cd^{2+}, Ga^{2+}, In^{3+}, Ge^{4+}
- ions with preference for B-sites Ni^{2+}, Cr^{3+}, Ti^{4+}, Sn^{4+}
- Indifferent ions Mg^{2+}, Al^{3+}, Fe^{2+}, Co^{2+}, Mn^{2+}, Fe^{3+}, Cu^{2+}

Moreover the electrostatic energy also affects the cation distribution in the spinel lattice. The cations of the smallest positive charge reside on the B-sites having six anions in surrounding i.e. the most favourable electrostatic conduction.

2.2.7 Magnetic Exchange Interaction

The exchange energy between the two atoms having spins S_i and S_j can be expressed universally in terms of Heigenburg Hamiltonian [2.14]

$$H = -\sum j_{ij} S_i . S_j \tag{2.1}$$

where, J_{ij} the exchange integral represents the strength of the exchange coupling between the spin angular momentum i an j. It is well known that the favored situation is the one with the lowest energy and there are two ways in which the wave functions can combine for lowering the energy by H. These are:

(i) If J_{ij} is positive, the parallel spin configuration will minimize the system total energy and all spins aligned to each other in the ground state. This is the case leading to ferromagnetic ordering.

(ii) If J_{ij} is negative, J_{ij} favors the antiparallel alignment of spins and consequently gives rise to antiferromagnetic ordering.

2.2.8 Super exchange Interaction

The magnetic interaction in magnetic oxide (ferrites) can not be explained on the basis of direct exchange interaction because of the following facts:

- The magnetic ions are located too far apart from each other shielded by the nonmagnetic anion (oxygen). This is because these are not band type semiconductor [2.10]. The non-magnetic anion is situated in the line joining magnetic cations.

- Superexchange interactions appear, i.e., indirect exchange via anion p-orbitals that may be strong enough to order the magnetic moments.
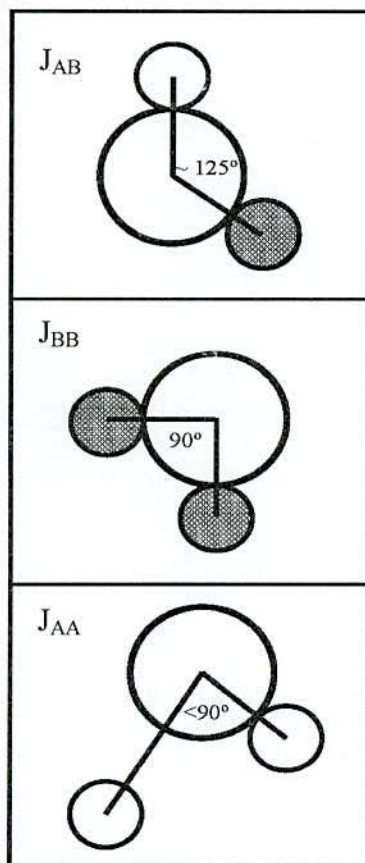
Fig. 2.6 Three major types of superexchange interactions in spinel ferrites are as follows: J_{AB}, J_{BB} and J_{AA}. The small empty circle is A site, the small solid circle is B site, and the large empty circle is oxygen anion

Ferrimagnetic oxides are one kind of magnetic systems in which there exist at least two inequivalent sublattices for the magnetic ions. The antiparallel alignment between these sublattices (ferrimagnetic ordering) may occur provided the inter-sublattice exchange interactions are antiferromagnetic (AF) and some requirements concerning the signs and strengths of the intra-sublattice interactions are fulfilled. Since usually in ferrimagnetic oxides the magnetic cations are surrounded by bigger oxygen

anions (almost excluding the direct overlap between cation orbitals) magnetic interactions occur via indirect superexchange mediated by the p oxygen orbitals. It is well-known that the sign of these superexchange interactions depends both on the electronic structure of the cations and their geometrical arrangement [2.15]. In most of ferrimagnetic oxides, the crystallographic and electronic structure give rise to antiferromagnetic inter and intra-sublattice competing interactions. The magnitude of negative exchange energies between two magnetic ions M and M′ depends upon the distances from these ions to the oxygen ion O^{2-}, via which the superexchange takes place, and on the angle M-O^{2-}-M′ (ϕ). According to the superexchange theory, the angle $\phi=180^0$ gives rise to the greatest exchange energy, and this energy decreases very rapidly as the distance between the ions increases. If A and B are the tetrahedral and octahedral ions respectively in a spinel structure, the A-B interaction is the greatest and A-A exchange interaction is the weakest [2.14].

2.2.9 Two Sublattices in Spinel Ferrites

The term "magnetic sublattice" is widely used in the study of magnetic structures of the whole spectrum of magnetic materials [2.16]. In the case of ferromagnetic materials, the "magnetic sublattice" is exactly the same as the crystal structure and no problem arises. In the case of antiferromagnetics, the importance of the direction of the magnetic moments is evident and makes clear the existence of two magnetic sublattices, as for example, in MnO. The difference between the two magnetic sublattices is the direction of their magnetic moment. However, ferrimagnetic materials are considerably more complex and the application of the molecular field theory to spinels has pointed to the problem of a clear definition of the concept of magnetic sublattices. In spinel ferrites the metal ions are separated by the oxygen ions and the exchange energy between spins of neighboring metal ions is found to be negative, that is, antiferromagnetic. This is explained in terms of superexchange interaction of the metal ions via the intermediate oxygen ions [2.17]. There are a few points to line out about the interaction between two ions in tetrahedral (A) sites:

- The distance between two A ions (~3.5 $\mathring{A}$) is very large compared with their ionic radius (0.67 $\mathring{A}$ for Fe^{3+}),

- The angle $A-O^{2-}-A$ ($\phi = 79^0 38'$) is unfavorable for superexchange interaction [2.14], and

- The distance from one A ion to O^{2-} is not the same as the distance from the other A ion to O^{2-} as there is only one A nearest neighbor to an oxygen ion (in Fig. 2.7, M and M' are A ions, r = 3.3 Å and q = 1.7 Å) [2.14]. As a result, two nearest A ions are connected via two oxygen ions.

These considerations led us to the conclusion that superexchange interaction between A ions is very unlikely. This conclusion together with the observation that direct exchange is also unlikely in this case [2.14] support the assumption that $J_{AA} = 0$ in the spinel ferrites. According to Neel's theory, the total magnetization of a ferrite divided into two sublattices A and B is:

$$M_T(T) = M_B(T) - M_A(T) \tag{2.2}$$

where, T is the temperature, $M_B(T)$ and $M_A(T)$ are A and B sublattice magnetizations.
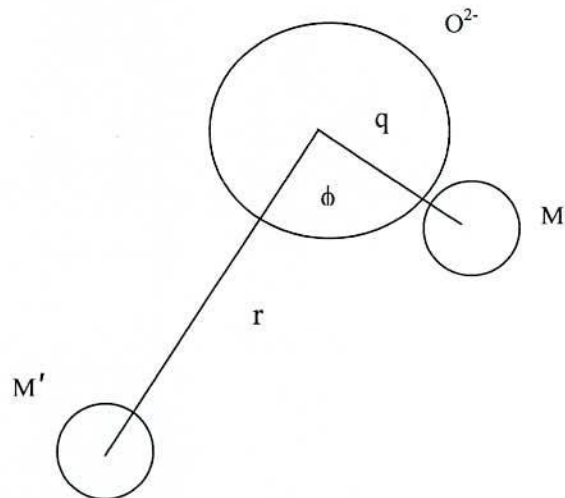
Fig. 2.7 Schematic representation of ions M and M' and the O^{2-} ion through which the superexchange is made. R and q are the centre to centre distances from M and M' respectively to O^{2-} and ϕ is the angle between them

Both $M_B(T)$ and $M_A(T)$ are given in terms of the Brillouin function $B_{S_i}(x_i)$;

$$M_B(T) = M_B(T = 0)B_{SB}(x_B) \tag{2.3}$$

$$M_A(T) = M_A(T = 0)B_{SA}(x_A) \tag{2.4}$$

with
$$x_A = \frac{\mu_B g_A S_A}{k_B T} M_B N_{AB} \qquad (2.5)$$

$$x_B = \frac{\mu_B g_B S_B}{k_B T} (M_B N_{BB} + M_A N_{AB}) \qquad (2.6)$$

The molecular field coefficients, N_{ij}, are related to the exchange constants J_{ij} by the following expression:

$$J_{ij} = \frac{n_j g_i g_j \mu_B^2}{2 z_{ij}} N_{ij} \qquad (2.7)$$

with n_j the number of magnetic ions per mole in the jth sublattice, g the Lande factor, μ_B is the Bohr magneton and z_{ij} the number of nearest neighbors on the jth sublattice that interact with the ith ion.

According to Neel's theory and using $J_{AA} = 0$, equating the inverse susceptibility $\frac{1}{\chi} = 0$ at $T = T_c$ we obtain for the coefficients of the molecular field theory N_{AB} and N_{BB} of the following expression:

$$N_{BB} = \frac{T_c}{C_B} - \frac{C_A N_{AB}^2}{T_c} \qquad (2.8)$$

where, C_A and C_B are the Curie constants for each sublattice. Eq^n (2.2) and eq^n (2.8) constitute a set of equations with two unknown, N_{AB} and N_{BB}, provided that M_A and M_B are a known function of T.

2.3   Magnetic Properties of Ferrites

Ferromagnetic materials are characterized by a high magnetization (magnetic moments per unit volume) which can be achieved even in polycrystalline materials by the application of relatively small magnetic field. In a ferromagnetic material; the individual atomic (atom with partly filled 3d or 4f shells) or ionic moments arising from unpaired spins are permanent, and interact strongly with one another in a manner which tends to cause parallel alignment of the nearby moments. The moments of a large number of neighbouring ions are thus parallel, even in the absence of an applied field. These regions or domains, of spontaneous magnetization exist in both single and polycrystalline materials, and within a domain the value of the saturation magnetization M is the maximum that can be achieved in the material at the given temperature.

The origin of the interaction lies in the so-called quantum mechanical exchange [2.18-2.19], but, in a phenomenological description of magnetism, it is possible to regard that the obliging forces are arising from an internal magnetic field called the Weiss molecular field [2.20]. Weiss assumed that spontaneous magnetization properties disappear at the curie point when the thermal energy is equal to the energy of the individual ionic moment in Weiss induction field then,

$$B_W = kT_c + \mu B_m \qquad (2.9)$$

Where k is Boltzmann constant, T_c is Curie temperature, μ's permeability and B_m is the Weiss molecular field. It is convenient to write $B_m = \mu_0 H$; below the Weiss molecular field H is used. Weiss assumed that the molecular field H_m was proportional to the magnetization M i.e.,

$$H_m = \gamma M \qquad (2.10)$$

where M is the magnetization in the material and γ is the constant of proportionality called molecular field coefficient.

A ferrite may be defined as the one, which below a certain temperature bears a spontaneous magnetization that, arises from non-parallel arrangement of the strongly coupled atomic dipoles. Ferrite is the substance consists of two sublattices with magnetic moments of one sublattice tending to antiparallel to those of other. When the sublattice magnetizations are not equal there will be a net magnetic moment. The term ferrimagnetism has been used in broad sense in order to include the materials with more then two sublattice and with other spin configurations, such as triangular or spiral configurations. It is usually assumed that a ferrimagnetic material has an appreciable net magnetization, although no precise definition of the term appreciable has been given. The two sublattices are denoted by A and B. If the magnetic moments of the ions at A and B-sites are unequal, this inequality may be due to;

- Presence of elements in different ionic states, e.g. Fe^{3+} and Fe^{2+}
- Different elements in the same or different ionic states, e.g. Fe^{3+} and Co^{2+}
- Different crystalline field acting at two sites.

The competition between the forces on the B spins may lead to the triangular configurations.

2.3.1 Electron Spin

With the concept of electron spin introduce by Goudsmit in 1925 and Uhlenbeck in 1926, the origin of magnetism was explained. Spin corresponds to movement of electric charge in the electron, hence an electric current which produces a magnetic moment in the atom. The net magnetic moment is the vector sum of the individual spin and orbital moments of the electrons in the outer shells [2.21]. Next figure illustrate these two phenomenons:

(a)   (b)
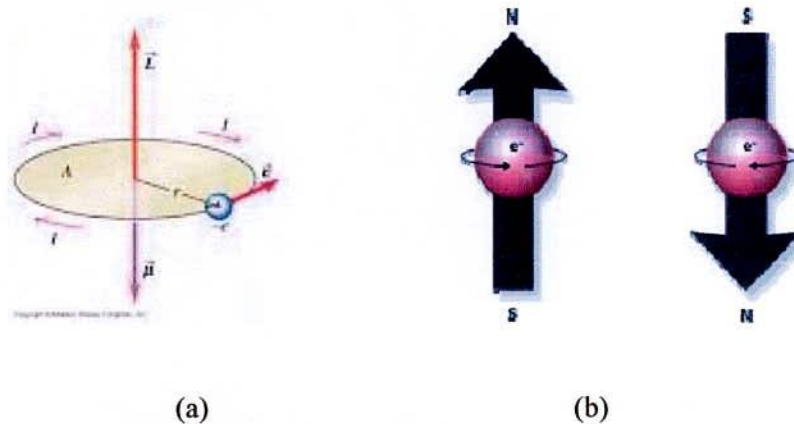
Fig.2.8 (a) Electron orbit around the nucleus (b) Electron spin

The electron spin can be represented in two modes pointed up or down. In an atom, with opposed paired spins cancel and do not result in magnetic moment, while the unpaired spins will give rise to a net magnetic moment.

2.3.2 Magnetic Dipole

The Earth's magnetic field, which is approximately a magnetic dipole. However, the N- pole and S-pole are labeled here geographically, which is the opposite of the convention for labeling the poles of a magnetic dipole moment

In physics, there are two kinds of dipoles:

• An electric dipole is a separation of positive and negative charges. The simplest example of this is a pair of electric charges of equal magnitude but opposite sign, separated by some (usually small) distance. A permanent electric dipole is called an electrets.

• A magnetic dipole is a closed circulation of electric current. A simple example of this is a single loop of wire with some constant current flowing through it [2.22, 2.23].

2.3.3 Magnetic Field

The magnetic field (B) is a vector field. The magnetic field vector at a given point in space is specified by two properties:

(i) Its direction, which is along the orientation of a compass needle.

(ii) Its magnitude (also called strength), which is proportional to how strongly the compass needle orients along that direction.

The units for magnetic field strength H are ampere/meter. A magnetic field strength of 1 ampere/meter is produced at the center of a single circular conductor with a one meter diameter carrying a steady current of 1 ampere.

2.3.4 Magnetic Moment

A magnet's magnetic moment (μ) is a vector that characterizes the magnet's overall magnetic properties. For a bar magnet, the direction of the magnetic moment points from the magnet's south pole to its north pole, and the magnitude relates to how strong and how far apart these poles are. In SI units, the magnetic moment is specified in terms of $A\text{-}m^2$. A magnet both produces its own magnetic field and it responds to magnetic fields. The strength of the magnetic field it produces is at any given point proportional to the magnitude of its magnetic moment. In addition, when the magnet is put into an external magnetic field, produced by a different source, it is subject to a torque tending to orient the magnetic moment parallel to the field. The amount of this torque is proportional both to the magnetic moment and the external field. A magnet may also be subject to a force driving it in one direction or another, according to the positions and orientations of the magnet and source. If the field is uniform in space, the magnet is subject to no net force, although it is subject to a torque.

2.3.5 Molecular Field Theory of Ferrimagnetism

In ferrimagnetism spontaneous magnetization is due to cooperation of between the atomic dipoles with in the single domain i.e. there must be some kind of interaction between the atoms which produces the tendency for parallel alignment of the atomic magnetic dipoles. In order to obtain a logical description of spontaneous magnetization, Weiss [2.20] assumed that the molecular field H_m acting on a dipole may be written as;

$$H_m = M + \lambda M \tag{2.11}$$

where λ is the molecular field constant, it is clear that λM provide the cooperative effect. The molecular field theory of ferrimagnetism with two sublattices A and B was developed by L. Neel [2.25].

The molecular field H_{mA} acting on an atom at an A-site is;

$$H_{mA} = -\lambda_{AA}M_A - \lambda_{AB}M_B \qquad (2.12)$$

The molecular field H_{mB} acting on an atom at B site be;

$$H_{mB} = -\lambda_{BA}M_A - \lambda_{BB}M_B \qquad (2.13)$$

where M_A, M_B be the magnetizations of A and B sublattices respectively. Where λ_{AB} is the molecular field constant for the nearrest neighbour interaction and λ_{BB} is a molecular field constant for the next nearest neighbour interaction, similarly λ_{BA} and λ_{AA}, If a field H_A is also applied, the fields H_A and H_B at an atom on the and B sublattices respectively.

$$H_A = H_a - \lambda_{AA}M_A - \lambda_{AB}M_B \qquad (2.14)$$

$$H_B = H_a - \lambda_{BA}M_A - \lambda_{BB}M_B \qquad (2.15)$$

At equilibrium $\lambda_{AB} = \lambda_{BA}$

$$\lambda_{AA} \neq \lambda_{BB}$$

$$M_A \neq M_B$$

than

$$H_A = H_a - \lambda_{AA}M_A - \lambda_{AB}M_B \qquad (2.16)$$

$$H_B = H_a - \lambda_{AB}M_A - \lambda_{BB}M_B \qquad (2.17)$$

Here $\lambda_{AB} > 0$, since the interaction between the two sublattices is antiferromagnetic. The other molecular field constants λ_{AA} and λ_{BB} may in principle be positive or negative but apparently are positive for great majority of ferrimagnetic materials. Usually $\lambda_{AA} < \lambda_{AB}$ and $\lambda_{BB} < \lambda_{AB}$. It is common to express λ_{AA} & λ_{BB} in terms of λ_{AB}.

$$\lambda_{AA} = \alpha\,\lambda_{AB}$$

$$\lambda_{BB} = \beta\,\lambda_{AB}$$

The magnetization of the sublattices at thermal equilibrium is given by;

$$M_A = \sum_i N_i g_i \mu_B S_i B_{S_i}(x_A) \qquad (2.18)$$

Where as

$$x_A = \left(\frac{\mu_B S_i B_{S_i}}{kT}\right)H_A$$

$$B_{S_i}(x_A) = \frac{2s_i+1}{2s_i}\coth\frac{2s_i+1}{2s_i}x_A - \frac{1}{2s_i}\coth\frac{x_A}{2s_i} \qquad (2.19)$$

$$M_B = \sum_j N_j g_j \mu_B S_j B_{S_j}(x_B) \qquad (2.20)$$

Here N_j is the number of atoms per unit volume with the spin quantum number s_i,

2.3.6 Paramagnetic Susceptibility above Curie Temperature

The temperature above, which the spontaneous magnetization of a ferrimagnet vanishes, is called the Curie or Neel's temperature. Above T_c the sublattice magnetizations are given by;

$$M_A = \left(\frac{C_A}{T}\right)H_A \text{ and } M_B = \left(\frac{C_B}{T}\right)H_B \tag{2.21}$$

$$C_A = \sum_i \frac{N_i g_i^2 \mu_B^2 S_i (S_i + 1)}{3k} \tag{2.22}$$

And $C_B = \sum_j \frac{N_j g_j^2 \mu_B^2 S_j (S_j + 1)}{3k} \tag{2.23}$

Substitution for the fields in equations (2.21) then leads to;

$$(T + C_A \lambda_{AA}) M_A + C_A N_{AB} M_B = C_A H \tag{2.24}$$

$$C_b \lambda_{AB} M_A + (T + C_B \lambda_{BB}) M_B = C_B H \tag{2.25}$$

These equations then give the sublattice magnetizations;

$$M_A = \frac{C_A(T + C_B \lambda_{BB}) - C_A C_B \lambda_{AB}}{(T + C_A \lambda_{AA})(T + C_B \lambda_{BB}) - C_A C_B \lambda^2_{AB}} \times H \tag{2.26}$$

$$M_B = \frac{C_B(T + C_A \lambda_{AA}) - C_A C_B \lambda_{AB}}{(T + C_A \lambda_{AA})(T + C_B \lambda_{BB}) - C_A C_B \lambda^2_{AB}} \times H \tag{2.27}$$

Addition of these equations gives an expression for the susceptibility $\chi = \frac{M_A + M_B}{H}$.

The inverse of susceptibility can be expressed in a more convenient form.

$$\frac{1}{\chi} = \frac{T}{C} - \frac{1}{\chi_0} - \frac{\sigma}{T - \theta'} \tag{2.28}$$

where $C = C_A + C_B$ and

$$\frac{1}{\chi_0} = -\frac{1}{c^2}\left\{ C_A^2 \lambda_{AA} + C_B^2 \lambda_{BB} + 2C_A C_B \lambda_{BB} \right\}$$

$$\sigma = \frac{C_A C_B}{C^3}\left\{ C_A^2 (\lambda_{AA} - \lambda_{AB})^2 + C_B^2 (\lambda_{BB} - \lambda_{AB})^2 - 2C_A C_B \left[\lambda_{AB}^2 - (\lambda_{AA} + \lambda_{BB})\lambda_{AB} + \lambda_{AA} \lambda_{BB} \right] \right\}$$

$$\theta' = -\frac{C_A C_B}{C}(\lambda_{AA} + \lambda_{Bb} - 2\lambda_{AB})$$

34

The graphical representation of the eq^n (2.28) is hyperbola as illustrated in Fig. 2.9. Its asymptote is given by;

$$\frac{1}{\chi} = \frac{T}{C} - \frac{1}{\chi_0}$$

(2.29)

Since usually $\lambda_{AB} > \lambda_{AA}$. λ_{BB} and also λ_{AB}. λ_{AA}. λ_{BB} are positive. If θ is defined as T-intercept found by the extrapolation of the line, then
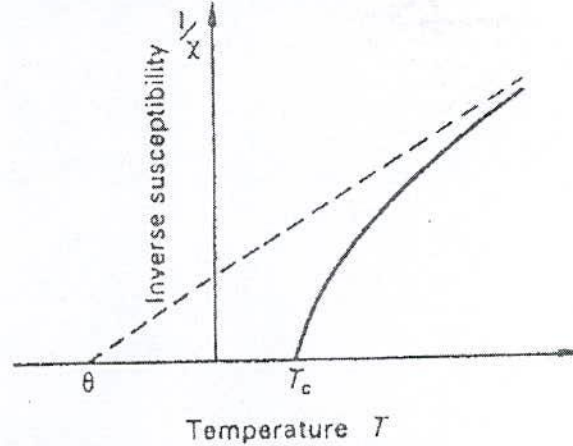
Fig. 2.9 Inverse of susceptibility of a ferrimagnetic material above its Curie point

$$\theta = -\frac{C}{\chi_0}$$

(2.30)

and the eq^n (2.29) may be written as;

$$\chi = \frac{C}{T + \theta}$$

(2.31)

where $\theta > 0$, eq^n (2.31) is the same for as that for the susceptibility of antiferromagnetic above T_c, where θ is the "paramagnetic" temperature. Therefore for a temperature sufficiently above T_c the $\frac{1}{\chi}$ Vs T plot has the same linear relationship as predicted by the molecular field theory for antiferromagnetic materials [2.24-2.25]. The rapid change of $\frac{1}{\chi}$ close to T_c shows marked deviation from ferromagnetic and antiferromagnetic cases. This phenomenon has its physical origin in the relative magnitudes of the sublatices because of antiparallel effect.

2.3.7 Spontaneous Magnetization

It is concluded that below Curie temperature T_c the sublattices are spontaneously magnetized with M_A and M_B being antiparallel. The magnetization of the individual

sublattices can not be observed individually but instead the net magnetization $M = M_A + M_B$, is measured. Since both M_A and M_B are antiparallel then,

$$|M| = |M_A| - |M_B| = |M_B| - |M_A| \qquad (2.32)$$

The temperature dependence spontaneous magnetization in ferrimagnetic materials is asserted only if N_{AB} is non-zero molecular field constant, also $N_{AB} \gg N_{AA}$ and N_{BB}.

The sublattice magnetizations may be given as;

$$M_A(T) = M_A(0) B_{sx}(x_A) \text{ and } M_B(T) = M_B(0) B_{sx}(x_B) \qquad (2.33)$$

$$\text{where } M_A(0) = N_A g \mu_B S_A$$

$$M_B(0) = N_B g \mu_B S_B$$

$$\text{and } x_A = \frac{g \mu_B S_A}{kT} \left(-N_{AA} M_A + N_{AB} M_A \right)$$

$$x_B = \frac{g \mu_B S_B}{kT} \left(N_{AB} M_A - N_{BB} M_B \right)$$

The summation sign has been omitted for simplicity and the applied field has been set equal to zero. The eq^n (2.33) are thus transcendental equations that can be solved for M_A and M_B. The magnitude of resultant spontaneous magnetization can be found from the eq^n (2.32).

2.3.8 Neel's Collinear Model of Ferrites

Soft ferrites belong to the cubic spinal structure. According to Neel's theory, the magnetic ions are assumed to be distributed among the tetrahedral A and octahedral B-sites of the spinel structure. The magnetic structure of such crystals essentially depends upon the type of magnetic ions residing on the A and B sites and the relative strengths of the inter- (J_{AB}) and intra-sublattice exchange interactions (J_{AA}, J_{BB}). Negative exchange interactions exist between A–A, A–B and B–B ions. When A–B antiferromagnetic interaction is the dominant one, A and B-sublattices will be magnetized in opposite direction below a transition temperature. When the A–A (or B–B) interaction is dominant, Neel found that the above transition will not take place and he concluded that the substance remains paramagnetic down to the lower temperature. But this conclusion

was not correct, as in the presence of strong interactions, some kind of ordering may be expected to occur at low temperature as claimed by Yafet and Kittel [2.26].

2.3.9 Non-collinear Model

In general, all the interactions are negative (antiferromagnetic) with $|J_{AB}| \gg |J_{BB}| \gg |J_{AA}|$. In such situation, collinear or Neel type of ordering is obtained. Yafet and Kittel theoretically considered the stability of the ground state of magnetic ordering, taking all the three exchange interactions into account and concluded that beyond a certain value of $\dfrac{J_{BB}}{J_{AB}}$, the stable structure was a non-collinear triangular configuration of moment wherein the B-site moments are oppositely canted relative to the A-site moments. Later on Leyons et. al. [2.27] extending these theoretical considerations showed that for normal spinel the lowest energy correspond to conical spinal structure for the value of $\dfrac{3J_{BB}S_B}{2J_{AB}S_A}$ greater than unity. Initially one can understand why the collinear Neel structure gets perturbed when $\dfrac{J_{BB}}{J_{AB}}$ increases. Since all these three exchange interations are negative (favoring antiferromagnetic alignment of moments) the inter- and intra-sublattice exchange interaction compete with each other in aligning the moment direction in the sublattice. This is one of the origins of topological frustration in the spinel lattice. By selective magnetic directions of say A-sublattice one can effectively decrease the influence of J_{AB} vis-à-vis J_{BB} and thus perturb the Neel ordering. The first neutron diffraction study of such system i.e., $Zn_xNi_{1-x}Fe_2O_4$ was done at Trombay [2.28] and it was shown to have the Y-K type of magnetic ordering followed by Neel ordering before passing on to the paramagnetic phase [2.29].

It was found that ferrites which have been substituted sufficiently with non-magnetic atoms showed significant departure from Neel collinear model. These theoretical models have been used to explain these departures:

- a paramagnetic centre model in which a number of magnetic nearest neighbours determines whether a magnetic ion remains paramagnetic or contributes to the magnetization
- a uniform spin canting relative to the average magnetization and

- a localized canting where the canting angle of a magnetic ion spin depends on the local magnetic environment.

The discrepancy in the Neel's theory was resolved by Yafet and Kittel [2.26] and they formulated the non-collinear model of ferrimagnetism. They concluded that the ground state at 0K might have one of the following configurations:

- have an antiparallel arrangement of the spins on two sites
- consists of triangular arrangements of the spins on the sublattices
- an antiferromagnetic in each of the sites separately.

2.3.10   Magnetic Moments of Ferrites

The determination of saturation moments of simple ferrites having the formula $Me^{2+}Fe_2^{3+}O_4$ where Me^{2+} is the divalent cation, such as Cu, Co, Ni, Fe, Mn etc. agrees with the Neel's collinear model. The A-B interactions are much larger than the A-A and B-B interactions respectively. The two kinds of magnetic ion forms two sublattices each saturated and magnetized in opposite direction at absolute zero.

Table- 2.1 Experimental and calculated saturation moments of some spinels

Ferrite	$M(\mu_B)$	$2SMe^{2+}$(cal.)
$MnFe_2O_4$	5 - 4.4	5
$FeFe_2O_4$	4.2 – 4.08	4
$CoFe_2O_4$	3.3 – 3.9	3
$NiFe_2O_4$	2.3 – 2.40	2
$CuFe_2O_4$	1.3 – 1.37	1
$MgFe_2O_4$	1.1 – 0.86	1.1
$Li_{0.5}Fe_{2.5}O_4$	2.6	2.5

Saturation magnetic moments of some selected spinels [2.9] are listed in the Table. (2.1), the first six ferrites are the inverse type i.e $Fe^{3+}[Me^{2+}Fe^{3+}]O_4$. The magnetic moments of the two Fe^{3+} cations compensate each other and the ferrite magnetization becomes equal to M_{Me}^{2+}. Since the theoretical magnetic moment is due to spin only value, the predicted theoretical moment is $M_{Me}^{2+}=2S_{Me}^{2+}$. These values are listed in the Table (2.1) and the experimental and calculated shows good agreement, except cobalt and copper series. The Li ferrite is also completely inverse and its moment is calculated based

on the cation distribution $Fe[Li_{0.5}Fe_{2.25}]O_4$ is equal to $2.5\mu_B$, per molecule, is in good agreement with the measured value.

There are two possible reasons for the discrepancies observed between calculated and observed magnetic moments as mentioned in the Table (2.1).

(i)   the orbital moments of the divalent ions may not be neglected, the crystal field effects therefore become important.

(ii)   the cation distribution must be taken into account.

2.4   Magnetization Process

A review of the magnetization process, namely the response of ferro-(ferri) magnetic material (bulk) to an applied field with a semi-microscopic approach is presented. In ferro-or ferri-magnetic material, the magnetization curves, especially in low magnetic fields differ widely from sample to sample and as a function of the magnetic history of the sample i.e., of the previous fields which have been successively applied.

2.4.1   Magnetization Curve

For unmagnetized bulk material, there is a zero net magnetic moment. It can be predicted that there will be an infinite number of degree of magnetization between the unmagnetized and saturation condition, when the material is subjected to an external magnetic field. These extreme situation correspond respectively, to random orientation of domains complete alignment is one direction with elimination of domain walls. If we start with the a demagnetized specimen and increase the applied magnetic field, the bulk material will be progressively magnetized by the domain dynamics. The magnetization of the sample will follow the course as shown in Fig 2.10 (2.5). The slope from the origin to a point on the curve or the ratio $\dfrac{M}{H}$ is defined as magnetic susceptibility. This curve is called Magnetization Curve. This curve is generally perceived as being made of three major portions.

The first, the lower section, is the initial susceptibility region and is characterized by reversible domain wall movements and rotations. By reversible means that after the magnetization slightly with an increase in field the original magnetization conditions can

be reversed if the field is reduced to initial value. The contribution of the displacement walls to an initial permeability is entirely dependent on the sort of material studied.
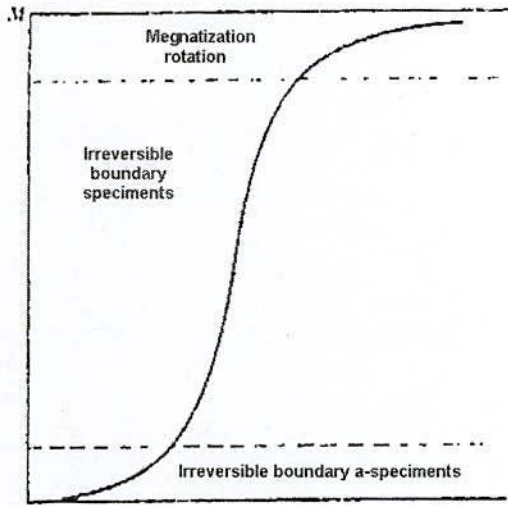
Fig. 2.10 Domain dynamics during various parts of the magnetization curve (2.5)

In the second stage magnetization curve, if the field is increased, the intensity of the magnetization increases more drastically, is called the irreversible magnetization range. This range is obtained mainly by the irreversible domain wall motion from one stable state to another.
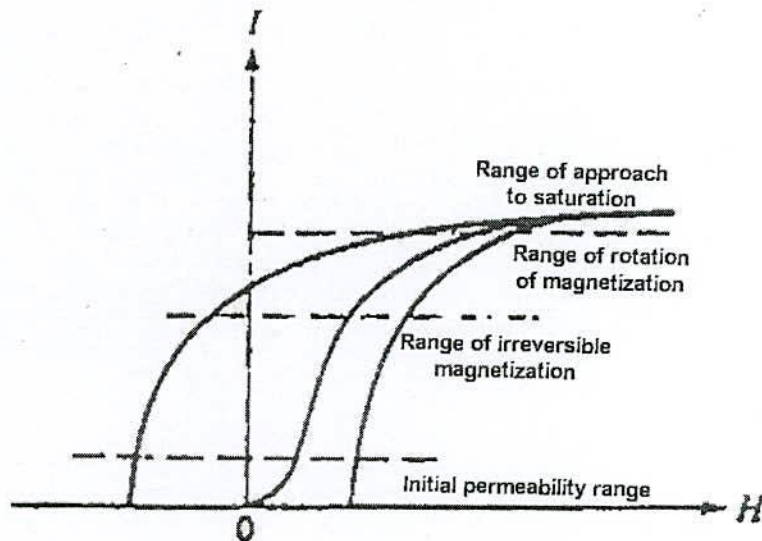
Fig. 2.11 Magnetization curve and the classification of magnetization mechanism

If the field is increased further, the magnetization curve become less steep and its process become reversible once more. In the third section of magnetization curve, the displacement of domain walls have already been completed and the magnetization take place by rotation magnetization. This range is called rotation magnetization range. Beyond this range the magnetization gradually approaches to saturation magnetization shown in Fig. 2.11.

2.4.2 Hysteresis

Magnetic hysteresis is an important phenomenon and refers to the irreversibility of the magnetization and demagnetization process, when a material shows a degree of irreversibility it is known as hysteretic. When a demagnetized ferromagnetic material is placed in as applied magnetic field grows at the expanse of the other domain wall. Such growth occurs by motion of the domain walls. Initially domain wall motion is reversible, and if the applied field is removes the magnetization will return to the initial demagnetized state. In this region the magnetization curve is reversible and therefore does not show hysteresis. The crystal will contain imperfections which the domain boundaries encounter during their movement. These imperfections have an associated magnetostatic energy when a domain wall intersects the crystal imperfection this magnetostatic energy can be eliminated as closure domains from this pins the domain wall to the imperfection as it if a local energy minima.

A great deal of information can be learned about the magnetic properties of a material by studying its hysteresis loop. A hysteresis loop shows the relationship between the induced magnetic flux density (**B**) and the magnetizing force (**H**). It is often referred to as the B-H loop. An example hysteresis loop is shown below.
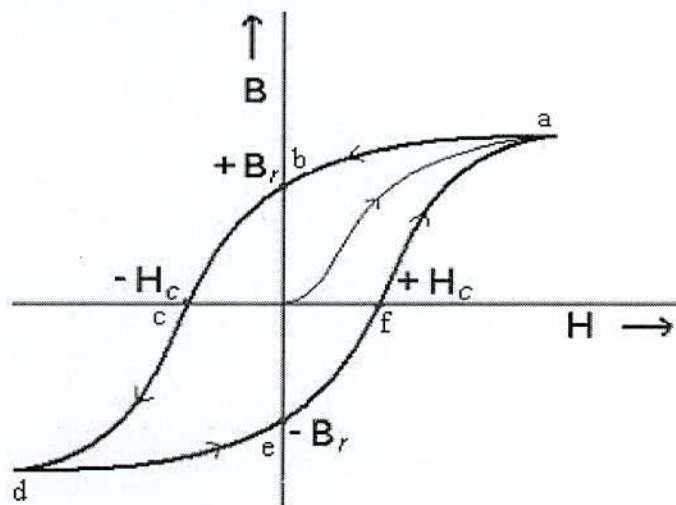
Fig. 2.12   Magnetic hysteresis loop

The loop is generated by measuring the magnetic flux of a ferromagnetic material while the magnetizing force is changed. A ferromagnetic material that has never been previously magnetized or has been thoroughly demagnetized will follow the dashed line as **H** is increased. As the line demonstrates, the greater the amount of current applied (+**H**), the stronger the magnetic field in the component (+**B**). At point "a" almost all of the magnetic domains are aligned and an additional increase in the magnetizing force will produce very little increase in magnetic flux. The material has reached the point of magnetic saturation. When **H** is reduced to zero, the curve will move from point "a" to point "b". At this point, it can be seen that some magnetic flux remains in the material even though the magnetizing force is zero. This is referred to as the point of retentivity on the graph and indicates the remanence (B_r) or level of residual magnetism in the material. (Some of the magnetic domains remain aligned but some have lost their alignment). As the magnetizing force is reversed, the curve moves to point "c", where the flux has been reduced to zero. This is called the point of coercivity on the curve (The reversed magnetizing force has flipped enough of the domains so that the net flux within the material is zero). The force required to remove the residual magnetism from the material is called the coercive force (H_c) or coercivity of the material. As the magnetizing force is increased in the negative direction, the material will again become magnetically saturated but in the opposite direction (point "d"). Reducing **H** to zero brings the curve to point "e." It will have a level of residual magnetism equal to that achieved in the other direction. Increasing **H** back in the positive direction will return **B** to zero. Notice that the curve did not return to the origin of the graph because some force is required to remove the residual magnetism. The curve will take a different path from point "f" back to the saturation point where it with complete the loop.

From the hysteresis loop, a number of primary magnetic properties of a material can be determined.

(i) **Retentivity:** A measure of the residual flux density corresponding to the saturation induction of a magnetic material. In other words, it is a material's ability to retain a certain amount of residual magnetic field when the magnetizing force is removed after achieving saturation. The value of **B** at point "b" on the hysteresis curve.

(ii) **Residual Magnetism** or **Residual Flux:** the magnetic flux density that remains in a material when the magnetizing force is zero. Residual magnetism and retentivity are the same when the material has been magnetized to the saturation point. However, the level of residual magnetism may be lower than the retentivity value when the magnetizing force did not reach the saturation level.

(iii) **Coercive Force:** The amount of reverse magnetic field which must be applied to a magnetic material to make the magnetic flux return to zero. The value of **H** at point "c" on the hysteresis curve.

2.4.3 Magnetization and Temperature

The influence of temperature on magnetic material can be determinate in the magnetic properties of dose materials. Rising the temperature of a solid, result in the increase of the thermal vibrations of atoms, with this the atomic magnetic moments are free to rotate. This phenomenon the atoms tend to randomize the directions of any moments that may be aligned [2.30]. With increasing temperature, the saturation magnetization diminishes gradually and abruptly drops to zero at what called the Curie temperature (T_c). The Curie point of a ferromagnetic material is the temperature above which it loses its characteristic ferromagnetic ability. At temperatures below the Curie point the magnetic moments are partially aligned within magnetic domains in ferromagnetic materials. As the temperature is increased from below the Curie point, thermal fluctuations increasingly destroy this alignment, until the net magnetization becomes zero at and above the Curie point.

Above the Curie point, the material is purely paramagnetic. At temperatures below the Curie point, an applied magnetic field has a paramagnetic effect on the magnetization, but the combination of paramagnetism with ferromagnetism leads to the magnetization following a hysteresis curve with the applied field strength. Table- 2.2 shows some examples of Curie temperature for various materials.
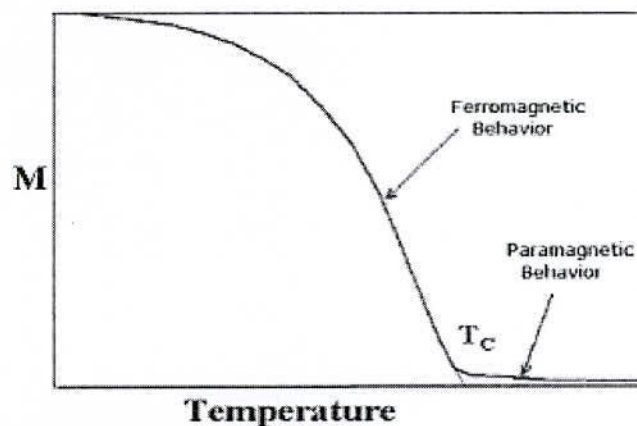
Fig. 2.13 Typical M-T curve for magnetic material

Table- 2.2 Curie temperature of selected materials

Material	Curie temperature (K)
Gadolinium	292
Nickel	631
Magnetite	858
Iron	1043
Cobalt	1393

2.4.4 Effect of Grain Size and Porosity on Hysteresis Loop Parameter

Smit and Wijn in 1954 [2.31] showed the variation of coercivity H_c with porosity in Ni-Zn ferrites. It was assumed that H_c increases with increasing porosity. This fact may be caused by the fact that higher porosity samples contain smaller (possibly single domain) particles, which have high coercive force. The coercive force of mixed ferrites Ni-Zn ferrites of varying porosity can be correlated fairly well with Neels' theoretical model treating the demagnetising influence of non magnetic materials in cubic crystals. In this method, the domain processes are considered rotational. Economos [2.32], showed that coercive force decreases in Mg ferrites as the porosity decreases. With regards to saturation, it is expected that saturation increases with increase in density or the packing of more magnetic material in a specified volume. Schwabe and Campel [2.33] showed that for square loop materials, the threshold field (close to H_c) varies with the grain size for lithium ferrite i.e., H_c is inversely proportional to the grain size.

Igarashi [2.34], separated porosity and grain size effects in studying Ni-Zn ferrites. He concluded that porosity changes the B-H loop as shown in Fig. 2.14. B_{max} would then be independent of grain size but would vary with porosity as $(1-p)4\pi M_o$, where M_o is the magnetization extrapolated to zero porosity. H_c is then proportional to $\frac{1}{r}$, where r being the grain radius, and independent of porosity. Fig. 2.15 shows the correlation of the experimental results with theoretical curves, as well as the correlation of the postulated and experimental B_r values. B_r is assumed to be independent of grain size. Li [2.35], found that saturation and remanance were independent of the grain size and H_c varying in a $\frac{1}{r}$ manner for commercial Ni-Zn and Mn-Zn ferrites.
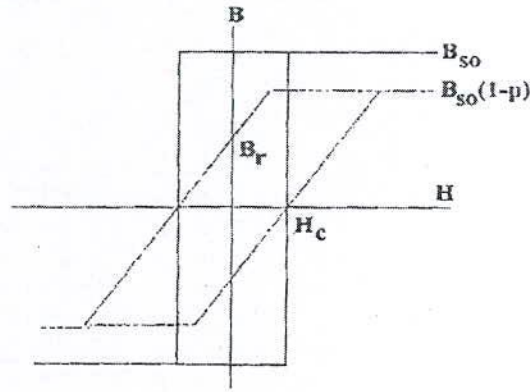
Fig. 2.14 Change of hysteresis loop of a Ni-Zn ferrite due to an increase in porosity from Igarishi (2.34)
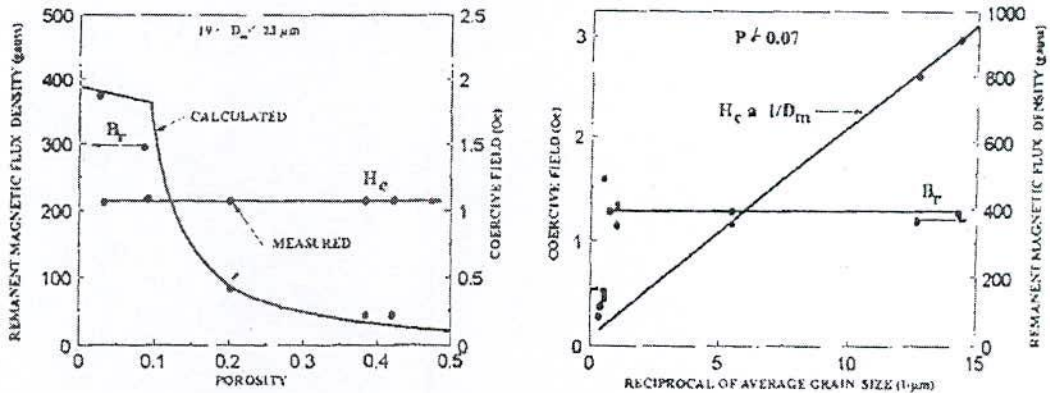
Fig. 2.15 (a) B_r and H_c force Vs porosity in Ni-Zn ferrites and the calculated (solid curve), b) B_r and H_c force Vs grain size in Ni-Zn ferrites and the calculated (solid) curves from Igarishi (2.34)

2.5 Magnetic Properties of Solids

Materials may be classified by their response to externally applied magnetic fields as diamagnetic, paramagnetic and ferromagnetic. These magnetic responses differ greatly in strength. Diamagnetism is property of all materials and opposes applied magnetic fields, but is very weak paramagnitism, when present, is stronger than diamagnetism and produces magnetization in the direction of the applied field and proportional to the applied field. Ferromagnetic effects are very large, producing magnetizations sometimes

orders of magnitude grater than the applied field and as such arte much larger than either diamagnetic or paramagnetic effects. The magnetization of a material is expressed in terms of density of net magnetic dipole moments μ in the material. We define a vector quantity called the magnetization M by

$$M = \frac{\mu_{total}}{V} \tag{2.34}$$

when the total magnetic field B in the material is given by

$$B = B_0 + \mu_0 M \tag{2.35}$$

where μ_0 is the magnetic permeability of space and B_0 is the externally applied magnetic field. When magnetic fields inside of materials are calculated using Ampere's law or the Biot- Savart law, then the μ_0 in those equations is typically replaced by just μ with the definition

$$\mu = \mu_r \mu_0 \tag{2.36}$$

where μ_r is called the relative permeability. If the material does not respond to the external magnetic field by producing any magnetization then $\mu_r = 1$. Another commonly used magnetic quantity is the magnetic susceptibility

$$\chi = \mu_r - 1 \tag{2.37}$$

For paramagnetic and diamagnetic materials the relative permeability is very close to 1 and the magnetic susceptibility very close to zero. For ferromagnetic materials, these quantities may be very large. Another way to deal with the magnetic fields which arise from magnetization of materials is to introduce a quantity called magnetic field strength H. It can be defined by the relationship

$$H = \frac{B_0}{\mu_0} = \frac{B}{H_0} - M \tag{2.38}$$

and has the value of unambiguously designating the driving magnetic influence from external currents in a material independent of the materials magnetic response. The relationship for B above can be written in the equivalent form

$$B = \mu_0 (H + M) \tag{2.39}$$

H and M will have the same units, amperes/meter

The magnetic susceptibility (χ) is defined as the ratio of magnetization to magnetic field

$$\chi = \frac{M}{H} \tag{2.40}$$

The permeability and susceptibility of a material is correlated with respect to each other by

$$\mu = \mu_0(1 + \chi) \tag{2.41}$$

2.5.1 Magnetic Domains and Domain Wall Motion

- In addition to susceptibility differences, the different types of magnetism can be distinguished by the structure of the magnetic dipoles in regions called domains.

- Each domain consists of magnetic moments that are aligned, giving rise to a permanent net magnetic moment per domain.

- Each of these domains is separated from the rest by domain boundaries / domain walls. Boundaries, also called Bolch walls, are narrow zones in which the direction of the magnetic moment gradually and continuously changes from that of one domain to that of the next.

- The domains are typically very small about 50 μm or less, while the Bloch walls are about 100 nm thick. For a polycrystalline specimen, each grain may have more than one microscopic sized domain.

- Domains exist even in absence of external field.

- In a material that has never been exposed to a magnetic field, the individual domains have a random orientation. This type of arrangement represents the lowest free energy.

- When the bulk material is un-magnetized, the net magnetization of these domains is zero, because adjacent domains may be orientated randomly in any number of directions, effectively canceling each other out.

- The average magnetic induction of a ferro-magnetic material is intimately related to the domain structure.

- When a magnetic field is imposed on the material, domains that are nearly lined up with the field grow at the expense of unaligned domains. This process continues until only the most favorably oriented domains remain.

- In order for the domains to grow, the Bloch walls must move, the external field provides the force required for this moment.
- When the domain growth is completed, a further increase in the magnetic field causes the domains to rotate and align parallel to the applied field. At this instant material reaches saturation magnetization and no further increase will take place on increasing the strength of the external field.
- Under these conditions the permeability of these materials becomes quite small.
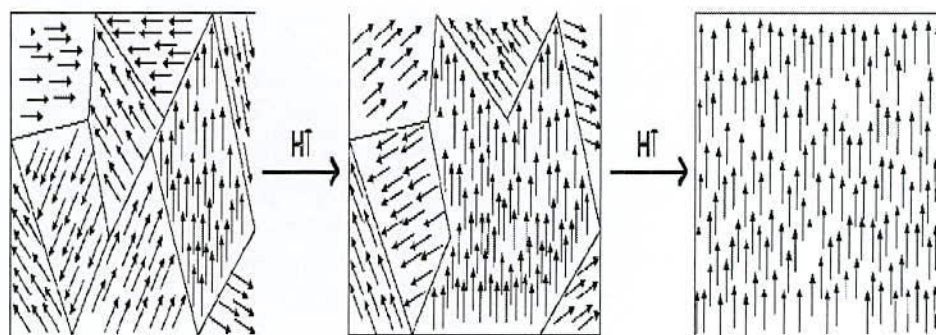
Fig. 2.16 Rotation of orientation and increase in size of magnetic domains due to an externally applied field

In magnetism, a domain wall is an interface separating magnetic domains. It is a transition between different magnetic moments and usually undergoes an angular displacement of 90° or 180°. Although they actually look like a very sharp change in magnetic moment orientation, when looked at in more detail there is actually a very gradual reorientation of individual moments across a finite distance [2.36]. The energy of a domain wall is simply the difference between the magnetic moments before and after the domain wall was created. This value is more often than not expressed as energy per unit wall area. The width of the domain wall varies due to the two opposing energies that create it: the Magnetocrystalline anisotropy energy and the exchange energy, both of which want to be as low as possible so as to be in a more favorable energetic state. The anisotropy energy is lowest when the individual magnetic moments are aligned with the crystal lattice axes thus reducing the width of the domain wall, whereas the exchange energy is reduced when the magnetic moments are aligned parallel to each other and thus makes the wall thicker, due to the repulsion between them (where anti-parallel alignment

would bring them closer - working to reduce the wall thickness). In the end equilibrium is reached between the two and the domain wall's width is set as such. An ideal domain wall would be fully independent of position; however, they are not ideal and so get stuck on inclusion sites within the medium, also known as crystallographic defects. These include missing or different (foreign) atoms, oxides, and insulators and even stresses within the crystal. In most bulk materials, we find the Bloch wall: the magnetization vector turns bit by bit like a screw out of the plane containing the magnetization to one side of the Bloch wall. In thin layers (oft the same material), however, **Neél walls** will dominate. The reason is that Bloch walls would produce stray fields, while Neél walls can contain the magnetic flux in the material [2.15]
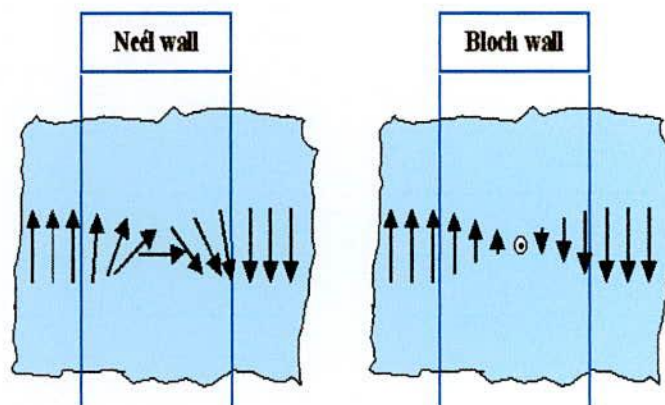
Fig. 2.17 The magnetization change from one direction to another one

2.5.2 Magnetostatic or Demagnetization Energy

If a material consists of a single domain than it behave as a block magnet. The external demagnetizing field has a magneto static energy that depends on the shape of the sample and is the field that slows work to be done by the magnetized sample in order to minimize static energy must be minimized .This can be achieved by decreasing the external demagnetizing field by dividing the material in to domain. Adding extra domains increase the exchange energy as the domain increase the exchange energy as the domains cannot align parallel, however the total energy has been decreased as the magneto static energy in the dominant effect. The magneto static energy can be reduced to zero by a domain structure that leaves no external demagnetizing field is the main driving force for the formation of domains.

49

2.5.3 Domain Wall Size Model

Domain wall size model [2.37, 2.38], has provided a phenomenological approach for the study of magnetization mechanism in polycrystalline ferrites. This model assumes a single Bloch wall which divides a spherical grain, for zero applied field. The domain wall is pinned t the grain boundary and a small applied field produces a reversible, spherical bulging. As the applied field increases, the domain wall is depinned from the gain boundary and is displaced with the bulged shape to a non-diametrical position with the grain. The value of the field for which the depinning occurs in the critical field, H_{ct} and this value separates the reversible magnetization range from the irreversible, hysteresis range. The critical field is proportional to the inverse of the grain size. As the applied field decreases, the domain wall becomes plane while pinned to the grain boundary in its new position, giving rise to non-zero magnetization value for zero applied field is the remanent magnetization. The application of an opposite field produces a bulging in the direction until the value of the critical field (for the new position) is attained. The domain wall is depinned and displaced to an equivalent position in the opposite side of the grain. The field is decreased and the domain wall becomes again a plane wall, leading to a remanent magnetization value for the opposite orientation. Cycling of the applied field thus produces a combination of bulging, depinning, and displacement that leads to a complete hysteresis loop. It has been shown that on the basis of these ideas, it is possible to establish the corresponding magnetization equation, as a function of an applied field, to obtain analytical prediction of the hysteresis loops [2.39]. This prediction can accurately model [2.40], experimental loop when the grain diameter distribution is taken into account.

2.5.4 Magnetocrystalline Anisotropy Energy

In some materials the domain magnetization tends to align in a particular crystal direction (the so-called easy axis). The material is easiest to magnetize to saturation or demagnetize from saturation if the field is applied along an easy axis. The energy difference between aligning the domain in the easy and another direction (hard direction) is called magnetocrystalline anisotropy energy. Anisotropy energy is the energy needed to rotate the moment from the easy direction to a hard direction. For materials with cubic

crystalline structure (such as ferrites), the energy is expressed in terms of anisotropy constants and the direction to which the magnetization rotates.

$$E_k = K_1 \sin^2 \theta + K_2 \sin^4 \theta ... \qquad \text{(hexagonal structure)} \qquad (2.42)$$

$$E_k = K_1 (\alpha_1^2 \alpha_2^2 + \alpha_2^2 \alpha_3^2 + \alpha_3^2 \alpha_1^2) + K_2 (\alpha_1^2 \alpha_2^2 \alpha_3^2 + ... \quad \text{(cubic structure)} \qquad (2.43)$$

where, K is the anisotropy constant, θ is the angle between the easy axis and the direction of magnetization, and α's are the direction cosines, which are the ratios of the individual components of the magnetization projected on each axis divided by the magnitude of the magnetization. A crystal is higher in anisotropy energy when the magnetization points in the hard direction rather than along the easy direction. The formation of domains permits the magnetization to point along the easy axis, resulting in a decrease in the net anisotropy energy.

i)   **Magnetostrictive energy:** In a magnetic field, the material may change its dimensions on the order of several parts per million. This change in dimension results in what is called magnetostrictive energy, which is lowered by a reduction in the size of the domains, requiring the formation of more domains.

ii)   **Domain wall energy:** This is energy resulting from the increase or decrease in the width of the walls due to the growth/shrinkage of domains.

The magnetization in a domain changes by two mechanisms: Rotation of the magnetic dipoles toward the direction of the applied field and change in the domain volume. In the first case, a certain amount of anisotropy energy is needed to rotate the magnetization in a crystal from the easy to another axis. In the second mechanism, the volume of the domain changes, changing its contribution to the bulk magnetization, while the magnetization direction is unchanged. The change in the magnetization intensity of a domain depends on how close its direction is to the direction of the applied field. If the magnetization direction is close, the intensity in the domain increases, whereas if it is far, the intensity decreases.

The domain volume changes due to motion of the domain wall. This movement is originated by a torque that rotates the moments of the domain in line with the field, moving the center of the wall toward the domain opposed to the field. Consequently, the volume of the domains whose direction is favorable is increased whereas the domains

with unfavorable direction decrease in volume [2.5]. In order to explain the fact that ferromagnetic materials with spontaneous magnetization could exist in the demagnetized state Weiss proposed the concept of magnetic domains. The magnetization within the domain is saturated and will always lie in the easy direction of magnetization when there is no externally applied field. The direction of the domain alignment across a large volume of material is more or less random and hence the magnetization of a specimen can be zero.

Magnetic domains exist in order to reduce the energy of the system. A uniformly magnetized specimen as shown in Fig. 2.18 (a) has a large magnetostatic energy associated with it. This is the result of the presence of magnetic free poles at the surface of the specimen generating a demagnetizing field, H_d. From the convention adopted for the definition of the magnetic moment for a magnetic dipole the magnetization within the specimen points from the south pole to the north pole, while the direction of the magnetic field points from north to south. Therefore, the demagnetizing field is in opposition to the magnetization of the specimen. The magnitude of H_d is dependent on the geometry and magnetization of the specimen. In general if the sample has a high length to diameter ratio (and is magnetized in the long axis) then the demagnetizing field and the magnetostatic energy will be low.
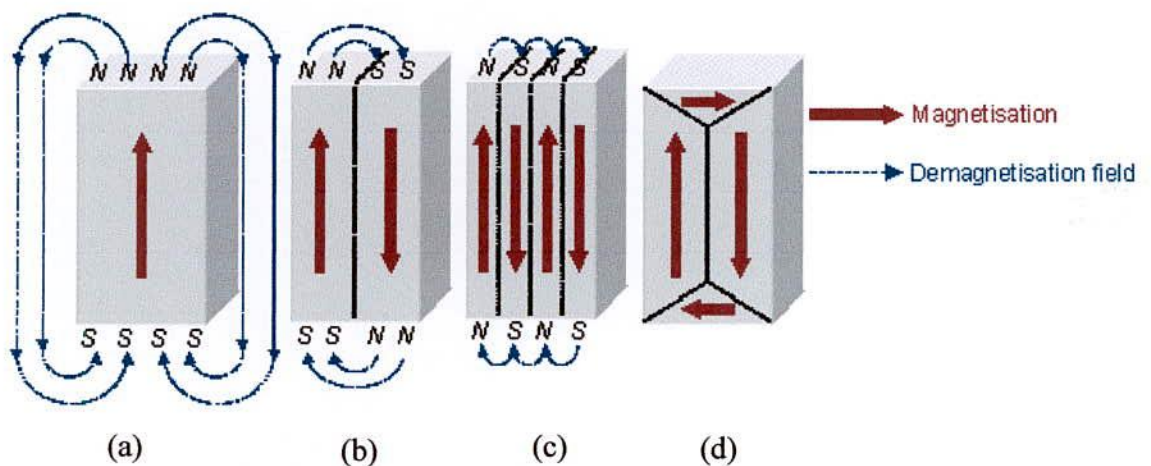
Fig. 2.18 Schematic illustration of the break up of magnetization into domains (a) single domain, (b) two domains, (c) four domains and (d) closure domains

The break up of the magnetization into two domains as illustrated in Fig. 2.18(b) reduces the magnetostatic energy by half. In fact if the magnet breaks down into N domains then the magnetostatic energy is reduced by a factor of $\frac{1}{N}$, hence Fig. 2.18(c) has a quarter of the magnetostatic energy of Fig. 2.18(a). Fig. 2.18(d) shows a closure domain structure where the magnetostatic energy is zero, however, this is only possible for materials that do not have a strong uniaxial anisotropy, and the neighbouring domains do not have to be at 180° to each other.

2.5.5 Magnetostriction

As a material showing magnetostrictive behavior can change its shape and size under the application of a varying magnetic field. The phenomenon was discovered in 1842 by J. Joule. In ferromagnets and ferrimagnets (such as iron, nickel, cobalt, gadolinium, and terbium, as well as a number of alloys and ferrites), magnetostriction reaches a significant magnitude (relative extension $\Delta l/l \sim 10^{-6}\text{-}10^{2}$). Magnetostriction is very small in antiferromagnets, paramagnets, and diamagnets. The change of length of a ferromagnetic substance when it is magnetized. More generally, magnetostriction is the phenomenon that the state of strain of a ferromagnetic sample depends on the direction and extent of magnetization. The phenomenon has an important application in devices known as magnetostriction transducers.

The magnetostrictive effect is exploited in transducers used for the reception and transmission of high-frequency sound vibrations. Nickel is often used for this application. The phenomenon that is the inverse of magnetostriction a change in the magnetization of a ferromagnetic specimen upon deformation is called the magnetoelastic effect, or sometimes the Villari effect.

In the modern theory of magnetism, magnetostriction is considered to be a result of the manifestation of the fundamental types of interactions in ferromagnetic bodies (electrical exchange interaction and magnetic interaction). Accordingly, two types of essentially different magnetostriction deformations of a crystal lattice are possible: those resulting from a change in magnetic forces (dipole-dipole and spin-orbital deformations) and those resulting from a change in exchange forces.

Magnetostriction caused by exchange forces is observed in ferromagnets in the region of magnetization above technical saturation, where the magnetic moments of the domains are fully oriented in the direction of the field and only an increase in the absolute magnitude of J_s (the paraprocess, or true magnetization) takes place. Magnetostriction caused by exchange forces in cubic crystals is isotropic that is, it is manifested in a change in the volume of the body. In hexagonal crystals (such as gadolinium), such magnetostriction is anisotropic. In most ferromagnetic substances at room temperature, magnetostriction resulting from the paraprocess is small; it is also small close to the Curie point, where the paraprocess almost entirely determines the ferromagnetic properties of a substance. Significant magnetostriction of the paraprocess is also found in ferrites upon annihilation or creation of noncollinear magnetic structures by a magnetic field. Magnetostriction is widely used in technology. It is the basis for the operation of magnetostriction transformers (sensors) and relays, ultrasonic radiators and receivers, filters and frequency stabilizers in electronic devices, and magnetostriction delay lines.

2.5.6 Theories of Permeability

Permeability is namely defines as the proportional constant between the magnetic field induction B and applied intensity H:

$$B = \mu H \tag{2.44}$$

If a magnetic material is subjected to an AC magnetic field as given below:

$$H = H_0 e^{i\omega t} \tag{2.45}$$

Then it is observed that the magnetic flux density B experiences a delay. The delay is caused due to presence of various losses and is thus expressed as

$$B = B_0 e^{i(\omega t - \delta)} \tag{2.46}$$

where δ is the phase angle and marks the delay of B with respect to H. The permeability is then given by

$$\mu = \frac{B}{H} = \frac{B_0 e^{i(\omega t - \delta)}}{H_0 e^{i\omega t}} \tag{2.47}$$

$$= \frac{B_0 e^{-i\delta}}{H_0} = \mu' - i\mu'' \tag{2.48}$$

$$\text{Where} \qquad \mu' = \frac{B_0}{H_0} \cos \delta \qquad\qquad (2.49)$$

$$\mu'' = \frac{B_0}{H_0} \sin \delta \qquad\qquad (2.50)$$

The real Part μ' of complex permeability μ as expressed in eqⁿ. (2.48) represent the component of B which is in phase with H, so it corresponds to the normal permeability. If there is no losses , we should have $\mu = \mu'$, The imaging part μ'' corresponds to the part of B which is delayed by phase angle arranging up to 90° from H . The presence of such a component requires a supply of energy to maintain the alternating magnetization regardless of the origin of delay.

The ratio of μ'' to μ' gives

$$\frac{\mu'}{\mu''} = \frac{\dfrac{B_0}{H_0} \sin \delta}{\dfrac{B_0}{H_0} \cos \delta} = \tan \delta \qquad\qquad (2.51)$$

This tan δ is called the loss Factor or loss tangent. The Q-Factor or quality factor is defined as the reciprocal of this loss factor, i.e

$$Q = \frac{1}{\tan \delta} \qquad\qquad (2.52)$$

2.6   Transport Properties

Ferrites are ferromagnetic semiconductors that could be used in electronic devices. The increasing demand for low loss ferrites resulted in detailed investigations on conductivity and on the influence of various substitutions on the electrical conductivity, thermoelectric power, etc. The conduction mechanism in ferrites is quite different from that in semiconductors. In ferrites, the temperature dependence of mobility affects the conductivity and the carrier concentration is almost unaffected by temperature variation. In semiconductors, the band type conduction occurs, where in ferrites, the cations are surrounded by closed pack oxygen anions and as a first approximation can well be treated as isolated from each other. There will be a little direct overlap of the anion charge clouds or orbital. In other words, the electrons associated with particular ion will largely remain isolated and hence a localized electron model is more appropriate than a collective electron (band) model. This accounts for the insulating nature of ferrites.

These factors led to the hopping electron model [2.41]. An appreciable conductivity in these ferrites is found to be due to the presence of iron ion ions with different valence states at crystallographically different equivalent lattice sites [2.42]. Conduction is due to exchange of 3d electron, localized at the metal ions, from Fe^{3+} to Fe^{2+}. Various models have been suggested to account for the electrical properties. These are as follows

- Hopping model of electrons
- Small polaron model

2.6.1 DC Resistivity of Ferrites

Extensive investigation into the origin of the electrical conductivity of the spinels has been carried out by Verwey [2.43] and later on by Van Uitert [2.44] and Jonker [2.45]. The resistivity of ferrites at room temperature can vary , depending on chemical composition between about 10^{-2} to higher than 10^{+11} ohm-cm [2.14]. The low value of resistivity is due to the simultaneous presence of ferrous and ferric ions on equivalent lattice sites (octahedral) as proposed by Verwey [2.43]. For example Fe_3O_4 at room temperature has resistivity of approximately 7×10^{-3} Ohm-cm and Fe_2O_4 with some deficiency in iron and sintered in a sufficiently oxidizing atmosphere so that the product contains no ferrous ions can have a resistivity higher than 7×10^6 ohm-cm. To make high resistivity ferrites one must sure that there are no ferrous ions in the stoichiometric ferrites.

Temperature dependent resistivity of ferrites follows Arrhenius relation [2.14]:

$$\rho = \rho_0 e^{\frac{E_a}{kT}}, \tag{2.53}$$

Where ρ is the resistively and E_a is the activation energy required for hopping of an electron from one lattice site to another.

2.6.2 AC Resistivity Ferrites

AC resistivity is an important property of ferrites material. Ferrites material has high intrinsic resistivity. It can be changed with change of frequency and temperature.

2.6.3 Thermopower

The Hall effect and the thermoelectric measurements usually describe the conduction mechanism in semiconductors. The Hall effect gives precise results, but in case of low mobility materials such as ferrites, it is sometime difficult to measure the Hall effect. Under such circumstances the thermoelectric power is the only alternative. The sign of the thermo-emf gives vital information about the type of conduction in semiconductors whether it is p- or n-type. There are two methods of thermopower measurement [2.46];

(i)   Integral Method

(ii) Differential Method

2.6.3.1   Integral Method

One end of the specimen is kept at a fixed temperature T_1 while the temperature T_2 of the other end is made to vary through the desired range. The thermoelectric power voltage V developed across the sample is measured as a function of the temperature T, i.e.

$$V(T) = \int_{T_1}^{T_2} a\, dT \tag{2.54}$$

2.6.3.2 Differential method

A small temperature difference ΔT is established across the sample to induce a small thermoelectric voltage $\Delta V(T)$. The Seebeck coefficient is then determined from the relation:

$$\alpha(T) = \lim_{\Delta T \to o} \frac{\Delta V(T)}{\Delta T} \tag{2.55}$$

The accuracy of the this method demands that the ΔT to be sufficiently small, so that $\alpha(T)$ changes in the temperature interval ΔT. On the other hand ΔT must be large enough to generate a voltage that can be detected to the desired precision.

2.6.4 Conduction Mechanisms

Ferrites are ferrimagnetic semiconductors and exhibit interesting properties that could be used in electronic devices. That is why ferrites attracted the attention of the physicist. The increasing demand for low loss ferrites resulted in detailed investigations on conductivity and on the influence of various substitutions on the electrical conductivity, thermoelectric power, etc.

The conduction mechanism in ferrites is quite different from that in semiconductors. In ferrites the temperature dependence of mobility affects the conductivity and the carrier concentration is almost unaffected by temperature variation. In semiconductors the band type conduction occurs, where in ferrites, the cations are surrounded by closed pack oxygen anions and as a first approximation can well be treated as isolated from each other. There will be a little direct overlap of the anion charge clouds or orbital. In other words the electrons associated with particular ion will largely remain isolated and hence a localized electron model is more appropriate than a collective electron (band) model.

This accounts for the insulating nature of ferrites. These factors led to the hopping electron model [2.47]. An appreciable conductivity in these ferrites is found to be due to the presence of iron with different valence states at crystallographically different equivalent lattice points [2.48]. Conduction is due to exchange of 3d electrons, localized at the metal ions, from Fe^{3+} to Fe^{2+} [2.10]. Assuming that all the Fe^{2+} ions in the B-site to participate in the in hopping transport, the number of charge carriers (n) worked out to be $\sim 10^{22}/cm^3$. Since mobility is low, even though n is large.

Many models have been suggested to account for the electrical properties. These are as follows;

    (i) Hopping Model of Electrons

    (ii) Small Poloron Model

    (iii)Phonon Induced Tunneling

2.6.4.1 Hopping Model of Electrons

Jonker [2.45] suggested that in materials like ferrites there is a possibility of exchanging the valency of a considerable fraction of metal ions and especially that of iron ions.

In the presence of lattice vibrations however the ions occasionally come close enough together for transfer to occur with a high degree of probability. Thus only the lattice vibrations induce the conduction and the consequence the carrier mobility shows temperature dependence characterized by activation energy. For such a process of jumping of electrons and holes the motilities are given by;

$$\mu_1 = el_1 \, f_1 \left[\frac{e^{-\frac{E_1}{k_B T}}}{kT} \right] \quad \text{and} \qquad (2.56)$$

$$\mu_2 = el_2 \, f_2 \left[\frac{e^{-\frac{E_2}{k_B T}}}{kT} \right] \qquad (2.57)$$

where subscripts represent the parameters for electrons and holes, I represent jumping length, f_t and f_2 lattice frequencies active in the jumping process, E_1 and E_2 are activation energies involved in the required lattice deformation.

The general expression for the total conductivity in this case where we have two types of charge carriers can be given as;

$$\sigma = n_1 e \, \mu_1 + n_2 e \mu_2 \qquad (2.58)$$

The temperature dependence of conductivity arises only due to mobility and not due to the number of charge carriers in the sample. It was concluded that for hopping conduction;

- The mobility has a minimum value much lower than the limiting value (0.1 cm^2/Vs) taken as minimum for band conduction [2.49].
- The independence of Seebeck coefficient on temperature is due to fact that in hopping model the number of charge carriers is fixed.
- Thermally activated process with activation energy E_a called hopping activation energy.

- Occurrence of n-p transitions with charge carriers in the Fe^{2+} or oxygen concentration in the system.

2.6.4.2 Small Polaron Model

A small polaron is a defect created when an electronic carrier becomes trapped at a given site as a consequence of the displacement of adjacent atoms or ions. The entire defect (carrier plus distortion) then migrates by an activated hopping mechanism. Small polaron formation can take place in materials whose conduction electrons belong to incomplete inner (d or f) shells which due to small electron overlap, tend to form extremely narrow bands [2.50-2.53, 2.10]. The migration of small polaron requires the hopping of both the electron and the polarized atomic configurations from one site to an adjacent site. For a fcc lattice the drift mobility takes the form;

$$\mu = (1-c)e\,a\frac{2\Gamma}{kT} \tag{2.59}$$

where e is the electronic charge, a is the lattice constant, c is the fraction of sited which contain an electron $C = \dfrac{n}{N}$, n is the number of electrons and N is the jump rate of the polaron from one site to the particular neighboring site given by;

$$\Gamma = P\mu_0\,e^{-\frac{E_H}{kT}} \tag{2.60}$$

Here μ_o is the appropriate optical phonon frequency; E_H is the activation energy; p is the probability of the electron transfer after the polarized configuration has moved to the adjacent site. The small polaron model also explains the low mobility, temperature independence of the Seebeck coefficient and thermally activated hopping.

Chapter - III

Experimental Procedure

Experimental Procedure

3.1 Methodology of Ferrite Preparation

The ferrite is not completely defined by its chemistry and crystal structure but also requires knowledge and control of parameters of its microstructure such as density grain size, porosity and their intra and intergranular distribution. It is well known that almost all ferrites decompose at the elevated temperature of we want to melt them under normal condition. This happens because the oxygen splits off at higher temperature reducing Fe^{3+} and Fe^{2+}. This necessarily implies that in case of metals ferrite preparation by melting as is not possible. The normal methods of preparation of ferrites comprise of the conventional ceramic method or powder metallurgy, chemical co-precipitation method and sol-gel method.

In the present investigation conventional ceramic method has been employed for the preparation of Ni-Cu-Zn ferrite samples for its relative simplicity and availability. The excellent powder preparation process and sintering facility available at the Magnetic Materials Division, Atomic Energy Centre, Dhaka has been utilized for the preparation of samples.

3.1.1 Compositions of the Studied Ferrite Systems

A series of mixed ferrites of various compositions were fabricated by solid state reaction technique keeping in view of their ionic radial and valances for maintaining the charge neutrality.

In the present research, several compositions of Ni-Cu-Zn soft ferrites are synthesized, characterized and investigated. The following compositions were fabricated characterized and investigated thoroughly:

(i) $(Ni_{0.28}Cu_{0.10}Zn_{0.62}O)(Fe_2O_3)_{1-x}$, [where x = 0.00, 0.02, 0.04, 0.06, 0.08]

(ii) $Ni_{0.28}Cu_{0.10+x}Zn_{0.62-x}Fe_{1.98}O_4$ [where x=0.00, 0.03, 0.06, 0.09, 0.12]

(iii) $Ni_{0.28}Cu_{0.10}Zn_{0.62}Fe_{1.98}O_4$ doped with V_2O_5, Li_2O [0.4 wt% each]

3.1.2 Sample Preparation Technique

The sample preparation of polycrystalline ferrites with optimum desired properties is still a complex and difficult task. Ferrites with optimized properties have always demanded delicate handling and caution approach in materials synthesis and appropriate knowledge of thermodynamics, control of the chemical composition and homogeneity. There are many processing methods such as solid state reaction method [3.1], high energy ball milling [3.2], Sol-gel method [3.3], chemical co-precipitation method [3.4], microwave sintering method [3.5], auto combustion method [3.6] etc for the preparation of polycrystalline ferrite materials. They are mainly divided into two groups.

(i)   Conventional Ceramic Method, i.e. Solid State reaction method, involves milling of reactants followed by sintering at elevated temperature.

(ii) Non-conventional method also called wet-method, which include processes: Sol-Gel synthesis, chemical co-precipitation method, organic precursor method, reverse micelle's method, co-spray roasting, activated sintering, etc.

In the present investigation solid state reaction has been employed for the preparation of Ni-Cu-Zn ferrite samples for its simplicity and availability.

The overall preparation process generally comprised of the following four major steps:

(i)   Preparing a mixture of desired composition
(ii)   Pre sintering the mixture to form ferrite
(iii) Converting the Raw ferrite into powder and pressing the powder
(iv)   Sintering.

The sintering process is irreversible in terms of microstructure, so that constant care could be maintained to keep conditions constant prior to and during sintering. A brief discussion given below will give us the idea about the above mentioned four major steps.

3.1.2.1 Preparing a Mixture of Materials

The extend of this work in these step greatly, depending on the starting materials, when component oxide are used, the corresponding step involves a mere mixing of the oxides by wet milling. To avoid iron contamination, mixing is done with stainless steel

balls in a steel ball milling machine and a fluid such as distilled water is used to prepare the mixture into slurry. Ferric oxide, Fe_2O_3 and whatever oxides, MO are required are taken in powder form with the captions in the ratio corresponding to that in the final product. Metal carbonate may also be used; during the later firing, Co_2 will be given off and they will be converted to oxides.

3.1.2.2 Pre-sintering the Mixture to Form Ferrite

The slurry prepared in step-1 is dried, palletized and then transferred to a porcelain crucible for pre sintering in a constant temperature of 850°C for $4\frac{1}{2}$ hours. Presintering of the materials were preformed in a furnace named Gallen Kamp at AECD (Atomic Energy Centre, Dhaka). The cooling and heating rates were 4°C/min. The pre-sintering is very crucial because in this step of sample preparation of ferrite is formed form its component oxides. The solid-state reactions, leading to the formation of ferrites, actually achieved by counter diffusion. This means that the diffusion involves two or more species of ions, which more in opposite direction initially across the interface of two contacting particles of different component oxides.

The following block diagram in Fig. 3.1 represents the method employed for the Ni-Cu-Zn-ferrites
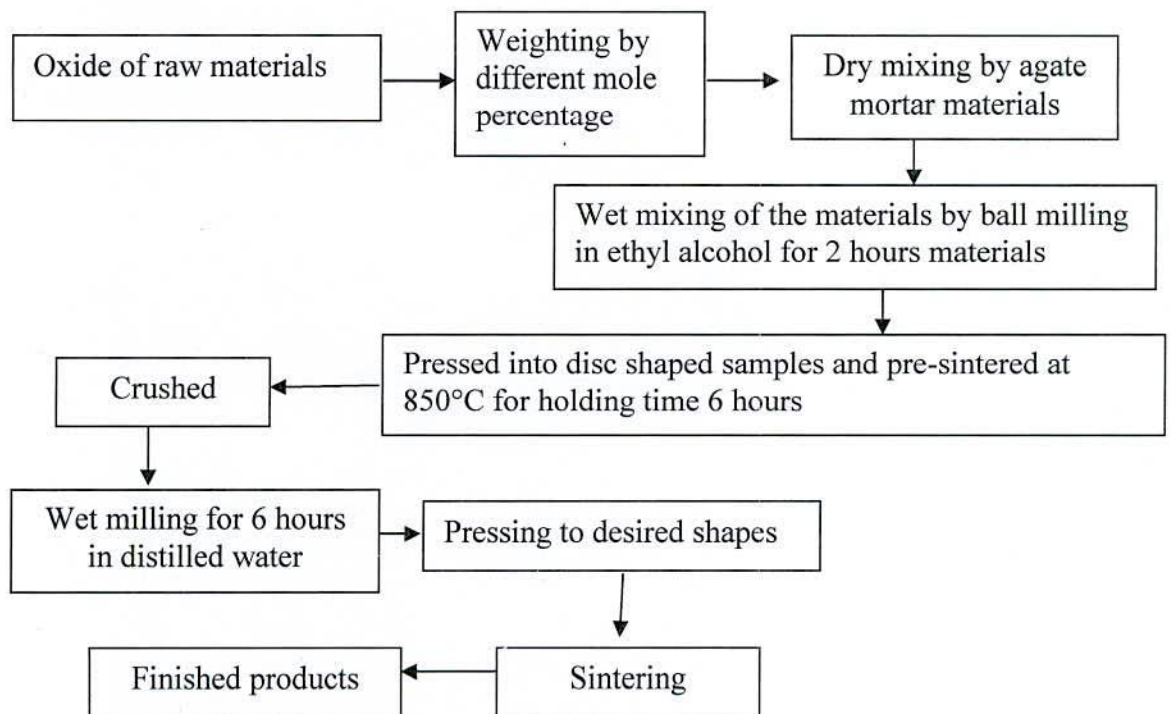
Fig.3.1 Flowchart of ferrite sample preparation

During the pre-sintering stage, the reaction of Fe_2O_3 with metal oxide of MO (M is divalent metal in) takes place in the solid state to form ferrite.

For Ni-ferrite

$NiO + Fe_2O_3 \rightarrow NiFe_2O_4$

For Ni-Zn ferrite

$(1-x) NiO + xZnO + Fe_2O_3 \rightarrow Ni_{1-x}Zn_xFe_2O_4$
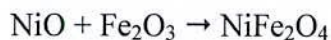
The reaction of the Ni-Cu-Zn ferrite is as follows

$(0.28)NiO + (0.62 - x) ZnO + (0.1+x) Cu + 1.98 Fe_2O_3 \rightarrow Ni_{0.28}Cu_{0.1+x} Zn_{0.62-x} Fe_{1.98}O_4$ [x= 0.00, 0.03, 0.06, 0.09, 0.12]

The reaction of the Ni-Cu-Zn ferrite finally

$0.28 NiO + 0.62 ZnO + 0.10 CuO + (Fe_2O_3)_{1-x} \rightarrow (Ni_{0.28}Cu_{0.10}Zn_{0.62}O) (Fe_2O_3)_{1-x}$ [where x = 0.00, 0.02, 0.04, 0.06, 0.08]
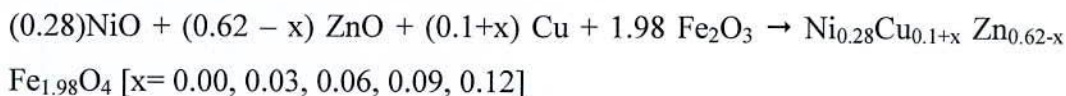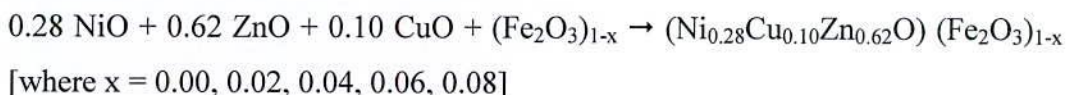
The ferrite is formed essentially in the pre-sintering step but the 'raw' ferrite formed has poor quality. In order to produce chemically homogeneous, dense and magnetically better material of desired shape and size, sintering at an elevated temperature is needed.

3.1.2.3 Converting the Raw Ferrite into Powder and Pressing the Powder

To promote successful sintering in the next step, the powder must be well characterized after grinding with respect to such factors as particle size and distribution particle shape, homogeneity, absorbed gases, impurities and intra particle porosity. Iron contamination due to continuous wear of the mill wall and still ball need to be closely watched and minimized. Now to the ground homogeneous powder polyvinyl alcohol is added as a binder. Pressing the powder into compacts of desired shapes is done either by conventional method in a die-punch assembly or by hydrostatic or isostatic compaction. By conventional method in a die-punch asembly a uniformly dense body is difficult owing to the friction gradient of the powder at the walls of the die and between the particles themselves. This problem is some what overcome by the addition of external and internal lubricant to the powder such as a satiric acid.

Mainly, we made three types of samples cylindrical, Tablet and toroidal. Specimen was prepared by a hydraulic press with a pressure at $1 - 10$ ton/cm^2 $14 - 140$

MPa. The die was designed and made in the workshop of AECD. This is made of nonmagnetic stainless steel.

3.1.2.4 Sintering

Sintering commonly refers to processes involved in the heat treatment of powder compacts at elevated temperatures where diffusion mass transport is appreciable. Sintering is traditionally used for manufacturing ceramic objects, and has also found uses in such fields as powder metallurgy. Successful sintering usually results in a dense polycrystalline solid. However, sintering can proceed only locally (i.e. at contact point of grains), without any appreciable change in the average overall density of a powder compact.

Ceramic processing is based on the sintering of powder compacts rather than melting / solidification / Cold working (Characteristics for metals), because:

(i)   Ceramics melt at high temperature

(ii)   As solidified microstructures cannot be modified through additional plastic deformation and re-crystallization due to brittleness of ceramics

(iii)   The resulting coarse grains would act as facture initiation sites

(iv)   Low thermal inductivities of ceramics (< 30 - 50 W/mK), in contract to thermal conductivity not metals (in the range 50 – 300 W/mK) cause large temperature gradients, and thus thermal stress and shock in melting-solidification of ceramics.

This is a heat treatment by which a mass of compacted powder is transformed into a dense object. This is the final and critical step of sample preparation. Sintering is the bonding together of a porous aggregate of particles at high temperature. The thermodynamic driving force is the reduction in the specific surface area of the particles. The sintering mechanism usually involves atomic transport over particle surfaces, along grain boundaries and through the particle interiors. Sintering may result in densification, depending on the predominant diffusion pathway. It is used in the fabrication of metal and ceramic components, the agglomeration of ore fines for further metallurgical processing and occurs during the formation of sandstones and glaciers. Sintering must fulfill three requirements

- to bond the particles together so as to impart sufficient strength to the product
- to density the grain compacts by eliminating the pores and

- to complete the reactions left unfinished in the pre-sintering step.

The theory of heat treatment is based on the principle that when a material has been heated above a certain temperature, it undergoes a structural adjustment or stabilization when cooled at room temperature. The cooling rate plays an important role on which the structural modification is mainly based.

Sintering can be enhanced by the presence of a liquid phase. If the constitution point of an alloy during sintering falls in a solid plus liquid region of the phase diagram, then the liquid persists throughout sintering. Transient liquid phase sintering occurs when the liquid phase is absorbed by the solid phase during sintering. Because the amount of liquid which forms, and the time for which it exists, is dependent on the sintering conditions, transient liquid phase sintering systems are process sensitive. The liquid phase can form directly from the elements when the sintering temperature is between the melting point of the matrix and the additive, by the melting of eutectic phase mixtures, which form by diffusion or by incipient melting. The liquid flows between the particles filling pores and causing densification by capillary action and through the provision of a fast diffusion pathway. Shrinkage occurs by particle rearrangement if the liquid volume is high enough and the green density is low enough, by the particles changing shape to allow better packing, by pore filling and by solid state sintering if a solid skeleton forms.

Why do we need Sintering?

The principal goal of sintering is the reduction of compact porosity. Sometimes the initial spaces between compacted grains of ceramics are called "voids", to differentiate them from the isolated spaces = pores, which occur in the final stages of sintering. The sintering process in usually accompanied by other changes within the material, some desirable and some undesirable. The largest changes occur in:

(i)   To bind the particles together so as to impart sufficient strength to the products

(ii)   To density the green compacts by eliminating the pores and

(iii)   To homogenize the materials by completing the reactions left unfinished in the pre-sintering step [3.7]

(iv)   To make strength of elastic modulus

(v)   To make hardness and fracture toughness

(vi)   To make homogenous distribution of grain number, grain size and shape

(vii)   To improve the average pore size and shape

(viii)   To get a stable chemical composition and crystal structure

Sintering is a widely used but very complex phenomenon. The fundamental mechanisms of sintering are still a matter of controversy. Experimental quantification of changes in pore fraction and geometry during sintering can be attempted by several techniques, such as: dilatometer, buoyancy, gas absorption, porosimetry, indirect methods (e.g. hardness) and quantitative microscopy etc. The description of the sintering process has been derived from model experiments (e.g., sintering of a few spheres) and by observing powdered compact behavior at elevated temperatures. The following phenomena were observed:

(i)   Increase of inter-particle contact area with time

(ii)   Rounding-off of sharp angles and points of contact

(iii)   In most cases, the approach of particle centers and overall densification

(iv)   Decrease in volume of interconnected pores

(v)   Continuing isolation of pores

(vi)   Grain growth and decrease in volume of isolated pores

3.1.3   Method of Sample Preparation

The ferrites of different compositions were prepared using ceramic technique involving solid state reaction from metal oxides (NiO, CuO, ZnO and Fe_2O_4) in the from of grained powder having 99.99%. Purity supplied by GmMH (E-merk, Germany). A series of polycrystalline, samples of mixed ferrites, were prepared by pressing and subsequent sintering. Different oxides were weighted precisely according to there molecular weight. The weight percentage of the oxide to be mixed for versions samples was calculated by using formula

$$\text{weight \% of oxide} = \frac{Molecular\ weigh\ of\ oxide \times required\ weight\ of\ the\ sample}{Sum\ of\ molecular\ weight\ of\ each\ oxide\ in\ a\ sample}$$

3.1.3.1 Solid state Reaction Method

The constituent in required stoichiometric proportions of materials were trough mixed using ceramic mortar and pestle for 4 hrs and then ball milled in a planetary ball mill in ethyl alcohol media for 2hrs with stainless steel balls of different sizes in diameter Fig. 3.2. The slurry was dried and the powder was pressed into disc shape. The disc shaped sample was pre-sintered at 850°C for 6hrs. The sample was then cooled down to room temperature at the same rate as that of heating. After that samples were crushed again and subsequently wet ball milled for 6hrs hours in distilled water to reduce it to small crystallites of uniform size. In order to produce chemically homogeneous and magnetically better material this prefired lump material was crushed.

These oxide mixtures were milled thoroughly for 4-6 hours to obtain homogeneous mixture. The mixture was dried and a small amount of saturated solution of polyvinyl alcohol (PVA) were added as a binder and pressed into pellet and toroid shape respectively under pressure 1.75 ton-cm^{-2} and 1.2 ton-cm^{-2} using hydraulic press Fig. 3.3. The prepared samples shown in Fig 3.4 were sintered at 1100°C-1200°C for 3 hrs with a microprocessor controlled muffle furnace. The samples were polished in order to remove any oxide layer formed during the process of sintering.
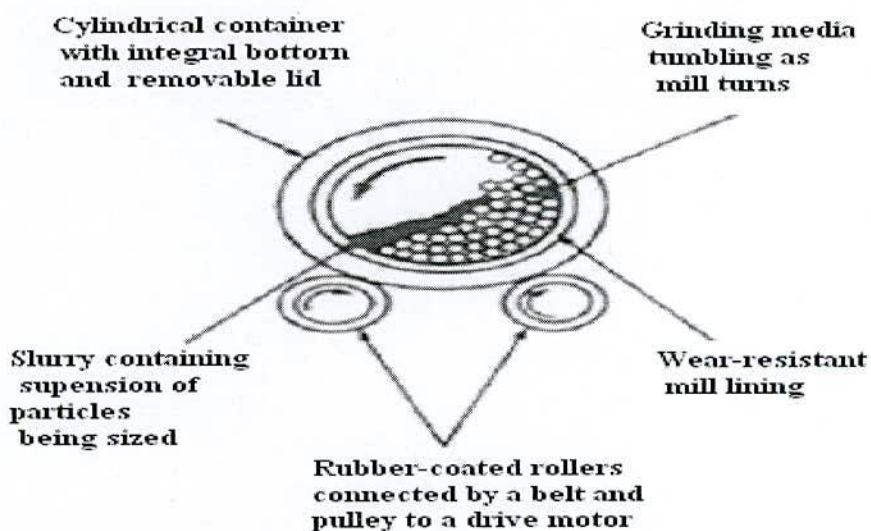
Fig. 3.2 Rubber-lined mill with stainless-steel balls

Fig. 3.3 Hydraulic press used to make different shaped samples
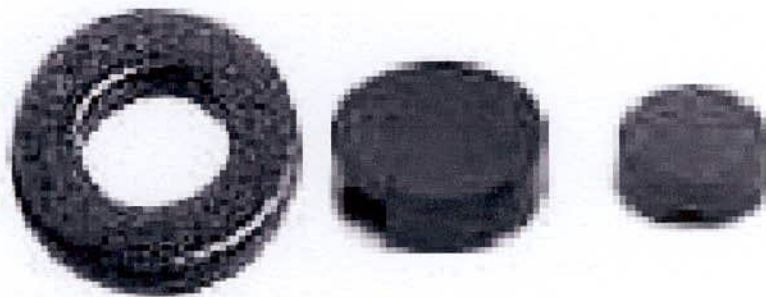
Fig. 3.4 Toroid and disk shape sample

3.2 X-ray Diffraction (XRD)

X-rays are the electromagnetic waves whose wavelength is in the neighborhood of 1Å. The wavelength of an X-ray is that the same order of magnitude as the lattice constant of crystals and it is this which makes X-ray so useful in structural analysis of crystals. X-ray diffraction (XRD) provides precise knowledge of the lattice parameter as well as the substantial information on the crystal structure of the material under study. X-ray diffraction is a versatile nondestructive analytical technique for identification and quantitative determination of various crystalline phases of powder or solid sample of any compound. When X-ray beam is incident on a material, the photons primarily interact with the electrons in atoms and get scattered. Diffracted waves from different atoms can interfere with each other and the resultant intensity distribution is strongly modulated by this interaction. If the atoms are arranged in a periodic fashion, as in crystals, the diffracted waves will consist of sharp interference maxima (peaks) with the same symmetry as in the distribution of atoms. Measuring the diffraction pattern therefore allows us to deduce the distribution of atoms in a material. It is to be noted here that, in diffraction experiments, only X-rays diffracted via elastic scattering are measured.

The peaks in an X-ray diffraction pattern are directly related to the atomic distance. Let us consider an incident X-ray beam interacting with the atoms arranged in a periodic manner as shown in two dimensions in Fig. 3.5. The atoms, represented as spheres in the illustration, can be viewed as forming different sets of planes in the crystal. For a given set of lattice planes with an inter-plane distance of d, the condition for a diffraction (peak) to occur can be simple written as

$$2d \sin n\theta = n\lambda \tag{3.1}$$
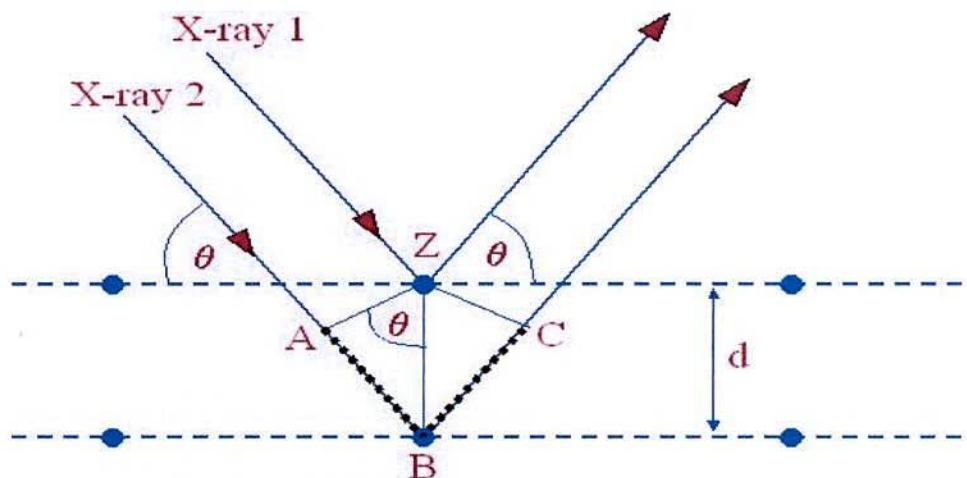
Fig. 3.5 Bragg's diffraction pattern

which is known as Bragg's law. In the equation, λ is the wavelength of the X-ray, θ is the scattering angle, and n is an integer representing the order of the diffraction peak. The Bragg's Law is one of the most important laws used for interpreting X - ray diffraction data. From the law, we find that the diffraction is only possible when $\lambda < 2d$ [3.8].

In the present work, A PHILIPS PW 3040 X'pert PRO X-ray diffractometer was used for the lattice parameter to study the crystalline phases of the prepared samples in the Materials Science division, Atomic Energy Centre, Dhaka. Fig. 3.6 shows the block diagram of X' pert XRD system.
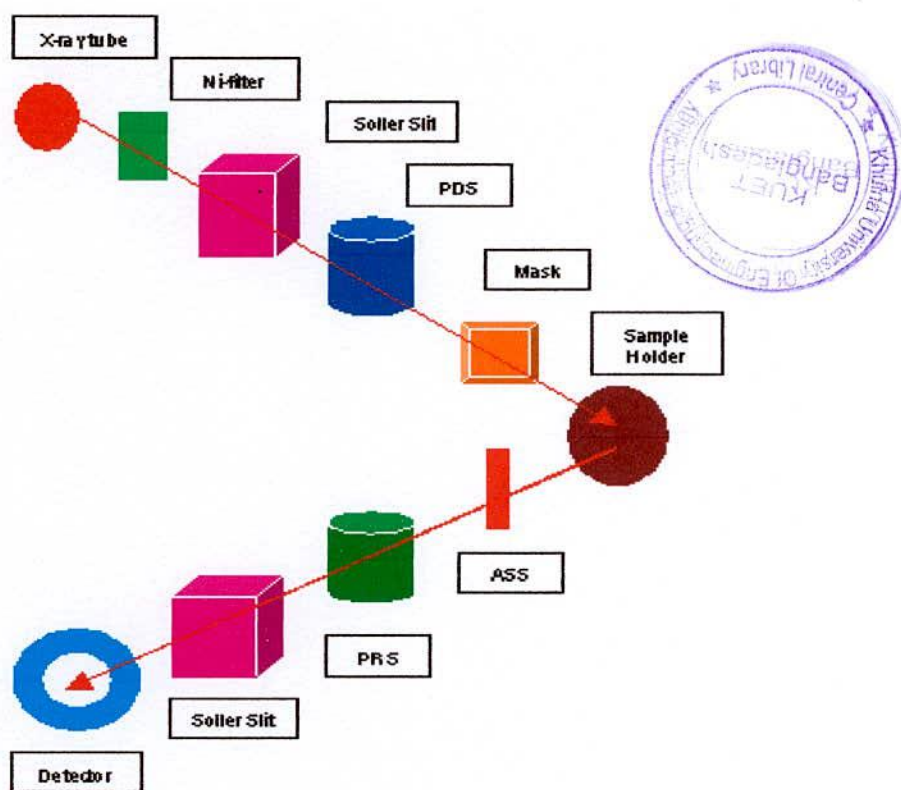
Fig. 3.6 Block diagram of the PHILIPS PW 3040 X' Pert PRO XRD system

The powder diffraction technique was used with a primary beam powder of 40 kV and 30mA for $Cu\text{-}K_{\alpha}$ radiation. A nickel filter was used to reduce $Cu\text{-}K_{\beta}$ radiation and finally $Cu\text{-}K_{\alpha}$ radiation was only used as the primary beam. The experimental has been performed at room temperature. A 2θ scan was taken from 15° to 75° to get possible fundamental peaks of the samples with the sampling pitch of 0.02° and time for each step data collection was 1.0 sec. Both the programmable divergence and receiving slits were

71

used to control the irradiated beam area and output intensity from the powder sample, respectively. An antiscatter slit was used just after the tube and in front of the detector to get parallel beam only. All the data of the samples were stored in the computer memory and later on analyzed them using computer "software, X' PERT HJGHS CORE". For XRD experiment each sample was set on a glass slide and fixed the sample by putting adhesive typed the two ends of the sample.

For each composition, the cylindrical samples of weight more than 2 gm are converted into powder. For XRD experiment each sample was set on a glass slide and fixed the sample by putting adhesive tape at the two ends of the sample X-ray diffraction patterns were carried out to confirm the crystal structure. Instrumental broadening of the system was determined from $\theta-2\theta$ scan of standard Si. At (311) reflection's position of the peak, the value of instrumental broadening was found to be $0.07°$. This value of instrumental broadening was subtracted from the pattern. After that, using the X-ray data, the lattice constant (a) and hence the X-ray densities were calculated.

3.2.1 Different Parts of the PHILIPS X' Pert PRO XRD System

Fig. 3.7 shows the inside view of the X' pert PRO XRD system. A complex of instruments of X- ray diffraction analysis has been established for both materials research and specimen characterization. These include facilities for studying single crystal defects, and a variety of other materials problems.

The PHILIPS X' Pert PRO XRD system comprised of the following parts;

(i)   "Cu-Tube" with maximum input power of 60 kV and 55 mA,

(ii)   "Ni- Filter" to remove $Cu-K_\alpha$ component,

(iii)   "Solar slit" to pass parallel beam only,

(iv)   "Programmable Divergent slits" (PDS) to reduce divergence of beam and control   irradiated beam area,

(v)   "Mask" to get desired beam area,

(vi)   "Sample holder" for powder sample,

(vii)   "Anti Scatter slit" (ASS) to reduce air scattering back ground,

(viii) "Programmable Receiving slit" (PRS) to control the diffracted beam intensity and

(ix)   "Solar slit" to stop scattered beam and pass parallel diffracted beam only.
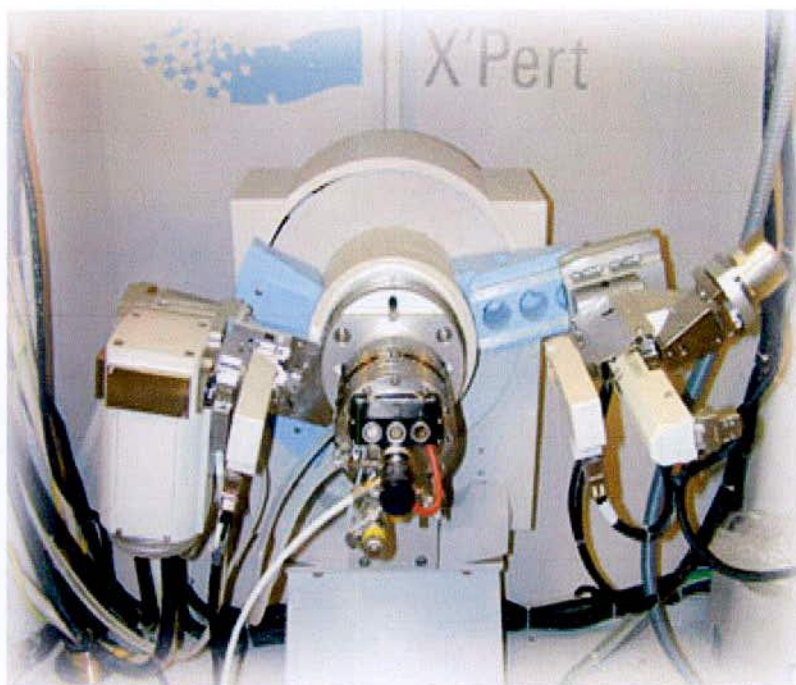
Fig. 3.7 Internal arrangement of a PHILIPS X' Pert PRO X-ray diffractometer

3.2.2 Interpretation of the XRD data

The XRD data consisting of θ_{hkl} and d_{hkl} values corresponding to the different crystallographic planes are used to determine the structural information of the samples like *lattice parameter and constituent phase*. *Lattice parameters of Co-ferrites samples* were determined. Normally, lattice parameter of an alloy composition is determined by the Debye-Scherrer method after extrapolation of the curve. We determine the lattice spacing (interplaner distance), d using these reflections from the equation which is known as Bragg's Law.

$$2d_{hkl}\, Sin\theta \,=\, \lambda$$

$$\text{i.e. } d_{hkl} \,=\, \frac{\lambda}{2\sin\theta} \tag{3.2}$$

where λ is the wavelength of the X-ray, θ is the diffraction angle and n is an integer representing the order of the diffraction.

The lattice parameter for each peak of each sample was calculated by using the formula:

73

$$a = d_{hkl} \times \sqrt{h^2 + k^2 + l^2} \qquad (3.3)$$

where h, k, l are the indices of the crystal planes. We get d_{hkl} values from the computer using software "X' Pert HJGHS CORE". So we got ten 'a' values for ten reflection planes such as a a_1 , a_2 a_3 ..... etc. Determine the exact lattice parameter for each sample, through the Nelson-Riley extrapolation method. The values of the lattice parameter obtained from each reflected plane are plotted against Nelson-Riley function [3.9]. The Nelson-Riley function F (θ), can be written as

$$F(\theta) = \frac{1}{2}\left[\frac{\cos^2 \theta}{\sin \theta} + \frac{\cos^2 \theta}{\theta}\right] \qquad (3.4)$$

where θ is the Bragg's angle. Now drawing the graph of 'a' vs F(θ) and using linear fitting of those points will give us the lattice parameter 'a_0'. This value of 'a_0' at F(θ) = 0 or θ = 90° .These 'a_0's are calculated with an error estimated to be ± 0.0001Å.

3.2.3 X-ray Density and Bulk Density

X-ray density, d_x was also calculated usual from the lattice constant. The relation between d_x and 'a' is as follows,

$$d_x = \frac{ZM}{Na^3} \qquad (3.5)$$

where M is the molecular weight of the corresponding composition, N is the Avogadro's number (6.023×10^{23} mole^{-1}), 'a' is the lattice parameter and Z is the number of molecules per unit cell (Z = 8 for the spinel cubic structure). The bulk density was calculated considering a cylindrical pellet of mass (m) and volume (V) of the pellets using the relation

$$d_B = \frac{m}{V} = \frac{m}{\pi r^2 h} \qquad (3.6)$$

where m is the mass of the pellet sample, r is the radius and h is the thickness of the pellet.

3.2.4 Porosity

Porosity is a parameter which is inevitable during the process of sintering of oxide materials. It is noteworthy that the physical and electromagnetic properties are strongly dependent on the porosity of the studied samples. Therefore an accurate idea of percentage of pores in a prepared sample is prerequisite for better understanding of the

various properties of the studied samples to correlate the microstructure property relationship of the samples under study. The porosity of a material depends on the shape, size of grains and on the degree of their storing and packing. The difference between the bulk density d_B and X-ray density d_x gave us the measure of porosity. Percentage of porosity has been calculated using the following relation [3.10]

$$P = (1 - \frac{d_B}{d_x}) \times 100\% \tag{3.7}$$

3.3 Permeability Measurement

3.3.1 Curie Temperature

Curie temperature measurement is one of the most important measurements because it provides substantial information on magnetic status of the substance in respect to the strength of exchange interaction. Above Curie temperature spontaneous magnetization vanishes and ferromagnetic materials behave like paramagnetic materials. So the determination of Curie temperature accurately is of great importance. The temperature dependence properties of ferrite materials depend upon its sublattice distribution and spin orientations of the metal ions and we can predict about the sublattice magnetization by measuring the Curie temperature.

There are several processes of measuring the Curie temperature; these are

(i)   by measuring magnetization against temperature,

(ii)   by measuring variation of initial permeability against temperature,

(iii)   by measuring susceptibility against temperature and

(iv)   by measuring the variation of resistivity of the sample against temperature.

In our present research work, we measured the Curie temperature of the samples by observing the variation of initial permeability of the ferrite samples with temperature and magnetization against temperature.

3.3.2 Measurement of Curie Temperature by Observing the Variation of Initial Permeability with Temperature

For ferrimagnetic materials in particular, for ferrite it is customary to determine the Curie temperature by measuring the permeability as a function of temperature. According

to Hopkinson effect [3.11] which arises mainly from the intrinsic anisotropy of the material has been utilized to determine the Curie temperature of the samples. According to this phenomenon, the permeability increases gradually with temperature and reaching to a maximum value just before the Curie temperature.

Curie temperature measurements were done by using Hewlett Packard 4192A LF Impedance Analyzer shown in Fig. 3.8. Impedance parameters absolute value of impedance ($|Z|$), absolute value of admittance ($|Y|$), phase angle (θ), resistance (R), reactance (X), conductance (G), susceptance (B), inductance (L), capacitance (C), dissipation (D) and quality factor (Q). Measurement range of $|Z|$ / R / X is $0.1 \text{m}\Omega$ to $1.2999 \text{ M}\Omega$, $|Y|$ /G/B is 1 ns to 12.999 s; θ is $-180°$ to $+180°$; L is 0.1mH to 1.000 kH; C is 0.1PF to 100.0 mF, D is 0.0001 to 19.999; Q is 0.1 to 1999.9. All have a basic accuracy of 0.1% and resolution of $4\frac{1}{2}$ digits. Number of display digits dependence on measuring frequency and OSC level setting. We made use of the excellent experimental facilities available at the Materials Science Division, Atomic Energy Centre, Dhaka.

The temperature dependent permeability was measured by using induction method. The specimen formed the core of the coil. The number of turns in each coil was 5. We used a constant frequency (100 kHz) of a sinusoidal wave, AC signal of 100mV. HP 4192A impedance analyzer with continuous heating rate of ≈ 5 K / min with very low applied ac field of $\approx 10^{-3}$ Oe. By varying temperature, inductance of the coil as a function of temperature was measured. Dividing this value of L_0 (inductance of the coil without core material), we got the permeability of the core i.e. the sample. When the magnetic state inside the ferrite sample changes from ferromagnetic to paramagnetic, the permeability falls sharply. From this sharp fall at specific temperature the Curie temperature was determined. For the measurement of Curie temperature, the sample was kept inside a cylindrical oven with a thermocouple placed at the middle of the sample. The thermocouple measures the temperature inside the oven and also of the sample.

The sample was kept just in the middle part of the cylindrical oven in order to minimize the temperature gradient. The temperature of the oven was then raised slowly. If the heating rate is very fast then the temperature of the sample may not follow the temperature inside the oven and there can be misleading information on the temperature

of the samples. The thermocouple showing the temperature in that case will be erroneous. Due to the closed winding of wires the sample may not receive the heat at once. So, a slow heating rate can eliminate this problem. The cooling and heating rates are maintained as approximately 0.5°C min^{-1} in order to ensure a homogeneous sample temperature. Also a slow heating ensures accuracy in the determination of Curie temperature.
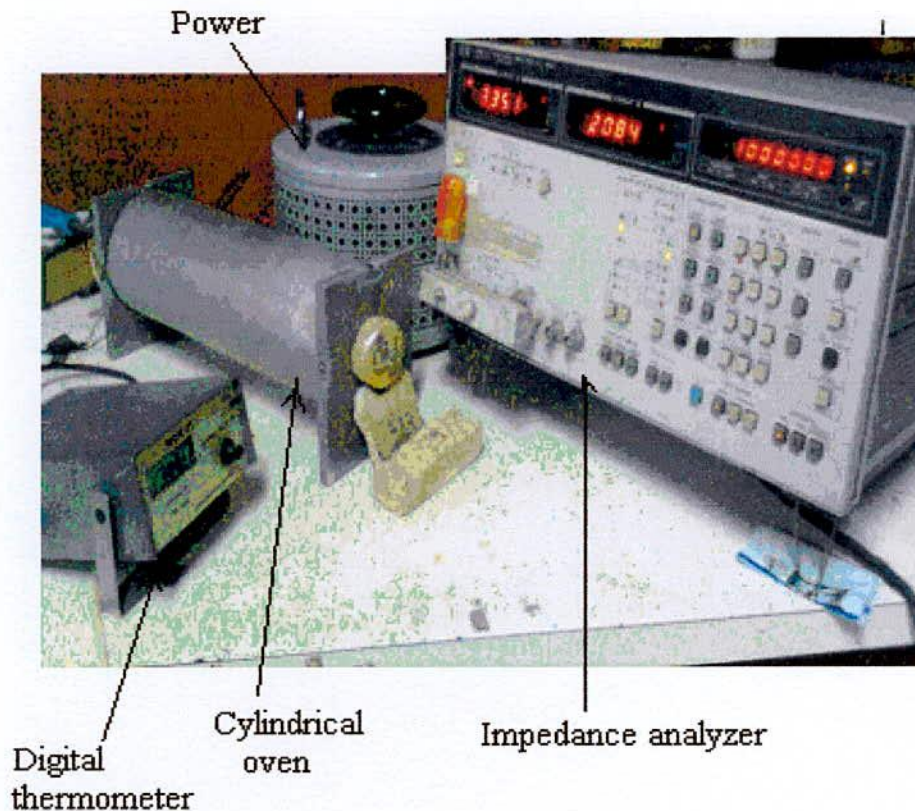
Fig. 3.8 Impedance Analyzer Model-Hewlett-Packard 4192A

The oven was kept thermally insulated from the surroundings. The temperature was measured with a digital thermometer attached close to the sample and put inside the furnace where the temperature fluctuation is almost negligible. Then the permeability versus temperature curve was plotted from which the Curie temperature was calculated.

3.3.3 Permeability

From the frequency dependence of complex permeability, evolution of permeability and magnetic loss component at different stages of ferrite sample as affected by thermal

treatment at different temperature was determined using toroids shape sample prepared with insulating Cu wire. The 4192 LF Impedance analyzer directly measure the value of inductance, L and loss factor.

$$D = \tan\delta \tag{3.8}$$

From inductance the value of real part of complex permeability, μ' can be obtained by using the relation

$$\mu' = \frac{L}{L_0} \tag{3.9}$$

where L is the inductance of the toroid and L_0 is the inductance of the coil of same geometric shape in vacuum, L_0 is determined by using the relation,

$$L_0 = \frac{\mu_0 N^2 S}{\pi \bar{d}} \tag{3.10}$$

Here μ_0 is the permeability of the vacuum, N is the number of turns (here N = 5), S is the cross-sectional area of the toroid shaped sample, S = dh, where, $d = \frac{d_1 \sim d_2}{2}$ and $\bar{d}$ is the average diameter of the toroid sample given as

$$\bar{d} = \frac{d_1 + d_2}{2} \tag{3.11}$$

where, d_1 and d_2 are the inner and outer diameter of the toroid samples.

3.3.4 Mechanisms of Permeability

Mechanisms of permeability can be explained as the following way: a demagnetized magnetic material is divided into number of Weiss domains separated by block walls. In each domain all the magnetic moments are oriented in parallel and the magnetization has its saturation value M_s. In the walls the magnetization direction changes gradually from the direction of magnetization in one domain to that in the next. The equilibrium positions of the walls results from the interactions with the magnetization in neighboring domains and from

the influence of pores; crystal boundaries and chemical in homogeneities which tend to favor certain wall positions.

3.3.5 Technique of Measurements of Permeability

Measurements of permeability normally involve the measurements of the change in self inductance of a coil presence of the magnetic core. The behavior of a self inductance can now be described as follows. Suppose we have an ideal lossless air coil of inductance L_o. On insertion of magnetic core with permeability μ, the inductance will be μL_o. The complex impedance Z of this coil can be expressed as,

$$Z = R + jX = j\omega L_o(\mu' - j\mu'') \tag{3.12}$$

where the resistive part is

$$R = \omega L_o \mu' \tag{3.13}$$

and the reactive part is

$$X = \omega L_o \mu'' \tag{3.14}$$

The radio frequency (RF) permeability can be derived from the complex impedance of a coil Z (Eqn. 3.12). The core is usually toroidal to avoid demagnetization effects. The quantity L_o is derived geometrically.

3.3.6   Frequency Characteristic of Ferrite Samples

The frequency characteristics of the cubic ferrite sample i.e. the permeability spectra were investigated using a Hewlett Packard Impedance Analyzer of Model No.4192A provide the value of inductance, L and loss factor, $D = \tan\delta$. The measurements of inductances were taken in the frequency range of 1 kHz to 13 MHz. The values of measured parameters obtained as a function of frequency and the real (μ') and imaginary part (μ'') of permeability and the loss factor are calculated. μ' is calculated by using the $Eq^n.3.9$ and $Eq^n.3.10$ and μ'' is calculated by using the following equation

$$\mu'' = \mu' \tan\delta \tag{3.15}$$

3.4 Low Field Hysteresis graph

Hysteresis is well known in ferromagnetic materials. When an external magnetic field is applied to a ferromagnet, the atomic dipoles align themselves with the external field. Even when the external field is removed, part of the alignment will be retained: the material has become magnetized.

Fig. 3.9 B-H loop tracer

A general view of the B-H loop tracer with its system components is shown in Fig. 3.9. A hysteresisgraph or BH- Meter allows for the magnetic properties of soft magnetic materials to be measured. A schematic diagram of commercial hysteresisgraph has been presented Fig. 3.10. A hysteresisgraphhas two major functions. It produces currrent to produce a magnetic field, and measures voltage over time to measure magnetic induction. By determining the induction response of the test sample to the applied current, the magnetic properties of the materialis determined. Most soft magnetic materials are measured using ring geometry. Two coils of wire are wound around the sample.

A current from a bi-polar power supply is passed through the primary coil to generate a magnetic field in the ring. The applied magnetic field is proportional to the current. As the sample magnetic induction changes in response to the applied magnetic field, a voltage is induced in the secondary windings. This induced voltage is integrated over time with a circuit often called a fluxmeter, as it is used in many applications to measure magnetic flux. The integrated voltage is proportional to the magnetic induction of the test samples. The current in the primary coil is determined by measuring the voltage across a resistor. All the data of the samples were analyzed using computer software to control the applied field and measure both B and H simultaneously.
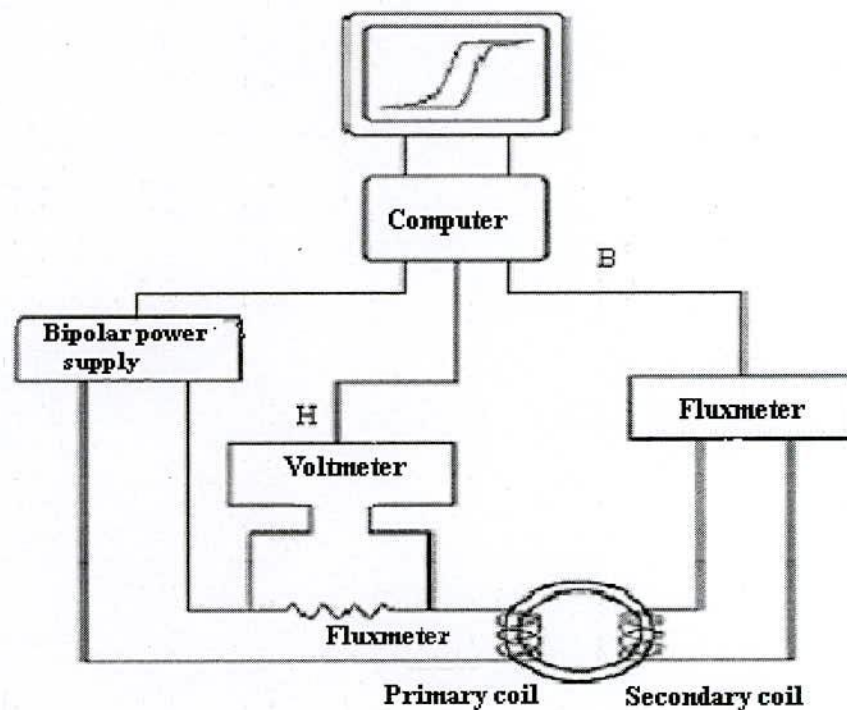
Fig. 3.10 Schematic diagram of commercial hysteresis graph

3.4.1 Measurement of an Initial B-H Curve

As these are important curves for magnetic design, these curves are measured using a hysteresis graph. For accurate initial curves, the sample must be demagnetized prior to the measurement. This demagnetization can be performed either externally, or in many cases, the sample can be demagnetized by the hysteresis graph. Residual magnetization can greatly distort the response of a soft magnetic material near zero field.

3.4.2 AC B-H Curve Measurement

In many applications, soft magnetic materials are subjected to cyclical magnetic field. The response of a soft magnetic material can be very complicated in this case, and is determined by both material parameters, such as sample permeability and material geometry. It can be exceedingly difficult to make accurate predictions of material performance through computer models. Therefore, the best way to determine the performance of these materials is to measure the BH-curve under cyclical applied magnetic fields. This can be performed using a hysteresis graph. The bi-polar power is driven at the test frequency, and the fluxmeter can measure the varying magnetic induction of the material. The resulting BH-curves are called AC BH-curves, and yield important information in regards to the material such as AC permeability and core loss. For these types of measurements, it is important that the hysteresis graph components have the appropriate frequency response to measure the AC BH-curve properly.

3.4.3 Materials Geometry

The AMH-series permeameter measures characteristics of soft magnetic materials, according to the IEC 60404-4 and IEC 60404-6 standards. The ideal sample geometry of soft magnetic material is a ring. Thus shape is preferable because ring shape eliminates factors   that can distort the magnetic test results. The main source of distortion of test data on soft magnetic materials is usually from air-gaps present in the magnetic test circuit. These air gaps lower the apparent permeability of the material, and can be difficult to control. As ring geometry is continuous path, the magnetic circuit is closed, without any air gaps that cause distortion. In addition, the magnetic path length, which is required to convert the applied current in the sense windings into applied magnetic field, is easy to calculate an unambiguous for ring samples. In ring shaped samples, primary winding are wound on the ring to generate a magnetic field in the sample via applied current to the primary windings.

A secondary coil is also wound onto the ring to inductively measure the magnetic induction of the sample. If this machining process is on a sample must be form of ring can be made in different methods:

(i)   made as an unique dense piece of material, obtained by mechanical works or by casting, sintering, etc.

(ii) made by stacking several disks with the same internal and external diameter, that can be obtained by punching, laser cutting, etc.

(iii) made by a unique thin strip wound as a clock-spring.

The external diameter D_e should be higher than 1.4 times the internal diameter D_i. The cross section A of the sample is calculated by the geometrical relation

$$A = \frac{(D_e - D_i)h}{2} \tag{3.16}$$

where h is the thickness of the sample. The thickness can be measured normally with a gauge if the sample is a solid ring. If it is made by stacked rings, sometimes it is preferred to use the mass and the density, calculating the thickness h with the formula:

$$h = \frac{4m}{\rho \pi (D_e^2 - D_i^2)} \tag{3.17}$$

where $\square$ is the density of the material.
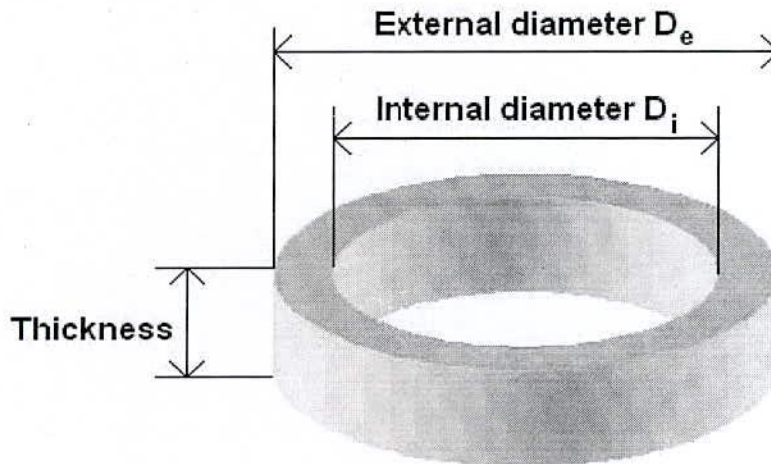
Fig. 3.11 Sample geometry

3.4.4 Windings

In these instances accurate magnetic measurements can still be performed, since the sample geometry creates a closed magnetic circuit. For these measurements, primary and secondary coils are wound onto the sample, as with ring measurement. The magnetic path

length   of the test circuit must be either determined or known in order to convert the applied primary current into applied magnetic field.

Two types of windings are necessary for the measure:

(i)   Magnetization winding (N_H number of turns) and

(ii)   Measuring winding (N_B number of turns)

The magnetization winding consists of a suitable number of turns N_H in which flows the magnetization current, i. The current produces the magnetic field H following the relationship:

$$H = \frac{N_H i}{l_m}$$
(3.18)

where l_m is the mean magnetic path length. If D_e does not exceed D_i more than 10 %, we can approximate l_m with the mean circumference:

$$l_m = \pi \frac{D_e + D_i}{2}$$
(3.19)

If $D_e \gg D_i$, then it is preferable to use the

$$l_m = \pi \frac{D_e - D_i}{\ln(\frac{D_e}{D_i})}$$
(3.20)

The value of l_m is automatically calculated by the software.

The magnetic flux induced in the sample under test is measured using a computer-controlled integrating fluxmeter attached to the secondary winding. The secondary winding produces the induced voltage V_2 from which the magnetic flux Φ is obtained:

$$\Phi = - \int V_2 dt$$
(3.21)

The integrating fluxmeter is the preferred method of measuring induced magnetic flux when the H field is being varied at frequencies from DC (typically 0.01Hz) to 10 kHz and numerically by the computer controlled software for AC measurements. The common method for implementing an electronic integrator consists of a DC amplifier with resistive–capacitive feedback and the magnetic induction, B is then obtained by the

flux by the relationship:

$$B = \frac{\Phi}{N_B A}$$

(3.22)

3.4.5 DC Measurement

DC measurements are made using a field that change very slowly, and that can be considered quasi-static. Since the variation of H, and in general the variation of B, is very slow, the inducted voltage is very small, and a numerical integration will give inaccurate results. The integration of the inducted voltage is performed by the fluxmeter, which is more precise and can follow very well the variation of B at such slow rate. After winding, the ring must be connected to the fluxmeter through the special cable for DC measure shown in Fig.3.12.
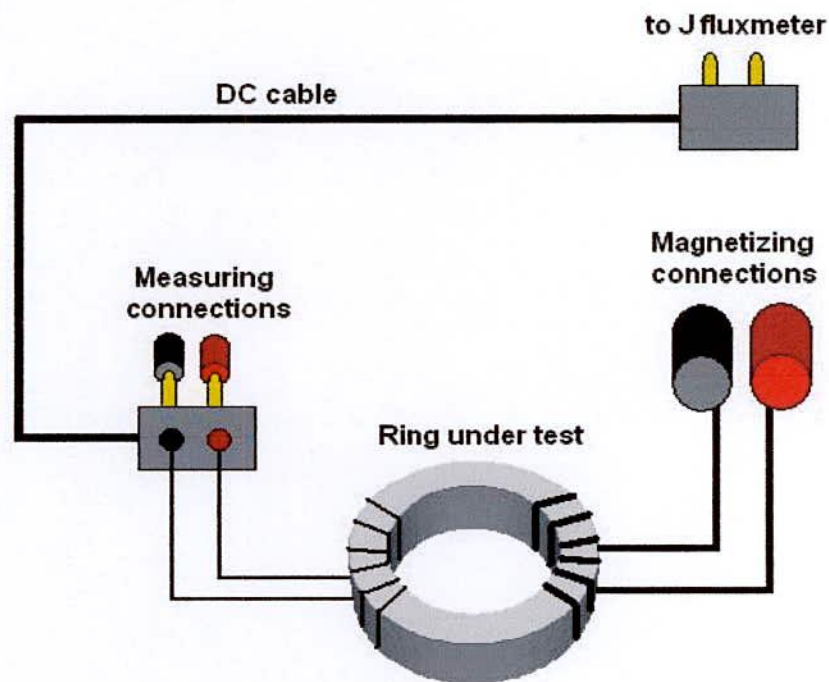
Fig. 3.12 DC measuring cable

This cable is simply an extension that takes signal from measuring connections to fluxmeter's inputs. For devices with two fluxmeters, use the $\frac{B}{J}$ fluxmeter. This fluxmeter is then connected by the analog output (in the back panel) to the PC board. A 4-poles connector permits the connection to auxiliary optional devices. Connect the H

turns to magnetization connectors and the B turns in the connections in the DC cable. Then connect the other terminals to the fluxmeter shown in Fig 3.13. The sample put on the fan grid.

AC/DC hysteresis graph for hard and soft magnetic materials of the prepared samples measured AMH-1K-1800-HS B-H loop tracer in the Materials Science division, Atomic Energy Centre, Dhaka. In DC conditions, H and B are always in phase, and the max value of H corresponds to the max value of B. The Hysteresis cycle always has some sharp vertex. The DC normal magnetization curve is the set of all the vertex of different amplitude. The ratio between B and $\mu_0 H$ is a ratio between two simultaneous values, and it is called relative permeability. In Ac conditions, this is not always true, because the max H and max B can be 'shifted' by a phase angle. In this case, the hysteresis cycle has rounded vertex shown in Fig. 3.14. The ratio between B and $\mu_0 H$ is a ratio between two non-simultaneous values, and it is called amplitude permeability.
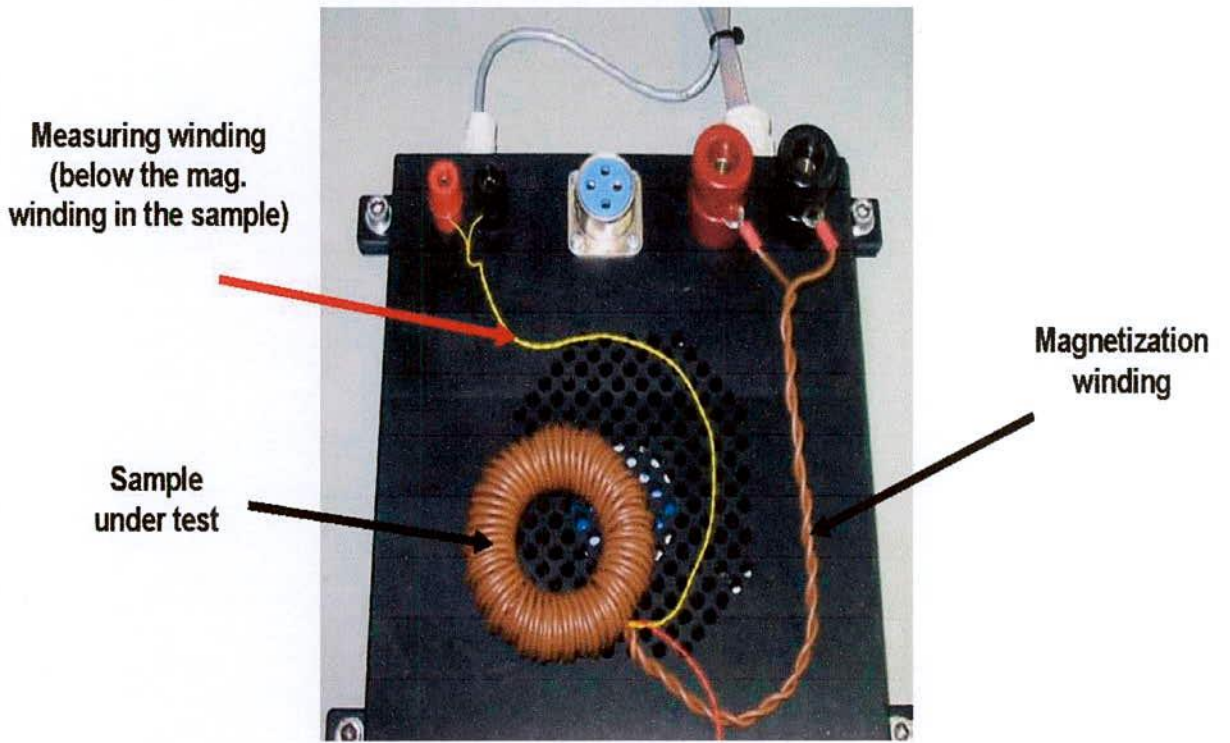
Fig. 3.13 The measuring and magnetizing connections are in the plastic tool inside the opening case
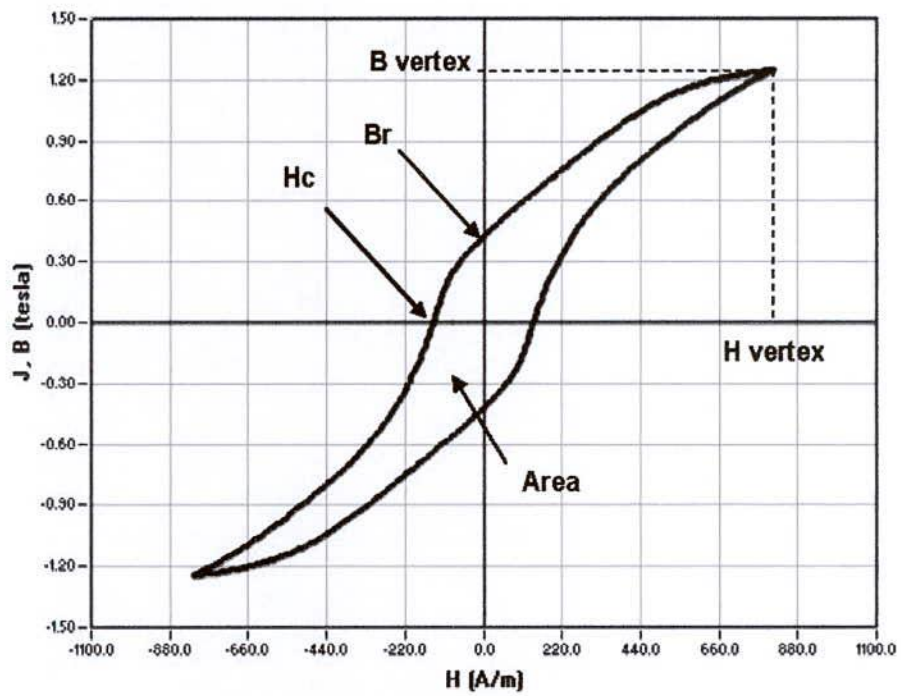
Fig. 3.14 Hysteresis cycle

3.5 Transport Property

3.5.1 DC and AC Resistivity

Resistivity is an intrinsic property of a material .The technical importance of ferrites lies primarily in their high resistivity. The electrical resistivity measurements carried out by a two probe method on silver painted sample a Keithley Electrometer using pellet samples of diameter 8.3-8.8mm and of thickness 1.2 - 2.5 mm by applying silver electrodes on the surfaces. Samples were prepared by sintering the samples at 1100°C to 1200°C for Ni-Cu-Zn ferrites for 3hours. The samples were polished using metallurgical polishing machine with the help of silicon carbide papers with grit size 600. After that the samples were clean with acetone and then again polished with special velvet type polishing cloth named as α-gam, for finer polishing using fine alumina powder of grain size 0.05 micron dispersed in a liquid. The powders were of various sizes starting with 1 micron to 0.05 micron. Samples are then cleaned in a ultrasonic cleaner and dried in surface at 150°C for several hours. Then the samples are again cleaned with acetone and silver paste was added to both the sides of the polished pellet samples together with two thin copper wires of 100 micron diameter for conduction. Again the samples are dried at 150°C to eliminate any absorbed moisture.

The DC and AC resistivity were measured as a function of frequency in the range 1 kHz-13MHz at room temperature by Electrometer Keithley model 6514 and impedance analyzer. Both the resistivity has been calculated using the formula:

$$\rho = \frac{RA}{l} = \frac{\pi r^2 R}{l} \qquad 3.23)$$

where R is the resistance of the Pellet, r is the radius of the pellet and l is the thickness of the pellet .

Ferrites are semiconductors and their resistivity decreases with increasing temperature according to the relation

$$\rho = \rho_\alpha e^{E_p / KT} \qquad (3.24)$$

where K the Boltzmann constant, T is the absolute temperature, E_p represents an activation energy which according to Verway and De Boer is the energy needed to

release an electron from the ion to jump to the neighboring ion, thus giving rise to electrical conductivity. If we plot $\log \rho$ vs $\frac{1}{T}$ for various ferrites, a straight line is found in a wide temperature range with a slope corresponding to E_p according to the relation

$$E_p = 0.198 \times 10^{-3} \frac{d(\log \rho)}{d(1/T)}$$

(3.25)

3.5.2 Dielectric Constant

Dielectric measurement as a function of frequency in the range 100Hz-13MHz at room temperature were carried out by using Hewlett Packrat impedance analyzer in conjunction with a laboratory made furnace which maintain the desired temperature with the help of a temperature controller The real part of dielectric constant was calculated using the formula

$$\varepsilon' = \frac{cd}{\varepsilon_o A}$$

(3.26)

where c is the capacitance of the pellet in Farad, d the thickens of the pellet in meter, A the cross-sectional area of the flat surface of the pellet in m^2 and do the constant of permittivity for free space.

3.6 Magnetization Measurement Techniques

In the present study magnetization has been performed using a Vibrating Sample Magnetometer (VSM).

3.6.1 Vibrating Sample Magnetometer (VSM)

A vibrating sample magnetometer (VSM) operates on Faraday's Law of Induction, which tells us that a changing magnetic field will produce an electric field. This electric field can be measured and can tell us information about the changing magnetic field. A VSM is used to measure the magnetic behavior of magnetic materials. Vibrating Sample Magnetometer is a versatile and sensitive method of measuring magnetic properties developed by S. Foner [3.12] and is based on the flux change in a coil when the sample is vibrated near it. The Vibrating Sample Magnetometer (VSM) is designed to continuously

measure the magnetic properties of materials as a function of temperature and field. In this type of magnetometer, the sample is vibrated up and down in a region surrounded by several pickup coils. The magnetic sample is thus acting as a time-changing magnetic flux, varying inside a particular region of fixed area. From Maxwell's law it is known that a time varying magnetic flux is accompanied by an electric field and the field induces a voltage in pickup coils. This alternating voltage signal is processed by a control unit system, in order to increase the signal to noise ratio. The result is a measure of the magnetization of the sample.

3.6.2 Principle of VSM

If a sample is placed in a uniform magnetic field, created between the poles of a electromagnet, a dipole moment will be induced. If the sample vibrates with sinusoidal motion a sinusoidal electrical signal can be induced in suitable placed pick-up coils. The signal has the same frequency of vibration and its amplitude will be proportional to the magnetic moment, amplitude, and relative position with respect to the pick-up coils system. Fig 3.15 shows the block diagram of vibrating sample magnetometer.
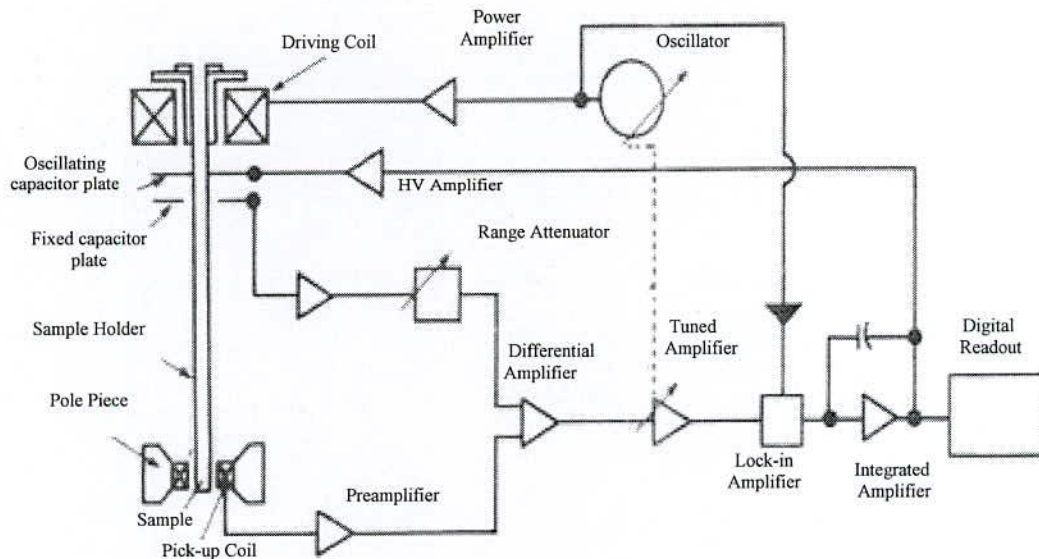
Fig. 3.15 Block diagram of vibrating sample magnetometer

The sample is fixed to a sample holder located at the end of a sample rod mounted in a electromechanical transducer. The transducer is driven by a power amplifier which itself is

driven by an oscillator at a frequency of 90 Hz. So, the sample vibrates along the Z axis perpendicular to the magnetizing field. The latter induced a signal in the pick-up coil system that is fed to a differential amplifier. The output of the differential amplifier is subsequently fed into a tuned amplifier and an internal lock-in amplifier that receives a reference signal supplied by the oscillator.

The output of this lock-in amplifier, or the output of the magnetometer itself, is a DC signal proportional to the magnetic moment of the sample being studied. The electromechanical transducer can move along X, Y and Z directions in order to find the saddle point. Calibration of the vibrating sample magnetometer is done by measuring the signal of a pure Ni standard of known saturation magnetic moment placed in the saddle point. The basic instrument includes the electromechanical system and the electronic system (including a personal computer). Laboratory electromagnets or superconducting coils of various maximum field strengths may be used.

Fig. 3.16 Vibrating sample magnetometer

3.7   Microstructure Study

Magnetic properties of the Ni-Cu-Zn ferrites samples are strongly dependent upon the sensitive control of the microstructure. Permeability is directly proportional to the grain size of the samples. At least up to a critical diameter of the grains causes the premeability to increase monotonically. Resistivity and density of the ferrite samples are also dependent on the porosity of the samples. Resistivity of the samples increases with the trapped intra-granular pores. Hence the microstructural studies of the samples are required for making prediction about the result of permeability and resistivity of the ferrite samples. For microstructure study the ferrite samples were polished step by step. Primarily the samples were polished by using Metaserv Universal Polisher, Model No. C 200/5V, Volts 240, Amp. 0.75. Secondly. using another polishing machine 99 Phoenix Ave, Enfield, CT06082 USA, Model No. LABPOL 8/12, keeping a speed of 300-450 rev/sec for about 1 hour using different grades of Al_2O_3 fine powders mixing with water.

In the tertiary stage the polished samples were cleaned ultrasonically for $\frac{1}{2}$ hour using an ultrasonic cleaner FRITSCH @ Laboratte, Model: 17.202, No. 1030. After the fine polishing and ultrasonic cleaning the samples were etched thermally under suitable temperature for the different samples down below 150 to 100°C of the sintering temperature for 2 minute sin air for every sample. As the thermal etching was finished the samples were ready for the microstructure study. The microstructure measurement of the samples were done by using a Scanning Electron Microscope (SEM), Model No. S-3400 N, Hitachi installed at Industrial Physics Division, Bangladesh Council for Scientific and Industrial research (BCSIR), Dhaka, Bangladesh.

3.7.1 The Scanning Electron Microscope (SEM)

Scanning electron microscopy (SEM) or electron probe microanalysis (FPMA) are generally considered micro-analytical techniques whch are able to *image* or *analyze* materials we can not generally observe with the resolution offered by visible techniques. By *image* we mean photograph of an object much smaller than we can see, even with the aid of an optical microscope. The SEM has a unique capability of giving view of a flea the same perspective as the Chevy driveway. By *analyze* we mean identify the elements

(e.g., silicon, iron. etc) of which the specimen is composed. Elemental analysis can also be accomplished at a micro-scale; for example, EPMA can probe a specimen as small as 5 thousands of a millimeter (5 microns), and not only identify the elements present but measure them with a small degree of error. These instruments represent two if the greatest advances in scientific instrumentation; however they do have their limits. For example, not all specimens can be exposed to the high vacuum within the specimen chamber. Also, elements lighter than atomic number 8 (oxygen) can not be measured without reservations, and EPMA is not sensitive to many elements below 100ppm. Still, this instrumentation has proved invaluable, especially for mineralogists and pathologists, and a good operator can very one parameter or another to circumvent instrumental weaknesses.

These instruments belong to a broad category of particle beam instruments. In this case we bombard materials with electrons which have high energies because they have mass and because they have been accelerated with thousands of volts. SEM has been historically used as cameras and microanalyzers for elemental analysis, modern electron probes offer both capabilities while optimizing for one or the other. For example, SEM can quantify X-rays with its energy dispersive X-ray detector (EDX), but it is designed for ease of use and for a variety of specimens. Scanning electron microscopes have been generally used as cameras, that is, for photographing specimens beyond the capabilities of ordinary optical microscopes. While the images obtained appear very real and as if they were photographed by ordinary means, the apparent illumination is a function of particle emission rather than radiation we're familiar with. These particles emitted are termed secondary electrons, and their detection via a SE detector is displayed on a scanning TV display. A bright image will be the result of high secondary electron emission, while the primary influence on high emission is the surface structure of the specimen. The end result is therefore brightness associated with surface characteristics and an image which looks very much like a normally illuminated subject.

The usefulness of quantifying elemental compositions is invaluable in the sciences of mineralogy, petrology and materials research. Students and investigators can measure the composition of several mineral phases which are, apparently or assumed, in equilibrium with each other. This information can be used to estimate the temperature and pressure at the time of crystallization. It is also able to measure the composition of a

rock-forming mineral relative to its growth history; for example, its core and rim compositions. Material science applications are even more varied, from thin film semi-conductors to photonics materials to super conductors. In the case of thin-films, by measuring various X-ray intensities at a number of different accelerating voltages, both the composition and thickness of various films deposited on a substrate may be determined with excellent accuracy. single crystal grown for various purposes can have their formula stoichiometry measured and compared with X-ray diffraction data. The following Fig. 3.17 show the pictorial diagram of SEM Model No. S-3700 N by Hitachi, Japan.
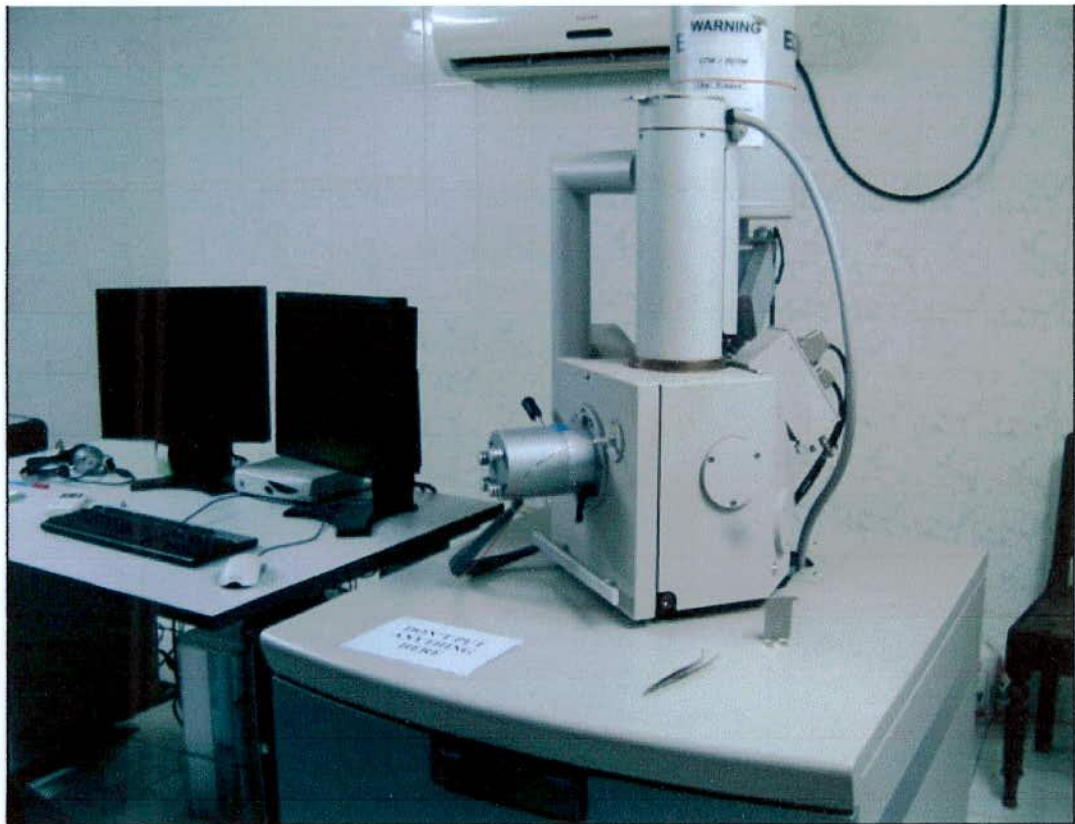
Fig. 3.17 Scanning Electron Microscope

Results and Discussion of $(Ni_{0.28}Cu_{0.10}Zn_{0.62}O)(Fe_2O_3)_{1-x}$ Ferrites

4.1 Introduction

There has been a growing interest in Ni-Cu-Zn ferrites for the applications in producing multi-layer-type chips mainly because these oxides can be sintered at relatively low temperatures with a wide range of compositions. Compared with the effect of compositions, microstructure of ferrites, influence the temperature dependence of relative initial permeability of Ni-Cu-Zn ferrites in a more complicated way. Unfortunately few reports can be found concerning the effects of microstructures, such as density concerning the effects of microstructures such as density, grain size, porosity and their intra and intergranular distribution, etc. on the temperature dependence of relative permeability of Ni-Cu-Zn ferrites. Nickel ferrite (Ni Fe_2O_4) is a partially single phase cubic spinel and it can be considered as a collinear ferrimagnet.

Ferrites have the spinel-type structures, which can be described in terms of a nearly cubic close-packed arrangement of anion with one half of the octahedral interstices (B-sites) and one- eight of the tetrahedral interstices (A-sites) filled with cations. By introduction of a relatively small amount of foreign ions, an important modification of both structure and electromagnetic properties can be obtained. Introduction of nonmagnetic ions such as Zn^{2+} in Ni-ferrites will drastically affect the magnetic properties such as magnetization, Curie temperature etc. Zn^{2+} ions are known [4.1] to occupy the tetrahedral (A) sites, Ni^{2+} ions have a preference for the octahedral (B) sites while the Fe^{3+} ions are distributed over both the sites.

Nickel ferrite with diamagnetic substitution for Ni^{2+} and Fe^{3+} ions has attracted the attention of number research workers who attempted to explain the magnetic properties on the basis of the distribution of the only magnetic in Fe^{3+} in tetrahedral and octahedral sites, which makes the analysis reliable. Zn and Cd substituted mixed ferrites such Ni-Zn [4.2], Fe-Zn [4.3] Cu-Zn [4.4], Cu-Cd [4.5], Ni-Cd [4.6], Mg-Cd [4.7] and Mg-Zn [4.8] show canted spin arrangement on the octahedral B-site. The individual compositions of Ni-Cu-Zn ferrites used for inductor vary to some extent; ferrites relative rich in Zn (31 mol% ZnO) [4.9] with intermediate (26 mol% ZnO) [4.10] or low Zn-concentrations (15.5 mol% ZnO) [4.11]. Although there have been many studies in the

last years focusing on ferrite powder morphology and preparation of dense microstructures with large permeability, there are only few reports on correlations between composition and properties of Ni-Cu-Zn ferrites. For example, Low et. al. [4.12] reported on property-composition diagrams of sol-gel derived samples with 50 mol% Fe_2O_3 and Murthy [4.13] studied the series $Ni_{0.65-x}$ Cu_x $Zn_{0.35}Fe_2O_4$. As shown in some studies a small deficiency of iron (<50 mol% Fe_2O_3; compositions are named sub-stoichiometric, whereas the term stoichiometric here refers to ferries with 50 mol% Fe_2O_3 or $MeFe_2O_4$) seems to be beneficial for optimizing the shrinkages and densification of Ni-Cu-Zn ferrites. To our knowledge no systematic study on the effect of composition on the sintering behavior and electromagnetic properties of Ni-Cu-Zn ferrites has been published.

The ferrite containing Ni, Cu and Zn exhibit several interesting properties which make them suitable for cellular phones, video cameras, note book computers, hard and floppy drives. In this study, a series of $(Ni_{0.28}Cu_{0.10}Zn_{0.62}O)(Fe_2O_3)_{1-x}$ [x = 0.00, 0.02, 0.04, 0.06, 0.08] were prepared by using solid state reaction method and investigated their magnetic and electrical properties.

4.2 X-ray Diffraction Analysis

4.2.1 Phase Analysis

Structural characteristic and identification of phases are prior for the study of ferrite properties. X-ray diffraction (XRD) studies of the samples were performed by using Philips X' PERT PRO X-ray Diffractometer using Cu-K$_\alpha$ radiation in the range of $2\theta = 20°$ to $65°$ in steps of $0.02°$. The X-ray diffraction (XRD) pattern of the system $(Ni_{0.28}Cu_{0.10}Zn_{0.62}O)(Fe_2O_3)_{1-x}$ [x = 0.00, 0.02, 0.04, 0.06, 0.08] sintered at 1150°C for 3 hours is shown in Fig. 4.1. The powder X-ray diffraction patterns exhibit that all the samples were identified as a single phase of cubic spinel structure with no extra lines corresponding to any other crystallographic phase or unrelated ingredient. The XRD patterns for all the samples were indexed for fcc spinel structure and the Bragg planes are shown in the patterns. It is obvious that the characteristic peaks for spinel Ni-Cu-Zn ferrites appear in the samples as the main crystalline phase with a slight shifting in the position of peaks towards the higher at spacing values. The peaks (220), (311), (222),

96

(400), (422), (511), and (440) which represent either odd or even indicating the samples are spinel cubic phase. Generally, for the spinel ferrites the peak intensity depends on the concentration of magnetic ions in the lattice. Using the X-ray data, the lattice parameter 'a', and hence the X-ray densities were calculated.
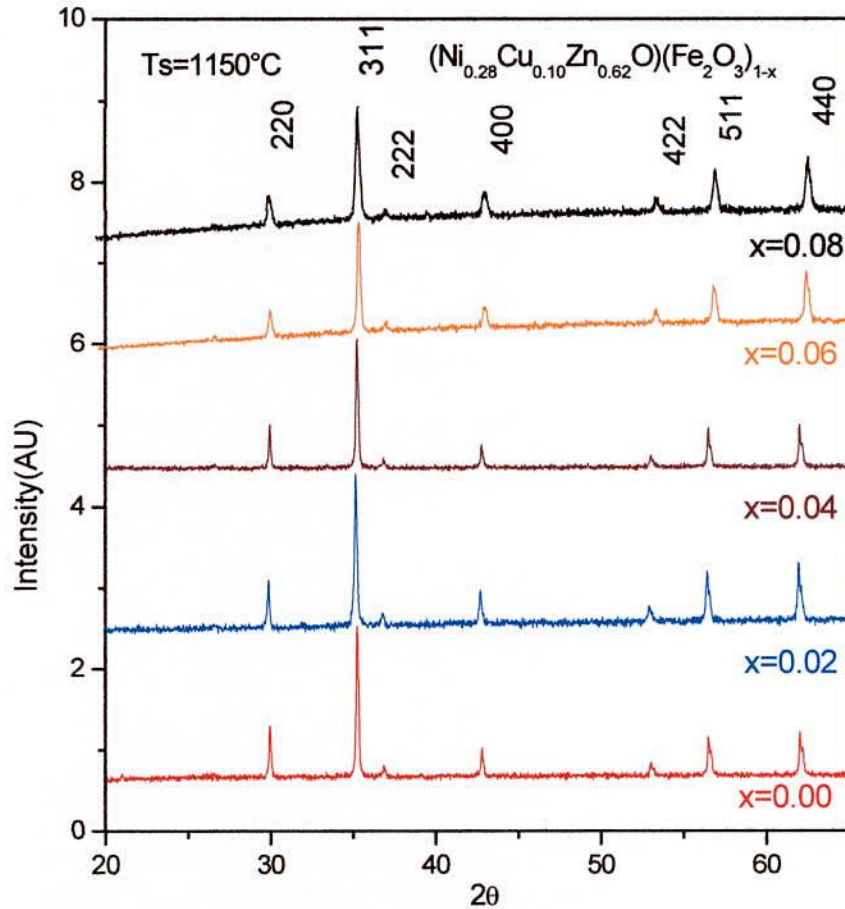
Fig. 4.1 XRD patterns of $(Ni_{0.28}Cu_{0.10}Zn_{0.62}O)$ $(Fe_2O_3)_{1-x}$ ferrites sintered at 1150°C (3 hrs)

4.2.2 Lattice Parameters

The values of the lattice parameter obtained from each plane are plotted against Nelson-Riley function [4.14] $F(\theta) = \frac{1}{2}\left[\frac{\cos^2\theta}{\sin\theta} + \frac{\cos^2\theta}{\theta}\right]$, where θ is the Bragg's angle, by extrapolation of these lines to $F(\theta) = 0$ or $\theta = 90°$. The variation of the lattice parameter 'a' as a function Fe-deficient content x is as in Fig. 4.2. A decrease in lattice constant is observed with the increase of Fe-deficient content (x) in the lattice. The linear decrease in lattice constant with Fe-content indicates that the present system obeys the Vegard's law

[4.15]. This decrease can be attributed to the vacancy created by Fe^{3+} deficiency with increasing its content. The unit cell is expected to reduce its size by contraction of the lattice resulting in decrease of lattice parameter gradually.
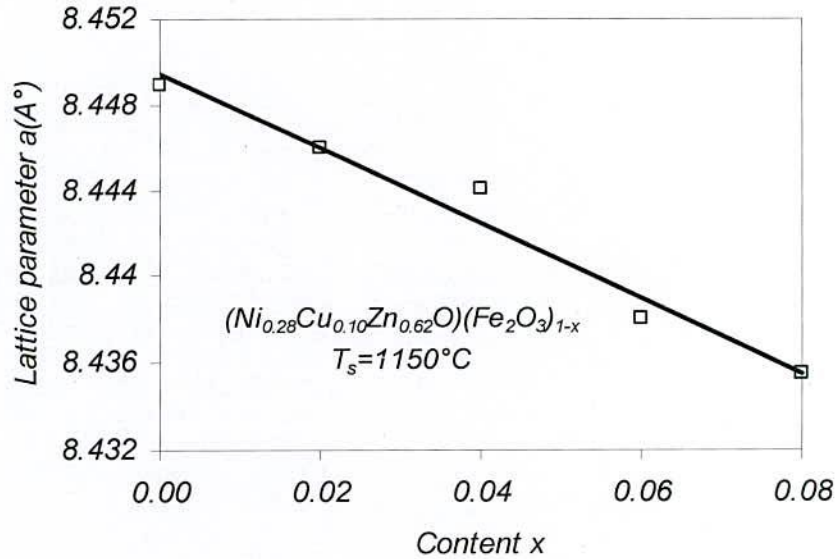
Fig. 4.2 Variation of lattice constant 'a' as a function of deficient of Fe-content of $(Ni_{0.28}Cu_{0.10}Zn_{0.62}O)$ $(Fe_2O_3)_{1-x}$ ferrites

4.2.3 Density

The variation of density with Fe-deficiency (x) is shown in Fig. 4.3. The bulk density, d_B was measured by usual mass and dimensional consideration whereas X-ray density, d_x was calculated from the molecular weight and the volume of the unit cell for each sample by using the eq^n (3.5). The bulk density (d_B) is lower than the X-ray density, (d_x). This may be due to the existence of pores, which are inevitable during ceramic processing and formed and developed during the sample preparation or the sintering process. The X-ray density slightly decreases with increasing Fe-deficiency and the bulk density increases continuously with increasing x content. This enhancement of bulk density is due to activated diffusion process triggered by the excess vacancies created by Fe^{3+} deficiency. Introduction of iron deficiency significantly reduces the Fe^{2+} ions in the sample and thereby inhibiting the electron hopping between Fe^{3+} and Fe^{2+} ions which causes to accelerate the sintering and densification [4.16]. Kimura et. al. [4.17] found that the decrease iron content from the stoichiometric value effectively lowers the sintering temperature. It may also be mentioned that reduction of Fe^{2+} due to Fe^{3+} deficiency is expected to increase the resistivity of the samples. It is worth while to mention that density play an important role on the magnetic properties especially on the structure

sensitive extrinsic property such as permeability and flux density. Table-4.1 shows the results of lattice parameter, theoretical density, bulk density calculated porosity. It is observed form the Table-4.1 that porosity decreases monotonically with increasing iron deficiency in contrast with bulk density which shows reverse behavior. The porosity which is intrinsic for any oxide materials plays an important role in deciding the magnetic and electrical properties.
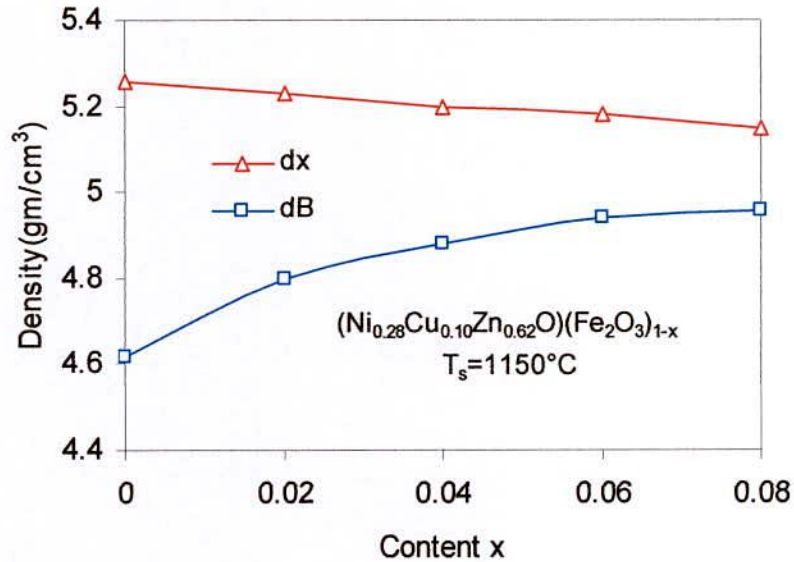
Fig. 4.3 Variation of density with Fe- deficient content (x) of $(Ni_{0.28}Cu_{0.10}Zn_{0.62}O)$ $(Fe_2O_3)_{1-x}$ ferrites

Table- 4.1 Data of the lattice parameter (a), X-ray density (d_x), bulk density (d_B), porosity (P%), molecular weight (M) of $(Ni_{0.28}Cu_{0.10}Zn_{0.62}O)$ $(Fe_2O_3)_{1-x}$ samples sintered at 1150°C/3hrs

Fe-deficient content (x)	a (Å)	d_x (g/cm^3)	d_B (g/cm^3)	P%	M (g)
0.00	8.4489	5.26	4.62	12.2	239.02
0.02	8.4460	5.23	4.80	8.2	237.42
0.04	8.4441	5.21	4.88	6.2	235.82
0.06	8.4380	5.18	4.94	4.6	234.23
0.08	8.4355	5.15	4.96	3.7	232.63

4.3   Magnetic Properties

4.3.1 Temperature Dependence of Initial Permeability

Fig. 4.4 shows the temperature dependence of initial permeability, μ' for the toroid shaped samples (where x = 0.00 - 0.08), which is measured at a constant frequency (100 kHz) of an AC signal by using Impedance Analyzer. Since the initial permeability is directly related to the magnetization and to the ionic structure, then the thermal spectra of permeability can be taken as a test of the formation and homogeneity of the ionic structure of the samples. It is observed that the initial permeability increase with the increase in Fe-deficiency throughout the entire range of compositions, while it falls abruptly close to the Curie point. This is because Fe-deficient in these compositions not only increases the magnetic moment but also lowers anisotropy, K_1 [4.18] since Fe^{3+} deficient composition do not contain any Fe^{2+} which generally increases K_1.

On the other hand permeability increases with the decrease of K_1 as the temperature increases according to the relation $\mu' \propto \dfrac{M_s^2 D}{\sqrt{K_1}}$ [4.19, 4.20] which is manifested in Fig. 4.4 (a,b). It is observed from Fig. 4.4 (a) and Fig. 4.4 (b) that the permeability falls sharply when the magnetic state of the ferrite samples changes from ferromagnetic to paramagnetic state. When the anisotropy constant reaches to zero just below the Curie temperature, μ' attains its maximum value known as Hopkinson peak [4.19] and then drops off sharply to minimum value at Curie point. The sharpness of the permeability drop at the Curie point can be used as a measure of the degree of compositional homogeneity according to Globus [4.16], which has also been confirmed by X-ray diffraction that no impurity phases could be detected.

The variation of initial permeability (μ') with temperature can be expressed as follows. The anisotropy constant (K_1) and saturation magnetization (M_S) usually decrease with increase in temperature. K_1 falls faster than the M_S as the temperature increases. When the anisotropy constant, reaches to zero, μ' attains its maximum value and then drops off to minimum value near the Curie point.

100
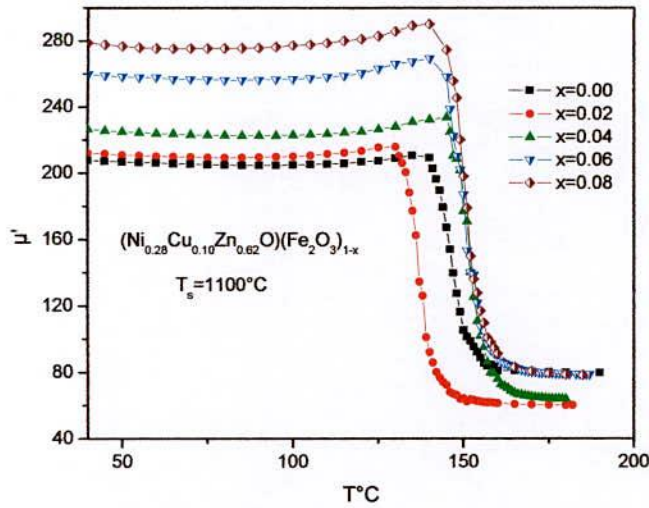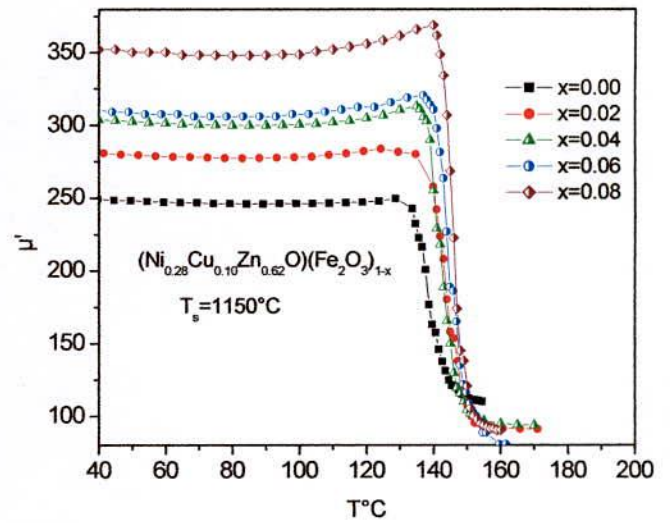
Fig. 4.4 Temperature dependence of real permeability, μ' for (a) T_s = 1100°C/3hrs and (b) T_s = 1150°C/3hrs of $(Ni_{0.28}Cu_{0.10}Zn_{0.62}O)$ $(Fe_2O_3)_{1-x}$ ferrites

The μ'-T plot does not show any secondary maximum that generally occurs due to excess formation of Fe^{2+} ions, there by indicating the single-phase formation of the samples. Fig. 4.5 (a,b) represents the variation of the complex permeability and temperature derivative of permeability as a function of temperature of the sample x = 0.04. It is observed that the imaginary part of permeability μ'' and temperature derivatives of permeability, $\dfrac{d\mu'}{dT}$ show peaks at temperature, T_c which matches well with the sharp fall of permeability at $T = T_C$.

Fig. 4.6 (a) and 4.6 (b) shows temperature dependence of initial permeability, μ' for x=0.00 and 0.08 samples of $(Ni_{0.28}Cu_{0.10}Zn_{0.62}O)$ $(Fe_2O_3)_{1-x}$ ferrites measured during heating and cooling cycles sintered at 1150°C for 3 hrs. A slight variation T_c during heating and cooling is due to thermal hysteresis effect.

101
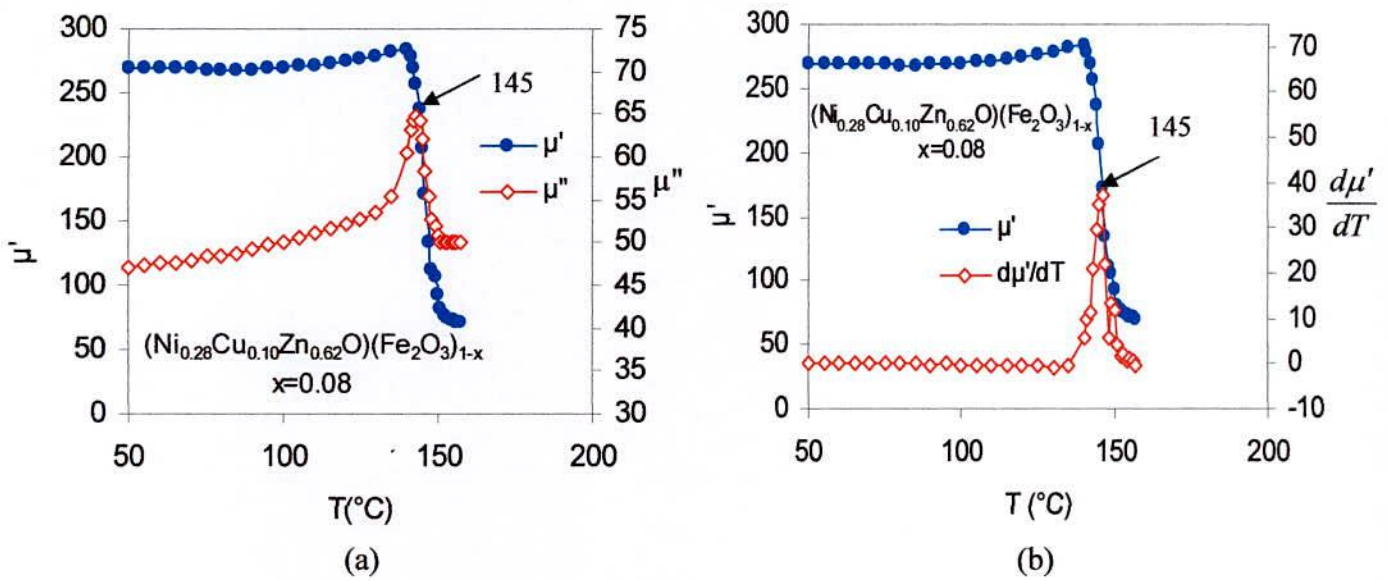
Fig. 4.5 (a,b) Determination of Curie temperature from the temperature dependence of μ', μ'' and $\dfrac{d\mu'}{dT}$ as a function of temperature of $(Ni_{0.28}Cu_{0.10}Zn_{0.62}O)\ (Fe_2O_3)_{1-x}$ ferrites sintered at 1150°C/3hrs
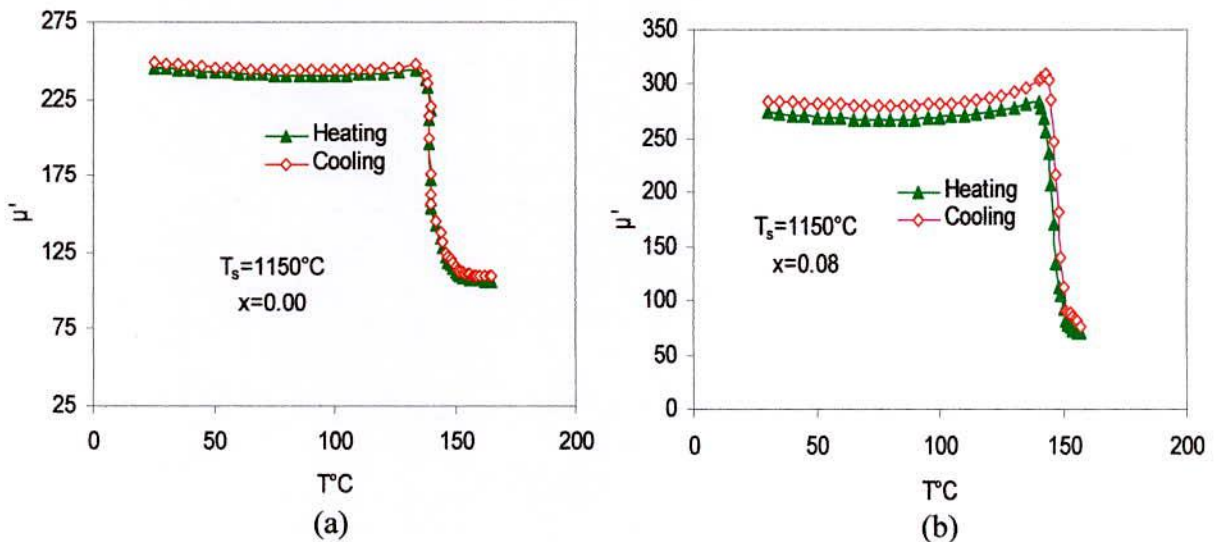
Fig. 4.6 (a, b) Temperature dependence of initial permeability, μ' for (a) x = 0.00 and (b) x = 0.08 of $(Ni_{0.28}Cu_{0.10}Zn_{0.62}O)\ (Fe_2O_3)_{1-x}$ ferrites samples sintered at 1150°C/3hrs

102

4.3.2 Compositional Dependence of Curie Temperature

Fig. 4.7 shows the variation of Curie temperature T_C with Fe-deficiency of $(Ni_{0.28}Cu_{0.10}Zn_{0.62}O)(Fe_2O_3)_{1-x}$ ferrites and the values are taken during heating the sample. T_c of the studied sample was determined from μ'-T curve. The temperature corresponding to the peak value of $\dfrac{d\mu'}{dT}$ has been taken as the Curie temperature of the sample. The T_c values are shown in Teble-4.2.

Table - 4.2 Data of Curie temperature (T_C) $(Ni_{0.28}Cu_{0.10}Zn_{0.62}O)(Fe_2O_3)_{1-x}$ ferrites

Fe- deficient Content x	T_s=1100°C	T_s=1150°C
	T_c (°C)	T_c (°C)
0.00	146	139
0.02	137	141
0.04	151	143
0.06	150	144
0.08	151	145

T_C is the transition temperature above which the ferrite material losses its magnetic properties. The Curie temperature gives an idea of the amount of energy required to break up the long range ordering in the ferromagnetic material. The Curie temperature mainly depends upon the strength of A-B exchange interaction.
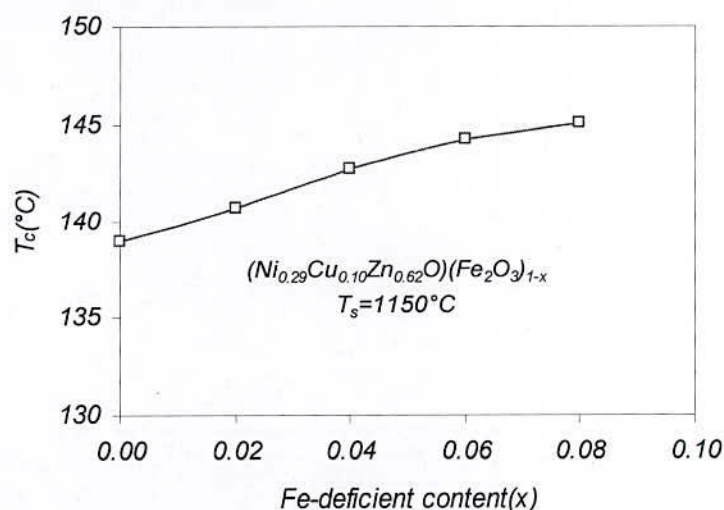
Fig. 4.7 Variation of Curie temperature (T_C) with Fe-deficient (x) of $(Ni_{0.28}Cu_{0.10}Zn_{0.62}O)(Fe_2O_3)_{1-x}$ ferrites

From Fig. 4.7 it is observed that Curie temperature slowly and gradually increases with increasing of Fe-deficiency. It has been observed that T_c increases with the introduction of iron deficiency. It is known that at T_c, the thermal energy wining over the exchange energy which results to disorder the system from an ordered one i.e., a ferrimagnatic substance transforms to a paramagnetic one. Curie temperature of ferrites is dependent on the strength of A-B exchange interaction [4.21]. As the iron deficiency is increased in the sample, the strength of the interactions between the tetrahedral A-sites and octahedral B-sites might be increased which enhances the Curie temperature. Our results have been found to be consistent with earlier results reported in Ref. [4.22] for Cd-Cr-Cu ferrites, According to the T_c data, it reveals that T_c data during heating and cooling are very close to each other in both cases. Small differences in the T_c measurement in heating and cooling processes may occur due to the reduced thermal disturbance taking place during the cooling cycle.

4.3.3 Frequency Dependence of Complex Permeability

The complex permeability can be separates into two components, μ' and μ''. μ' represents the real permeability with the magnetization in phase with the alternating magnetic field and μ'' the imaginary permeability with the magnetization 90° out of phase with the alternating magnetic field. The complex permeability is given by $\mu = \mu' - i\mu''$, where μ' is the real permeability (in phase) and μ'' the imaginary permeability (90° out of phase). Complex permeability has been determined as a function of frequency, f up to 13 MHz at room temperature for all the samples of series $(Ni_{0.28}Cu_{0.10}Zn_{0.62}O)$ $(Fe_2O_3)_{1-x}$ ferrites by using the conventional technique based on the determination of the complex impedance of circuit loaded with toroid shaped sample. Fig. 4.8 represents the results of the real part of the permeability, μ' and Fig. 4.9 imaginary part, μ'' as a function of frequency for the whole series of ferrite samples sintered at 1100°C, 1150°C and 1200°C for 3 hours.
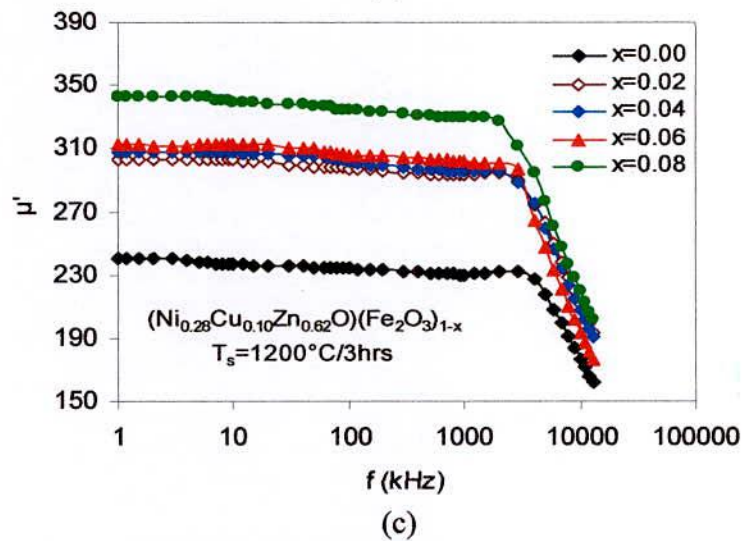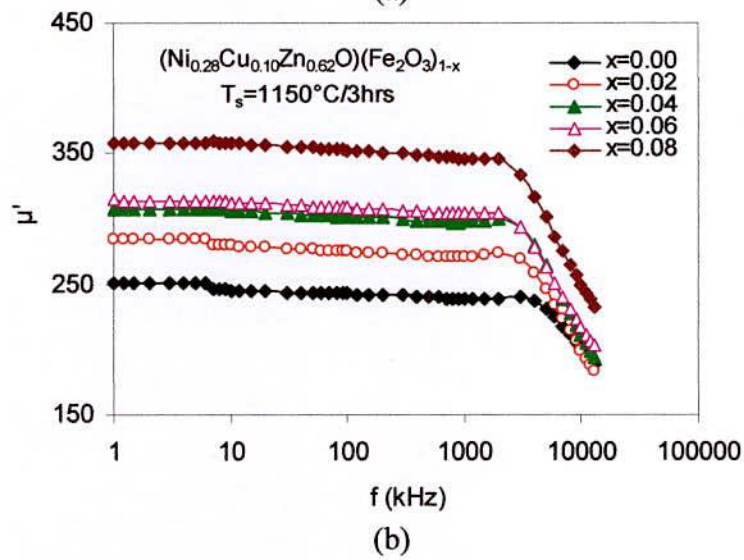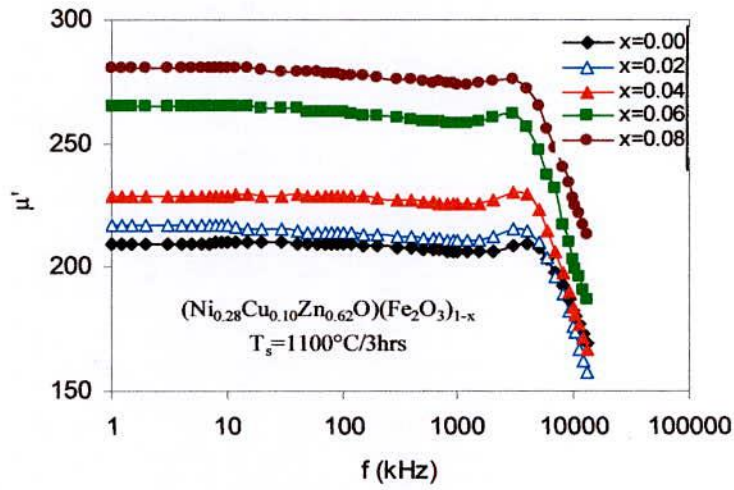
Fig. 4.8 Frequency dependence of the real part of the permeability, μ' of $(Ni_{0.28}Cu_{0.10}Zn_{0.62}O)$ $(Fe_2O_3)_{1-x}$ ferrites at (a)1100°C, (b) 1150°C and (c) 1200°C for 3 hrs

From Fig. 4.8 it is noticed that the real component of permeability, μ' is fairly constant with frequency up to certain frequency range, and then falls rather rapidly to very low value at higher frequency. We can call this real part of the permeability, μ' as initial permeability. The permeability of compositions with x=0.00-0.08 were stable up to 2-4 MHz and the cut-off frequencies of samples were above 4 MHz. It is clearly evident from these figures that the initial permeability as a function of frequency increases with Fe-deficiency, x i.e the permeability μ' increases monotonically with x content. However, the imaginary part of the permeability gradually increases with the increase in frequency, took a broad maximum at a certain frequency while the real part has been observed to be decreased. This type of feature is known as the ferrimagnatic resonance [4.23, 4.24]. The permeability increases with a decrease in K, according to the relation $\mu' \approx \dfrac{M_s^2 D}{\sqrt{K_1}}$ [4.25].

In the present study the increase of μ' on x content may be related to grain size which increases with x content and possible due to reduction of K_1. An insignificant effect of slightly increasing M_s with x content cannot be also ruled out. High permeability in the low frequency side remarkably show the dominant role played by the motion of the domain wall. In addition, in the low frequency region, ferrites work as a low loss constant self-inductor where the core is mostly inductive and thereby rejects electromagnetic interference signal to the source. On the other hand, in the high frequency side, inductive core show high impedance and becomes more resistive and dissipates the interfering signals rather than reflecting these to the source [4.26]. Resonance peaks are the results of the absorption of energy due to the coincidence of the frequency of the magnetic dipoles and applied field. At resonance, highest amount of energy is transmitted from the applied ac magnetic field to the lattice. It might also be explained using the fact that at high frequency side, magnetization of the sample cannot follow the frequency of the applied ac filed. Moreover, in the high frequency region, permeability has been found to be governed by the spin rotation due to the damping of the domain walls. Spins are relaxed at higher frequencies which in turn cause to reduce the permeability to a lower value. Considering this facts a perfect frequency band can be successfully identified at which the sample can be used. From permeability spectrum as shown in Figs. 4.8 (a, b, c) it is also observed that the higher the permeability the lower the resonance frequency. This behavior of our sample proves the validity of the Snoek's model [4.27] that defines the relationship between resonance frequency and initial permeability as $f_r\mu' = $ content,

where f_r is the resonance frequency for the domain wall motion above which initial permeability, μ' gets decreased. That is the product of initial permeability and resonance frequency always remains constant. The lower the permeability values, the higher the frequencies at which resonance will take place. This way, an effective limit of the product of these two parameters (high f_r and high μ') could be identified so that the pair is mutually incompatible. Since the onset of resonance frequency determines the upper limit of the operational frequency of any device, it infers that the operational frequency range of the samples is below 2-4 MHz depending on the composition and sintering temperature. The resonance frequency, Snoek's limits $f_r.\mu'$ along with the permeability of the samples are shown in Table – 4.3.

From Fig. 4.9, the imaginary component μ'' first rises slowly and then increases quite abruptly making a peak at a certain frequency (called resonance frequency, f_r), where the real component μ' is falling sharply. This phenomenon is attributed to the ferrimagnatic resonance. Resonance frequency (f_r) was determined from the maximum of imaginary permeability of the ferrites. It is observed from the Fig. 4.9 that the higher the permeability the lower the resonance frequency of the material. This really confirms with

Snoek's limit [4.27]. $f_r\,(\mu_i - 1) = \left(\dfrac{4}{3}\right)\gamma\,M_S,$ (4.1)

where, f_r is the resonance frequency for domain wall motion, γ is the gyromagnetic ratio and M_S is the saturation magnetization. This means that there is an effective limit to the product of resonance frequency and permeability. The resonance frequency peaks are the results of the absorption of energy due to matching of the oscillation frequency, of the magnetic dipoles and the applied frequency.
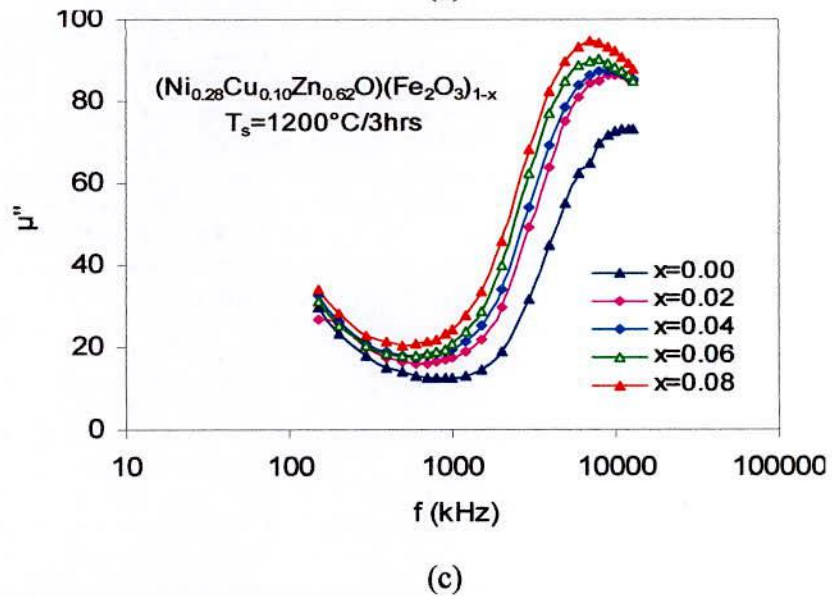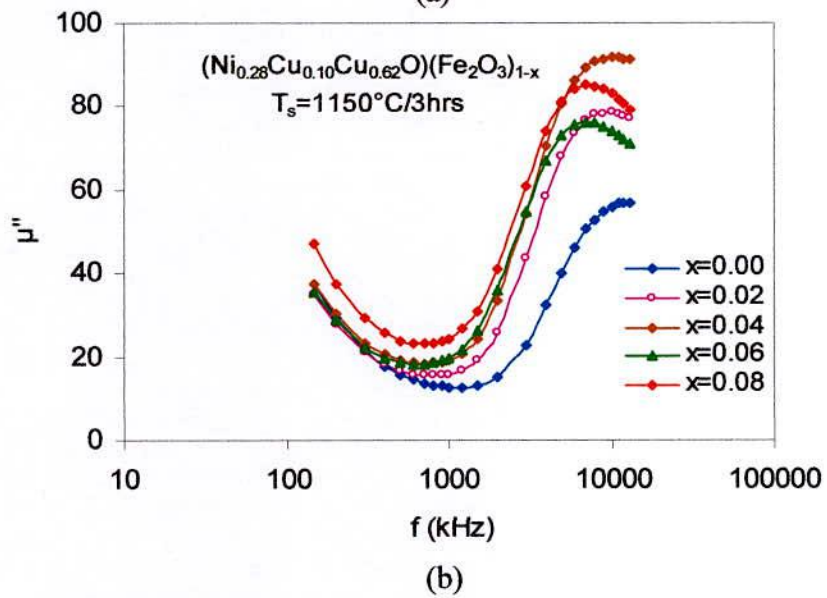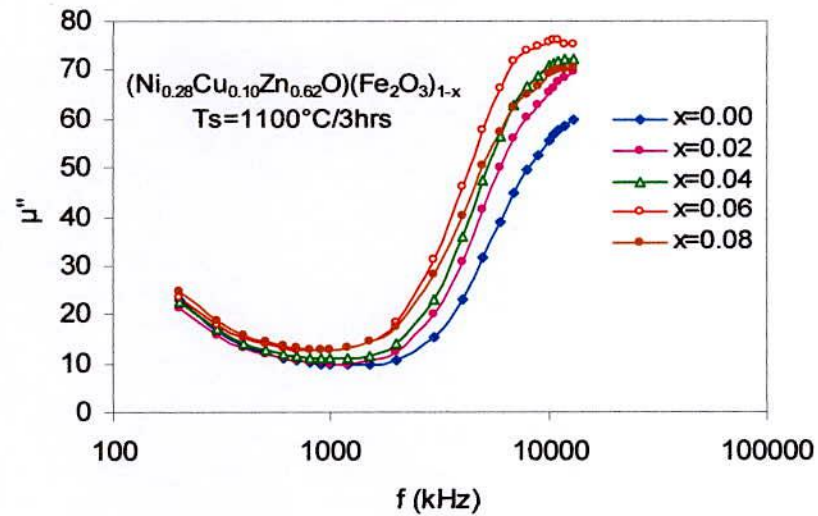
Fig. 4.9 Complex initial permeability spectra for $(Ni_{0.28}Cu_{0.10}Zn_{0.62}O)$ $(Fe_2O_3)_{1-x}$ ferrites at (a) 1100°C, (b) 1150°C and (c) 1200°C for 3 hrs

Table-4.3 Data for permeability (μ'), resonance frequency (f_r) and Snoek's Limit ($\mu'.f_r$) of $(Ni_{0.28}Cu_{0.10}Zn_{0.62}O)(Fe_2O_3)_{1-x}$ ferrites

Fe-deficient content (x)	Ts=1100°C			Ts=1150°C			Ts=1200°C		
	μ' (10kHz)	f_r (MHz)	Snoek's $\mu.f_r$(GHz)	μ' (10kHz)	f_r (MHz)	Snoek's $\mu.f_r$(GHz)	μ' (10kHz)	f_r (MHz)	Snoek's $\mu.f_r$(GHz)
0.00	209	13	2717	251	11	2761	240	12	2880
0.02	217	12	2604	284	10	2840	303	9	2781
0.04	229	12	2748	308	09	2772	311	8.5	2643
0.06	265	10.5	2782	316	08	2528	313	8.5	2660
0.08	280	10	2800	358	7.50	2685	343	7.5	2572
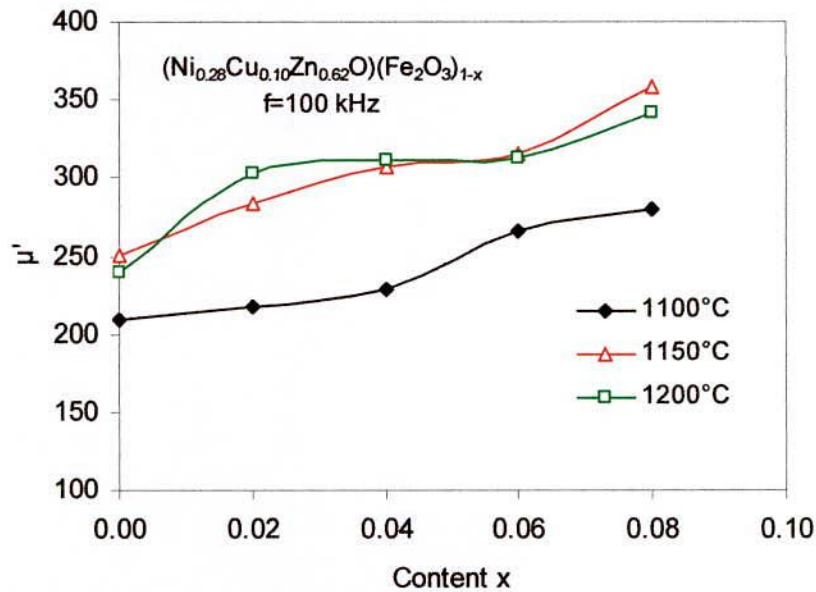
Fig. 4.10 Variation of initial permeability, μ' at frequency 100 kHz with Fe-deficient of $(Ni_{0.28}Cu_{0.10}Zn_{0.62}O)(Fe_2O_3)_{1-x}$ ferrites

Fig. 4.10 shows that the variation of initial permeability at frequency 100 kHz with Fe-deficient of $(Ni_{0.28}Cu_{0.10}Zn_{0.62}O)(Fe_2O_3)_{1-x}$ ferrites sintered at 1100°C, 1150°C and 1200°C for 3 hours. It was observed that the permeability increases slowly with increase in Fe-deficiency as well as with increasing T_s. For the sample with x = 0.08 the maximum initial permeability is observed at a sintering temperature of T_S = 1150°C for 3 hrs. The increase of permeability with Fe-deficient is connected with increased magnetization, density, grain size and possible reduction of anisotropy energy. Moreover as the sintering temperature increases dispersion of μ'-f spectra also shifts to the lower

109

frequency range as a result of increasing density and grain size, as proposed by Nakamura [4.28]. An increase in the density of ferrites not only results in the reduction of demagnetization field due to the presence of pores but also raise the spin rotational contribution, which in turn increases the permeability [4.29].

4.3.4 Frequency Dependence of Quality Factor

Frequency dependence of quality factor (QF) of the samples sintered at Ts=1100, 1150 and 1200°C for 3 hours were measured and Fig. 4.11 shows the results of the samples sintered at Ts=1150°C/3hrs. Quality factor signifies the merit of the material from the application point of view. The variation of the quality factor with frequency showed a similar trend for all the samples. Q-factor increases with increases of frequency showing a peak and then decreases with further increase of frequency. It is seen that quality factor deteriorates beyond 5 MHz i.e., the loss tangent is minimum up to 5 MHz and then it rises rapidly. The loss is due to lag of domain wall motion with respect to the applied alternating magnetic field and is attributed to various domain defects [4.30], which include non-uniform and non-repetitive domain wall motion, domain wall bowing, localized variation of flux density and nucleation and annihilation of domain walls.
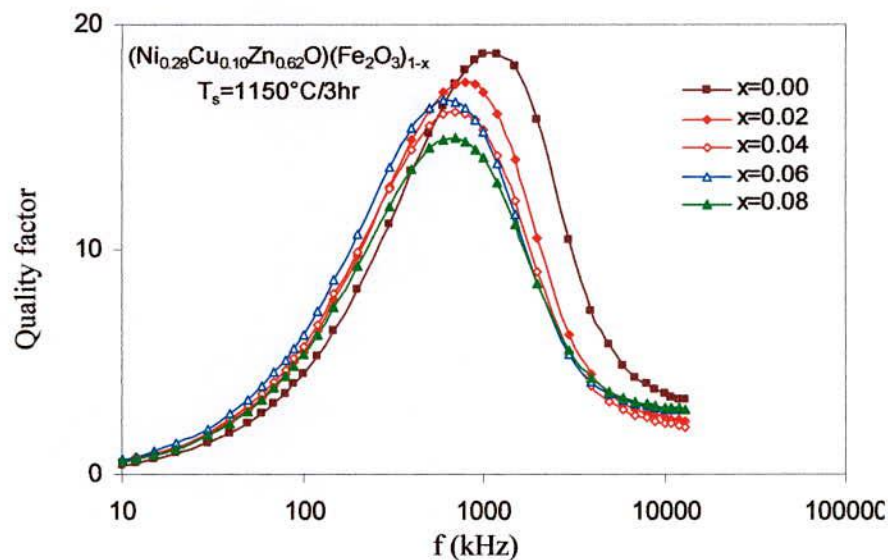
Fig. 4.11 Frequency dependence of Quality factor of $(Ni_{0.28}Cu_{0.10}Zn_{0.62}O)$ $(Fe_2O_3)_{1-x}$ ferrites sintered at 1150°C for 3 hours

This happens at the frequency where the permeability begins to drop with frequency. This was manifested in the frequency dependence of permeability of samples shown in Fig. 4.8. This phenomenon is associated with the ferrimagnatic resonance within the domains and at the resonance maximum energy is transferred from the applied magnetic field to the lattice resulting in the rapid decrease in quality factor. The peak corresponding to maxima in Q-factor shifts to lower frequency range as Fe-deficiency increases. Sample with x = 00 posses the maximum value of quality factor.

4.3.5 Low Field B-H loop at Room Temperature

The B-H loops at room temperature of the investigated compositions ($Ni_{0.28}Cu_{0.10}Zn_{0.62}O$) $(Fe_2O_3)_{1-x}$ sintered at 1100°C, 1150°C and 1200°C were measured at constant frequency (f = 1kHz) shown in Fig. 4.12 (a), (b) and (c). From the B-H loops, the remanence induction, (B_r) Saturation induction, (B_s) and coercive force (H_c) were determined as a function of x and sintering temperature. From these loops, the high coercivity, H_c is observed at x=0.00 and it decrease almost linearly with increasing Fe-deficiency for all the studied samples sintered at different temperatures.

(a)
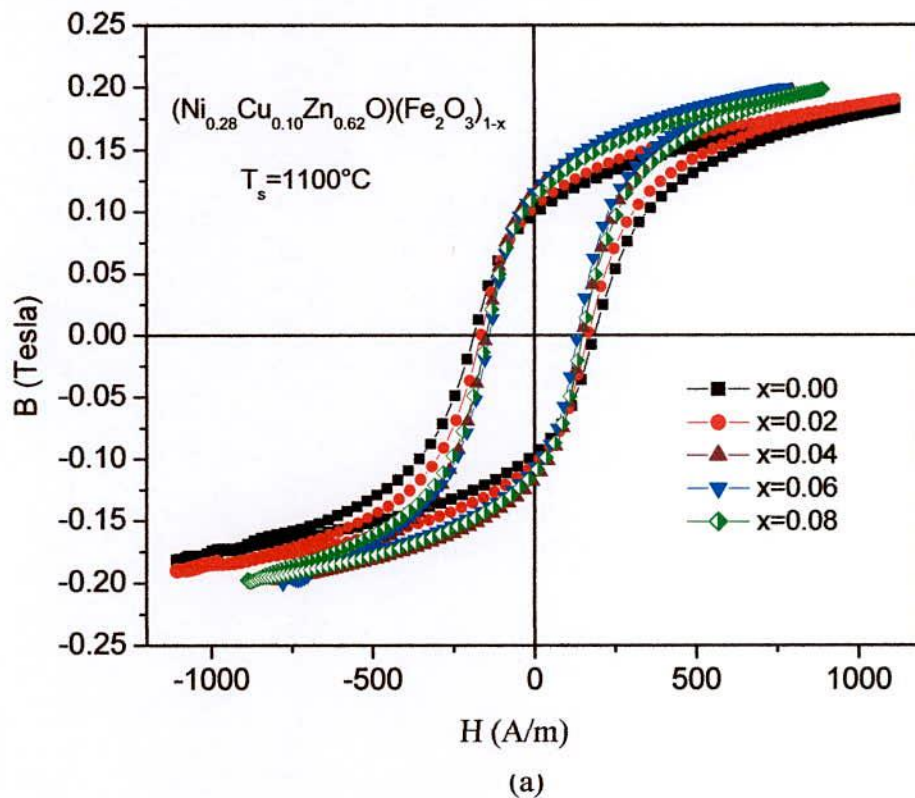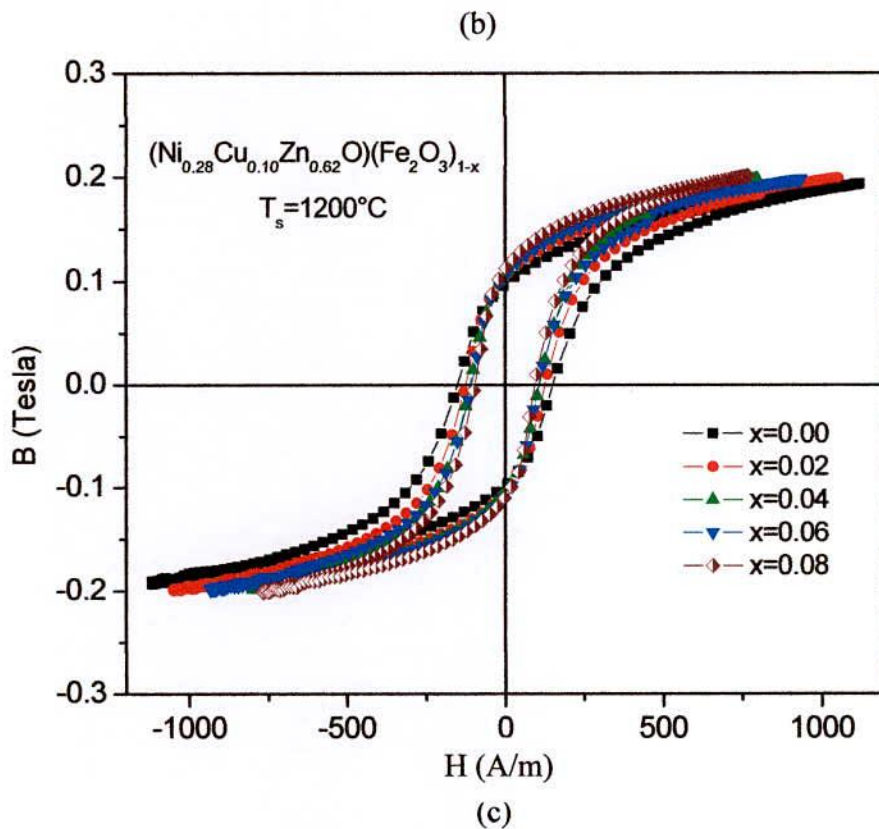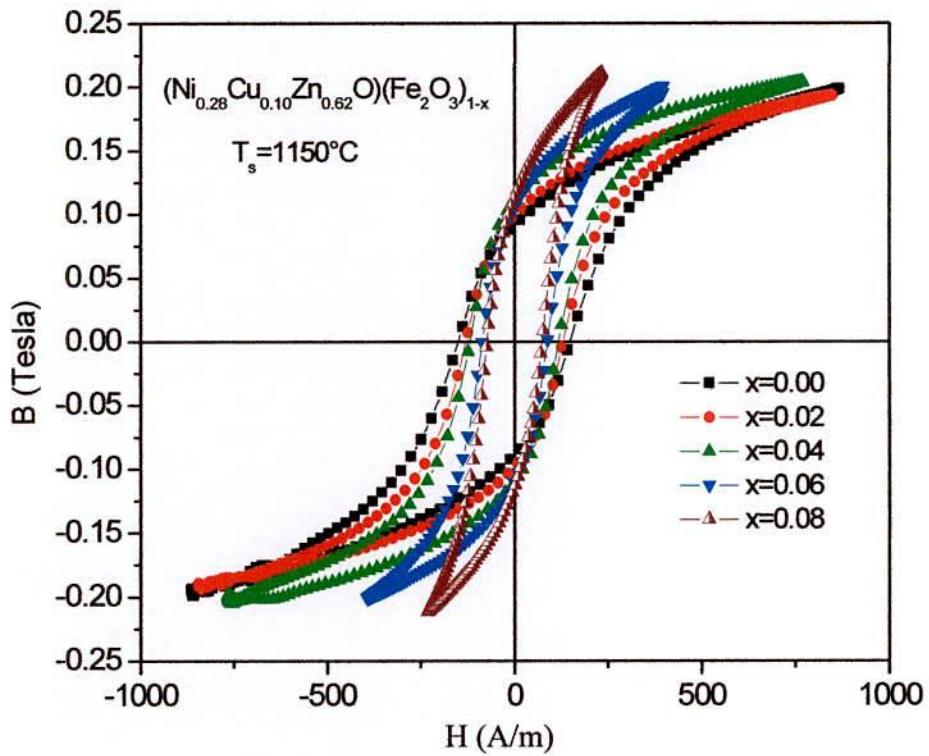
Fig. 4.12 Magnetic hysteresis graphs of $(Ni_{0.28}Cu_{0.10}Zn_{0.62}O)(Fe_2O_3)_{1-x}$ ferrite with x sintered at (a) 1100°C (b) 1150°C and (c) 1200°C for 3 hours at constant frequency f = 1kHz

These results are shown in Table 4.4. It is observed that the B_r and B_s both increase with x content. For high permeability material a low coersivity is a prime requirement which is fulfilled in the present study since permeability is inversely related to Coercivity i.e. $\mu' \propto \dfrac{1}{H_c}$. Again a high B_s is also a requirement for high permeability which is also manifested in the studied sample (see Table 4.4). Fig. 4.13 shows the dependence of permeability, μ' and Coercivity, H_c with x content. And excellent correlation between μ' and H_c is observed.

Table-4.4 The experimental values of coercive force (H_c), remanence induction (B_r), saturation induction (B_s), $\left(\dfrac{B_r}{B_s}\right)$ ratio and losses of $(Ni_{0.28}Cu_{0.10}Zn_{0.62}O)$ $(Fe_2O_3)_{1-x}$ samples at room temperature with constant frequency (f = 1kHz) at different sintering temperature

Fe-deficient content (x)	T_S (°C) / 3hrs	H_C (Oe)	B_r (kG)	B_s (kG)	B_r/B_s	Losses (W/kg)
0.00	1100	2.34	0.97	1.84	0.53	22.13
	1150	1.93	0.91	2.15	0.42	14.75
	1200	1.89	0.97	1.93	0.50	19.85
0.02	1100	2.08	1.03	1.90	0.54	21.11
	1150	1.74	1.04	2.08	0.50	19.11
	1200	1.59	1.03	2.00	0.52	17.71
0.04	1100	1.87	1.17	1.97	0.59	20.39
	1150	1.60	1.16	2.24	0.52	19.97
	1200	1.49	1.10	2.14	0.51	18.92
0.06	1100	1.87	1.21	2.13	0.56	23.64
	1150	1.38	1.32	2.70	0.49	16.66
	1200	1.34	1.06	1.99	0.53	16.82
0.08	1100	1.94	1.10	2.10	0.52	23.85
	1150	1.29	1.73	3.42	0.50	14.29
	1200	1.29	1.15	2.16	0.53	16.78

These results are shown in Table 4.4. It is observed that the B_r and B_s both increase with x content. For high permeability material a low coersivity is a prime requirement which is fulfilled in the present study since permeability is inversely related to Coercivity i.e. $\mu' \propto \dfrac{1}{H_c}$. Again a high B_s is also a requirement for high permeability

which is also manifested in the studied sample (see Table 4.4). Fig. 4.13 shows the dependence of permeability, μ' and Coercivity, H_c with x content. And excellent correlation between μ' and H_c is observed.
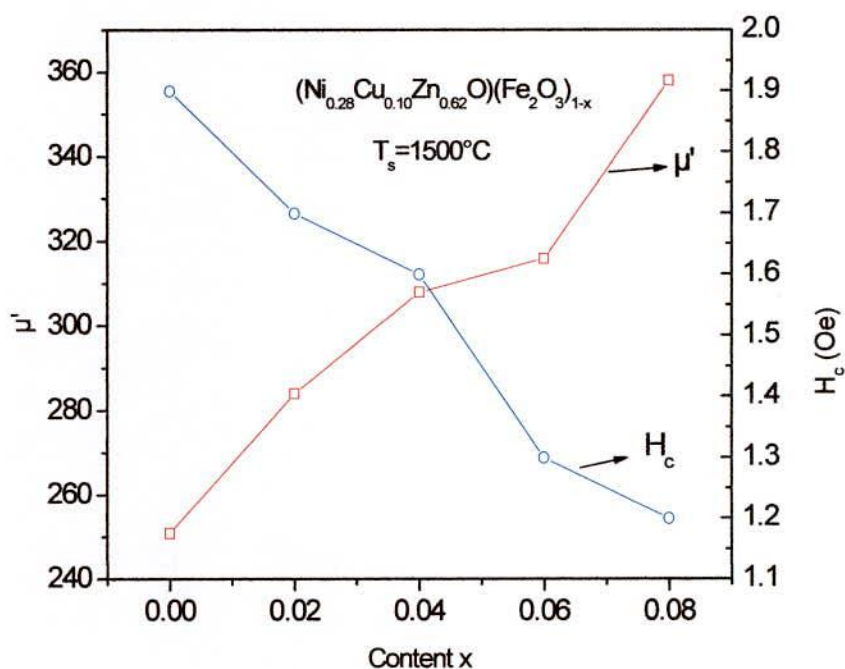
Fig. 4.13 Magnetic hysteresis graph of $(Ni_{0.28}Cu_{0.10}Zn_{0.62}O)(Fe_2O_3)_{1-x}$ ferrite sintered for 1150°C at constant frequency f=1 kHz and μ' and H_c versus composition x

The low coercive force and higher permeability, confirms that the development of soft magnetic characteristic properties of Ni-Cu-Zn ferrite with increasing Fe-deficiency, which is well known as soft magnetic materials from application point of view. It is also observed that the coercivity decreases with increase in sintering temperature. The decrease in the H_c with T_s values is understandable because of the substantial increase in grain size in response to the increase in sintering temperature which facilitating the movement of the magnetic domain. Thus, because the magnetic properties (magnetization, permeability) are dependent on the domains wall movement, large grains tend to consist of a greater number of domain walls. The magnetization / demagnetization caused by domain wall movement require lower energy compared to that required for domain rotation. Therefore, the larger the grain size, easier the displacement of domain walls.

The area of the B-H loops in Fig. 4.12 (a), (b) and (c) reveals the characteristic soft or permeable magnetic material of the $(Ni_{0.28}Cu_{0.10}Zn_{0.62}O)$ $(Fe_2O_3)_{1-x}$ with increase of Fe-deficiency. In this case, the effect of the microstructure on the magnetic properties for operation at low frequencies has stronger effect than that of composition. The increase of Fe-deficiency decreased the coercive field and the hysteresis losses, increase the samples magnetization and permeability. Saturation induction (B_s), is found to increase with increasing Fe-deficient. The different values of retentivity and $\dfrac{B_r}{B_s}$ ratio observed are interpreted in a quantitative way by means of domain theory. The predominant losses in Ni-Cu-Zn ferrite are hysteresis and eddy current at operating frequencies lower than the relaxation frequency of the wall displacement. The loss in hysteresis depends on the magnetostriction, magnetocrystalline anisotropy, saturation magnetization and microstructure. The values of maximum flux density, coercive field, and hysteresis loss of the system has been found with x=0.08.

4.3.6 Magnetization Measurement

Magnetization as a function of applied magnetic field up to 20 kOe measured with vibrating sample magnetometer (VSM) at room temperature of $(Ni_{0.28}Cu_{0.10}Zn_{0.62}O)$ $(Fe_2O_3)_{1-x}$ sintered at 1150°C for 3 hrs samples has been measured and is presented in Fig. 4.14. It is observed that the magnetization increases sharply at very low field (H < 1 kOe) which corresponds to magnetic domain reorientation due to domain wall displacement and thereafter increase slowly up to saturation due to spin rotation. This magnetization process is connected with soft magnetic of behavior of magnetic material. The slow process of magnetization toward the saturation value is connected with the magnetic anisotropy effect. Actual saturation could not be attained even with magnetic field as high as 16000 Oe.

Fig. 4.15 Shows the variation saturation magnetization (M_s) of the samples as a function x content. It is observed from the Fig. 4.15 and Table 4.5 that M_s increases up to x = 0.06 and then it decrease slightly with x content. The insignificant decrease of M_s may be experimental uncertainty.
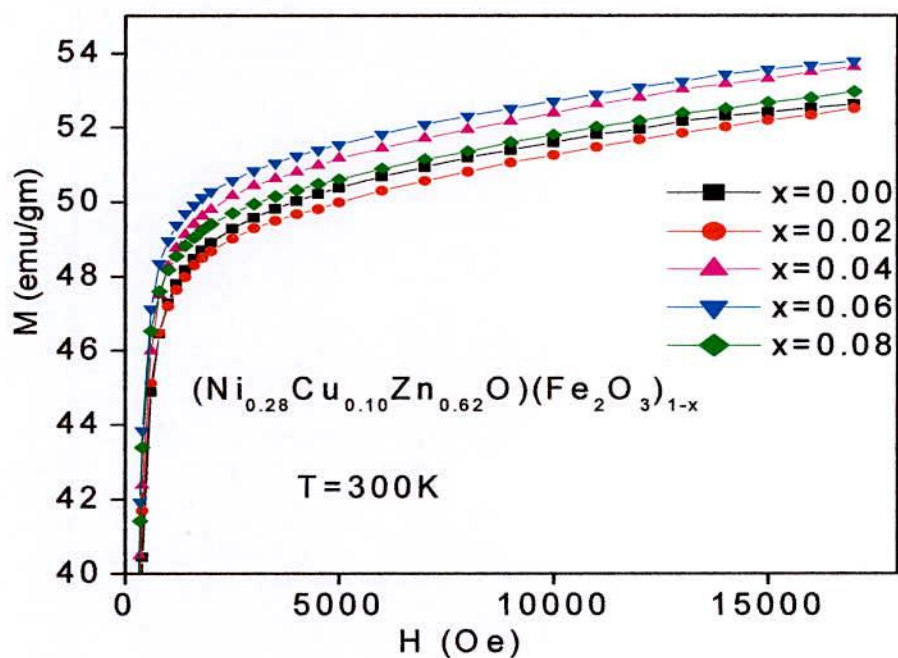
Fig. 4.14 Field dependence of magnetization for x = 0.00-0.08 for $(Ni_{0.28}Cu_{0.10}Zn_{0.62}O)$ $(Fe_2O_3)_{1-x}$ ferrites at room temperature
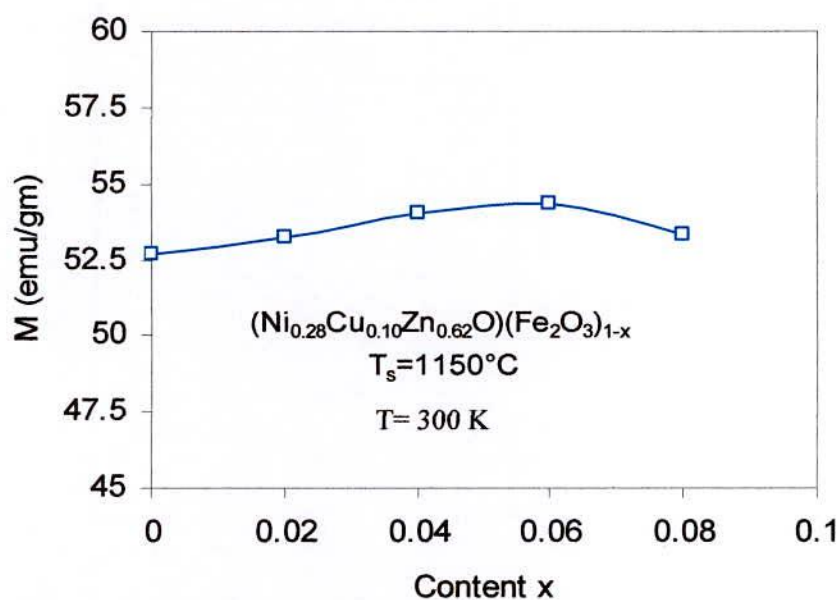
Fig. 4.15 Saturation magnetization, M_s versus Fe deficient in $(Ni_{0.28}Cu_{0.10}Zn_{0.62}O)$ $(Fe_2O_3)_{1-x}$ ferrites

The observed variation in saturation magnetization can be explained on the basis of cation distribution and the exchange interactions between A and B sites. The increase in M_s with increase of Fe-deficiency is due to the increase of resultant sub-lattice magnetic moment, which can be explained on the basis of Neel's two sub-lattice model. Neel [4.31] considered three types of exchange interactions between unpaired electrons of two ions lying in A and B sites. In perfect ferrites, the A-B exchange interaction is normally anti-ferromagnetic having pre-dominant role. Therefore, the spins at the A-sites will be anti-parallel to the spins at B-sites below a transition temperature (called Curie temperature).

Table-4.5 Saturation magnetization (M_s) Coercive filed (H_c) and remanence (M_r) of ($Ni_{0.28}Cu_{0.10}Zn_{0.62}O$) ($Fe_2O_3$)$_{1-x}$ ferrite with different x-values

Fe-deficient Content (x)	T_s=1150°C				
	M (emu/g)	B_s (kG)	H_c (Oe)	B_r (kG)	Losses (W/kg)
0.00	52.70	2.15	1.93	0.91	14.75
0.02	53.22	2.10	1.74	1.04	19.11
0.04	54.05	2.24	1.60	1.16	19.97
0.06	54.32	2.70	1.38	1.32	16.66
0.08	53.35	3.42	1.30	1.73	14.29

Fig. 4.16 shows the Temperature dependence of saturation magnetization measured with an applied magnetic field of H=5 kOe. It is observed that magnetization, M_s decreases monotonically with increasing temperature and finally tends toward zero above the Curie temperature, T_c. The slow decrease of magnetization around the T_c is due to the decrease of M_s from the two sublattice magnetization unlike ferromagnet where much sharper fall of M_s is observed that at $T=T_c$. From the graph 4.16, it is observed that at low temperature magnetization increases slightly with increasing x content.
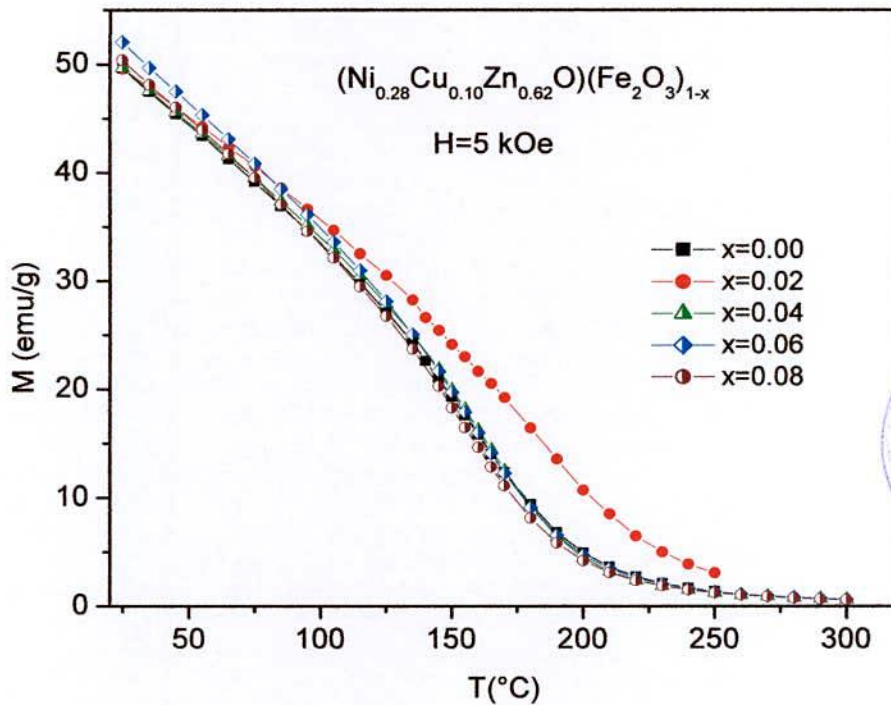
Fig. 4.16 Temperature dependence of magnetization of $(Ni_{0.28}Cu_{0.10}Zn_{0.62}O)$ $(Fe_2O_3)_{1-x}$ ferrites with an applied field 5 kOe

4.3.7 Scanning Electron Microscope (SEM) Microstructure Analysis

Microstructure significantly affects the magnetic and electrical properties of ferrites. Domain behavior and its relation to microstructure of magnetic materials and the critical grain size, necessary to maintain a single domain can be obtained from microstructure study of the ferrite samples. Grain growth is closely related to the grain boundary mobility. Recrystallization and grain growth involve the movement of grain boundaries. It is seen from the micrographs that the dense microstructure are obtained for all the samples. The average grain size was obtained from SEM picture by linear intercept method [4.32]. Fig. 4.17, Fig. 4.18 and Fig. 4.19 show the SEM microstructure of $(Ni_{0.28}Cu_{0.10}Zn_{0.62}O)$ $(Fe_2O_3)_{1-x}$ ferrites sintered at 1100°C, 1150°C and 1200°C. It is clear that the microstructure of Ni-Zn-Cu ferrite strongly depends on the amount of Fe-deficient in the samples. Fe-deficient influents the microstructure of the Ni-Cu-Zn ferrites by the presence of Cu which activates the sintering process.
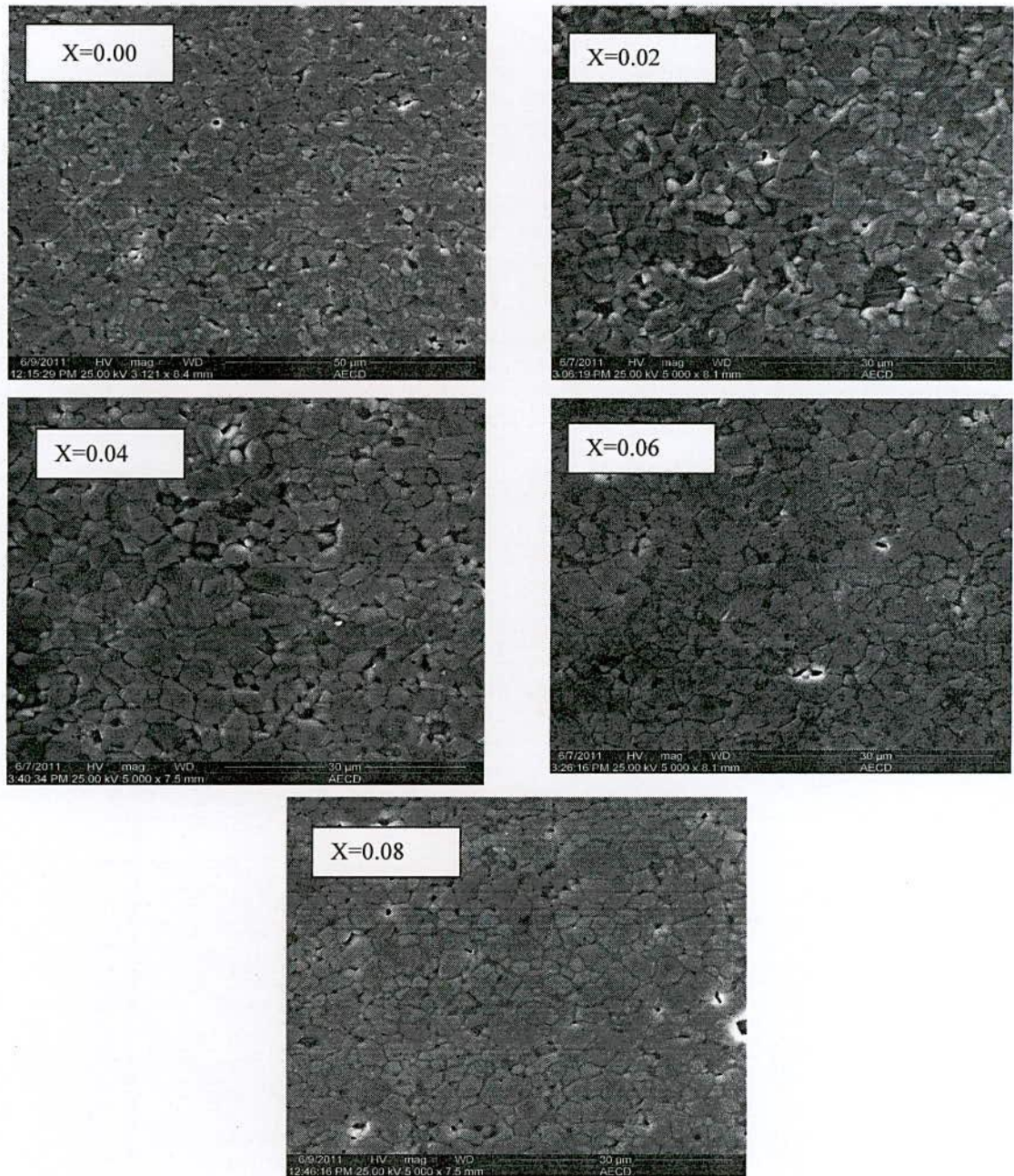
Fig. 4.17 SEM micrographs of the system ($Ni_{0.28}Cu_{0.10}Zn_{0.62}O$) ($Fe_2O_3$)$_{1-x}$ sintered at 1100°C
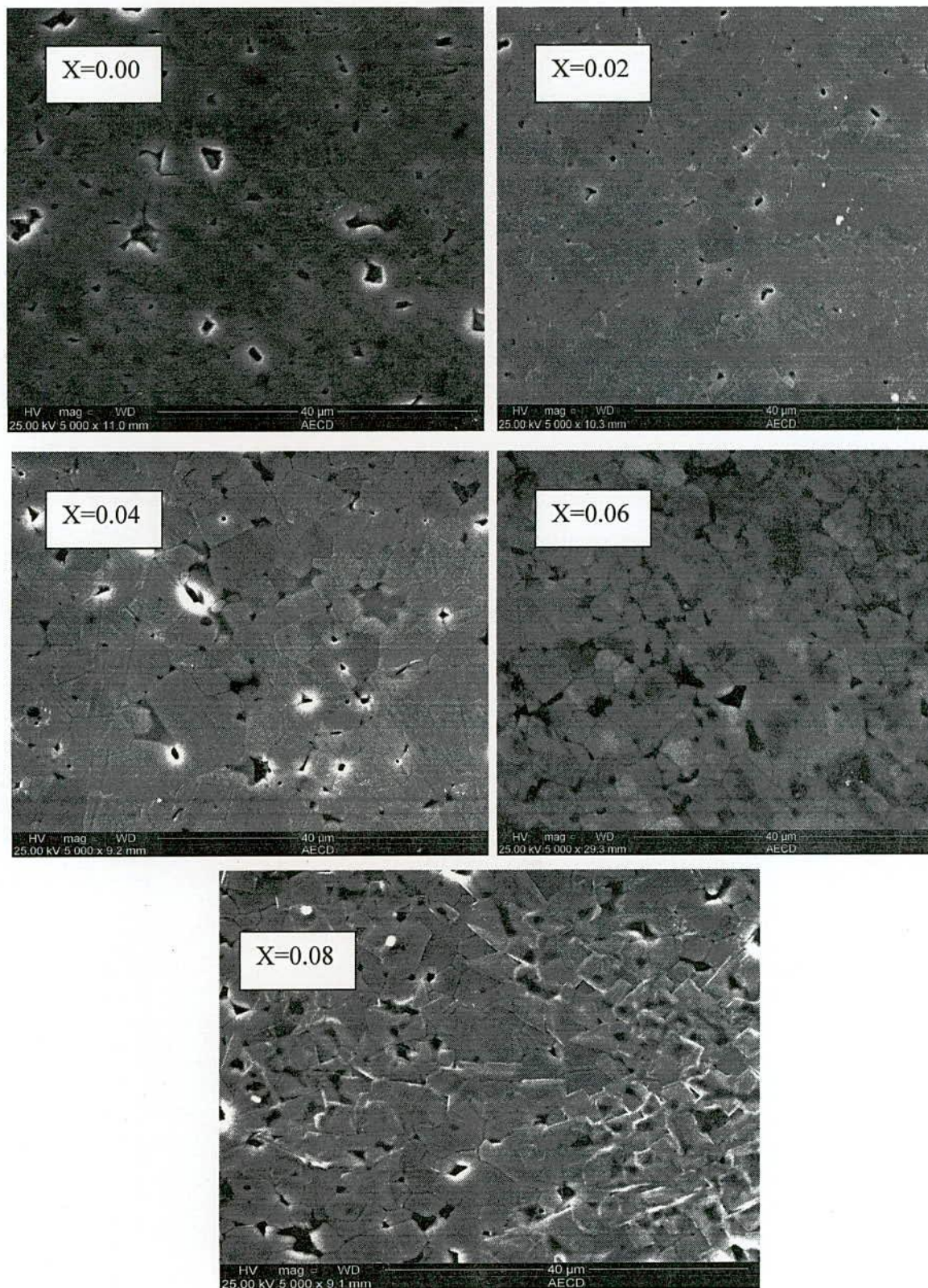
Fig. 4.18 SEM micrographs of the system $(Ni_{0.28}Cu_{0.10}Zn_{0.62}O)(Fe_2O_3)_{1-x}$ sintered at 1150°C
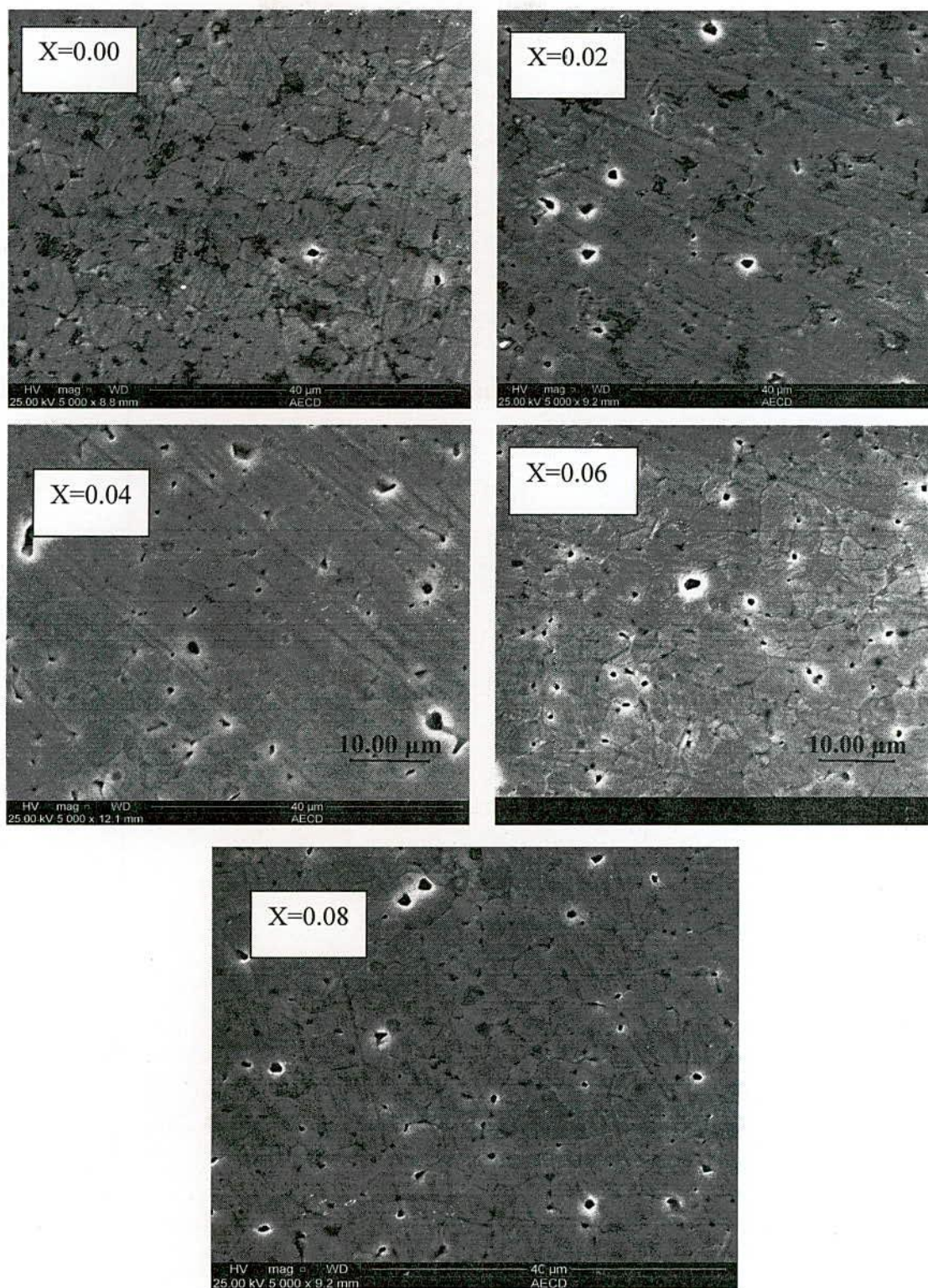
Fig. 4.19 SEM micrographs of the system $(Ni_{0.28}Cu_{0.10}Zn_{0.62}O)(Fe_2O_3)_{1-x}$ sintered at 1200°C

It facilitates the grain growth by increasing the rate of cation interdiffusion as a result of its segregations to the grain boundaries [4.24]. The behavior of grain growth reflects the competition between the driving force for grain boundary movement and the retarding force that drives the grain boundaries to grow over pores, thereby decreasing the pore volume and making the material dense. When the driving force of the grain boundary in each grain is homogeneous, the sintered body attains a uniform grain size distribution. Abnormal grain growth occurs if this driving force is inhomogeneous. During our investigation it has also been noticed that the grain size of the samples increases with the increasing in sintering temperature.

During the early stage of sintering the volume fraction of pores is very large and no grain growth occurs at all. As the sintering proceeds, the porosity decreases and many of the small pares disappear. The grains that grow consume their neighbors, grow larger and add more sides. As the grain size increases it is expected that the permeability of the samples also will be increased due the domain wall motion. Resistivity of the samples depends upon the porosity and high resistivity is needed for low losses. Considering the entire factors, we can select an optimum sintering temperature for each sample from the microstructure study. For the samples with small grains, pores are formed at the grain boundaries whereas samples with large grains, the majority of pores are trapped inside the grains at large distance from the grain boundaries as well as some pores may migrate to the grain boundary, which might effect the permeability, density and resistivity of Ni-Cu-Zn ferrites. During the liquid phase sintering, grain growth occurs via a dissolving/solution – precipitation process. Energetically, small grains are less stable than large grains due to their higher specific surface areas. As a consequence, small grains would be dissolved in the liquid-phase layers. Once the concentration of the dissolved phase reached a critical level, precipitation would take place. It seems that small grains have to "Swim" through a barrier (liquid-phase layer) to combine with a large grain.

It is observed that an increase in the Fe-deficient results in an increase in the coverage of the grain by the liquid-phase layers, and this is beneficial to grain growth. As a result the average grain size increases with increasing Fe-deficient. Effect of sintering temperature on the grain growth of $(Ni_{0.28}Cu_{0.10}Zn_{0.62}O)$ $(Fe_2O_3)_{1-x}$ ferrites has been investigated. Fig. 4.17 to Fig. 4.19 shows the SEM micrographs of the sample x = 0.00-

0.08 sintered at different temperature. The increase in grain size with sintering temperature is clearly visible. The average grain size continuous to increase from 2.75 μm to 4.16 μm for x=0.00 while increasing the sintering temperature from 1100°C to 1200°C similar behavior is observed for other samples of the series. Fig. 4.20 represent the average grain diameter as a function Fe-deficient(x) sintered at 1100°C, 1150°C and 1200°C. From this figure it is observed that the grain sizes markedly increased with the Fe-deficiency and sintering temperature. The values of average grain size of the samples are presented in Table-4.5.
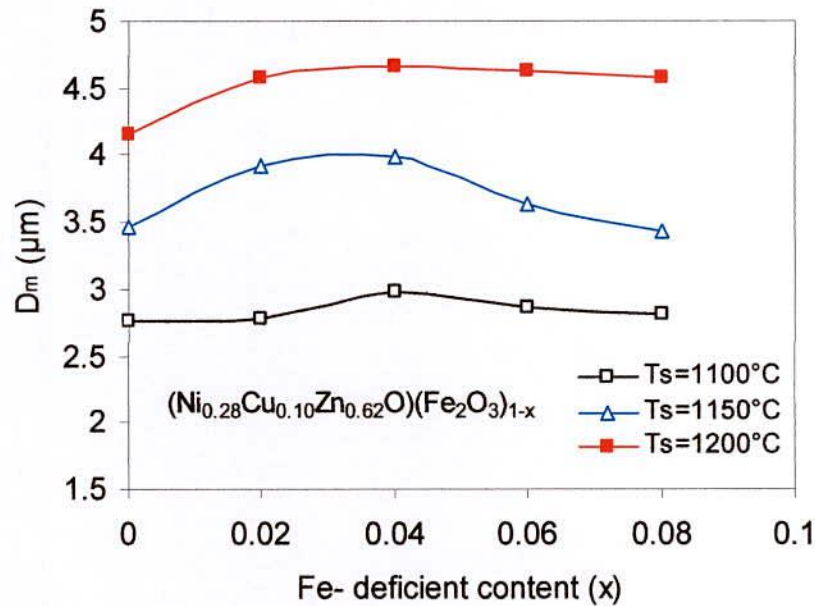
Fig. 4.20 Average grain size (D_m) as a function Fe-deficient (x) of the samples

Table-4.6 The average grain size of the $(Ni_{0.28}Cu_{0.10}Zn_{0.62}O)$ $(Fe_2O_3)_{1-x}$ ferrites sintered at 1100°C, 1150°C and 1200°C

Fe-deficient Content (x)	T_s=1100°C D_m (μm)	T_s=1150°C D_m (μm)	T_s=1200°C D_m (μm)
0.00	2.75	3.47	4.16
0.02	2.78	3.91	4.58
0.04	2.98	3.99	4.66
0.06	2.87	3.64	4.63
0.08	2.81	3.44	4.58

4.4 Electrical Transport Property

4.4.1 Compositional Dependence of DC Electrical Resistivity

DC resistivity is an important electrical property of ferrites in high frequency application Fig. 4.21 gives the room temperature values of resistivity (ρ_{dc}) versus Fe-deficient of samples of series ($Ni_{0.28}Cu_{0.10}Zn_{0.62}O$) ($Fe_2O_3$)$_{1-x}$ ferrites by using a Keithley Electrometer. For measurements, the pellet shaped samples were coated with silver paint on the both surfaces of each sample under study. The DC resistivity is found to increase with Fe-deficient up to x = 0.06. Resistivity is found to decrease with further increase of Fe-deficient.
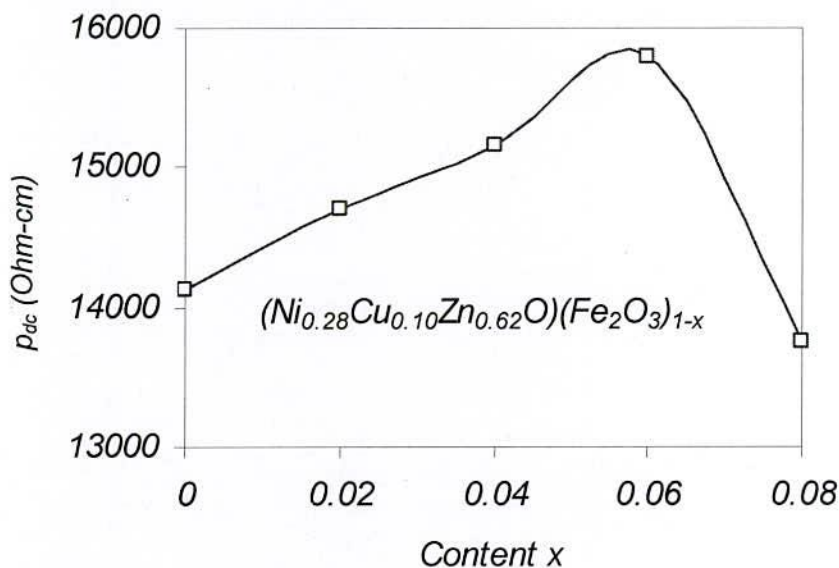
Fig. 4.21 Room temperature DC resistivity as a function Fe-deficient of ($Ni_{0.28}Cu_{0.10}Zn_{0.62}O$)($Fe_2O_3$)$_{1-x}$ ferrites at1150°C

This decrease of resistivity may be attributed to the entrapped intragranular porosity, Sankpal et. al. and Shaikh et. al. measured resistivity as a function of composition in their work on Ni-Cu and Li-Cd ferrites [4.33-4.34]. Electrical conduction in Ni-Cu-Zn ferrites can be explained by Verway–de-Boer mechanism [4.35] involving electron exchange between ions of the same element existing in more than one valence

state and distributed randomly over crystallographically equivalent lattice sites. Thus the variation in resistivity may be explained either by probabilities of the cations present in B-sites or by the micro structural modification brought about the sintering conditions or by both. The highest value of DC resistivity for x = 0.06 same is observed to be 1.57×10^4 Ω-cm. The observed decrease in resistivity with the increase of Fe-deficient has been related to the decrease of porosity since pores are non-conductive. Obviously the more the Fe^{2+} ions the higher the conduction mechanism and consequently a decrease in the resistivity.

4.4.2 Frequency Dependence of AC Resistivity

The electrical properties of ferrite materials depend upon the method of preparation, chemical composition, grain size and sintering temperature. The frequency dependence of AC electrical resistivity of ferrites is crucial because of its huge applications with frequency increases from 1 kHz to 13 MHz and is shown in Fig. 4.22 and Fig. 4.23 at room temperature.
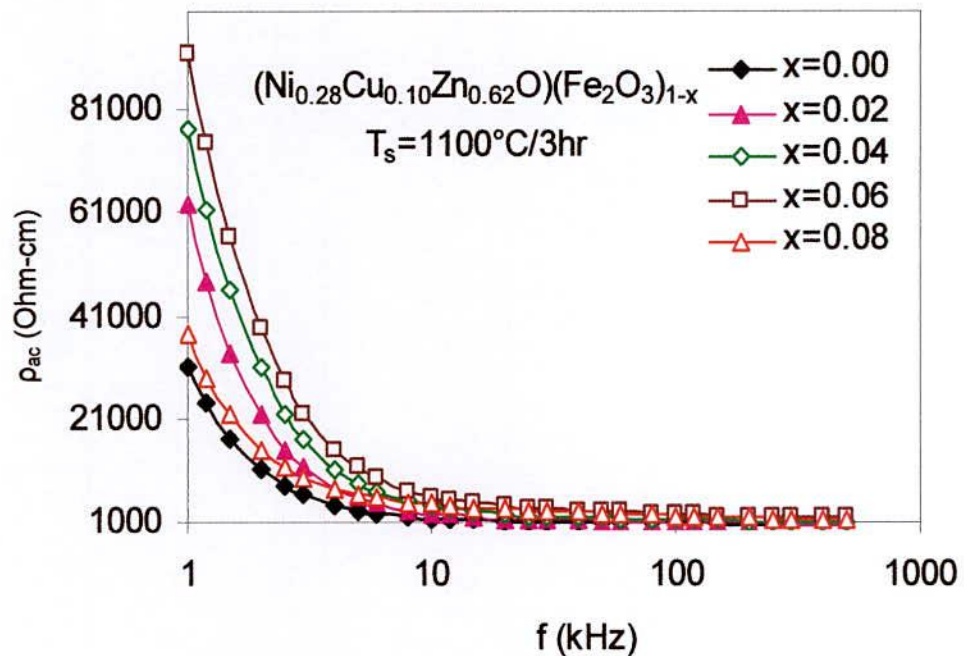
Fig. 4.22 Frequency dependence of AC resistivity of $(Ni_{0.28}Cu_{0.10}Zn_{0.62}O)(Fe_2O_3)_{1-x}$ ferrites at 1100°C/3hrs

All the samples show the significant dispersion with frequency which is the normal ferrimagnetic behavior. The resistivity of the ferrites is expected to decrease with an increase in the frequency; this may be due to the low dielectric constant and also depends on the porosity and composition [4.36]. From the results, it is determined that dielectric constant with low ac resistivity at a low frequency such as 10 kHz, is much higher than with high ac resistivity.
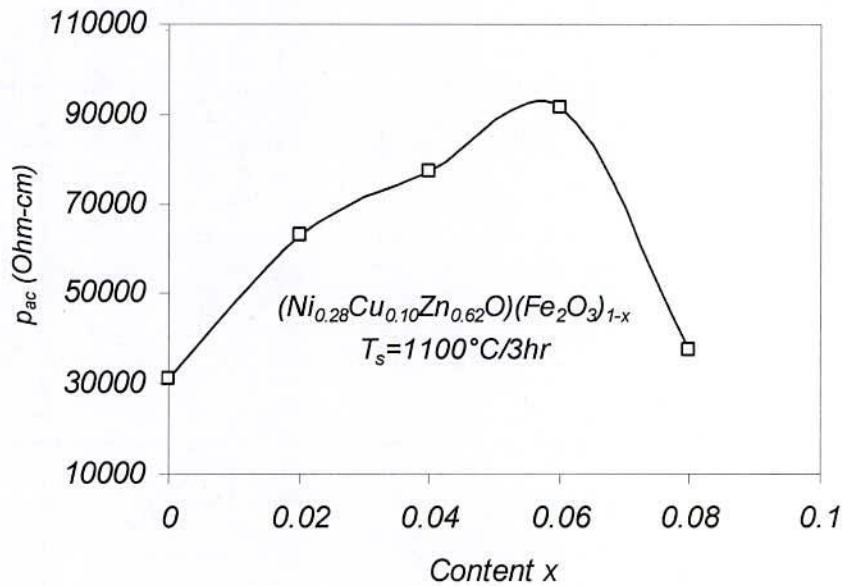
Fig. 4.23 Room temperature Ac resistivity as function of Fe-deficient of $(Ni_{0.28}Cu_{0.10}Zn_{0.62}O)(Fe_2O_3)_{1-x}$ ferrites at 1100°C/3hrs

4.4.3 Frequency Dependence of Dielectric Constant

Fig. 4.24 (a) and Fig 4.24 (b) shows are the variation of dielectric constant ε', with frequency for different composition of $(Ni_{0.28}Cu_{0.10}Zn_{0.62}O)(Fe_2O_3)_{1-x}$ ferrites at 1150°C/ 3hrs and1200°C/ 3hrs from 1kHz to 13MHz at room temperature. It can be seen that all samples show the frequency dependent phenomena i.e., the dielectric constant decreases with increasing frequency exhibiting a normal ferrimagnetic behavior. A more dielectric dispersion is observed at lower frequency region and it remains almost independent of applied external field at high frequency side. The dielectric behavior of

126

ferrites may be explained on the basis of dielectric polarization process is similar to that of the conduction mechanism and are mainly by the hopping conduction mechanism. Electrical conduction in ferrites can be explained by Verway-de-Boer hopping mechanism [4.35]. Verway explained that the electronic conduction in ferrites is mainly due to hopping of electrons between ions of the same element exiting in more than one value state and distributed randomly over crystallography equivalent lattice sites. A number of such ions are formed during the sintering.
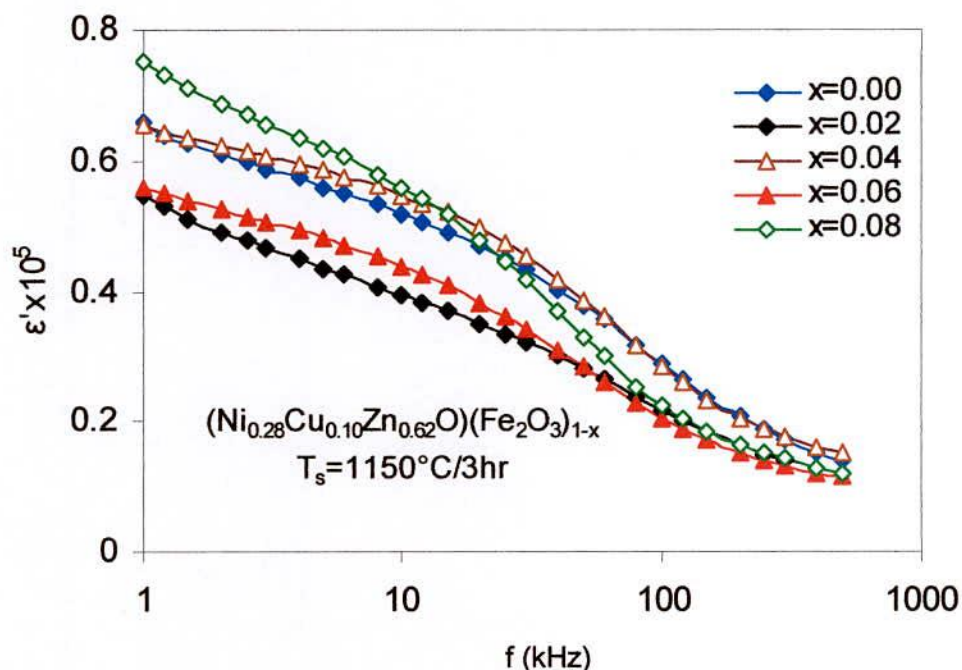
Fig. 4.24 (a) Dielectric constant as a function of frequency for $(Ni_{0.28}Cu_{0.10}Zn_{0.62}O)$ $(Fe_2O_3)_{1-x}$ ferrites sintered at 1150°C/3hrs

Fe^{2+} ion concentration is a characteristic properly of a ferrite material and depends upon several factors such as sintering temperature/time and atmosphere including the grain structure. Creation of Fe^{2+} ions gives rise to electron hopping between Fe ions in +2 and +3 valence states. The electronic exchange between Fe^{2+} and Fe^{3+} ions results the local displacement of charges in the direction of applied electric field, which is responsible for the polarization in ferrites [4.37, 4.38]. The magnitude of exchange depends on the concentration of Fe^{2+}/Fe^{3+} ion pairs present on B-site. Since Fe^{2+} ions are easily polarizable, the larger the number of Fe^{2+} ions the higher would be the dielectric

constant. The dielectric constant decreases with increasing frequency and then reaches almost constant value due to the fact that beyond a certain frequency of external AC field the electron exchange between Fe^{2+} and Fe^{3+} cannot follow the alternating field. This type of dielectric behavior was observed in a number of ferrites such as Cu-Cd [4.39], Mg-Cu-Zn ferrites [4.40] and Li-Co ferrites [4.41].
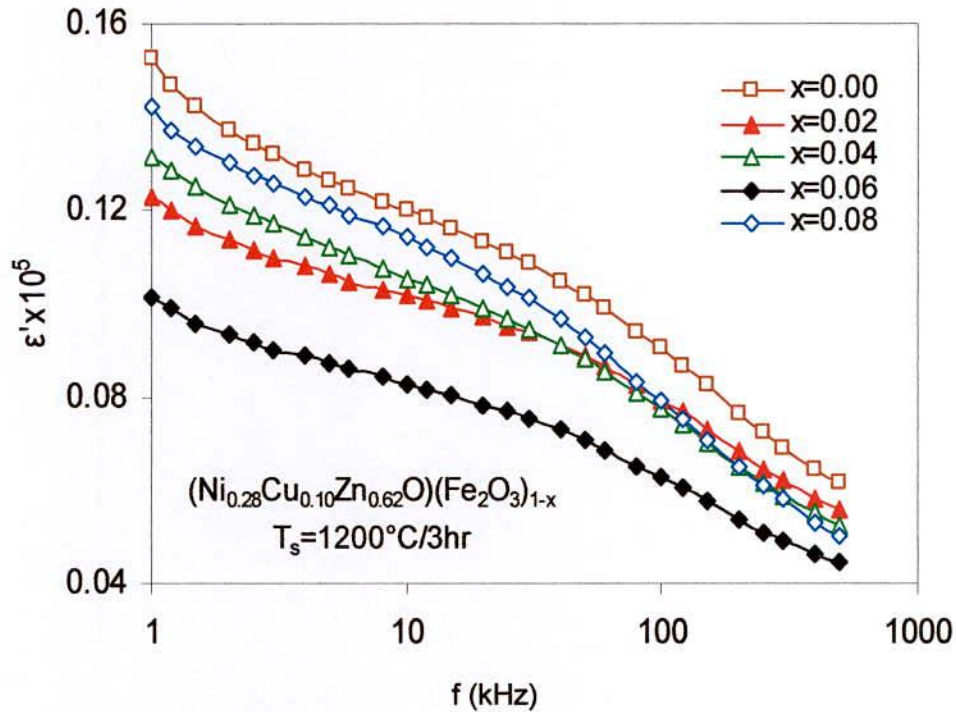
Fig. 4.24 (b) Dielectric constant as a function of frequency for $(Ni_{0.28}Cu_{0.10}Zn_{0.62}O)$ $(Fe_2O_3)_{1-x}$ ferrites sintered at 1200°C/3hrs

All the samples have high value of ε' in the order of 10^5 at low frequencies. The inhomogeneous dielectric structure was supposed to be consisted by two layers. The first one is the fairly well conducting large ferrite grain which is separated by the second thin layer of the poorly conducting grain boundaries. The grain boundaries of lower conductivity and higher dielectric constant are found to be more effective at lower frequencies while the ferrite grains of higher conductivity and lower dielectric constant are more effective at high frequencies.

4.5 Summary

The x-ray diffraction confirmed the single phase cubic spinal structure of the samples. The lattice constant decreases with increasing Fe-deficient content obeying Vegard's law. Bulk density is found to increase white porosity decreases with decreasing Fe-deficient content. Curic temperature slightly increases linearly with the addition of Fe-deficient content. The initial permeability increases slowly at low Fe-deficient and the increase sharply for all the sintering temperature. The hysteresis behavior the decrease of coercivity with increases in sintering temperature. Saturation magnetization increases with Fe-deficient content up to $x = 0.06$ there after it decreases. The grain size of the samples increases with increasing sintering temperature. The DC electrical resistivity increases with increasing Fe-deficient content up to $x = 0.06$ there after decrease. The AC electrical resitivity decrease with an increase in frequency. The dielectric content decreases with increasing frequency.

Chapter - V

Results and Discussion of $Ni_{0.28}Cu_{0.10+x}Zn_{0.62-x}Fe_{1.98}O_4$

Results and Discussion of $Ni_{0.28}Cu_{0.10+x}Zn_{0.62-x}Fe_{1.98}O_4$ Ferrites

5.1 Introduction

The properties of Ni-Zn ferrites can be tailored by substituting them with different metal ions such as Co^{2+}, Mg^{2+}, Mn^{2+}, Cu^{2+} etc. The Ni-Zn ferrites are one of the most versatile, reasonable cost magnetic materials for general use in both low- and high frequency devices because of their high resistivity, low dielectric losses, mechanical hardness, high Curie temperature and chemical stability. Sintering temperature can be reduced by using CuO with Ni-Zn ferrites composition is known to play, a crucial role in increasing the sintering density and lowering the sintering temperature [5.1-5.2]. There has been a growing interest in Ni-Cu-Zn ferrites for the applications in producing multilayer-type chips mainly because these oxides can be sintered at a relatively low temperature with a wide range of composition. In particular the addition of Cu in the composition, has been known to play a crucial role in dropping the firing temperature. The purpose of this study is to investigate the effects of Cu-substitution on the electrical and magnetic properties of Ni-Zn ferrites sintered at high temperature with various compositions. Ni-Cu-Zn ferrites with composition of $Ni_{0.28}Cu_{0.10+x}Zn_{0.62-x}Fe_{1.98}O_4$ [where x=0.00, 0.03, 0.06, 0.09 & 0.12] were prepared by standard double sintering technique using high purity oxides of Fe_2O_3, CuO, ZnO, NiO and reported in the present work.

5.2   X-ray Diffraction Analysis

5.2.1 Phase Analysis

Structural characterization and identification of phases is a prior for the study of ferrite properties. Optimum magnetic and transport properties of the ferrites necessitate having single phase cubic spinel structure. X-ray diffraction patterns for $Ni_{0.28}Cu_{0.10+x}Zn_{0.62-x}Fe_{1.98}O_4$ samples sintered at 1150°C for 3hrs are shown in Fig-5.1. The XRD pattern for all the samples were indexed for fcc spinel structure and the Bragg planes are shown in patterns. The XRD pattern of all the samples of $Ni_{0.28}Cu_{0.10+x}Zn_{0.62-x}Fe_{1.98}O_4$ with [hkl] values corresponding to the diffraction peaks of different planes (111), (220), (311), (222), (400), (422), (511) and (440), which represent either odd or even indicating the spinel phase of the sample. All the samples show good crystallization with well defined diffraction line with no extra lines confirms the formation of single phase spinel structure. This also demonstrates the homogeneity of the prepared samples.
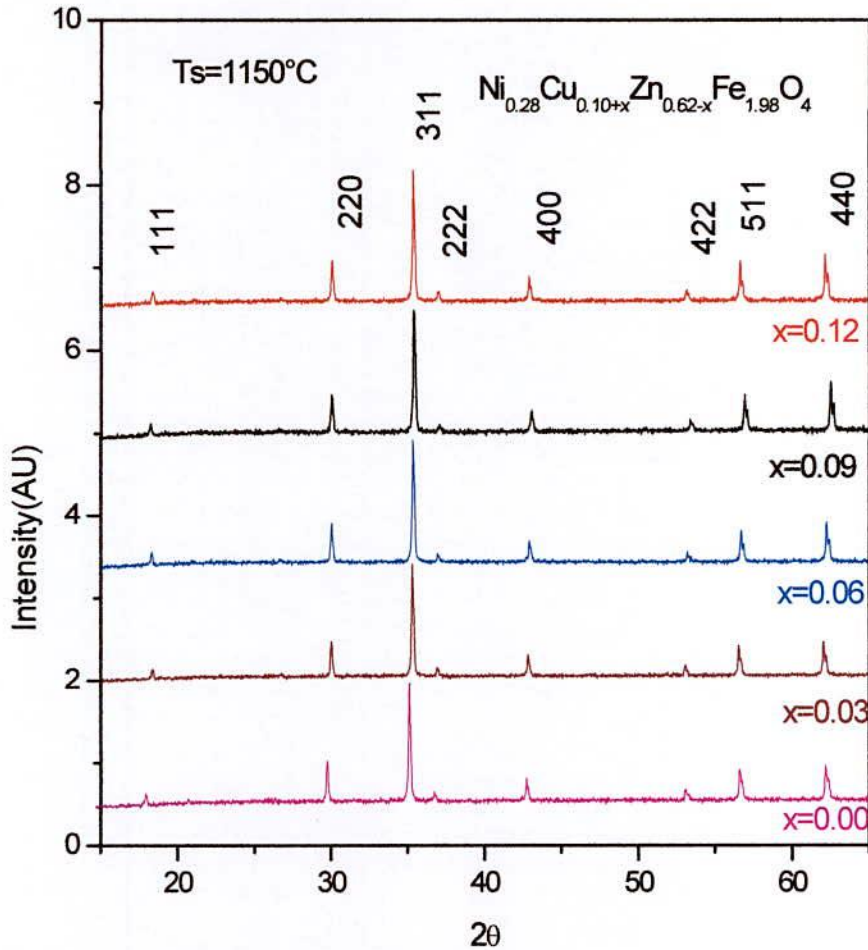
Fig. 5.1 XRD patterns of $Ni_{0.28} Cu_{0.10+x} Zn_{0.62-x} Fe_{1.98}O_4$ ferrites sintered at 1150°C/3 hrs

5.2.2 Lattice Parameters

The lattice parameter of all the samples has been precisely determined considering the reflection with the $Cu-K_\alpha$ radiation using the extrapolated Nelson-Riley function $F(\theta) = 0$ at $\theta = 90°$ [4.14]. The variation of the lattice parameter 'a' as a function of Cu^{2+} content (x) is depicted in Fig. 5.2 and also shown in Table 5.1. From the Fig. 5.2 it is observed that the lattice parameter decreases linearly with increase of Cu content as the ionic radii of Cu^{2+} (0.70 A°) which is smaller than Zn^{2+} (0.82 A°). Since the radius of the substituted ions in smaller than that of the replaced ions, lattice constant is expected to decrease.
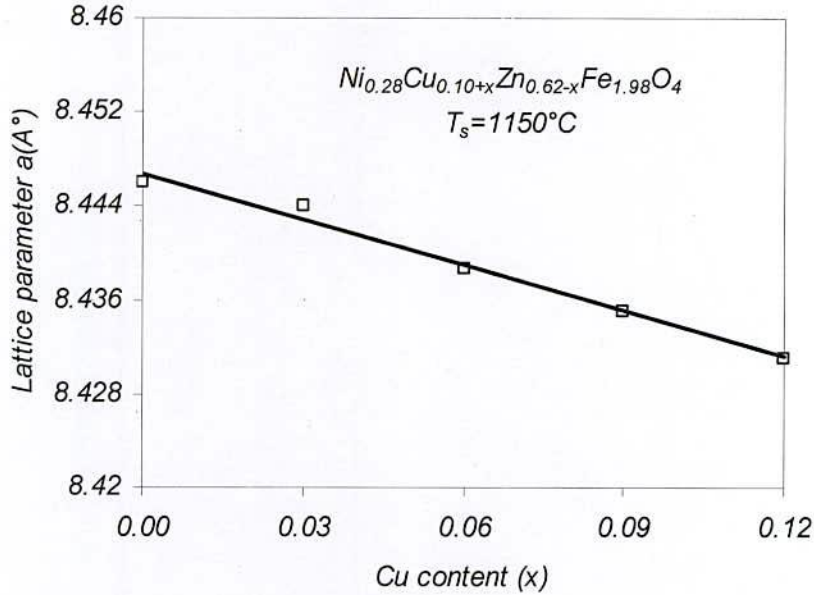
Fig. 5.2 Variation of lattice constant 'a' as a function of Cu content (x) of $Ni_{0.28}$ $Cu_{0.10+x}$ $Zn_{0.62-x}$ $Fe_{1.98}O_4$ ferrites sintered at 1150°/3hrs

5.2.3 Density

Density plays a key role in controlling the properties of polycrystalline ferrites. A significant increase in the bulk density is observed with copper content. The beneficial effect of Cu ions on the densification of Ni-Cu-Zn ferrite can be reasonably explained by the possible sintering mechanism that takes place through a high atomic mobility of Cu-ions at relatively low temperature. A possible explanation may be the formation of solid solution. It is supposed that all Cu ions enter into the spinel lattice during sintering and activate the lattice diffusion. The dependence of bulk density (d_B) and X-ray density (d_x) upon Cu content (x) is shown in Fig. 5.3. The balk density slightly increases with increasing Cu-content as shown in Fig. 5.3 and also shown in Table – 5.1. The densities of Cu^{2+} and Zn^{2+} are 8.96 gm/cc and 7.14 gm/cc respectively. It was also observed that bulk density was less then X-ray density. The replacements of Zn^{2+} by Cu^{2+} ions in the spinel leads to a variation in bonding and consequently affect interatomic distance and density. The oxygen ions which diffuse through the material during sintering also accelerate the densification of the material. The apparent density of the same composition reflects the same general behavior of the X-ray density. The percentage of porosity was also calculated using the eq^n (3.6). Porosity changes slightly with Cu content (x). It is understood from the data of Table-5.1, porosity values are found to decrease significantly

with increasing Cu-content, thereby giving an impression that Cu might be helping in the densification of the materials. The composition X=0.09 has the highest density and lowest porosity which may be due to the increase of oxygen vacancies.
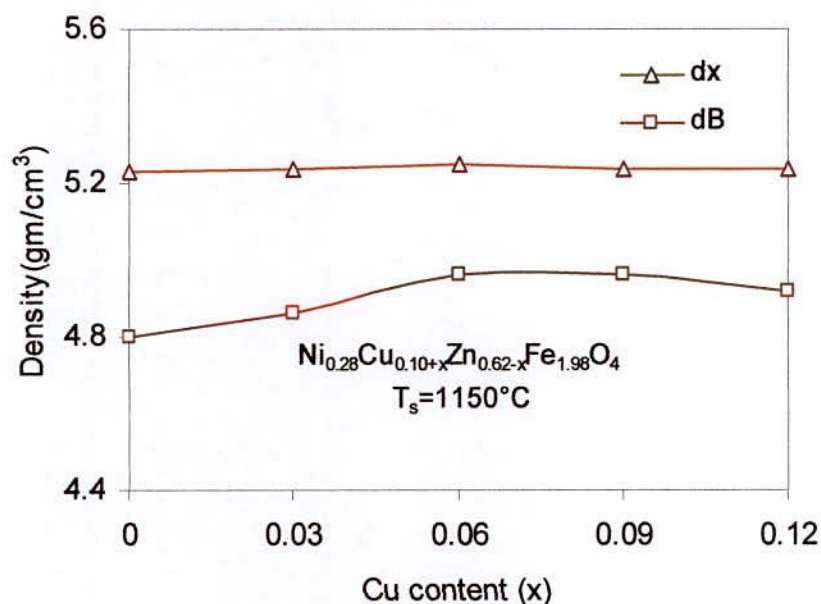
Fig. 5.3 Variation of density with Cu content (x) of $Ni_{0.28}$ $Cu_{0.10+x}$ $Zn_{0.62-x}$ $Fe_{1.98}O_4$ ferrites sintered at 1150°C/3hrs

Table- 5.1 Lattice parameter (a), X-ray density (d_x), bulk density (d_B), Porosity (P%) of $Ni_{0.28}$ $Cu_{0.10+x}$ $Zn_{0.62-x}$ $Fe_{1.98}O_4$ ferrites with different Cu content sintered at 1150°C/3hrs

Cu content (x)	a (Å)	d_x (g/cm^3)	d_B (g/cm^3)	P%	M (g)
0.00	8.4460	5.23	4.80	8.2	237.42
0.03	8.4441	5.24	4.86	7.3	237.37
0.06	8.4387	5.25	4.96	5.5	237.31
0.09	8.4350	5.24	4.96	5.3	237.26
0.12	8.4310	5.24	4.92	6.2	237.20

5.3   Magnetic Properties

5.3.1 Temperature Dependence of Initial Permeability

Temperature dependence of initial permeability is important for applications. Fig. 5.4(a,b) shows the thermal variation of initial permeability (μ') for the toroid shaped

133

ferrite samples of the series sintered at $T_s=1100°$ and $1150°C$. Since the initial permeability is directly related to the magnetization and to the ionic structure, the thermal spectra of permeability can be taken as a test of the formation and homogeneity of the ionic structure of the samples. In general, it was found that the initial permeability increases with increase in temperature, while it falls abruptly close to Curie point.

Knows as Hopkinson effect near the T_c with the manifestation of a peak followed by sharp fall of permeability. The sharpness of the permeability drop at the Curie point can be used as a measure of degree of compositional homogeneity according to Globus [5.1]. The present ferrites show good homogeneity as shown in Fig. 5.4, where an abrupt drop in permeability occurs within the temperature range less than $5°C$ near Curie point. The anisotropy constant (K_1) and saturation magnetization (M_s) usually decreases with increase in temperature. But decrease of (K_1) with temperature is faster than that of (M_s). When the anisotropy constant reaches to zero, μ' attains its maximum value and then drops off to minimum value near the Curie point. According to the equation $\mu' \propto \dfrac{M^2{}_s D}{\sqrt{K_1}}$

[4.19, 4.20], μ' must show a maximum at temperature at which K_1 vanishes, where D is the diameter of the grain.

(a)

134
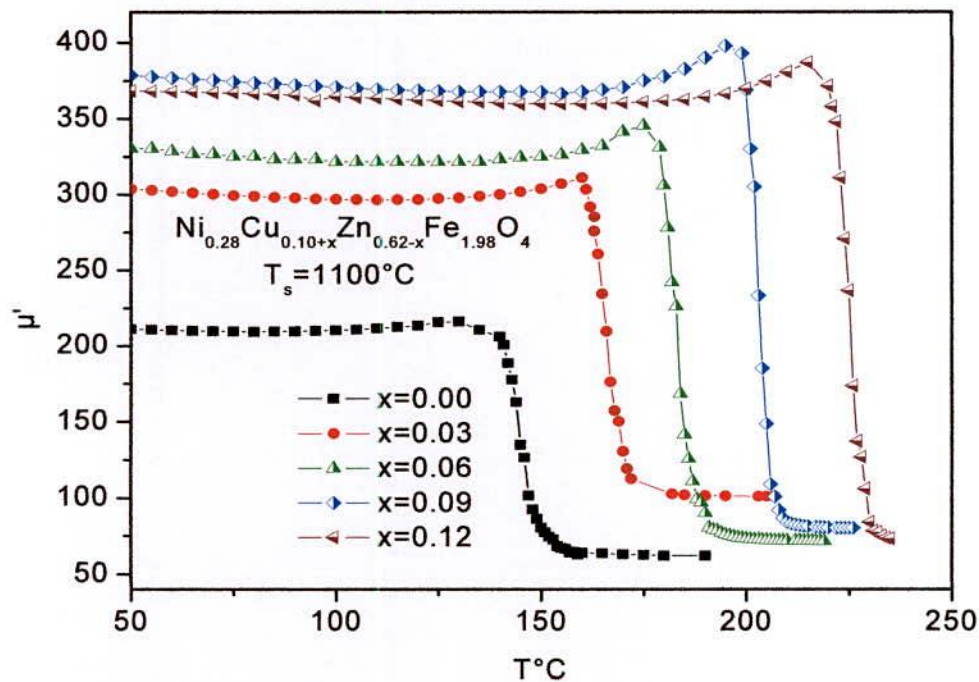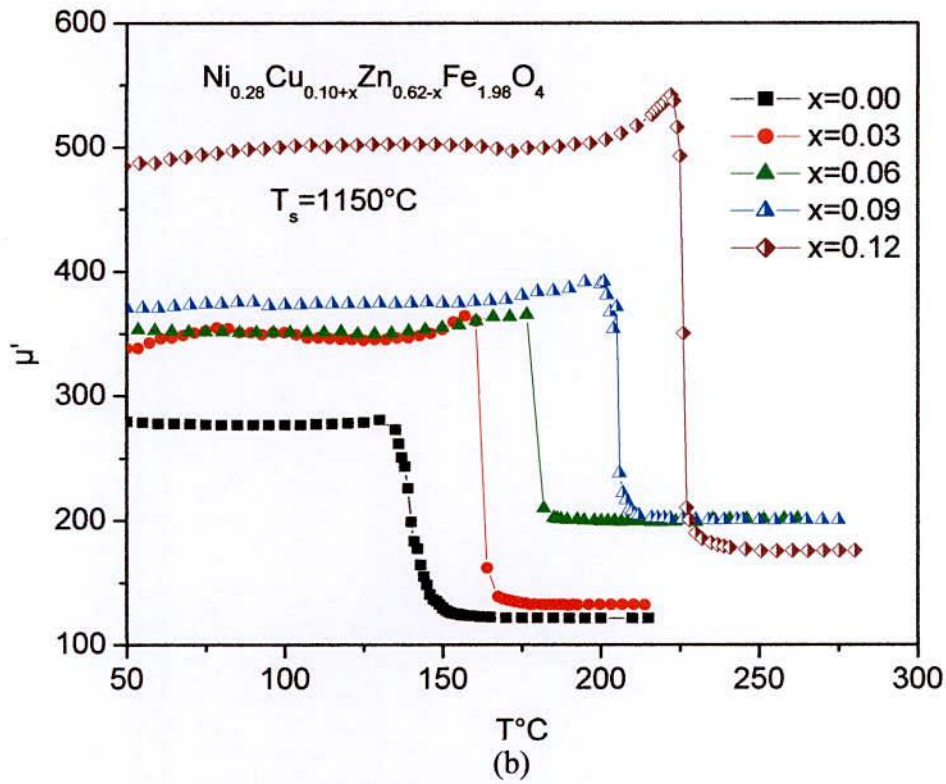
Fig. 5.4 Temperature dependence of permeability for $Ni_{0.28}$ $Cu_{0.10+x}$ $Zn_{0.62-x}$ $Fe_{1.98}O_4$ ferrites sintered at (a) 1100°C & (b) 1150°C for 3 hrs

The T_c values of the samples have been determined from μ'-T curves. Fig. 5.5 shows the variation of T_c with Cu content (x).
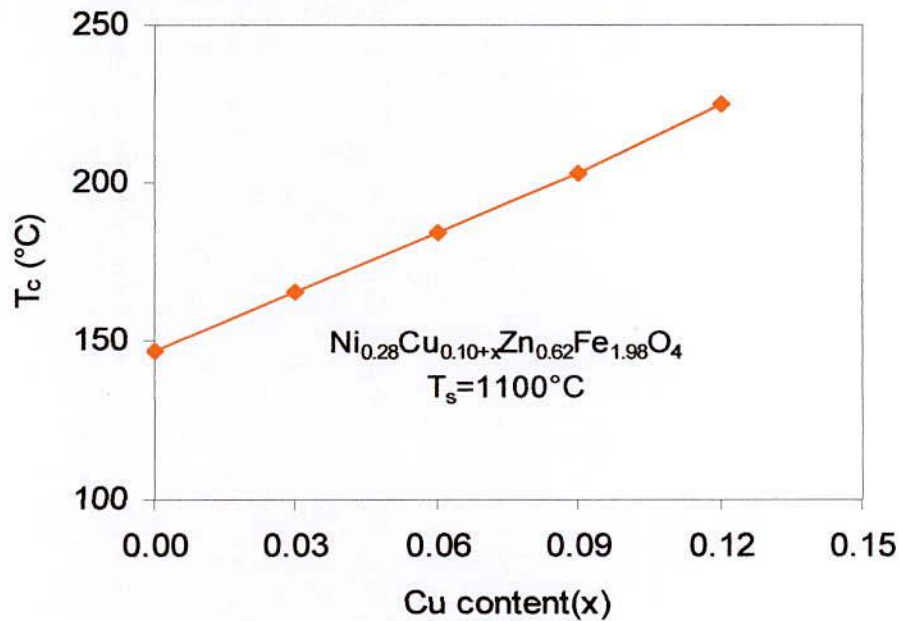
Fig. 5.5 Variation of Curie temperatures as a function of copper content (x)

The T_c values increase linearly with x content. The change in T_c is attributed probably due to the change of A-B exchange interaction as a result of the modification of cation distribution between A and B sub lattice due to CuO substitution. Fig. 5.6 represents the variation of the complex permeability, μ', μ'' and temperature derivative of permeability, $\frac{d\mu'}{dT}$ as a function of temperature of $Ni_{0.28} Cu_{0.10+x} Zn_{0.62-x} Fe_{1.98}O_4$ with x = 0.03. At the T_c, where complete spin disorder takes place corresponds to maximum of imaginary part and the temperature derivative of the real part of permeability. From this figure it is observed that imaginary part of permeability and temperature derivatives of permeability show peaks at a temperature, T which excellently matches with the sharp fall of permeability at $T = T_c$
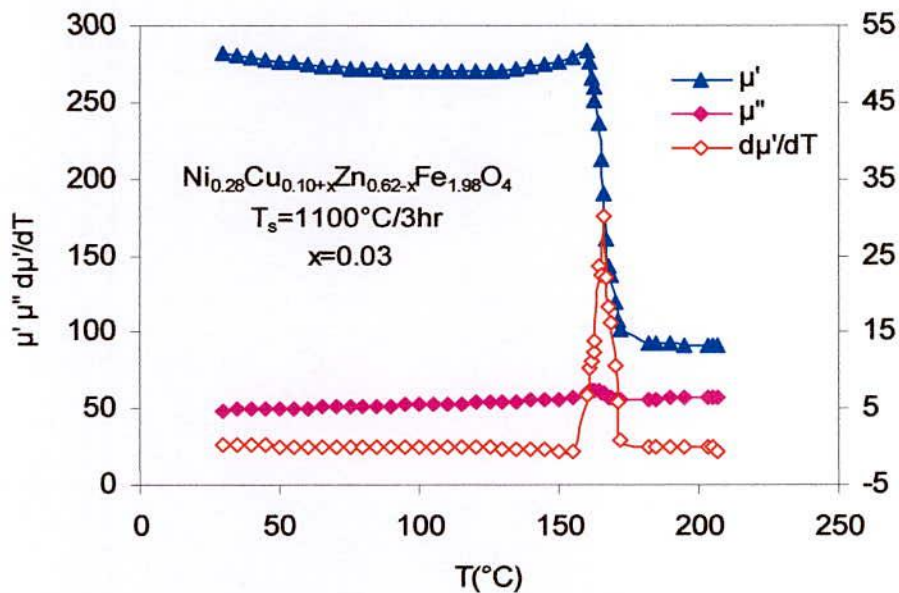
Fig. 5.6 Determination of Curie temperature from the temperature dependence of μ', μ'' and $\frac{d\mu'}{dT}$ as a function of temperature of $Ni_{0.28} Cu_{0.10+x} Zn_{0.62-x} Fe_{1.98}O_4$ with x = 0.03

5.3.2 Complex Initial Magnetic Permeability

Fig. 5.7 (a, b, c) and Fig. 5.8 (a, b, c) shows the variation of the Complex permeability spectra with frequency of the system $Ni_{0.28}Cu_{0.10+x}Zn_{0.62-x}Fe_{1.98}O_4$ for different values of x at different sintering temperature 1100°C, 1150°C and 1200°C for 3 hours. For all the samples sintered at 1100°C, 1150°C and 1200°C the values of initial

permeability increases with increasing Cu-content, because the sintered density increases and porosity decreases with increase of Cu-content. From these figures, it is seen that the real part of the permeability μ' remained almost constant until the frequency was raised to a certain value (4-5 MHz) and then drops to a very low values at higher frequencies. The imaginary part μ'' gradually increased with the frequency and attain a broad maximum at a certain frequency where the real part of permeability rapidly decreased. This feature is well known as the ferrimagnatic resonance [5.3]. At low frequencies, a ferrite inductor is a low loss constant self-inductor where μ' is highest and the core is mostly inductive, rejecting the electromagnetic interference (EMI) signal to the source. At high frequencies where the μ'' parameters becomes more significant, the inductors show high impedance and become resistive and dissipate interfering signals rather than reflecting these to the source [4.26]. The resonance frequency peaks are the results of the absorption of energy due to matching of the oscillation frequency of the magnetic dipoles and the applied frequency. At the resonance, maximum energy is transferred from the applied field to the lattice resulting in the rapid increase in $\tan \delta$ ($\tan \delta = \dfrac{\mu''}{\mu'}$).

(a)
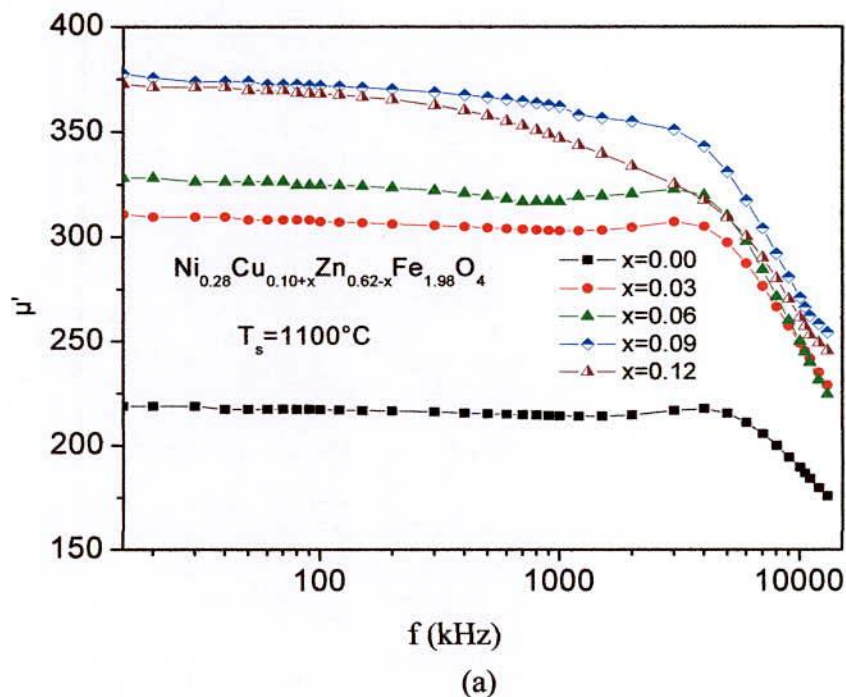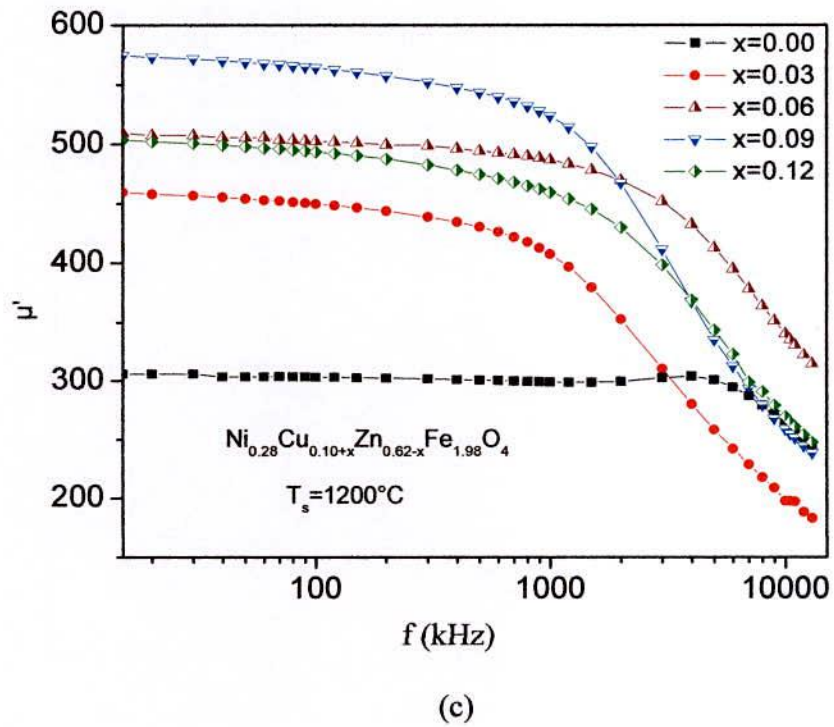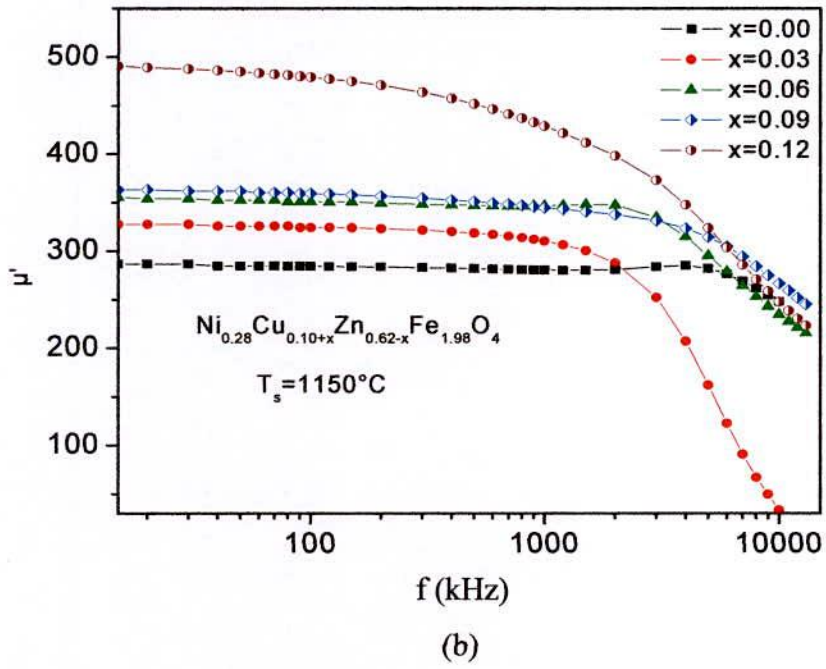
Fig. 5.7 Frequency dispersion of real part of the permeability, μ' of $Ni_{0.28}$ $Cu_{0.10+x}$ $Zn_{0.62-x}$ $Fe_{1.98}O_4$ ferrites at (a) 1100°C, (b) 1150°C and (c) 1200°C for 3 hrs
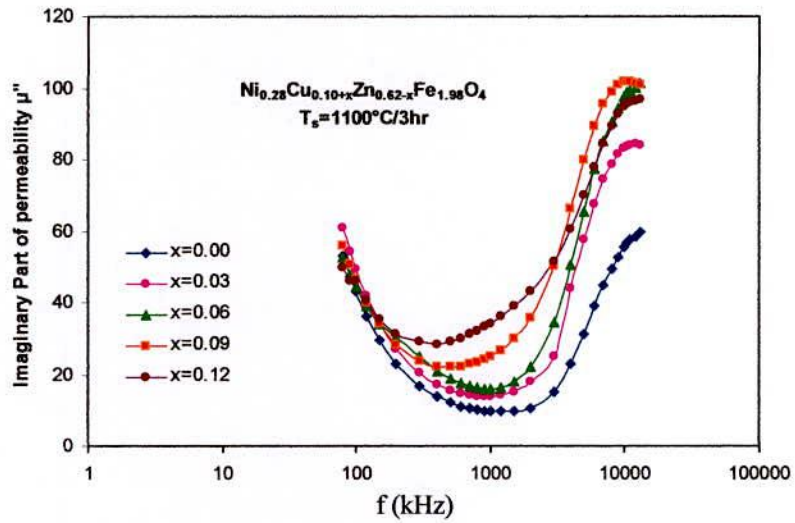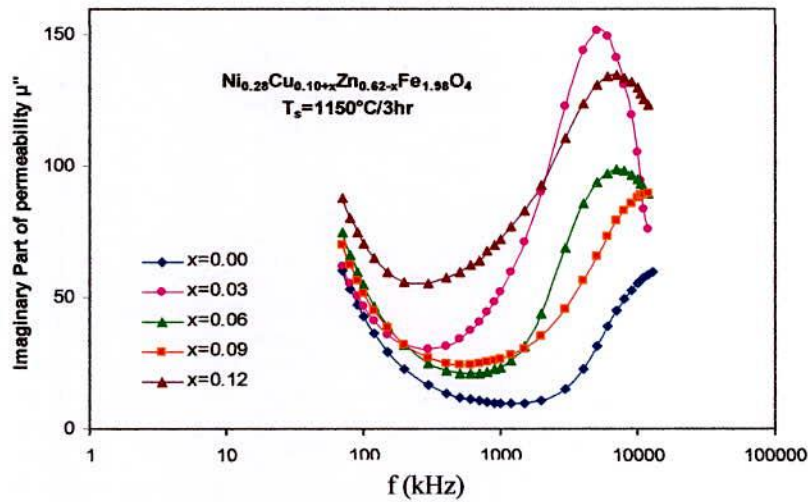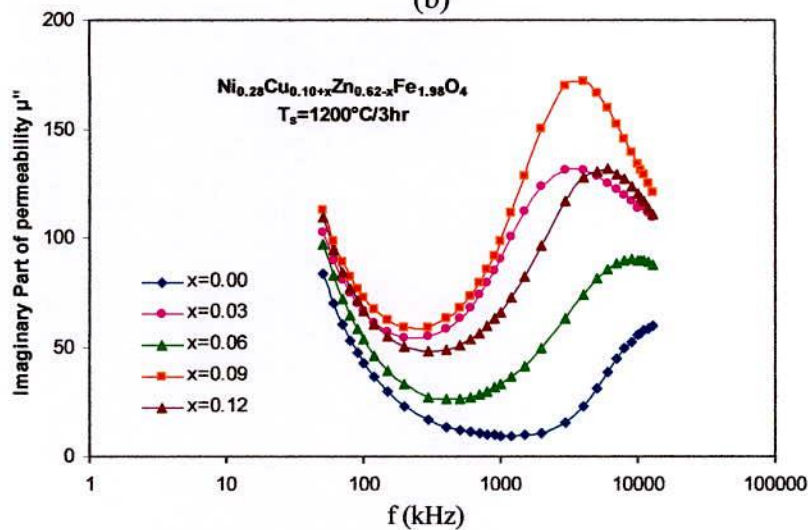
Fig. 5.8 Complex initial permeability spectra for $Ni_{0.28}$ $Cu_{0.10+x}$ $Zn_{0.62-x}$ $Fe_{1.98}O_4$ ferrites sintered at (a) 1100°C, (b) 1150°C and (c) 1200°C for 3 hrs

The values of initial permeability and resonance frequencies for all the samples sintered at 1100°C, 1150°C and 1200°C are presented in Table 5.2. The resonance frequencies of the ferrites (f_r) were determined from the maximum of imaginary permeability. The resonance frequencies shifts from 10 MHz to 7 MHz as the copper content (x) increases from x = 0.00 to 0.12 sintered at 1150°C. The product of μ and f_r is al most constant proving the Snoek's limit. This indicates that lower the permeability values, the higher the frequencies at which resonance phenomenon occurs. When frequency is low, permeability is high and when frequency is high, permeability is tow. Thus, an effective limit of product of frequency and permeability is established. So that high frequency and high permeability are mutually incompatible.

Table- 5.2 The Curie temperature (T_c), initial permeability (μ') (at 10kHz) and resonance frequency (f_r) of the $Ni_{0.28} Cu_{0.10+x} Zn_{0.62-x} Fe_{1.98}O_4$ ferrites sintered at 1100°C, 1150°C and 1200°C for 3 hours

Cu content (x)	Ts=1100°C			Ts=1150°C			Ts=1200°C		
	μ'	T_c	f_r(MHz)	μ'	T_c	f_r(MHz)	μ'	T_c	f_r(MHz)
0.00	217	143	13	284	140	10	303	141	10
0.03	313	166	10	325	164	8	466	165	8
0.06	340	184	9	356	182	7.5	520	181	7
0.09	383	204	8	370	206	9	586	206	6
0.12	370	225	8	480	226	7	504	226	6

5.3.3 Frequency Dependence of Quality Factor

Fig. 5.9 represents the frequency dependence of quality factor (QF) of x = 0.00 and x = 0.09 samples sintered at different sintering temperatures. It is seen from this that the samples sintered at 1100°C exhibit maximum quality factor. Fig. 5.9 shows the frequency dependence of QF of the samples sintered at different temperatures. The quality factors were calculated from the magnetic loss tangent measured on the coil wound torodial samples. The variation of the QF with frequency showed a similar trend for all the samples. Q-factor increases with an increase of frequency showing a peak and then decreases with further increases of frequency. It is seen that QF deteriorates beyond 5-10 MHz depending on T_s. i.e. the loss tangent is minimum up to 5-10 MHz and then it

rises rapidly. The loss is due to lag of domain wall motion with the applied alternating magnetic field and is attributed to various domain defects [4.30] which include non-uniform and non-repetitive domain wall motion, domain wall bowing, localized variation of flux density nucleation and annihilation of domain walls. This happens at the frequency where the permeability begins to drop. This phenomenon is associated with the ferrimagnatic resonance within the domains [4.24] and at the resonance, maximum energy is transferred from the applied magnetic field to the lattice resulting in the rapid decrease in QF. The peak corresponding to maxima in Q-factor shifts to lower frequency range as copper content increases.

(a)

(b)
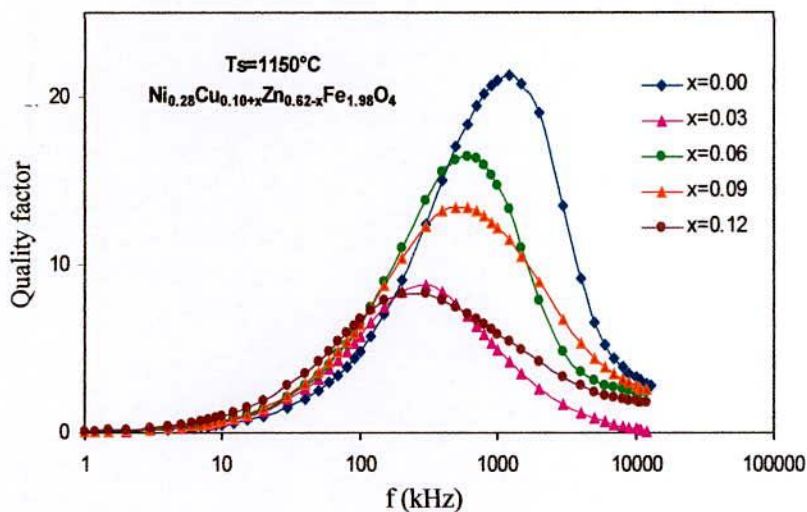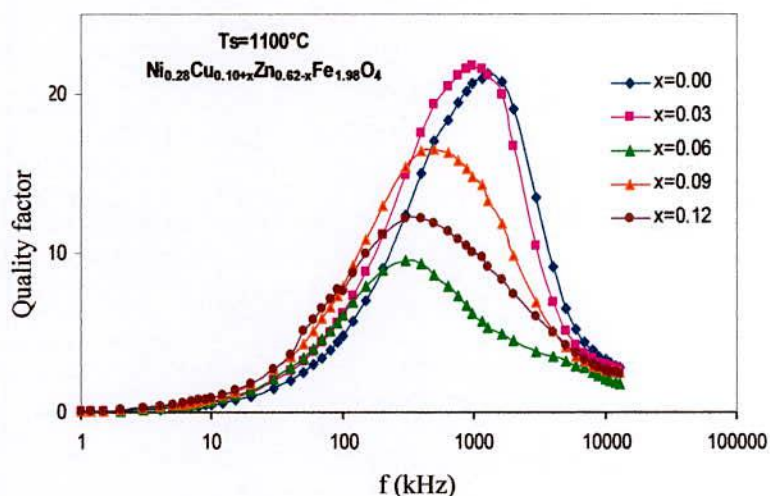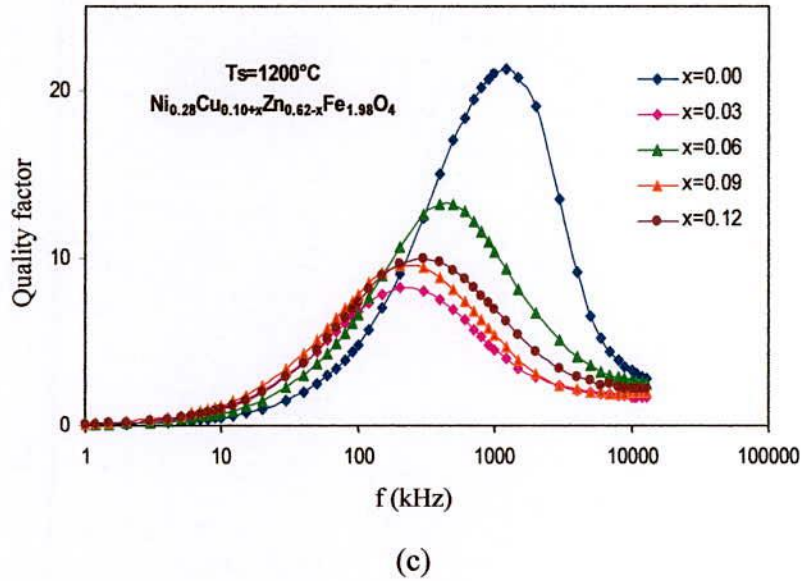
Fig. 5.9 Quality factor (QF) of the $Ni_{0.28}$ $Cu_{0.10+x}$ $Zn_{0.62-x}$ $Fe_{1.98}O_4$ ferrites sintered at (a) 1100°C, (b) 1150°C and (c) 1200°C/3hrs

5.3.4 Low Field B-H loop at Room Temperature

The B-H loops at room temperature of the investigated composition $Ni_{0.28}$ $Cu_{0.10+x}$ $Zn_{0.62-x}$ $Fe_{1.98}O_4$ sintered at 1100°C, 1150°C and 1200°/3hrs were measured at constant frequency (f = 1kHz) shown in Fig. 5.10 (a, b, c). From the B-H loops, the remanence induction (B_r), saturation induction (B_s) and coercive force (H_c) were determined and studied with respect to x and sintering temperature. From this loops the high coercivity, H_c is observed at x = 0.00 and it decreases almost linearly with increasing Cu-content for all the sintering temperature which are listed in Table-5.3. The low coercive force and higher permeability, confirms that the development of soft magnetic characteristic properties of Ni-Cu-Zn ferrites. It is also observed that coercivity decreases with increase in sintering temperature. The difference in the H_c values is understandable because of the substantial increase in grain size in response to the increase in sintering temperature which facilitating the movement of the magnetic domain. Saturation induction (B_s) is found to increase with increasing Cu-content. The different values of retentivity, and $\dfrac{B_r}{B_s}$ ratio observed are interpreted in a quantitative way by means of domain theory.

Table-5.3 The experimental values of coercive force (H_c), remanence induction (B_r), saturation induction (B_s), $\dfrac{B_r}{B_s}$ ratio and losses of $Ni_{0.28}$ $Cu_{0.10+x}$ $Zn_{0.62-x}$ $Fe_{1.98}O_4$ samples at room temperature with constant frequency (f = 1kHz) at different sintering temperature

Cu content (x)	T_S (°C) / 3hrs	H_C (Oe)	B_r (kG)	B_s (kG)	B_r/B_s	Losses (W/kg)
	1100	2.08	1.03	1.90	0.54	21.11
0.00	1150	1.74	1.04	2.10	0.50	19.10
	1200	1.59	1.03	2.00	0.51	17.70
	1100	1.76	1.38	2.42	0.57	25.54
0.03	1150	1.59	1.73	3.23	0.54	25.10
	1200	0.94	1.48	2.70	0.55	20.21
	1100	1.64	1.58	2.74	0.57	27.53
0.06	1150	1.30	1.28	2.57	0.50	15.54
	1200	1.42	1.24	2.34	0.53	21.32
	1100	1.31	1.71	3.00	0.57	24.38
0.09	1150	1.43	2.00	3.58	0.56	25.68
	1200	0.75	1.40	2.81	0.50	15.51
	1100	1.30	1.88	3.14	0.60	26.04
0.12	1150	0.98	1.80	2.83	0.63	20.49
	1200	0.88	1.13	2.80	0.40	14.40

(a)

(b)

(c)
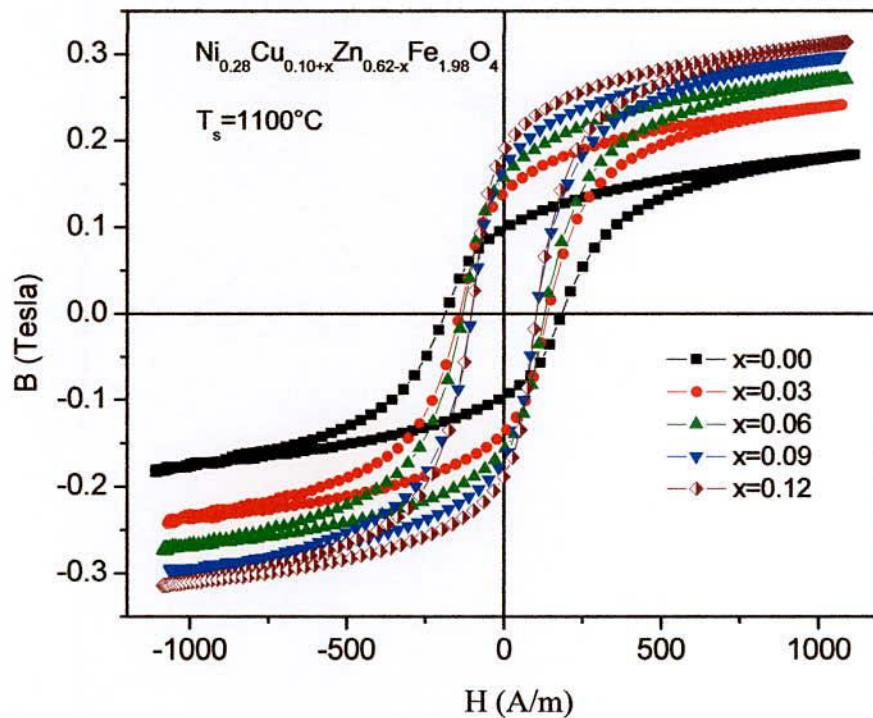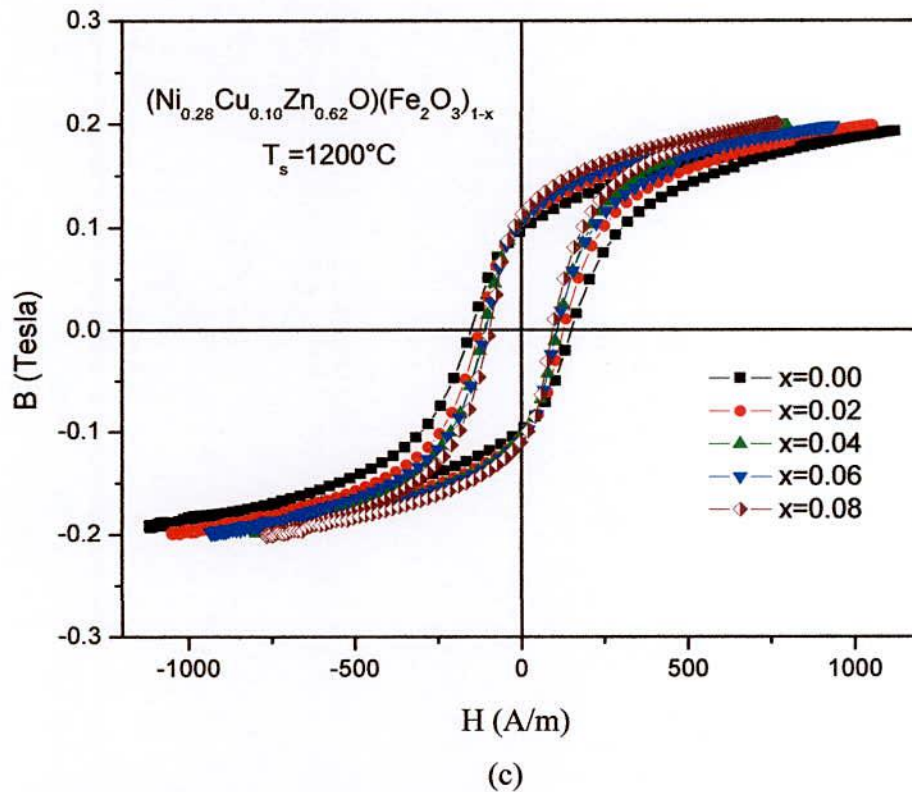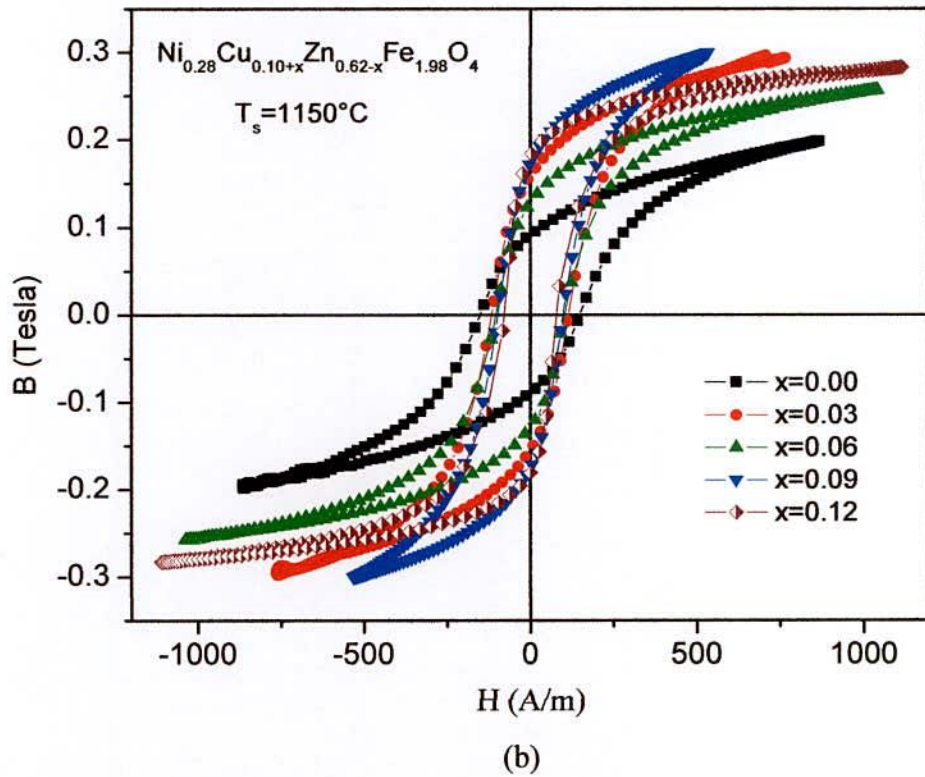
Fig. 5.10 Magnetic hysteretic graphs of $Ni_{0.28}$ $Cu_{0.10+x}$ $Zn_{0.62-x}$ $Fe_{1.98}O_4$ ferrites with x sintered at (a) 1100°C (b) 1150°C and (c) 1200°C for 3 hours at constant frequency f = 1kHz

144

5.3.5 Magnetization Measurement

The room temperature magnetization M (H) as a function of field of the samples have been measured and is presented in Fig. 5.11. It is observed that M is saturated with an applied of H=18000 Oe. It is also observed that saturation magnetization increases gradually with increase of Cu content. The value of saturation magnetization increases from 53.22 emu/g for x= 0.00 to 63.3 emu/g for x= 0.12. This may be attributed to the modified cation distribution between A and B sites. Fig. 5.12 shows the dependence of saturation magnetization, M_s with Cu content x. Fig. 5.13 shows the temperature dependence of magnetization with an applied magnetic field of H=5 kOe. It is observed that M_s increases gradually with x content and decreases with increasing temperature. The magnetization decreases toward zero above the Curie temperature, T_c. The T_c value increases linearly with the increase in copper content.

The observed variation in saturation magnetization can be explained on the basis of cation distribution and the exchange interactions between A and B sites, respectively. Neel [4.31] considered three types of exchange interactions between unpaired electrons of two ions lying in A and B sites. In perfect ferrites, the A-A, B-B and A-B nearest neighbor exchange couplings are normally antiferromagnetic and the A-B exchange coupling is usually heavily predominant. Therefore, the spins at the A-sites will be antiparalle to the spins at B-sites below a transition temperature (called Curie temperature). The net magnetization is therefore, the difference between the magnetic moments of B and A sub lattices, i.e. $M_s = M_B - M_A$ and will normally be parallel to the B-sublattice magnetization because the number of cations on B-sites is twice the number of cations on A- sites. The magnetization of each composition depends on the distribution of Fe^{3+} ions between the two sublattices A and B, where Cu^{2+} and Zn^{2+} ions are non-magnetic. The initial rise in the M_s value is attributed magnetizations, respectively. The initial rise in the M_s value is attributed to the fact Cu^{2+} ions preferably tend to go to the B-sites by replacing Zn^{2+} ions and only a slight increase in the magnetic moment of the B-sites. So that the net magnetic moment increases can be attributed to two factors:

(i) The increase of canting angle between the moments in the B-sites leads to a decrease in the magnetization [5.4].

(ii) The increase in the magnitude of the total magnetic moments in the B-sites lead to a magnetization increase.

The actual cation distribution can through light on the variation of saturation magnetization. If there is migration of Cu^{2+} to A-sites, the accompanied migration of Fe^{3+} ions to B-sites will lead to an increase in magnetization in B-sites, leading to the increase of the saturation magnetization (M_s) of the Ni-Cu-Zn ferrite.
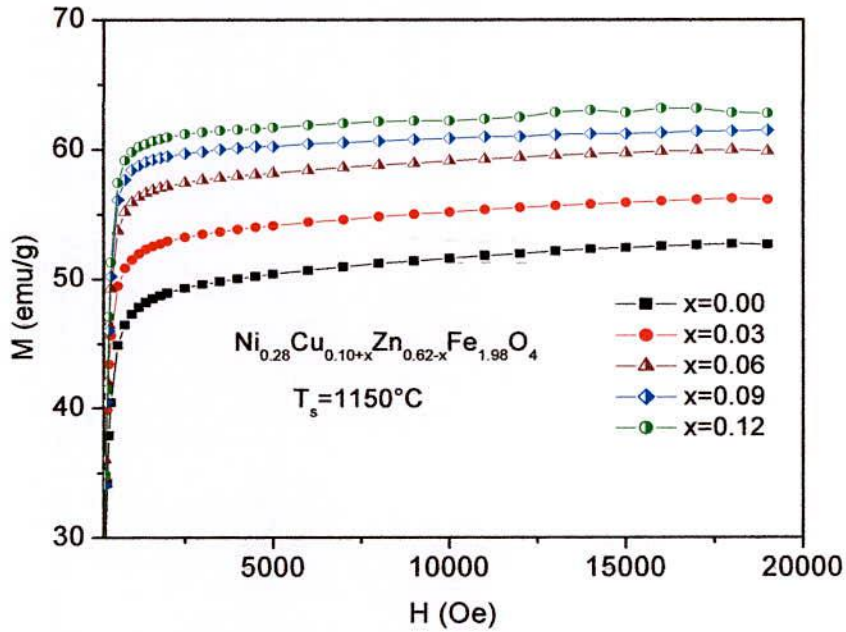
Fig. 5.11 Field dependence of magnetization for x = 0.00-0.12 of $Ni_{0.28}$ $Cu_{0.10+x}$ $Zn_{0.62-x}$ $Fe_{1.98}O_4$ ferrites at room temperature
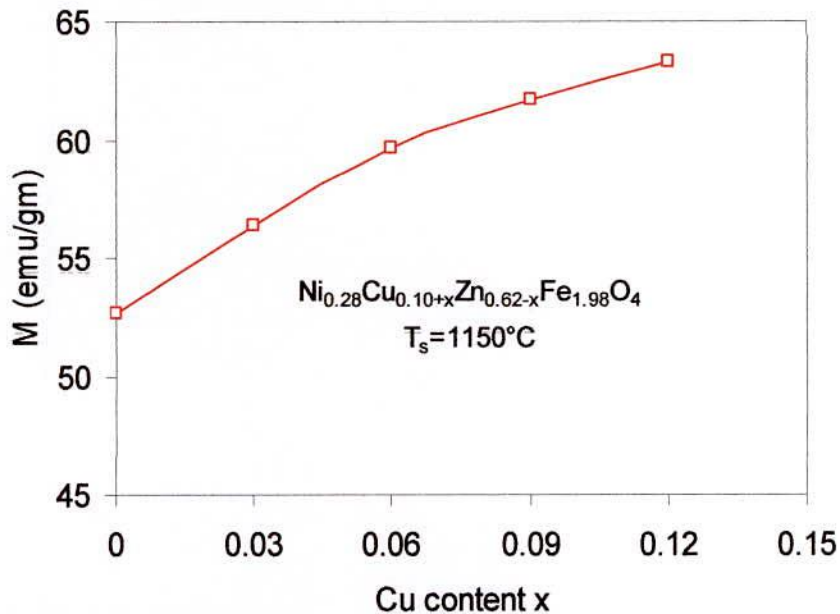
Fig. 5.12 Saturation magnetization M versus Cu-content in $Ni_{0.28}$ $Cu_{0.10+x}$ $Zn_{0.62-x}$ $Fe_{1.98}O_4$ ferrites

146

Fig. 5.13 shows the temperature dependent of saturation magnetization measured with an applied field of H= 5 kOe. It is observed that magnetization, M_s decreases monotonically with increasing temperature and finally towards zero above the Curie temperature, T_c. The slow decrease of M_s from the two sublattice magnetization unlike ferromagnetic. From the Fig. 5.13 it is observed that low temperature magnetization increase with increasing Cu-content.
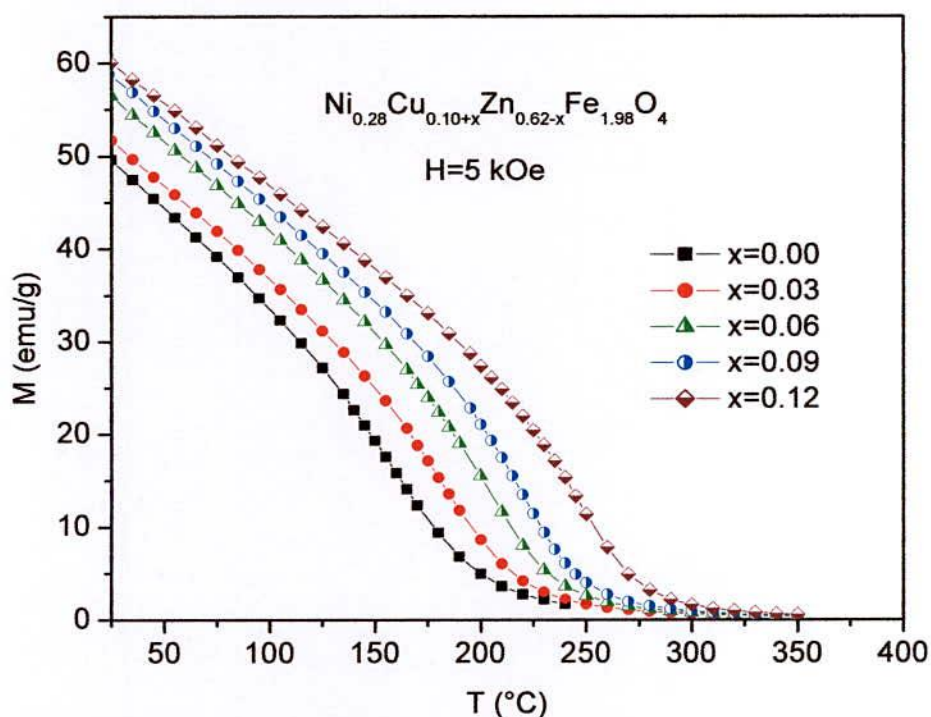
Fig. 5.13 Temperature dependence of magnetization of $Ni_{0.28}$ $Cu_{0.10+x}$ $Zn_{0.62-x}$ $Fe_{1.98}O_4$ ferrites with applied field 5 kOe

5.4 Scanning Electron Microscope (SEM) Microstructure Analysis

Fig. 5.14, 5.15 and 5.16 shows the SEM microstructure of $Ni_{0.28}Cu_{0.10+x}Zn_{0.62-x}Fe_{1.98}O_4$ ferrites sintered at 1100°C, 1150°C, and 1200°C. It is clear that the microstructure of Ni-Cu-Zn ferrite strongly depends on the amount of Cu content in the samples. As the Cu content increases, the grain size increases gradually. It is also noticed from the microstructure that with increasing sintering temperature grain grows bigger. This reflected in the permeability value that permeability also increases with Cu content since permeability is directly proportional to grain size D and M_s which also increase with increasing M_s. i.e. $\mu' \propto \dfrac{M_s^2 D}{\sqrt{K_1}}$. The increase in grain size with sintering

147

temperature is clearly visible. The average grain size continuous to increase from 2.78 µm to 4.58 µm for x= 0.00 while increase the sintering temperature from 1100°C to 1200°C similar behavior is observed for other samples of the series. Fig. 5.17 represents the average grain diameter as a function of Cu-content sintered at 1100°C, 1150°C and 1200°C.From this figure it is observed that the grain sizes markedly increased with the Cu-content and sintering temperature, the values of average grain size of the samples of the series.
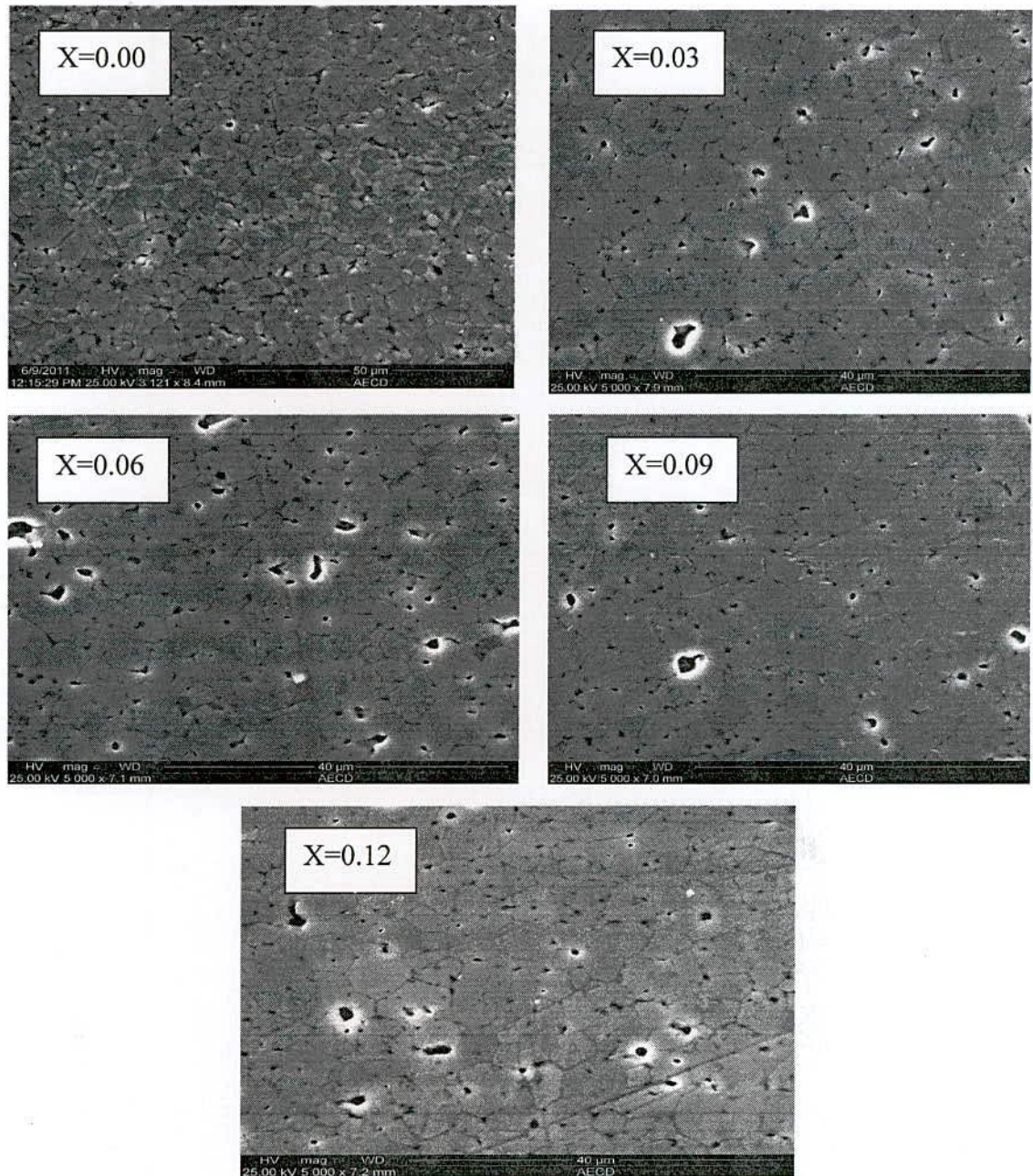
Fig. 5.14 SEM micrographs of the system $Ni_{0.28}Cu_{0.10}Zn_{0.62}Fe_{1.98}O_4$ sintered at 1100°C
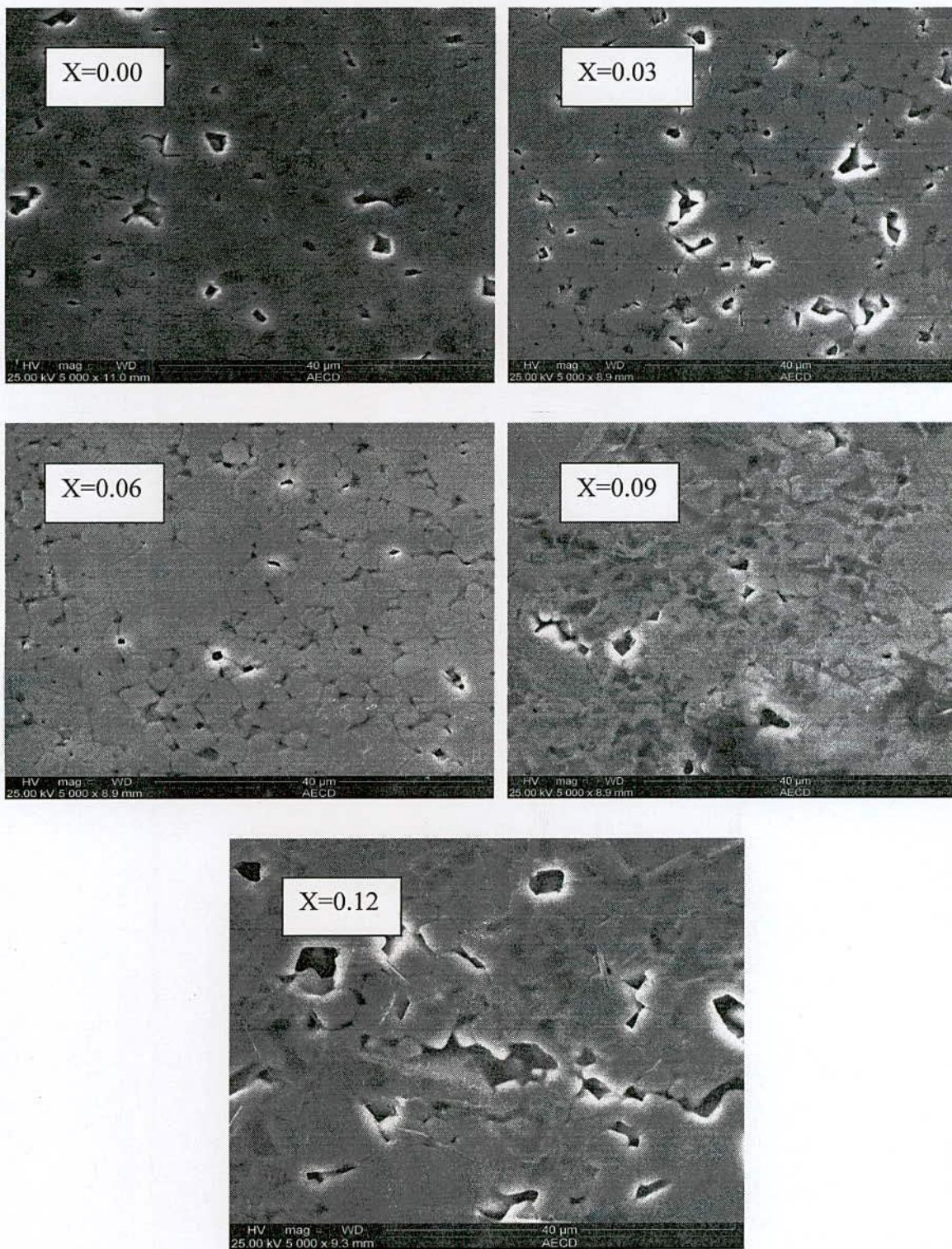
Fig. 5.15 SEM micrographs of the system $Ni_{0.28}Cu_{0.10}Zn_{0.62}Fe_{1.98}O_4$ sintered at 1150°C
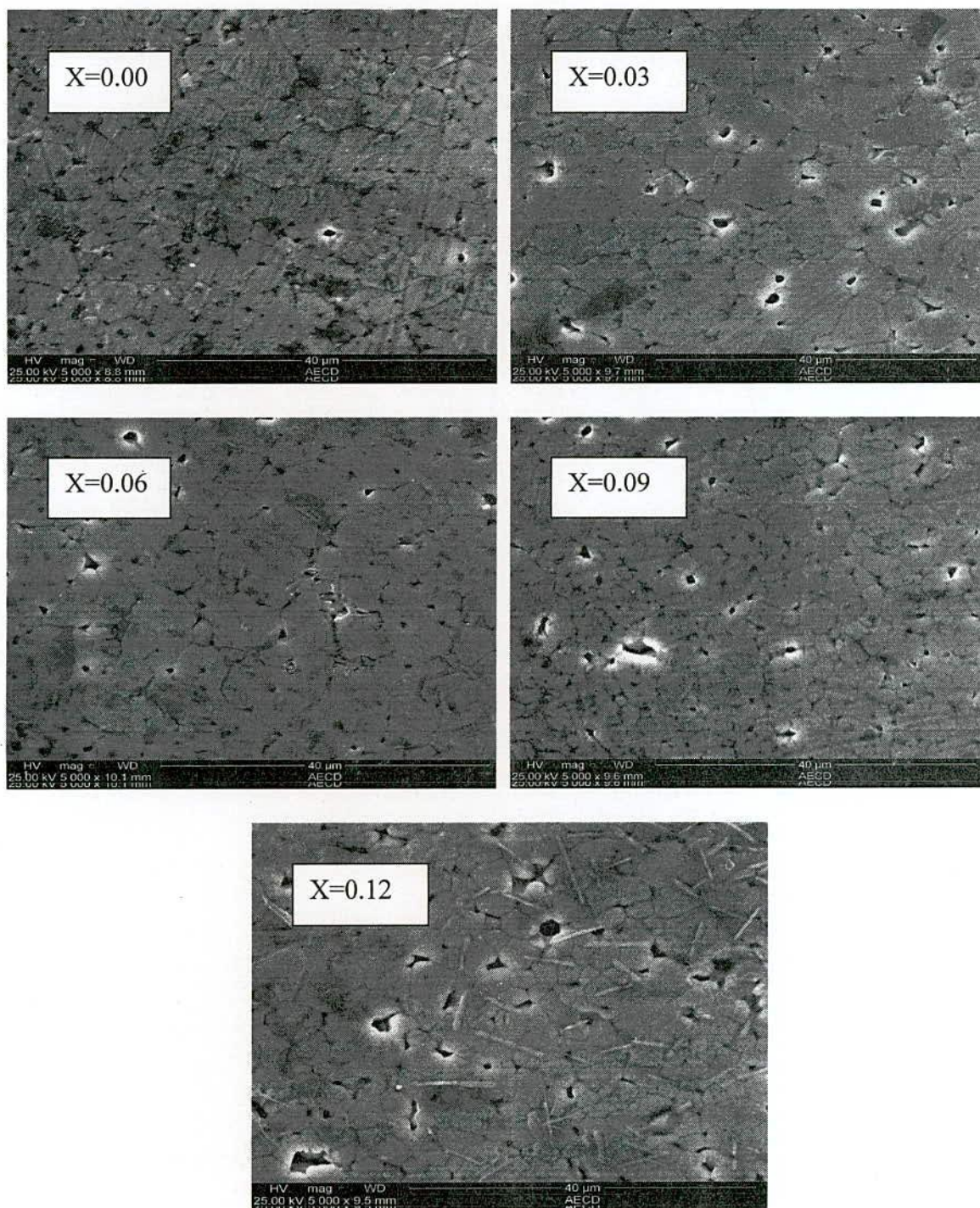
Fig. 5.16 SEM micrographs of the system $Ni_{0.28}Cu_{0.10}Zn_{0.62}Fe_{1.98}O_4$ sintered at 1200°C
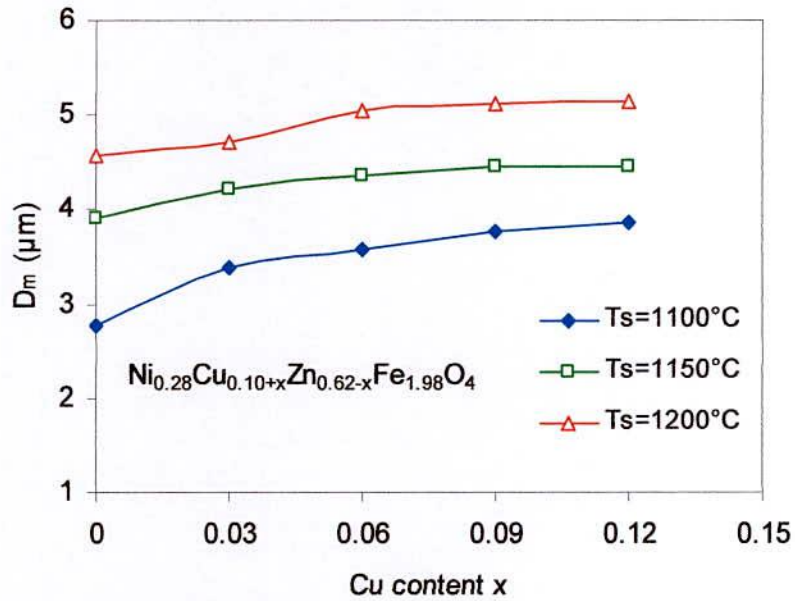
Fig. 5.17 Average grain size (D_m) as a function Cu content (x) of $Ni_{0.28}Cu_{0.10+x}Zn_{0.62-x}$ $Fe_{1.98}O_4$ ferrites

Table-5.4 The average grain size of the $Ni_{0.28}Cu_{0.10+x}Zn_{0.62-x}$ $Fe_{1.98}O_4$ ferrites sintered at 1100°C, 1150°C and 1200°C

Cu-content (x)	$T_s=1100°C$ D_m (μm)	$T_s=1150°C$ D_m (μm)	$T_s=1200°C$ D_m (μm)
0.00	2.78	3.91	4.58
0.03	3.40	4.22	4.72
0.06	3.58	4.36	5.05
0.09	3.77	4.46	5.12
0.12	3.87	4.46	5.15

5.5 Electrical Transport Properties

5.5.1 DC Electrical Resistively

DC resistivity (ρ_{dc}) versus x of $Ni_{0.28}Cu_{0.10+x}Zn_{0.62-x}Fe_{1.98}O_4$ ferrites measured at room temperature is presented as a function of Cu-content in Fig. 5.18. It was found that resistivity increases markedly with the addition of Cu^{2+} up to x = 0.09 and there after decreases.
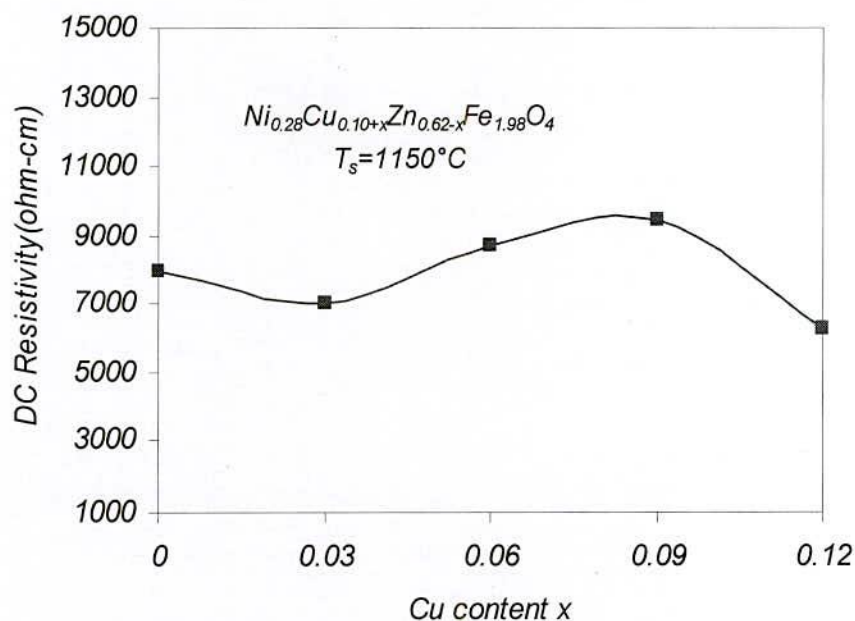
Fig. 5.18 Room temperature DC resistivity as a function of Cu-content (x) $Ni_{0.28}Cu_{0.10+x}Zn_{0.62-x}Fe_{1.98}O_4$ sintered at 1150°C

The conduction mechanism in ferrite is considered as the electron hopping between Fe^{2+} and Fe^{3+} ions in B-sites [5.5]. DC resistivity is an important parameter and depends upon several factors such as sintering temperatures time and atmosphere including the grain structure. It is well known that resistivity of ferrites depends on their chemical composition [5.6] and heat treatment. Fe^{3+} ions in the lattice are created due to Zn loss during the sintering process. In general, the dominant electrical conductivity mechanism in the iron different Ni-Cu-Zn ferrite in P-type up to a firing temperature 1150°C. The effect of the Cu to Zn composition ratio on the electrical conductivity cannot be negligible at a low sintering temperature; so that Cu substituted for Zn plays a significant role in the conductivity of Ni-Cu-Zn ferrites. High resistivity of Ni-Cu-Zn ferrites can be obtained from the Ni^{2+}-Ni^{3+} electron transition but the resistivity is decreased by Cu^{2+}- Cu^{+} transition as the variation of Cu content in Ni-Cu-Zn ferrites. The highest value of DC resistivity for x = 0.09 sample is observed to be $9.48x10^3$ □ - cm.

5.5.2 Variation of AC Resistivity with Frequency

Fig. 5.19 shows the variation of AC resistivity as log ρ versus frequency a log f of the sample at room temperature. All the samples show the significant dispersion with frequency, which is the normal ferrimagnatic behavior. The extent of dispersions is

largely affected by Cu-content. With increasing Cu-content the frequency dispersion is enlarged significantly. The conduction mechanism in ferrites is explained on the basis of hopping of charge carriers between the Fe^{2+} and Fe^{3+} ions on octahedral site. The increase in frequency enhances the hoping frequency of charge carriers resulting in an increase in the conduction process thereby decreasing the resistivity.
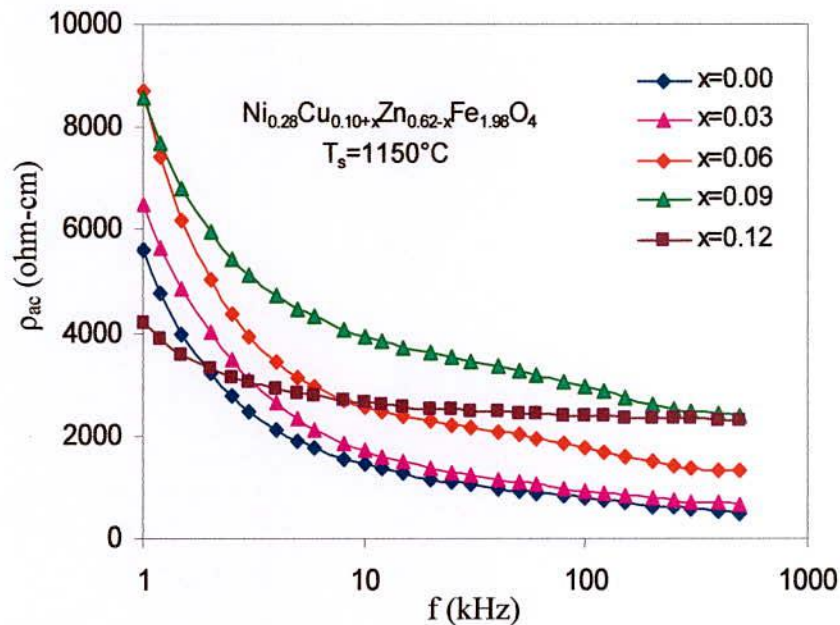
Fig. 5.19 Frequency dependence of AC resistivity of $Ni_{0.28}$ $Cu_{0.10+x}$ $Zn_{0.62-x}$ $Fe_{1.98}O_4$ ferrites sintered at 1150°C/ 3hrs

The dispersion of polycrystalline ferrite with frequency can be explained by the model of separated microstructure, of grains with low resistivity and grain boundaries with high resistivity, such as an equivalent circuit consisting of a resister and capacitor. The ferrite resistivity increases at a low frequency because motion of electron occurs readily through grains under an electric filed but is interrupted if they reach the interfaces. The ferrite permittivity also increases with the large polarization formed on the grain boundary interface at a low frequency [5.7].

5.5.3 Frequency Dependence of Dielectric Constant

Fig. 5.20 shows the variation of dielectric constant ε' with frequency for different compositions of $Ni_{0.28}$ $Cu_{0.10+x}$ $Zn_{0.62-x}$ $Fe_{1.98}O_4$ ferrites at 1150°. It can be seen from the figures that the dielectric constant is found to decrease continuously with increasing

frequency for all specimens exhibiting a normal dielectric behaviors of ferrites. The dielectric dispersion is rapid at lower frequency region and it remains almost independent at high frequency side. The incorporation of Cu into Ni-Cu-Zn ferrites has no pronounced effect on the dielectric constant at high frequency, but significantly decreases the dielectric constant in the low frequency range.
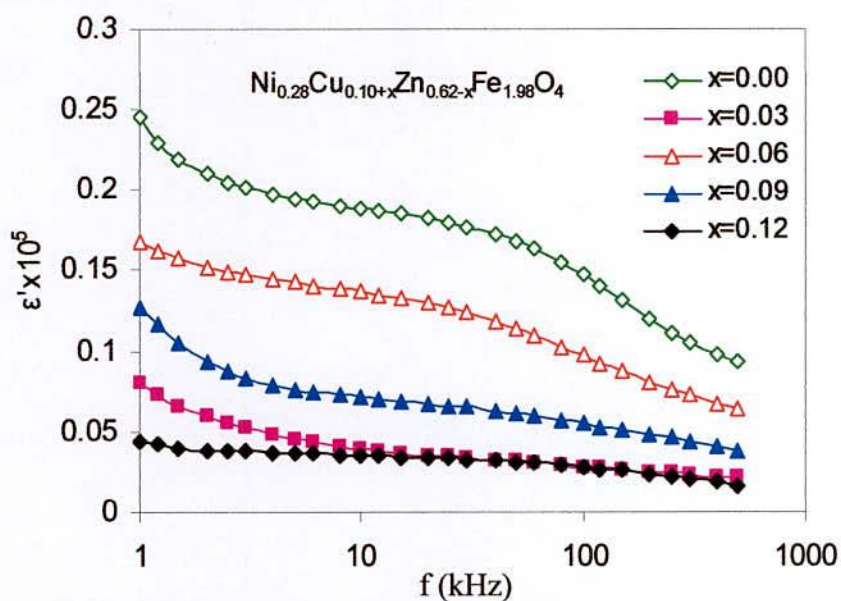
Fig. 5.20 Dielectric constant (ε') as a function of frequency of the ferrite system $Ni_{0.28}$ $Cu_{0.10+x}$ $Zn_{0.62-x}$ $Fe_{1.98}O_4$ ferrites sintered at 1150°C/3hrs

The values of dielectric constant decrease sharply at low frequency up to 1kHz which is because of the interfacial polarization taking place at low frequencies. This can be explained by the model of granular microstructure having grains of low resistivity separated by grain boundaries of high resistivity [5.8-5.9]. The decrease in the values can be explained on the basis of the decrease in Fe^{2+} ions, which are easily polarizable ions. Fe^{2+} ions are easily available in the ferrites prepared by ceramic method because of the sintering at high temperature. The fine grains resulting from the citrate method and Cu-addition reduces the sintering temperature, which results in lowering of Fe^{2+} ions and hence the decrease in values of ε' as compared to the ferrite prepared by ceramic method. The observed decrease in dielectric constant with increase in frequency is due to the fact that above certain frequencies the electronic exchanges between Fe^{2+} and Fe^{3+} ions does not follow the frequency of the applied AC field.

154

5.6 Summary

The XRD pattern confirmed the single phase cubic spinel structure of the samples. The lattice parameter 'a' decreases with the increase of copper content. Bulk density was less than X-ray density. Curie temperature increases with increasing Cu-content. The initial permeability increases with Cu content and sintering temperature but resonance frequency shifted toward the lower frequency which really confirms with Snoek's relation. From the low field B-H loop the coercivity decreases with increasing Cu content it reveals the softer ferromagnetic nature of the studied sample. Grain size increases with increasing sintering temperature. Saturation magnetization increases with increasing Cu content. DC resistivity increases markedly with the addition of Cu content. AC electrical resistivity decreases with increasing frequency. The dielectric constant decreases with increasing frequency.

Chapter - VI

Results and Discussion of $Ni_{0.28}Cu_{0.10}Zn_{0.62}Fe_{1.98}O_4$ Doped with V_2O_5 and Li_2O

6.0 Results and Discussion of $Ni_{0.28}Cu_{0.10}Zn_{0.62}Fe_{1.98}O_4$ doped with V_2O_5 and Li_2O

6.1 Introduction

Ni-Cu-Zn ferrite materials with V_2O_5 and Li_2O additives are prepared by the conventional ceramic technique. The use of sintering additives was found to be an effective method in practical manufacturing to lower the sintering temperature without degrading the electromagnetic properties [6.1] of the ferrites. Many researchers used Bi_2O_3 [6.2-6.4], V_2O_5 [6.5-6.7], MoO_3 [6.8-6.9], Glass [6.10], PbO [6.11] and WO_3 [6.3-6.12], as sintering aids in Ni-Cu-Zn ferrite.

These additives form liquid phases either due to the additives or due to the eutectic liquid phase formation between the additives and ferrite. Amount of liquid phase increases with increasing amount of sintering aids which results in increased densification. However, excessive amount of sintering additives will deteriorate electromagnetic properties of ferrites. So optimum content of sintering aids is necessary to achieve good sinterability as well as better magnetic properties. Hsu et.al. [6.6] stated that 0.5 mol% (~0.20 wt%) V_2O_5 addition had better densification in Ni-Cu-Zn ferrites. In Jeong et al. [6.3] study, 0.25 wt%. Bi_2O_3 addition showed optimum electromagnetic properties in the ferrite. Seo et. al. [6.9] reported that 0.02 wt%. MoO_3 addition had given highest bulk density and maximum initial permeability in the ferrite.

In this study the concentration of two sintering additives were fixed at 0.40 wt%. for V_2O_5 and Li_2O. The green samples containing different additives were sintered at temperature in the range of 1100°C to 1200°C with 3 hrs holding time, Effects of those sintering additives on the densification behavior were investigated. The X-ray diffraction analysis proves that the additives do not affect the final crystal phase of the Ni-Cu-Zn ferrite in our testing range. The V_2O_5 additive more easily enters the crystal lattice of the Ni-Cu-Zn ferrite than the Li_2O additive. These characteristics evidently affect the magnetic properties, such as SEM, saturation flux density, ratio of remanence B_r to saturation flux density B_s, coercive force of the Ni-Cu-Zn. The mechanisms involved are discussed. Structural and Magnetic properties of sintered specimens were also measured.

6.2 X-ray Diffraction Analysis (XRD)

The phase purity of sintered specimens was studied by XRD. The XRD pattern of the system $Ni_{0.28}Cu_{0.10}Zn_{0.62}Fe_{1.98}O_4$ + 0.4 wt% V_2O_5 ferrites sintered at 1150°C for 3 hrs is shown in Fig. 6.1. The XRD patterns for all the samples were indexed for fcc spinel structure and the Bragg planes are shown in patterns. It is obvious that the characteristics peaks for spinel Ni-Cu-Zn ferrite appear in the main crystalline phase with a slight shifting in the position of peaks towards the lowered spacing values. The peaks (111), (220), (311), (222), (400), (422), (511) and (440) which represent either odd or even indicating the samples are spinel cubic phase. It is observed from the Table 6.1 that a slight decrease in lattice parameter took place due to doping of V_2O_5 and Li_2O.
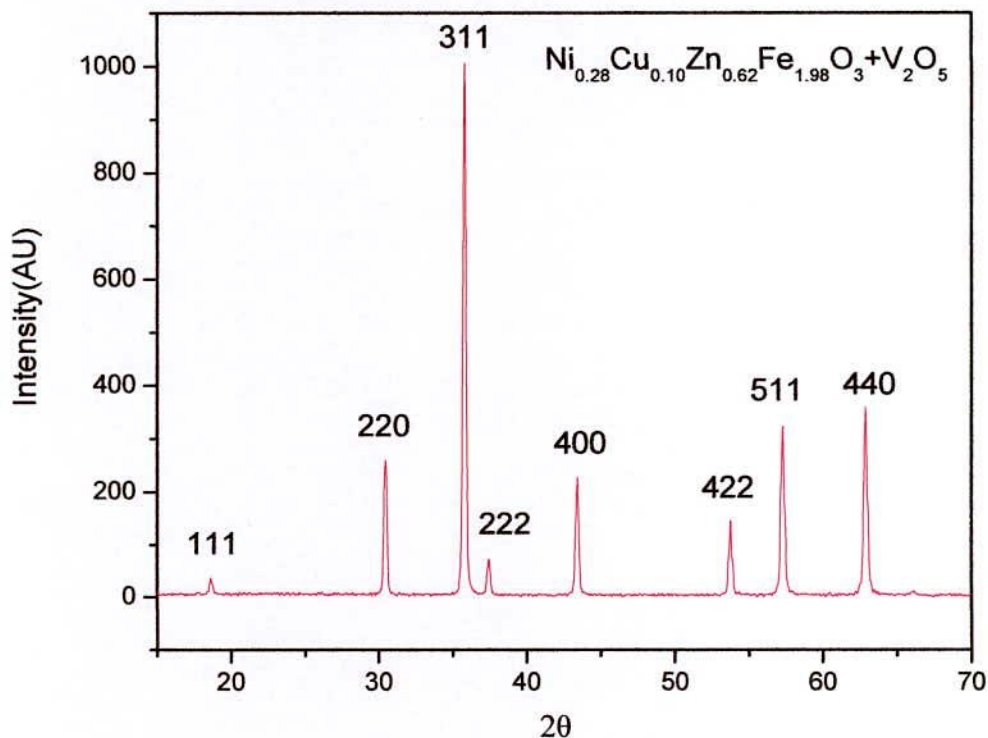
Fig. 6.1 XRD patterns of $Ni_{0.28}Cu_{0.10}Zn_{0.62}Fe_{1.98}O_4$ doped with V_2O_5 sintered at 1150°C (3hrs)

The bulk density increased, lattice parameter decreased and porosity increased with sintering aids compared to undoped one. Results are shown in Table- 6.1.

Table-6.1 Data of the lattice parameter (a), X-ray density (d_x), bulk density (d_B), porosity (P%), $Ni_{0.28}Cu_{0.10}Zn_{0.62}Fe_{1.98}O_4$ doped with V_2O_5 and Li_2O samples sintered at 1150°C/3hrs

Composition	a (A°)	d_x (g/cm^3)	d_B (g/cm^3)	P%
Un doped	8.4460	5.23	4.80	8.2
DopedwithV_2O_5 (0.4wt %)	8.4033	5.39	5.05	10.8
DopedwithLi_2O (0.4wt %)	8.4024	5.36	4.95	11.9

It is found that densification has taken place by the addition of sintering aids. The enhanced densification of the ferrite was attributed to the liquid phase assisted densification through recrystallization [6.10]. Liquid phase formation in these systems was either due to the melting of the sintering additives or due to the lowering of eutectic temperatures in presence of additives.

6.3 Magnetic Properties

6.3.1 Temperature dependence of initial permeability

Fig. 6.2 shows the temperature dependence of initial permeability, μ' for the toroid shaped samples with additives such as V_2O_5 and Li_2O, which were measured at a constant frequency (100 kHz) of an AC signal by using Impedance Analyzer. The change in Curie temperature, T_c of the ferrite with V_2O_5 and Li_2O substitution was also evaluated. It is found that T_c of the doped sample has increased compared with undoped sample. The T_c for undoped sample is 140°C while that of V_2O_5 and Li_2O doped samples are 150°C and 145°C respectively. This slight increase in T_c is probably due to decrease in lattice parameter and also may be due to increase in density. The decrease in lattice parameter may have influence on the strengthening of exchange interaction and coupling between magnetic ions.
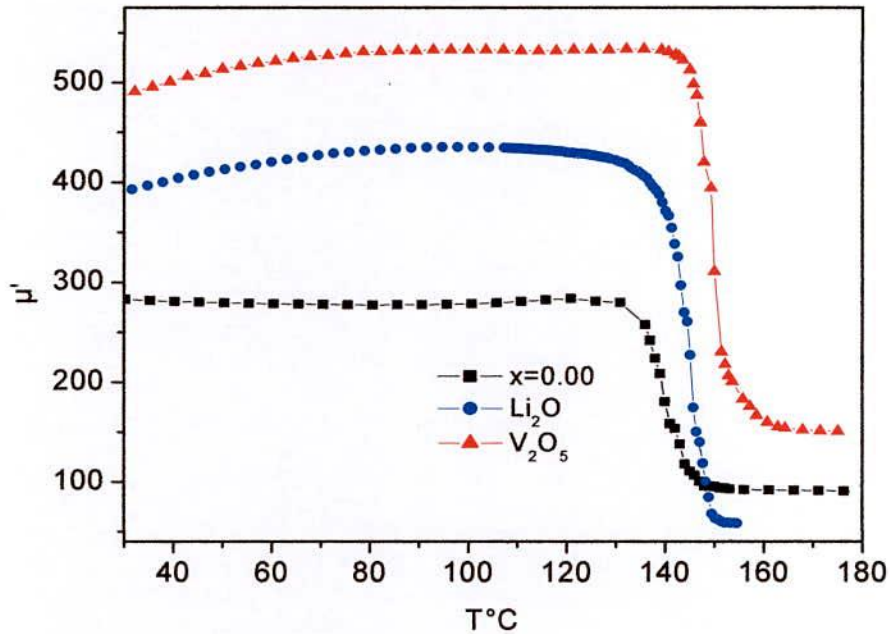
Fig. 6.2 Temperature dependence of permeability in $Ni_{0.28}Cu_{0.10}Zn_{0.62}Fe_{1.98}O_4$ doped with V_2O_5 and Li_2O sintered at $1150°$ for 3 hrs

6.3.2 Frequency dependence of Complex permeability

Permeability curves for the samples sintered at $1150°C$ for 3hrs are shown in Fig. 6.3 (a) and Fig. 6.3 (b). Fig's depicts the permeability spectra over the frequency range from 1 kHz to 13 MHz. From the Fig. 6.3(a), it is remarkably observed that, a large enhancement of permeability of 476 and 380 for the V_2O_5 and Li_2O doped samples compared with 284 for the undoped samples. This large enhancement of permeability is due increased density and larger grain size. The grain size of undoped sample is 3.9 μm while it is 6 μm for V_2O_5 doping. Fig. 6.3 (b) shows the imaginary part of permeability as a function of frequency. It is observed that the resonance frequency, f_r for the doped sample could not determined due to the limitation of the equipment up to 13 MHz, while f_r for the undoped sample has been estimated to be 12 MHz. It is noticed that though the permeability of the doped samples are much higher than undoped, the f_r has shifted to

higher frequency which may be due to increased density, grain size and defect free microstructure as can be seen in the microstructure of V_2O_5 doped sample (see Fig. 6.4)
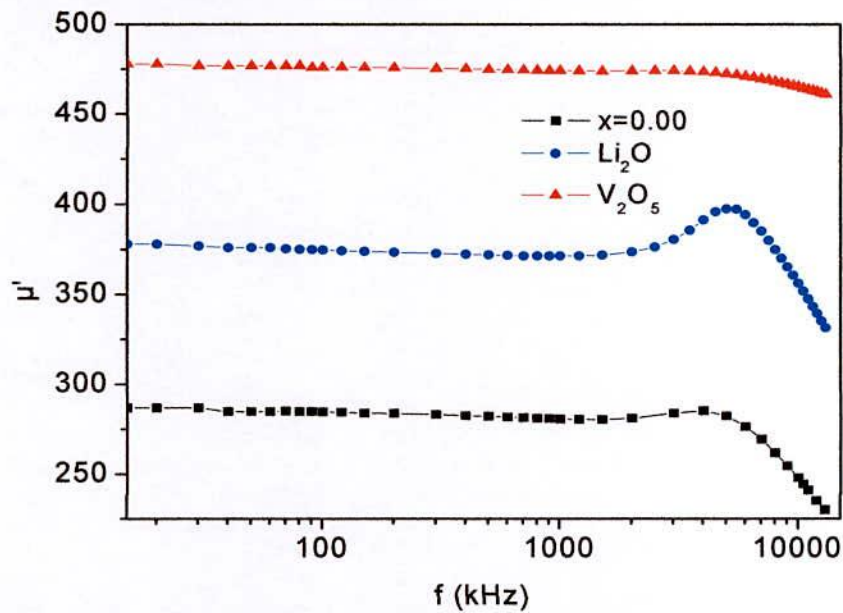
Fig. 6.3 (a) Frequency dependence of the real part of the permeability, μ' of $Ni_{0.28}Cu_{0.10}$ $Zn_{0.62}Fe_{1.98}O_4$ doped with V_2O_5 and Li_2O sintered at 1150°C for 3hrs
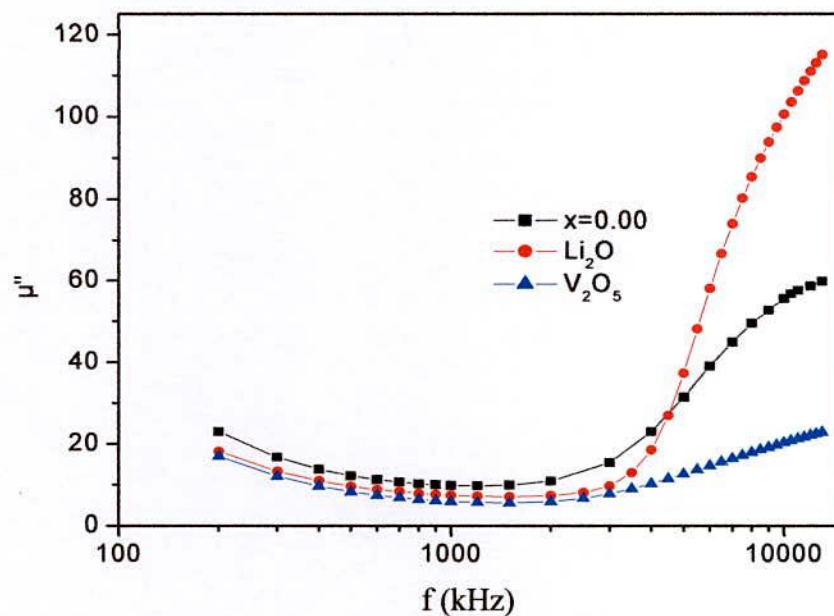
Fig-6.3 (b) Frequency dependence of the imaginary part of complex permeability, μ'' of $Ni_{0.28}Cu_{0.10}Zn_{0.62}Fe_{1.98}O_4$ doped with V_2O_5 and Li_2O sintered at 1150°C for 3hrs

160

6.4 SEM Microstructure

Fig. 6.4(a) and Fig. 6.4(b) show microstructure of sintered specimen that were sintered at 1150° for 3 hrs. It was evidenced from SEM analysis that grain has become larger in the presence of V_2O_5 additives. A rapid grain growth of a limited number of grains to size much larger than those of the average grain population was observed. It might be due to lower melting point of V_2O_5 having liquid phase sintering effect. The liquid phase act as driving force during sintering facilitating higher densification and grain growth. The microstructure of undoped sample is hizzy and less dense than doped sample. The undoped sample has more porosity as evidenced from the microstructure than V_2O_5 doped samples. The average grain size is 3.9 μm for the undoped sample while 6 μm for the sample doped with 0.4 wt% V_2O_5. The grains that grow consume their neighbors, grow larger and add more sides. The values of permeability of Ni-Cu-Zn ferrite increase with increasing grain size as well as with density because domain wall motion increases with increasing grain size, which is responsible for increasing the value of permeability.
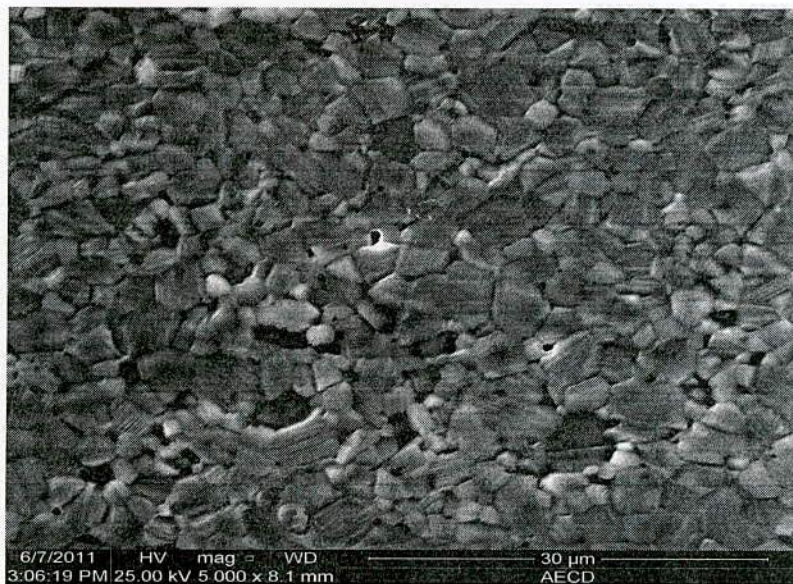
Fig. 6.4 (a) Microstructure of $Ni_{0.28}Cu_{0.10}Zn_{0.62}Fe_{1.98}O_4$ undoped sintered at 1150°C for 3 hrs

161
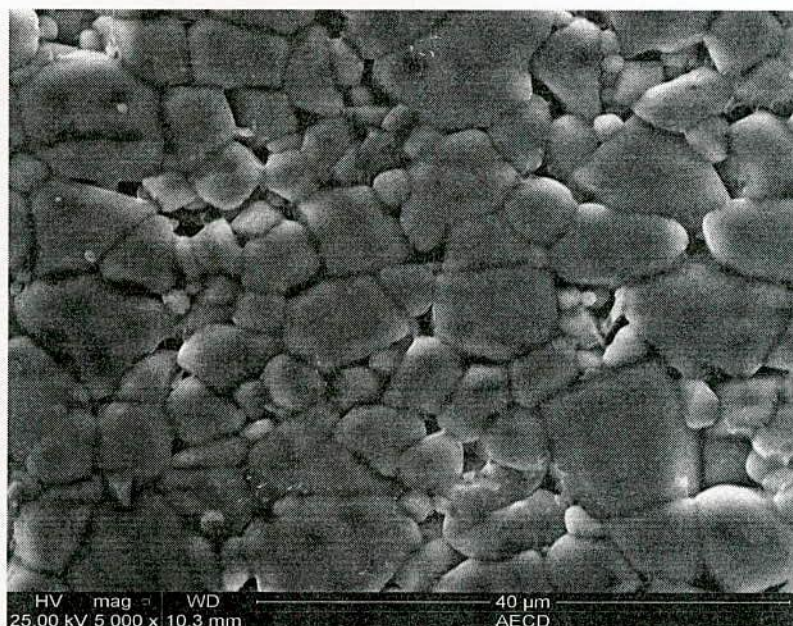
Fig-6.4 (b) Microstructure of $Ni_{0.28}Cu_{0.10}Zn_{0.62}Fe_{1.98}O_4$ doped with 0.4 wt% V_2O_5 sintered at 1150°C for 3 hrs

6.5 Low field B-H loop at Room Temperature

The magnetic properties of the investigated composition $Ni_{0.28}Cu_{0.10}Zn_{0.62}Fe_{1.98}O_4$ doped with V_2O_5 and Li_2O were measured in experiment. The magnetic hysteresis graphs of the toroid samples prepared from Ni-Cu-Zn ferrite doped with V_2O_5 (0.4 wt%) and Li_2O (0.4 wt%) sintered at 1100°C and 1150°C for 3hrs at constant frequency (f=1kHz) are depicted in Fig. 6.5(a) and 6.5(b). The important magnetic parameters obtained from the hysteresis data are tabulated in Table-6.2.

From the B-H loops, the remenance induction (B_r), saturation induction (B_s) and coercive force (H_c) were determined and compared with V_2O_5 and Li_2O doped samples at different sintering temperatures. It is observed from the Fig. 6.5(a, b) and Table 6.2 that magnetic induction, B_s has increased from 2.10 kG for undoped sample to 3.26 and 2.84 kG for doped with V_2O_5 and Li_2O respectively. The coercivity, H_c has substantially decreased from 1.74 Oe for undoped to 0.90 and 1.64 Oe for V_2O_5 and Li_2O doped

162

samples respectively. These features show that additives have beneficial effect of magnetic softening of the ferrites. Comparing this data with the bulk density and microstructure of the samples, the increased B_s and lower H_c values are closely correlated to the densification and grain size. This shows that a soft magnetic ferrite with higher bulk density, large average grain size and pore-free microstructure possesses higher B_s and lower H_c [6.13]. However, the 0.4 wt% V_2O_5 added Ni-Cu-Zn ferrite has enhanced the grain growth, and pore free dense microstructure.

Further more, the coercive field strength (H_c) of a magnetic material is the opposing magnetic field strength required reducing remanent flux density (B_r) to zero; low H_c value in magnetic material arises from the lower pinning forces between the magnetic domain walls. Igarashi and Okazaki have reported that in soft magnetic ferrites, the coercivity was independent of the density but depended highly on the grain size of ferrite [6.13]. On the other hand, Bogdanovich also reported the existence of a strong dependency between coercivity and porosity. The low coercive force and higher permeability, confirms that the development of soft magnetic characteristics properties of Ni-Cu-Zn ferrite doped with 0.4 wt% V_2O_5. It is also observed coercivity decreases with increase in sintering temperature (Table-6.2). The difference in the H_c values is understandable because of the substantia! increase in grain size in response to the increase in sintering temperature which facilitating the movement of the magnetic domain.

The hysteresis loss of the undoped specimen is higher, which might arise from its porous (Table-6.2) structure. It is known that hysteresis loss is mainly cussed by the irreversible rotation of magnetization vector. The magnetization in the present ferrite may be primarily controlled by domain wall motion Porosity, which acts as extra pinning centre, hinders the domain wall motion. In that case, higher field is required to switch the domain, which causes higher hysteresis losses. The lower hysteresis loss of the doped samples V_2O_5 and Li_2O is observed.
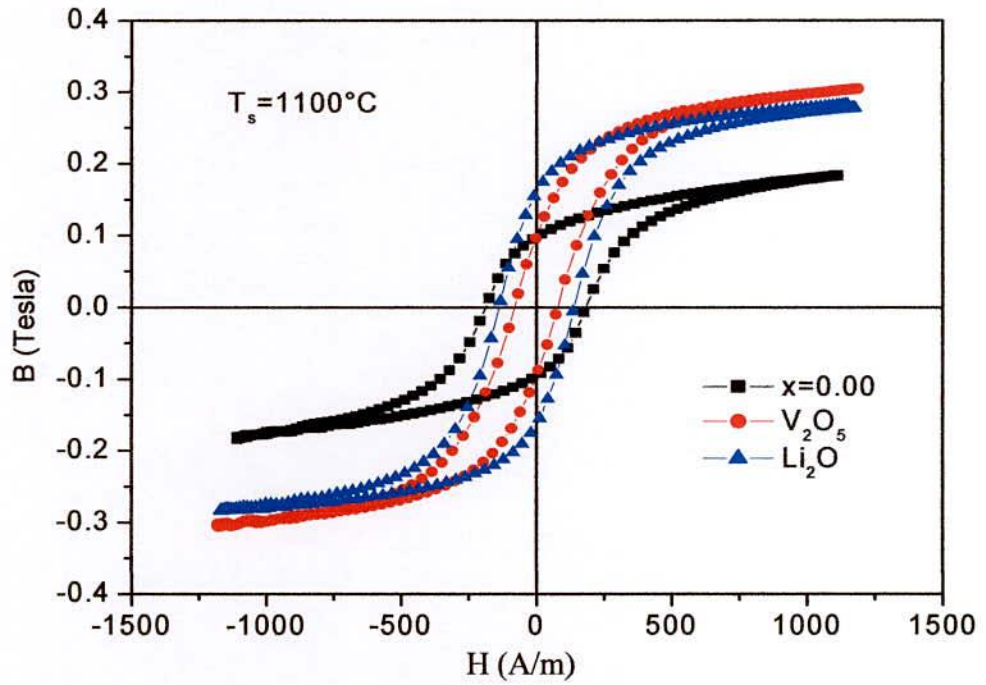
Fig. 6.5 (a) Magnetic hysteresis graphs of $Ni_{0.28}Cu_{0.10}Zn_{0.62}Fe_{1.98}O_4$ doped with V_2O_5, Li_2O sintered at 1100°C/3h
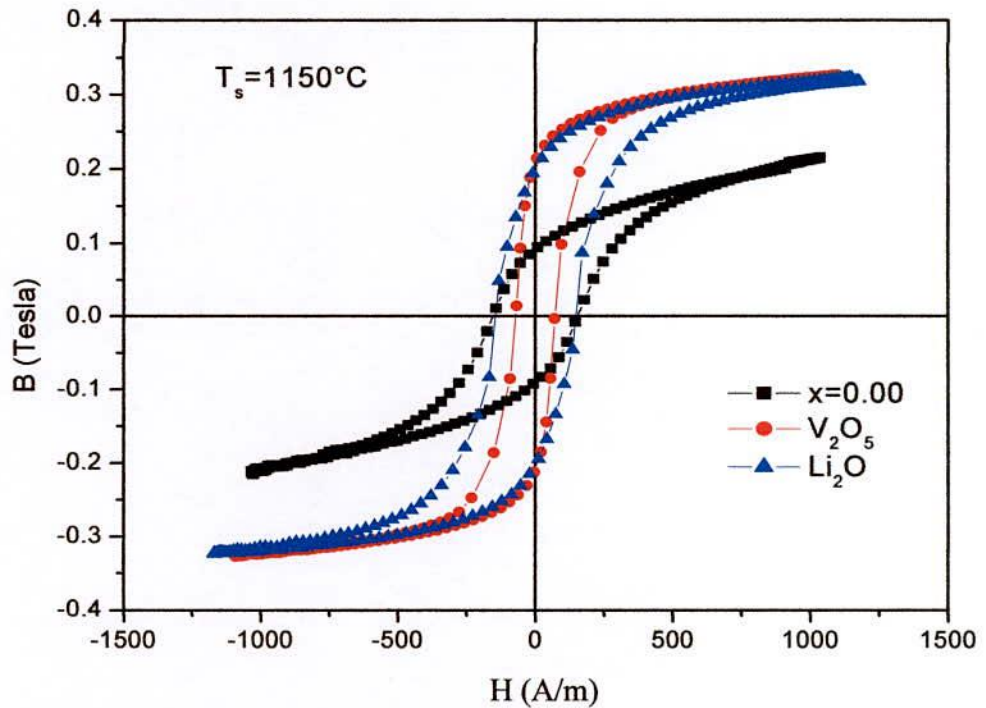
Fig. 6.5 (b) Magnetic hysteresis graphs of $Ni_{0.28}Cu_{0.10}Zn_{0.62}Fe_{1.98}O_4$ doped with V_2O_5, Li_2O sintered at 1150°C/3hrs

Table-6.2 The experimental values of T_c, μ', H_c, B_r, B_s & $\dfrac{B_r}{B_s}$ ratio and hysteresis loss of

$Ni_{0.28}Cu_{0.10}Zn_{0.62}Fe_{1.98}O_4$ doped with V_2O_5 and Li_2O samples sintered at 1150°C/3hrs

Composition	T_S (°C) / 3hrs	T_c	μ'	H_c (Oe)	B_r (kG)	B_s (kG)	B_r/B_s	Losses (W/kg)
Undoped	1150	140	284	1.74	1.04	2.10	0.50	19.1
Doped with V_2O_5	1150	150	476	0.90	2.08	3.26	0.63	16.8
Doped with Li_2O	1150	145	380	1.64	1.61	2.84	0.57	18.2

6.6 Magnetization Measurement

Magnetization as a function of applied magnetic field up to 20 kOe was measured with vibrating sample magnetometer (VSM) at room temperature of $Ni_{0.28}Cu_{0.10}Zn_{0.62}Fe_{1.98}O_4$ and doped with V_2O_5 and Li_2O sintered at 1150°C for 3hrs shown in Fig. 6.6. It is observed that the magnetization increases sharply at very low field (H < 1 kOe) which corresponds to magnetic domain reorientation and thereafter increase slowly up to saturation. The saturation magnetization of doped samples is higher than undoped samples. This may be due to higher of the doped ferrite. M_s of 0.4 wt% V_2O_5 composition are higher than 0.4 wt% Li_2O composition. Fig. 6.6 shows the magnetization curve for $Ni_{0.28}Cu_{0.10}Zn_{0.62}Fe_{1.98}O_4$ with doped V_2O_5 and Li_2O ferrites. The value of M_s for undoped sample is 53.22 emu/g and that of doped with V_2O_5 and Li_2O are 58.0 and 56.0 emu/g.
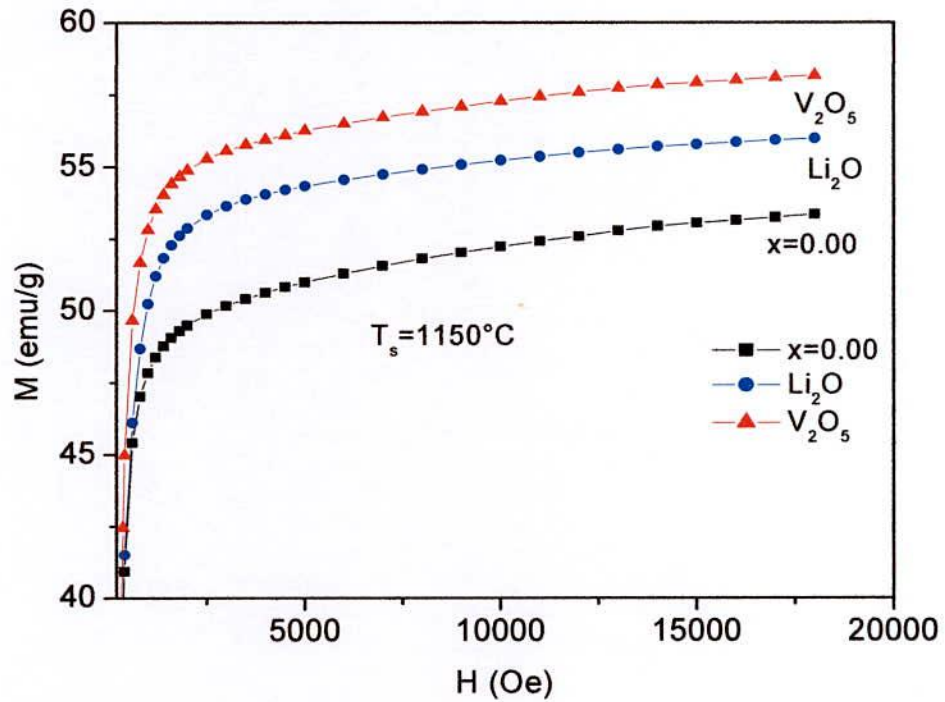
Fig. 6.6 Field dependence of magnetization of $Ni_{0.28}Cu_{0.10}Zn_{0.62}Fe_{1.98}O_4$ doped with V_2O_5 and Li_2O sintered at 1150°C for 3 hrs

6.7 Summary

Effect of sintering additives on densification behaviors and electromagnetic properties of Ni-Cu-Zn ferrites were studied. The results showed that small amount of additives was able to enhance the densification. A significant increase in initial permeability of the ferrite was found at small fraction doped with 0.4 wt% of V_2O_5 and 0.4 wt% of Li_2O substitution. The increased permeability was due to better densification and increased grain size in substituted ferrites. Better densification had also resulted improved electromagnetic properties of the V_2O_5 modified ferrites.

166

CHAPTER - VII

Conclusions and Future Work

7.1 Conclusions

The present work was focused on the synthesis, characterization and detail study of electromagnetic properties of iron deficient $(Ni_{0.28}Cu_{0.10}Zn_{0.62}O)$ $(Fe_2O_3)_{1-x}$ (x = 0.00, 0.02, 0.04, 0.06 & 0.08) and $Ni_{0.28}Cu_{0.10+x}Zn_{0.62-x}Fe_{1.98}O_4$ ferrite samples (x = 0.00, 0.03, 0.06, 0.09 & 0.12) using standard double sintering ceramic method, sintered at 1100°C - 1200°C for 3 hours. The effects of dopiness as V_2O_5 and Li_2O as sintering aids on the densification kinetics and magnetic properties of the ferrites were also investigated. The X-ray diffraction pattern confirmed the single phase cubic spinel structure of both Fe-deficient and Cu-additive ferrites.

The significant findings of this work are as follows:

(i)   The lattice constant of $(Ni_{0.28}Cu_{0.10}Zn_{0.62}O)$ $(Fe_2O_3)_{1-x}$ decreases linearly with increasing Fe-deficiency obeying Vegard's law.

(ii)   Curie temperature slightly increases with increasing x content possibly due to strengthening of A-B exchange interaction due to increased number of Fe^{3+} ions at A site as well as decrease of lattice parameter of the studied samples. This increases linkages between the magnetic ions and exchange coupling that determines the magnitude of the Curie temperature.

(iii) Saturation magnetization and magnetic moment are found to increase with increasing Fe-deficiency up to 0.06 and thereafter it slightly decreases. This may be due to modified cation distribution on two sublattices.

(iv)   The low field hysteresis parameter such as coercivity, (H_c) decreases with increasing of x content and sintering temperature.

(v)   The remanence, (B_r) and flux density or induction, (B_s) increase gradually with x content and B_s increases with sintering temperature. Decrease of H_c comes from the reduction of pinning force between domain walls and grain boundaries resulting from larger grain size and increased density or reduced porosity.

(vi)   Bulk density increases with increasing of x content.

(vii) SEM micrograph results indicate that the grain size of the samples increases with increasing Fe-deficiency.

(viii) Grain size has a great influence on the domain wall contribution and hence on permeability. The initial permeability increases gradually with

increasing x content and sintering temperature. The initial permeability is constant up to 2-4 MHz region dependent on sintering temperature.

(ix)   Ferrimagnatic resonance f_r shifts to lower frequency with the increases of permeability validating Snoek's relation $\mu_i.f_r$ = constant.

(x)   The DC electrical resistivity increase with increasing Fe-deficiency.

(xi)   Dielectric constant decreases with increasing frequency exhibiting normally dielectric behavior of ferrites.

(xii)   Based on the experimental results in terms of soft magnetic properties it may be concluded that optimum composition of iron deficient $(Ni_{0.28}Cu_{0.10}Zn_{0.62}O)(Fe_2O_3)_{1-x}$ series is x = 0.08 with high initial permeability of 358, low H_c of 1.3 Oe and minimum hysteresis loss of 14.3 W/kg.

The CuO has great influence on microstructure and electromagnetic properties of NiCuZn ferrites. The presence of Cu-ions causes appreciable changes in physical, magnetic, electrical and dielectric properties of Cu-substituted $Ni_{0.28}Cu_{0.10+x}Zn_{0.62-x}Fe_{1.98}O_4$ ferrites.

(xiii)   The lattice parameter decreases with the copper content due to smaller ionic radius of Cu^{2+} (0.70Å) compared to that of Zn^{2+}(0.82Å).

(xiv)   A slightly increase in bulk density has been found with increasing Cu content substituting Zn in Ni-Cu-Zn ferrite. The average gain size increases significantly with increasing Cu-content. The increase in density and grain growth of the samples may be attributed to the liquid phase sintering due to the presence of CuO.

(xv)   The initial permeability increases with Cu-content and sintering temperature attaining a value of permeability μ=586 for the sample x=0.09 sintered at T_s=1200°C compared to μ=303 for x=0.00 in this series. The resonance frequency shifts toward the lower frequency, as the permeability of the samples increases which really confirms with Snoek's relation. The increase in the permeability can be attributed to the presence of Cu-ions activating the sintering process in ferrites and leading to increase in density and grain size.

(xvi)   From the low field B-H loop it was observed that the coercivity and hysteresis losses decrease with increasing Cu-content revealing the softer ferrimagnetic nature of the studied sample. H_c as low as 0.75 Oe for x=0.09 sintered at 1200°C with hysteresis losses of 15.5 W/kg has been observed compared with H_c =1.6 Oe and hysteresis loss of 17.7 W/kg for the sample x=0.00 in the series. A decrease in coercivity is also observed with increase in sintering temperature. Flux density, B_s is found to increase with x content.

(xvii)   Saturation magnetization, M_s increases with increasing Cu-content with a value of M_s = 53.2 emu/g for x=0.00 compared with M_s =61.8 emu/g for x=0.09.

(xviii) The dc electrical resistivity is found to increase with the increase in Cu-content which is attributed to the fact that the incorporation of Cu in B-site of ferrite may decrease the concentration of Fe^{2+}/Fe^{3+} ion pairs. The compositional variation of resistivity and dielectric constant indicates the inverse trends with each other. Both ac resistivity and dielectric constant decreases as the frequency of applied ac electrical field increases. The increase in frequency enhances the hopping frequency of charge carriers, resulting in an increase in the conduction process, thereby decreasing the resistivity. Dielectric constant decreases with increasing frequency exhibiting normal dielectric behavior of ferrites.

(xix)   Analysis of the experimental results of $Ni_{0.28}Cu_{0.10+x}Zn_{0.62-x}Fe_{1.98}O_4$ series, it appeared that the sample with x=0.09 shows the best soft magnetic properties sintered at T_s=1200°C having high permeability and low magnetic losses.

(xx)   Addition of Li_2O and V_2O_5 plays a crucial role in improving the magnetic properties of $Ni_{0.28}Cu_{0.10}Zn_{0.62}Fe_{1.98}O_4$ ferrite. Ionic radius of V^{5+} and Li^{2+} are 0.6 Å and 0.59 Å respectively. So, addition of vanadium in Ni-Cu-Zn ferrite may show some interesting properties because they can enter into lattice for solid solution and they have lower melting point assisting liquid phase sintering. A significant increase in initial permeability of the ferrite was found at small fraction of dopants with 0.4 wt% of V_2O_5 and Li_2O additions. The increased permeability was due to higher densification and increased grain size of the ferrites samples. The saturation magnetization

increases substantially by addition of Li and V. Decreasing tendency of coercivity (H_c) and large enhancement of B_s is observed for the samples with larger grains. Such an effect comes from the reduction of the pinning force between the domain walls and the grain boundaries due to the decrease in the total grain boundary area of the samples with larger grains. Finally it may be concluded that Li_2O and V_2O_5 doped samples can be sintered at much lower temperature of $T_s=1150°C$ for obtaining optimum magnetic properties. It reduces the energy consumption and enables cost effective material synthesis hence a large enhancement of permeability from 284 for undoped to 476 and a drastic decrease of H_c from 1.74 Oe to 0.9 Oe for the V_2O_5 doped sample have been observed.

7.2 Scope for Future Work

With the development and advancement of nanotechnology a tremendous growth in research on miniaturization and high efficiency electronic devices is taking place. For these efficient miniaturized devices we need soft magnetic materials as its basic magnetic component. Soft ferrites are extensively used in inductor cores which form a basic requirement in modern technology. NiCuZn ferrites are suitable for these devices for future advanced technology. Fabrication and characterizations of multilayer chip inductor using improved NiCuZn ferrites is of high demand. Therefore future work on these types of systems may be carried out using nanoparticle and nanosysthesis techniques for the development of efficient miniaturized device for advance technology.

References

References

Chapter- I

[1.1] E. C. Snelling; Soft Ferrites: Properties and Applications, 2nd edition, Butter worths, London; 1988, p- 1.

[1.2] J. Kulikowski; 1984, "Soft magnetic ferrites development or staqguation" J. Magn. Magn. Mater. Vol. 41, pp. 56 – 62.

[1.3] A. verma, T. C. Goel, R. G. Mendiratta, R. G. Gupta; 1999, "High-resistivity nickel-Zinc ferrites by the citrate precursor method" J. Magn. Magn. Mater. Vol. 192, pp. 271 – 276.

[1.4] T. Nakamura, T. Miyaonoto, Y. Yamada; 2003, "Complex Permeability spectra of Polycrystalline Li-Zn ferrite and application of EM – wave absorber" J. Magn. Magn. Mater. Vol. 256, pp. 340 – 347.

[1.5] A. Lakshman, K. H. Rao, R. G. Mendiratta; 2002, "Magnetic Properties of In^{3+} and Cr^{3+} substituted Mg – Mn ferrites", J. Magn. Magn. Mater. Vol. 250, pp. 92-97.

[1.6] Toshiyuki Suzuki, Termitsu Tanaka, Kaoru Inkmzu; "High density recording capability for advanced particulate media", J. Magn. Magn. Mater. 235 (2001) 159.

[1.7] T. Ginnakopoulou, L. Kompotiatis, A. Kontogeorgakos, G. Kordas; "Microwave behavior of ferrites prepared via sol-gel method", J. Magn. Magn. Mater. 246 (2002) 360.

[1.8] E. Olsen, J. Thonstad; "Nickel ferrites as inert anodes in aluminium electrodes : Part I Material fabrication and preliminary testing", J. Appl. Electrochem. 29 (1999) 293.

[1.9] C. O. Augustin, D. Prabhakaran. L. K. Srinivasan; "Fabrication and Characterization of NiCr$_2$O$_4$ Spinel", J. Mater. Sci. Lett. 12(1993) 383.

[1.10] I. S. Jacobs, J.A.P. 40, 917, 1969.

[1.11] A. Balayachi, J. L. Dormann and M. Nogues; "Critical analysis of magnetically semi disordered systems: critical exponents at various transitions", J. Phys. Condens. Matter. 10 (1998) 1599.

[1.12] M. A. Hakim, M. Manjurul Haque, M. Huq, SK. Manjura Hoque and P. Norblad; "Reentrant Spin Glass and Spin Glass Behavior of Diluted Mg – Zn Ferrites", CP 1003, Magnetic Materials, International Conference on Magnetic Materials (ICMM-2007) AIP. p- 295.

[1.13] H. Martinho, N. O. Moreno, J. A. Sanjurjo, C. Rettori, D. L. Huber, S. B. O Seroff, W. Ratcliff, S. W. Cheong; "Magnetic properties of the frustrated antiferromagnetic spinel ZnCr$_2$O$_4$ and the spin-glass Zn$_{1+x}$Cd$_x$Cr$_2$O$_4$ (x=0.05,0.10)", Phys. Rev. B 64 (2001) 024408.

[1.14] N. Rezlescu, L. Rezlescu, P. D. Popa, Rezlescu; "Influence of additives on the properties of a Ni-Zn ferrite with low Curie point", J. Magn. Magn. Mater. (2000), pp. 215-216.

[1.15] H. M. Zaki, S. F. Mansour; "The influence of Ge^{4+} and Ti^{4+} ions substitutions on the magnetic properties of copper ferrite", Materials Chemistry and Physica. Vol. 88 (2004), pp. 326-332.

[1.16] E. Rezlescu, L. Sachelarie, P. D. Popa and N. Rezlescu; "Effect of substitution of divalent ions on the Electrical and Magnetic", Chemistry and Physica. Vol. 88 (2004), pp. 326-332.

[1.17] M. Manjurul Haque, M. Huq and M. A. Hakim; "Thermal hysteresis of permeability and transport properties of Mn substituted Mg-Cu-Zn ferrites", (2008), 055007, pp. 1-10.

[1.18] S. H. Seo and J. H. Oh; 1999, "Effect of MoO_3 Addition of Sintering Behaviors and Magnetic Properties of NiCuZn Ferrite for Multilayer Chip Inductor" IEEE TRANSACTIONS ON MAGNETICS, Vol. 35, No. 5.

[1.19] M. Manjurul Haque, M. Huq, M .A. Hakim; 2008, "Influence of CuO and sintering temperature on the microstructure and magnetic properties of Mg-Cu-Zn ferrites", J. Magn. Magn. Mater. Vol. 320, pp. 2792-2799.

[1.20] J. Bera, P. K. Roy; 2005, "Effect of grain size on electromagnetic properties of $Ni_{0.7}Zn_{0.3}Fe_2O_4$ ferrite", Physica B Vol. 363, pp. 128 – 132.

[1.21] Amarendra K. S., T. C. Goel and R. G. Mendiratta; 2002; "Magnetic Properties of Mn –substituted Ni – Zn ferrites; J. Applied Phys., Vol. 92. pp. 3872-3876.

[1.22] A. A Sattar, H. M. El- sayed, K. M. EL- Shokrofy and M. M. El- Tabey; 2005, "Improvement of the Magnetic Properties of Mn – Ni – Zn Ferrite by the Non magnetic Al^{3+}- Ion Substitution"; Journal of Applied Sciences, Vol. 5 (1), pp. 162 – 168.

[1.23] T. T. Ahemd, I. Z. Rahman and S. A. M Tofail; 2004, "Effect of Copper ion distribution on the magnetization of nano scaled Ni-Zn ferrite"; J. Magn. Magn. Mater., Vol. 272 – 276, pp. 2250 – 2252.

[1.24] T. Nomura and M. Takaya; Hybrids 3(1987) 15.

[1.25] T. Nomura and A. Nakano, Proc. 6th Int. Conf. on Ferrites (1992) 1198.

[1.26] A. Nakano, H. Momoi and T. Nomura; Proc. 6th Int. Conf. On Ferrites (1992) 1225.

[1.27] T. Nakamura; "Low-temperature sintering of Ni-Zn-Cu ferrite and its permeability spectra", J. Magn. Magn. Mater., 168 (1997) 285 – 291.

[1.28] Hui Zhong, Huai Wu Zhang, hai Tao Zhou and Li Jun Jia; "Effects of WO_3 substitution on electromagnetic properties of Ni-Cu-Zn ferrite", J. Magn. Magn. Mater., 300 (2006) 445.

[1.29] Takanori Tsutoka; "Frequency dispersion of complex permeability in Mn – Zn and Ni – Zn spinel ferrites and their composite materials", J. Appl. Phys. 93(5) (2003) 2789.

[1.30] Nakamura T., Tsutaka T., Hatakeyana K.; "Frequency dispersion of permeability in ferrite composite materials" J. Magn. Magn. Mater., 138 (1994) 319.

[1.31] Abdeen A. M.; "Electrical conduction in Ni – Zn ferrites", J. Magn. Magn. Mater., 185 (1998) 199.

[1.32] K. O. Low, F. R. Sale; "Sintering of gel-derived Ni-Cu-Zn ferrites"; Ferrites: Proceedings of ICF 8, Kyoto, Tokyo, Japan.; The Japan Society of Power and Powder Metalurgy, 2000, pp. 548 – 550.

[1.33] Kin O. Low, Frank R. Sale, "Electromagnetic properties of gel – derived Ni-Cu-Zn ferrites"; J. Magn. Magn. Mater., 246 (2002) 30 – 35.

[1.34] S. Manjura Hoque, M. Amanullah Choudhury and M. Fakhrul Islam "Characterization of Ni – Cu mixed spinel ferrite", J. Magn. Magn. Mater., 251 (2002) 292.

[1.35] Rahman I. Z., Ahmed T. T., "Study of Ni-Cu-Zn based ferrite powders: Processing and characterization"; The 2nd International conference on structure, Processing and properties of materials, 25-27 February 2004, Dhaka, Bangladesh, pp. 113 – 120.

[1.36] K. Hirota, T. Aoyama, S. Enomoto, M. Yoshinaka, O. Yamaguchi; "Microstructures and magnetic and electric properties of low-temperature sintering Mn-Zn ferrites without and with addition of lithum borosilicate glass", J. Magn. Magn. Mater., 205 (1999) 283.

[1.37] T. Aoyama, K. Hirota, O. Yamaguchi; "Characterization and low- Temperature Sintering of Reactive Mn-Zn Ferrite Powder", J. Am. Ceram. Soc. 79 (10) (1996) 2792.

[1.38] D. Stoppels; "Development in soft magnetic power ferrites", J. Magn. Magn. Mater., 160 (1996) 323.

[1.39] H. M. Sung, C. J. Chen, L. J. Wang, W. S. Ko; "The characteristics of low temperature co-fired multilayer chip LC ferrites", IEEE Trans. Magn. 34 (4) (1998) 1363-1365.

[1.40] Jingling Sun, Jianbao Li, Geliang Sun; "Effects of La_2O_3 and Gd_2O_3 on some properties of Ni-Zn ferrites"; J. Magn. Magn. Mater., 250 (2002) 20.

[1.41] J. Hu, M. Yan and W. Luo; "Preparation of high – permeability Ni – Zn ferrites at low sintering temperatures", Physica B 368 (2005) 251.

[1.42] V. Tsakloudi, E. Elaftheriou, M. Stoukises and V. Zaspalis; "Electromagnetic properties of Mn-doped Ni-Cu-Zn ferrites", J. Magn. Magn. Mater. 318 (2007) 58.

[1.43] T. Nakamura and Y. Okano; "Low Temperature Sintered Ni-Zn-Cu Ferrite", J. Phys. IV France, 7, CI- 91 (1997).

[1.44] K. Yasuda, Y. Mochizuki, and M. Takaya; Proceedings of the Eight International Conference of Ferrites (ICF8), (Kyoto, 2000), p. 1162.

[1.45] K. O. Low and F. R. Sale; J. Magn. Magn. Mater., 30, 246 (2002).

[1.46] Z. Yue, K. Zhou, L. Li, H. Zhang, and Z. Gui; "Synthesis of nanocrystalline NiCuZn ferrites powders by sol-gel auto-combustion method", J. Magn. Magn. Mater., 208, 55-60 (2000).

[1.47] J. Töpfer and J. Mürbe; Proceedings of the Ninth International Conference of Ferrites (ICF9), (San Francisco, 2004), P. 885.

[1.48] J. Y. Hsu, W. S. Ko. and C. J. Chen; "The effect of V_2O_5 on the sintering of NiCuZn ferrites", IEEE Trans. Magn., 31, 3994 (1995).

[1.49] J. H. Jean and C. H. Lee; "Effects of Lead (11) Oxide on Processing and Properties of Low-Temperature Cofirable Ni-Cu-Zn Ferrite", J. Am. Ceram. Soc., 82, (1999) 343-350.

[1.50] J. Jeong, Y. H. Han, and B. C. Moon; "Effects of Bi_2O_3 addition on the microstructure and electromagnetic properties of NiCuZn ferrites", J. Mater. Sci: Mater. Electronics, 15 (5), (2004) 303 – 306.

[1.51] M. A. Hakim, D. K. Saha and A. K. M. Fazle Kibria,"Synthesis and temperature dependent structural study of nanocrystalline Mg-ferrite materials"; Bang. J. Phys. 3 (2007) 57.

[1.52] A. K. M. Akther Hossain, S. T. Mahmud, M. Seki, T. Kawai and H. Tabata, "Structural, electrical transport and magnetic properties of $Ni_{1-x}Zn_xFe_2O_4$"; J. Magn. Magn Mater. 312(2007) 210.

[1.53] H. I. Hsiang, W. C. Liao, Y. J. Wang, Y.F. Cheng, J. Euro; "Interfacial reaction of TiO_2/NiCuZn ferrites in multilayer composites", Ceram. Soc. 24(7) (2004) 2015-2021.

[1.54] L. Zhao, Y. Cui, H. Yang, L. Yu, W. Jin, S. Feng; "The magnetic properties of $Ni_{0.7}Mn_{0.3}Gd_xFe_{2-x}O_4$ ferrite", Mater. Lett. 60 (1) (2006) 104-108.

[1.55] E. Rezlescu, N. Rezlescu, P. D. Popa, L. Reslescu, C. Pasnicu; "The Influence of R_2O_4 (R=Yb, Er, Dy, Tb, Gd, Sm and Ce) on the Electric and Mechanical Properties of a Nickel-Zinc Ferrite", Physica (a). Status Solidi, A 162 (1997) 673-678.

[1.56] L. Zhao, H. Yang, L. Yu, Y. Cui, X. Zhao, S. Feng; "Study on magnetic properties of nanocrystalline La-, Nd-, or Gd-, substituted Ni-Mn ferrite at low temperatures", J. Magn. Magn. Mater. 305 (2006) 91-94.

[1.57] J. Sun, J. Li, G. Sun; "Effects of La_2O_3 and Gd_2O_3 on some properties of Ni-Zn ferrite", J. Magn. Magn. Mater. 250 (2002) 20-24.

[1.58] M. A. Ahmed, N. Okasha, M. M. El-Sayed; "Enhancement of the physical properties of rare-earth substituted Mn-Zn ferrites prepared by flash method", Ceramics International, 33, 1 (2007) 49-58.

[1.59] P. K. Roy, J. Bera; "Enhancement of the magnetic properties of Ni-Cu-Zn ferrites with the substitution of a small fraction of lanthanum for iron", Mater. Res. Bull. 42 (2007) 77-83.

[1.60] O. F. Caltum, L. Spinu, Al. Stancu, L. D. Thung, W. Zhou; "Study of the microstructure and of the permeability spectra of Ni-Zn-Cu ferrites", J. Magn. Magn. Mater. 242-245 (2002) 160.

CHAPTER- II

[2.1] http://en.wikipedia.org/wiki/crystalstructure.

[2.2] B. D. Cullity; "Element of X-ray Diffraction", Addition – Wesley Publishing Company, Inc. (1967).

[2.3] T. Ogasawara and M. A. S. Oliveira; "Microstructure and hysteresis curves of the barium hexaferrite from co-precipitation by organic agent", J. Magn. Magn. Mater. 217 (2000) 147.

[2.4] W. H. Bragg; "The structure of magnetite and the spinels", Nature, 95 (1915), 561.

[2.5] Alex Goldman; "Modern Ferrite Technology", Van Nostrand Reinhold, New York, (1940) p.15.

[2.6] N. Spaldin; Magnetic materials: Fundamentals and device applications combridge: Cambridge University press, 2003.

[2.7] "International Tables for X-ray Crystallography"; The Kyvoch Press, Birmingam, England (1965).

[2.8] Alex Goldman; "Modern Ferrite Techonology", Van Nosttrand Reinhold New York, 1990.

[2.9] R. W. Cahn, P. Haasen, E. J. Kramer; "Materials Science and Technology", Vol. 3B, VCH Publishers Inc., New York, NY (USA) & Verlagsgesellschaft mbH, weinheim (Federal Republic of Germany), (1994).

[2.10] B. Viswanathan, V. R. K Murthy; "Ferrite Materials Science and Technology", Spring Verlag, Noarosa Publishing House, New Delhi, (1990).

[2.11] D. J. Craik; 1975, Magnetic Oxide, Part 1, John Wiley & Sons, Ltd, Bristol England.

[2.12] E. J. W Verwaw and E. L Heilmann; T. Cham. Phys. 15(4), (1947), 174 – 180.

[2.13] F. C Romeign; Philips Res. Rep. 8, NR- 5 (1953), 304 – 342.

[2.14] Smit and W. J. P. Wijn; Ferrites, Philips Technical Library (Wiley, New York, 1959).

[2.15] S. Knepicka and P Novak; Oxide spinels. In E. P. Wohlfarth, editor, Ferromagnetic Materials, Volume 3, Chapter 4, Pages 184-304, North-Holland, The Netherlands, 1982.

[2.16] Virginia Fuentes, S. Aburto and R Velenzuela; "Magnetic Sublattices in nickel ferrite", J. Magn. Magn. Mater 69 (1987) 233.

[2.17] P. W. Anderson; in Magnetism, Vol. I, Eds, G. T. Rado and H. Suhl (Academic Press, New York, 1963).

[2.18] A. Land; "Quantum Mechanics", Pitman, London (1951).

[2.19] J. H. Van Vleck; "Theories of Electric and Magnetic susceptibilities", Clarendon Press, Oxford (1932).

[2.20] P. Weiss; "L′ hypothese du champ moleculaire et la propriete ferromagnetique", J. Phys. Theor. Appl. 6, (1907) 661.

[2.21] B. Jeyadevan, C. N. Chinnasamy, K. Shinoda, K. Tohji; "Mn – Zn ferrite with higher magnetization for temperature sensitive magnetic fluid", J. Appl. Phys., Vol. 93 (2003) pp. 8450.

[2.22] Fowler, Michael; "Historical Beginning" of Theories of Electricity and Magnetism; Retrieved 2008.

[2.23] Vowles, P. Hugh; "Early Evolution of Power Engineering", Isis (University of Chicago Press) 17(2): (1932) 412.

[2.24] Allan H. Morrish; "The Physical Principles of Magnetism", John Wiley & Sons (1965).

[2.25] L. Neel; "Anistropic magnetique superficielle et surstructures d′ tation", J. Phy. Radium 15(4), (1954), 225-239.

[2.26] Y. Yafet and C. Kittel; "Antiferromagnetic arrangements in ferrites", Phys. Rev. 87(1952) 290.

[2.27] D. H. Leyons, T. A. Keplan, K. Dwight and N. Menyuk; "Classical Theory of the ground spin-state in cubic spinels", Phys. Rev. 126 (1962) 540.

[2.28] N. S. S. Murthy, M. G. Natera, S. I. Yousuf, R. J. Begum and C. M. Srivatava; "Yafet-Kittel angles in Zinc-Nickel ferrites", Phys. Rev. 181 (2) (1969) 969.

[2.29] M. Nogues, J. L. Dorman, J. Tellet and G. Villers; "Randomly canted structures in the ferrite $Zn_xMg_{1-x}Fe_2O_4$", J. Magn. Magn. Mater. 104-107 (1992) 415.

[2.30] William D. Cattister; the University of Utah, Materials Science and Engineering 6th ed., Wiley 2003.

[2.31] J. Smit and H. P. J. Wijn; Advances in Electronics and Electron Physics, 6, 69 (1954).

[2.32] C. Economos; Ceramic fabrication processes, New York: John Wiley and Sons, 201, (1954).

[2.33] E. A. Schwabe and D. A. Campbell; "Influence of Grain Size on Square-loop Properties of Lithium Ferrites", J. Appl. Phys. 34 (4), (1963) 1251-1253.

[2.34] Igarashi H. and Dkazaki; "Effects of Porosity and Grain Size on the Magnetic Properties of NiZn Ferrite", K. J. Am. Cer. Soc. 60 [1-2], (1977) 51-54.

[2.35] Li, S.; "Grain size effects on magnetic properties and core process of recording head Ferrites", IEEE. Trans. Mag. 22 (1), 1986 14-18.

[2.36] Kip Thorne; Spacetime Warps and the Quantum: A Glimpse of the Future, ITP & Cal Tech, 1999.

[2.37] L. F. Magana, E. Amano and R. Valenzuala; Proc. ICF- 5 India (1984) pp. 813.

[2.38] Globus; A. J de Physque 38, CI-I (1977).

[2.39] M. A. Escobar, R. Valenzuela and L. F. Magana; "Analytical prediction of the magnetization curve and the ferromagnetic hysteresis loop", J. Appl. Phys. 54, (1983) 5935.

[2.40] L. F. Magana, M. A. Escobar, and R. J. Valenzuela; R. Phys Stat. Sol. (a) 97, 495 (1986).

[2.41] A. A. Samokhvalov and A. G. Rustamov; Sov. Phys. Solid State, 6(1964) 749.

[2.42] A. J. Bossmann and C. Crevecoeur; "Mechanism of the electrical conduction in Li-doped NiO", Phys. Rev. 144 (1966) 763.

[2.43] E. J. Verway, P. W. Haayman, and F. C. Romeijn; "Physical Properties and Cation Arrangement of Oxides with Spinel Structure 11. Electronic conductivity", J. Chem. Phys. 15(4), (1947), 181-187.

[2.44] L. G. Van Uitert; "High-Resistivity Nickel Ferrites-The Effect of Minor Additions of Manganese or Cobalt", J. Chem. Phys 24(2), (1956) 306-310.

[2.45] G. H. Jonker; "Analysis of the semiconducting properties of cobalt ferrite", J. Phys. Chem. Solids, 9(2), (1959). 165-175.

[2.46] S. Mandal, D. Banerjee, R. N Bhattacharya and A. A. Ghosh; "Thermoelectric power of unconventional lead vanadate glass", J. Phys: Condens Matter 8, (1996), 2865-2868.

[2.47] A. A. Samokhvalov and A. G. Rustamov; Sov. Phys. Solid state, 6, (1964), 744.

[2.48] A. J. Bosman and C. Crevecour; "Mechanism of the Electrical Conduction in Li Doped NiO", Phys. Rev. 144 (2), (1966), 763-770.

[2.49] G. H Jonker, J. H. Van Santen; "Magnetic Compounds with perovskite structure 111. ferromagnetic compounds of cobalt", J. Physica, 19(1-12), (1953) 120-130.

[2.50] R. V. Bhise, V. C. Mahajan, M. G Patil, S. D. Lotke and S. A Patil; Indian J. Physics 33, (1995), 454-462.

[2.51] B. V. Bhise, A. K Ghatage, B. M Kulkarni, S. D. Lotke and S. A Patil; Bull. Mater. Sci; 19(3), (1996).

[2.52] M. G Patil, V. C. Mahajan, B. V Bhise, S. M Chendke, and S. A Patil; Phys. Stat. Sol. (a) 144, (1994), 415.

[2.53] B. L. Patil, A. B Patil, M, G Patil, V. C. Mahajan, B. V Bhise, S. M Chandke, S. R. Sawant and S. A Patil; Materials Research Lab. Shivaji Univ. India.

177

CHAPTER- III

[3.1] L. B. Kong, Z. W. Li, G. Q. Lin and Y. B. Gan; "Magneto-dielectric properties of Mg-Cu-Co ferrite ceramics: II. Electrical, dielectric and magnetic properties", J. Am. Ceram. Soc. 90 (7) (2007) 2104.

[3.2] S. K. Sharma, Ravi Kumar, Shalendra Kumar, M. Knobel, C. T. Meneses, V. V. Siva Kumar, V. R. Reddy, M. Singh and C. G. Lee; "Role of interparticle interactions on the magnetic behavior of $Mg_{0.95}$ $Mn_{0.05}Fe_2O_4$ ferrite nanoparticles", J. Phys. : Condens. Matter 20(2008) 235214.

[3.3] Soilah Zahi, Mansor Hashim and A. R. Daud; "Synthesis, magnetic and microstructure of Ni-Zn ferrite by sol-gel technique", J. Magn. Magn. Mater. 308 (2007) 177.

[3.4] M. A. Hakim, D. K. Saha and A. K. M. Fazle Kibria; "Synthesis and temperature dependent structural study of nanocrystalline Mg-ferrite materials", Bang. J. Phys. 3 (2007) 57.

[3.5] A. Bhaskar, B. Ragini Kanth and S. R. Murthy; "Electrical properties of Mn added Mg-Cu-Zn ferrites prepared by microwave sintering method", J. Magn. Magn. Mater. 283 (2004) 109.

[3.6] Zhenxing Yue, Ji Zhou, Longtu Li and Zhilun Gui; "Effects of MnO_2 on the electromagnetic properties of Ni-Cu-Zn ferrites prepared by sol-gel auto combustion", J. Magn. Magn. Mater. 233 (2001) 224.

[3.7] C. W. Chen; Magnetism and Metallurgy, Soft Mag. Mat., North-Holland Pub. Com. xv (1977) 288.

[3.8] C. Kittel; "Introduction to Solid State Physics", 7th edition, John Wiley and sons, Inc., Singapore (1996).

[3.9] J. B. Nelson, D. P. Riley; "An experimental investigation of extrapolation methods in the derivation of accurate unit-cell dimensions of crystals", Proc. Phys. Soc London 57 (1945) 160.

[3.10] Tahir Abbas, M. U Islam and M. Ashraf Ch; Mod. Phy. Letts. B. 9(22), (1995), 1419.

[3.11] J. Smit and H. P. J Wijin; Ferrites, Wiely, New York, (1959) 250.

[3.12] Simon Foner; "Versatile and sensitive Vibrating Sample Magnetometer", Rev. Sci. Instr. 30(1959) 548.

CHAPTER- IV

[4.1] J. Smit, H. P. J. Wijn; "Ferrites", Philips Technical Library. Findhoven, Netherlands, 1959, p.150.

[4.2] J. M. Daniels and A. Rosencwaig; "Mossbauer study of the Ni-Zn ferrite system", Can. J. Phys. 48 (1970) 381.

[4.3]   C. M. Srivastava, S. N. Shringi, R. G. srivastava and N. G. Nandikar; " Magnetic ordering and domain-wall relaxation in zinc ferrous ferrite", Phys. Rev B 14 (1976) 2032.

[4.4]   R. G. Kulkarni and V. U. Patil; "Magnetic ordering in Cu-Zn ferrites", J. Mater. Sci 17 (1982) 843.

[4.5]   R. G Kulkarni and V. G Panicker; "Study of canted spin structure in Cu-Cd ferrites", J. Mater. Sci. 19 (1984) 890.

[4.6]   V. G Panicker, R. V Upadhay, S. N. Rao and R. G Kulkarni; "non-collinear spin structure in Ni-Cd ferrite system", J. Mat. Sci Lett. 3 (1984) 385.

[4.7]   R. V. Upadhyay, S. N. Rao and R. G Kulkarni; "Yafet-Kittel type of magnetic ordering in Mg-Cd ferrites", Mater, Lett. 3 (1985) 273.

[4.8]   R. B. Pujar, S. S. Bellad, S. C. watawe and B. K. Chougule; "Magnetic properties and microstructure of Z_r^{4+} substituted Mg-Zn ferrties", Mater. Chem. Phys. 57 (1999) 264.

[4.9]   S. C Byeon, H. J. Je and K. S. Hong; J pn. J. Appl. Phys., 36, 5103 (1997).

[4.10]   T. Nakamura and Y. Okano; J. Phys, IV France 7, CI-91 (1997).

[4.11]   A. Nakano and T. Nomura; Ceram. Trasactions, 97, 285 (1999).

[4.12]   K. O. Low and F. R. Sale; "The development and analysis of property-composition diagrams on gel-derived stoichiometric Ni Cu Zn ferrite", J. Magn. Magn. Mater., 256. 221 (2003).

[4.13]   S. R. Murthy; "Low temperature sintering of Ni Cu Zn ferrite and its electrical, magnetic and elastic properties", J. Mater. Sci. Lett., 21(8), (2002) 657-660.

[4.14]   J. B. Nelson, D. P. Riley; "An experimental investigation of extrapolation methods in the derivation of accurate unit-cell dimensions of crystals", Proc. Phys. Soc. London 57 (1945) 160.

[4.15]   L. Vegard; "Die constitution der mischkristalle und die raumfullung der atome", Z. Phys. 5 (1921) 17.

[4.16]   A. Globus, R. V. Monjaras; "Influence of the deviation from stoichiometry on the magnetic properties of Zn-rich Ni Zn ferrites", IEEE Trans. Magn. 11(5) (1975) 1300-1302.

[4.17]   O. Kimura, M. Matsumoto, M. Sakakura; "Enhanced Dispersion Frequency of Hot-Pressed Z-type Magnetoplumbite Ferrite with the Composition $2Co_{O.3}Ba_{0.5}Sr_{0.5}O10.8Fe_2O_3$", J. Am. Ceran. Soc. 78(10) (1995) 2857.

[4.18]   B. D Cullity; "Introduction to magnetic materials", Addison-Wesley publishing company, Inc. (1972).

[4.19]   B. D Cullity, C. D Graham; " Introduction to magnetic materials", 2nd ed., 2009.

[4.20]   J. Smit, and H. P. J. Wijin; "Ferrites", Wiley, New York, 1959, p. 157.

[4.21] A. M. Shaikh, S. C. Watawe, S. A. Jadhav, B. K. Chougule; Mater. Res. Bull. 37 (2002) 2547.

[4.22] C. Greskovich, K. W. Lay; "Grain Growth in Very Porous Al_2O_3 Compacts", J. Am. Ceram. SOC. 55 (1972) 142.

[4.23] T. Nakamura; J. Appl. phys. 88 (2000) 348.

[4.24] K. O. Low, F. R. Sale; "Electromagnetic properties of gel-derived Ni-Cu-Zn ferrites", J. Magn. Magn. Mater, 246 (2002) 30.

[4.25] R. Valenzuela; Magnetic Ceramic, Cambridge University press. Cambridge, 1994.

[4.26] E. C. Snelling; "Soft Ferrites; Properties and Applications", Second ed., Butterworth, London, 1988.

[4.27] J. L. Snoek; "Dispersion and absorption in magnetic ferrites at frequencies above one Mc/S," Physica, 14 (4) (1948) 207.

[4.28] T. Nakamura; "Low temperature sintering of Ni-Zn-Cu ferrite and its permeability spectra", J. Magn. Magn. Mater., 168 (1997) 285.

[4.29] J. J. Shrotri, S. D. Kulkarni, C. E. Deshpande, S. K. Date; "Effect of Cu substitution on the magnetic and electrical properties of Ni-Zn ferrite synthesized by soft chemical method," Meter, Chem., Phys. 59 (1999) 1.

[4.30] K. Overshott; "The causes of the anomalous Coss in amorphous ribbon materials", IEEE Trans. Magn. 17 (1981) 2698.

[4.31] L. Neel; Ann. Phys. 3 (1948) 137.

[4.32] M. I. Mendelson; "Average Grain size in Polycrystalline Ceramics", J. Am. Ceram, Soc. 52 (8) (1969) 443-446.

[4.33] A. M. Sankpal, S. R. Sawant, A. S. Vaingankar, I. J. Pure; Appl. Phys. 26 (1988) 459.

[4.34] A. M. Shaikh, S. S. Bellad, B. K. Chougule; "Temperature and frequency dependent dielectric properties of Zn substituted Li-Mg ferrites", J. Magn. Magn. Mater. 195 (1999) 384.

[4.35] E. J. W. Verwey and P.W. Haayman; "Electronic conductivity and transition point of magnetic (Fe_3O_4)", Physica 8 (1941) 979.

[4.36] A. Globus, P. Duplex; "Effective Anisotropy in Polycrystalline Materials. Separation of Components", J. Appl. Phys. 39 (1968) 727.

[4.37] K. I wauchi; "Dielectric properties of Fine Particles of Fe_3O_4 and Some Ferrites", Jpn. J. Appl. Phys. 10 (1971) 1520.

[4.38] C. B. Kolekar, P. N. Kamble, S. G. Kulkarni and A. S. Vainganker; "Effect of Gd^{3+} substitution on dielectric behavior of copper cadmium ferrites", J. Mater. Sci. 30 (1995) 5784.

[4.39] C. B. Kolekar, P. N. Kamble, S. G. Kulkarni and A. S. Vainganker; "Effect of GD^{3+} substitution on dielectric behavior of copper cadmium ferrites", J. Mater. Sci. 30 (1995) 5784.

[4.40] Zhenxing Yue, Ji Zhou, Longtu Li, Xiaohui Wang and Zhilun Gui; "Effect of copper on the electromagnetic properties of Mg-Zn-Cu ferrites prepared by sol-gel auto –combustion method", Mater. Sci. Eng. B 86 (2001) 64.

[4.41] Nutan Gupta, S. C. Kashyap and D. C. Dube; "Dielectric and magnetic properties of citrateroute- processed Li-Co spinel ferrites", Phys. Stat, Solidi (a) 204 (7) (2007) 2441.

CHAPTER- V

[5.1] A. Globus, H. Pascard and V. Cagan; "Distance between magnetic ions and fundamental properties in ferrites", J. Physique Coll. 38 (1977) C 1-163.

[5.2] G. C. Jain, B. K Das, R. S. Khanduja and S. C. Gupta; "Effect of intragranular porosity of initial permeability and coercive force in a manganese zinc ferrite", J. Mater. Sci, 11 (1976) 1335.

[5.3] F. G. Brockman, P. H. Dowling, W. G. Steneck; "Dimensional Effects Resulting from a High Dielectric Constant Found in Ferromagnetic Ferrite", Phys. Rev. 77 (1950) 85.

[5.4] R. G. Kulkarini and V. U. Patial; "Magnetic Ordering in Cu-Zn Ferrite", J. Mater. Sci., Vol 17, 1982, p 843.

[5.5] M. A. El Hiti; "DC conductivity for $Zn_x Mg_{0.8-x}Ni_{0.2}Fe_2O_4$ ferrites", J. Magn. Magn. Mater. 136 (1994) 138.

[5.6] J. Smit, H. P. J. wijn; "Ferrites", Wiley, New York, 1959, p.157.

[5.7] Hsui-Fung Cheng; "Modeling of electrical response for semi conducting ferrite", J. Appl. Phys., Vol. 56, No.6, pp. 1831-1837, 1984.

[5.8] C. G. Koops; "On the Dispersion of Resistivity and Dielectric Constant of Some Semiconductors at Audiofrequency", Phys. Rev., 83, (1951) 121-124.

[5.9] H. F. Cheng; "Modeling of electrical response for semi conducting ferrite", J. Appl. Phys. 56(6), (1984) 1831-1837.

CHAPTER- VI

[6.1] S. F. Wang, Y. R. Wang, T. C. K. Yang, C. F. Chen, C. A. Lu, C. Y. Huang; "Densification and magnetic properties of low fire NiCuZn ferrites", J. Magn. Magn. Mater. 220 (2000) 129-138.

[6.2] J. Jeong, H. Y. Han, C. B. Moon; "Effects of Bi_2O_3 addition on the microstructure and electromagnetic properties of NiCuZn ferrites", J. Mat. Sci. Mat. In Elect. 15 (5) (2004) 303.

[6.3] H. Su, H. Zhang, X. Tang; "Effects of Bi_2O_3-WO_3 additions on sintering behaviors and magnetic properties of NiCuZn ferrites'', Mat, Sci. Engg. B 117 (2005) 231.

[6.4] K. Kawano, N. Sakurai, S. Kusumi, H. Kishi; "Magnetic permeability and microstructure of the Bi, Si oxides-doped NiZnCu ferrite composite material", J. Magn. Magn. Mater. 297(1) (2006) 26-32.

[6.5] M. Yan, J. Hu, W. Luo, W.Y. Zhang; "Preparation and investigation of low firing temperature Ni Cu Zn ferrites with high relative initial permeability", J, Magn. Magn. Mater. 303 (1) (2006) 249.

[6.6] J. Y. Hsu, W. S. Ko, C. J. Chen; "The effect of V_2O_5 on the sintering of NiCuZn ferrites", IEEE Trans. Magn. 31 (6) (1995) 3994.

[6.7] R. Lebourgeois, S. Duguey, J. P. Ganne, J. M. Heintz; "Influence of V_2O_5 on the magnetic properties of nickel-zinc-copper ferrites", J. Magn. Magn. Mater. 312 (2007) 328.

[6.8] H. Su, H. Zhang, X. Tang, X. Xiang; "High-permeability and high-Curie temperature NiCuZn ferrite'', J. Magn. Magn. Mater. 283 (2004) 157.

[6.9] S. H. Seo, J. H. Oh; "Effect of MoO_3 addition on sintering behaviors and magnetic properties of Ni Cu Zn ferrite for multilayer chip inductor", IEEE Trans. Magn 35 (5) (1999) 3412-3414.

[6.10] S. F. Wang, Y. R. Wang, T. C. K. Yang, F. J. Wang, C. A. Lu; "Densification and properties of fluxed sintered NiCuZn ferrites", J. Magn. Magn. Mater. 217 (2000) 35.

[6.11] J. H. Jean, C. H. Lee, W. S. Kou; "Effects of Lead (11) Oxide on Processing and Properties of Low-Temperature Cofirable Ni-Cu-Zn Ferrite", J. Am. Ceram. Soc. 82 (2) (1999) 343-350.

[6.12] K. S. Park, J. H. Nam, J. H. Oh; "Magnetic properties of NiCuZn ferrites with addition of tungsten trioxide", J. Magn. Magn. Maer. 226-230 (2001) 1415.

[6.13] H. Igarashi, K. Okazaki; "Effects of Porosity and Grain Size on the Magnetic Properties of NiZn Ferrite", J. Am. Ceram. Soc. 60 (1-2) (1977) 51.

Publications List

a) National & International Journals :

1. "Complex permeability of Fe-deficient Ni-Cu-Zn ferrites"
   Z. H. Khan, M. Mahbubur Rahman, S. S. Sikder, M. A Hakim and D. K. Saha; Journal of Alloys and Compounds 548 (2013) 208-215.

2. "Thermal hysteresis of permeability and transport properties of Cu substituted $Ni_{0.28}Cu_{0.10+x}Zn_{0.62-x}Fe_{1.98}O_4$ ferrites"
   Z. H. Khan, M. Mahbubur Rahman, S. S. Sikder, M. A. Hakim, Shireen Akhter, H. N. Das and B. Anjuman; Journal of Advanced Chemistry Letters (ACL) ,American Scientific Publishers (USA), Accepted Vol. 01, 2013.

3. "Structural and Magnetic Properties of Cu Substituted Ni-Cu-Zn Ferrites".
   Z. H. Khan, S. S. Sikder, M. A Hakim, D. K. Saha and S. Noor; Journal of Engineering Science 02 (2011) 81-85.

4. "Effect of Cu addition on the temperature dependence of relative permeability of Ni-Cu-Zn ferrites."
   Z. H. Khan, S. S. Sikder and M. A. Hakim; Proceedings of national conference, Chittagong University of Engineering & Technology, 8th November, 2009, 16-20.

b) Under Publication / Paper Presented in National & International Conferences / Seminars / Symposium / Workshops:

1. "Effects of magnetic properties on the temperature dependence of relative permeability of Ni-Cu-Zn ferrites."

   Z. H. Khan, S. S. Sikder and M. A. Hakim; National Conference Theme: Materia;s science & Technology For Sustainable Development: Bangladesh Perspective, in the 8 November, 2009, Chittagong University of Engineering & Technology (CUET).

2. "Effect of CuO on the Magnetic Properties of $Ni_{0.28}Cu_{0.10+x}Zn_{0.62-x}Fe_{1.98}O_4$"

   Z. H. Khan, S. S. Sikder, Md. Masud Rana and M. A. Hakim; International Conference on Magnetism and Advanced Materials (ICMAM-2010), in the March 3 - 7, 2010, Department of Physics, BUET and Meterials Science Division, AECD, Dhaka, Bangladesh.

3. "Complex Magnetic Permeability of Fe deficient Ni - Cu - Zn Ferrites"

   Z. H. Khan, S. S. Sikder, H. N. Das and M. A. Hakim; International Conference on Magnetism and Advanced Materials (ICMAM-2010), in the March 3 - 7, 2010, Department of Physics, BUET and Meterials Science Division, AECD, Dhaka, Bangladesh.

4. "The effect of Fe-Deficient of Structural and Magnetic Properties of Ni-Cu-Zn Ferrites"

    Z. H. Khan, S. S. Sikder, M. A. Hakim, D. K. Saha, Saroaut Noor and H. N. Das; National conference on Physics for Development in the 10-11, February, 2011, Bangladesh University of Engineering and Technology (BUET).

5. "Structural and Magnetic Properties of Fe-deficient Ni-Cu-Zn Ferrites"
    Z. H. Khan, S. S. Sikder, M. A. Hakim, D. K. Saha, Al Mamun and H. N. Das; International Conference (BPS), Theme: Physics of Today, in the March 15-16 ,2012, Bangladesh University of Engineering and Technology (BUET), Dhaka, Bangladesh.

6. "Frequency Dispersion of Permeability in Cu Substitution on Ni-Cu-Zn Ferrites"
    Z. H. Khan, S. S. Sikder, M. A. Hakim, D. K. Saha, H. N. Das and B. Anjuman; National Conference on Physics for Technology Development, Theme: Physics for Technology Development in the 27-28 December 2012, Atomic Energy Centre, Dhaka, Bangladesh.

7. "Effect of Copper Additives on the Magnetic Hysteresis of $Ni_{0.28}Cu_{0.10+x}Zn_{0.62-x}Fe_{1.98}O_4$ Ferrites"
    Z. H. Khan, S. S. Sikder, M. A. Hakim, D. K. Saha, H. N. Das and Al Mamun; National Conference on Physics for Technology Development, Theme: Physics for Technology Development in the 27-28 December 2012, Atomic Energy Centre, Dhaka, Bangladesh.

8. "Magnetic and Electrical Properties of High Temperature Sintered Ni-Cu-Zn Ferrites"

    S. Bahadur, S. S. Sikder, Shireen Akhter, **Z. H. Khan** and D. K. Saha; National Conference on Physics for Technology Development, Theme: Physics for Technology Development in the 27-28 December 2012, Atomic Energy Centre, Dhaka, Bangladesh.

9. "Effect of V_2O_5 and Li_2O on the magnetic properties of Ni-Cu-Zn ferrites"
    Z. H Khan, S. S. Sikder, M. A. Hakim, S. Manjura Hoque and Shireen Akhter; International Conference on Advances in Physics in the 4th February 2013, Department of Physics, University of Dhaka, Bangladesh.